frontiers | Research Topics

Neuronal network dysfunction in neurodegenerative disorders

Edited by
Andrea Kwakowsky, Asheeta Prasad, Fernando Peña-Ortega and Sean Austin O. Lim

Published in
Frontiers in Neuroscience

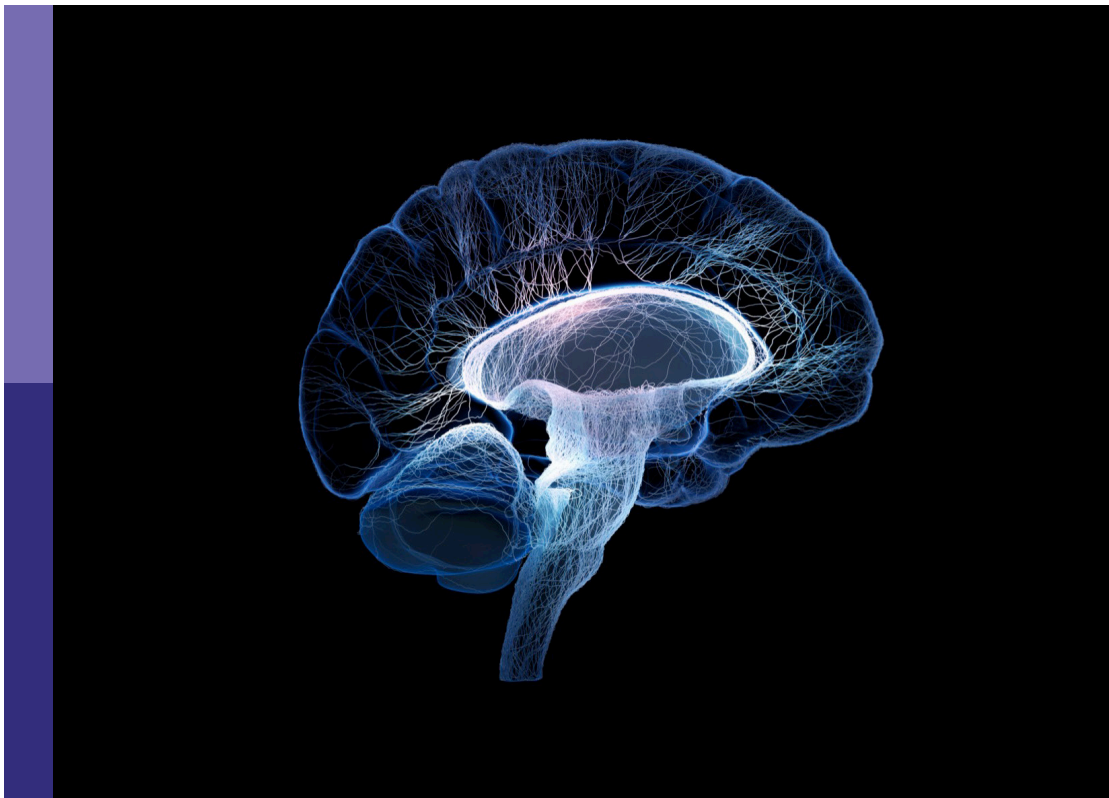

ISSN 1664-8714
ISBN 978-2-83251-876-2
DOI 10.3389/978-2-83251-876-2

About Frontiers

Frontiers is more than just an open access publisher of scholarly articles: it is a pioneering approach to the world of academia, radically improving the way scholarly research is managed. The grand vision of Frontiers is a world where all people have an equal opportunity to seek, share and generate knowledge. Frontiers provides immediate and permanent online open access to all its publications, but this alone is not enough to realize our grand goals.

Frontiers journal series

The Frontiers journal series is a multi-tier and interdisciplinary set of open-access, online journals, promising a paradigm shift from the current review, selection and dissemination processes in academic publishing. All Frontiers journals are driven by researchers for researchers; therefore, they constitute a service to the scholarly community. At the same time, the *Frontiers journal series* operates on a revolutionary invention, the tiered publishing system, initially addressing specific communities of scholars, and gradually climbing up to broader public understanding, thus serving the interests of the lay society, too.

Dedication to quality

Each Frontiers article is a landmark of the highest quality, thanks to genuinely collaborative interactions between authors and review editors, who include some of the world's best academicians. Research must be certified by peers before entering a stream of knowledge that may eventually reach the public - and shape society; therefore, Frontiers only applies the most rigorous and unbiased reviews. Frontiers revolutionizes research publishing by freely delivering the most outstanding research, evaluated with no bias from both the academic and social point of view. By applying the most advanced information technologies, Frontiers is catapulting scholarly publishing into a new generation.

What are Frontiers Research Topics?

Frontiers Research Topics are very popular trademarks of the *Frontiers journals series*: they are collections of at least ten articles, all centered on a particular subject. With their unique mix of varied contributions from Original Research to Review Articles, Frontiers Research Topics unify the most influential researchers, the latest key findings and historical advances in a hot research area.

Find out more on how to host your own Frontiers Research Topic or contribute to one as an author by contacting the Frontiers editorial office: frontiersin.org/about/contact

Neuronal network dysfunction in neurodegenerative disorders

Topic editors

Andrea Kwakowsky — University of Galway, Ireland

Asheeta Prasad — The University of Sydney, Australia

Fernando Peña-Ortega — National Autonomous University of Mexico, Mexico

Sean Austin O. Lim — DePaul University, United States

Citation

Kwakowsky, A., Prasad, A., Peña-Ortega, F., Lim, S. A. O., eds. (2023). *Neuronal network dysfunction in neurodegenerative disorders*. Lausanne: Frontiers Media SA. doi: 10.3389/978-2-83251-876-2

Table of contents

frontiers | Frontiers in Neuroscience

TYPE Editorial
PUBLISHED 24 February 2023
DOI 10.3389/fnins.2023.1151156

OPEN ACCESS

EDITED BY
Victor Tapias,
Cornell University, United States

REVIEWED BY
Carmen Castro,
Universidad de Cádiz, Spain
Savina Apolloni,
University of Rome Tor Vergata, Italy

*CORRESPONDENCE
Andrea Kwakowsky
✉ a.kwakowsky@auckland.ac.nz

SPECIALTY SECTION
This article was submitted to Neurodegeneration, a section of the journal Frontiers in Neuroscience

RECEIVED 25 January 2023
ACCEPTED 08 February 2023
PUBLISHED 24 February 2023

CITATION
Kwakowsky A, Prasad AA, Peña-Ortega F and Lim SAO (2023) Editorial: Neuronal network dysfunction in neurodegenerative disorders. *Front. Neurosci.* 17:1151156. doi: 10.3389/fnins.2023.1151156

Editorial: Neuronal network dysfunction in neurodegenerative disorders

Andrea Kwakowsky[1,2]*, Asheeta A. Prasad[3], Fernando Peña-Ortega[4] and Sean Austin Ong Lim[5]

[1]Pharmacology and Therapeutics, School of Medicine, Galway Neuroscience Centre, Ollscoil na Gaillimhe - University of Galway, Galway, Ireland, [2]Department of Anatomy and Medical Imaging, Centre for Brain Research, Faculty of Medical and Health Science, University of Auckland, Auckland, New Zealand, [3]Faculty of Medicine and Health, School of Medical Sciences, University of Sydney, Sydney, NSW, Australia, [4]Departamento de Neurobiología del Desarrollo y Neurofisiología, Instituto de Neurobiología, Universidad Nacional Autónoma de México, Querétaro, Mexico, [5]Neuroscience Program, College of Science and Health, DePaul University, Chicago, IL, United States

KEYWORDS

neurodegeneration, neurotransmitter, neurodegenerative diseases, neuronal network remodeling, neuronal network dysfunction

Editorial on the Research Topic
Neuronal network dysfunction in neurodegenerative disorders

The prevalence of neurodegenerative diseases is predicted to increase rapidly in the coming decades. There is a great need for therapies to prevent and/or slow the progression of these disorders as current therapies for most neurodegenerative diseases are symptomatic only. Neurodegenerative diseases such as Alzheimer's, Parkinson's, and Huntington's diseases as well as amyotrophic lateral sclerosis pose extraordinary challenges for drug development (Revi, 2020; Ferguson et al., 2022; Mead et al., 2022; Chopade et al., 2023). Several factors likely contribute to neurodegeneration, including oxidative stress, excitotoxicity, protein aggregation, vascular dysfunction, and neuroinflammation, and these processes culminate in the death of specific neuronal populations, leading to cognitive and/or motor impairments. The pathogenesis of neurodegenerative diseases is associated with significant dysfunction in multiple neurotransmitter systems, including altered levels of these neurotransmitters and the massive degeneration and remodeling of neuronal networks (Palop et al., 2006; Brichta et al., 2013; Ahmed et al., 2016; Govindpani et al., 2017; Kwakowsky et al., 2018; Yeung et al., 2021).

This editorial summarizes the contributions to the Frontiers Research Topic "*Neuronal network dysfunction in neurodegenerative disorders*." The objective of this Research Topic was to bring together a cross-section of studies on the advances in human and non-human research focusing on deciphering the mechanisms of neuronal network dysfunction and exploring the use of new therapeutics with selected neuronal target specificity in neurodegenerative diseases.

For this Research Topic, we received a large number of submissions from which 10 articles by a total of 54 authors from 8 countries were published. The articles included 7 original research papers along with two systematic reviews and one multi-scale computational modeling study. These articles range from brain imaging studies performed on patients (Wei et al.; Zheng et al.) to studies exploring post-mortem anatomical changes (Mazumder et al.) and using *in vitro* human (Peppercorn et al.) and animal models to explore the role of neuronal networks in neurodegenerative diseases (Xie et al.) and critical

review of a proposed therapeutic target (Wood et al.) and a suggested new model of disease mechanisms in PD (Muddapu et al.).

The selective loss of neurons and other mechanisms, such as abnormal expression and function of receptors and transporters, and mutations that affect their activity lead to dysfunctional network activity in neurodegenerative diseases. Importantly, the consequences of these alterations on neuronal network activity on behavior/cognition and/or motor function are not yet well-understood (Palop et al., 2006; Govindpani et al., 2017; Yeung et al., 2021; Elbasiouny, 2022). The underlying mechanisms of selective neuronal and regional vulnerability have been difficult to dissect (Surmeier et al., 2017; Giguere et al., 2018; Wang et al., 2020). Recent developments in whole-genome technologies, *in vitro* and *in vivo* disease models, and the extensive examination of anatomical, electrophysiological, and biochemical properties of vulnerable cell populations are beginning to elucidate these basic characteristics of neurodegenerative diseases. The collection of articles in this Research Topic showcases an array of tools applied to examine neuronal network dysfunction such as diffusion tensor imaging (DTI) (Huang et al.), functional and structural magnetic resonance imaging (MRI) (Wei et al.; Zheng et al.), multi-scale computational modeling (Muddapu et al.), optogenetics (Xie et al.), deep brain stimulation and post-mortem human brain analysis (Mazumder et al.), iPSc technology (Peppercorn et al.), RNA sequencing, and Sequential Window Acquisition of All Theoretical Fragment Ion Spectra-Mass Spectrometry (SWATH-MS) (Peppercorn et al.).

With respect to network dysfunction in Parkinson's Disease (PD), Muddapu et al. developed a computational model of cortico-basal ganglia networks that are strongly implicated in levodopa-induced dyskinesia (LID). The model also considers the scale at the level of oxidative stress and calcium-driven excitotoxicity. Collectively, their model proposes that neuronal cell loss in the substantia nigra pars compacta is affected differently at the terminals compared to the soma. Brain imaging techniques have also provided more insight into clinical PD. Wei et al. specifically looked at network connectivity in different presentations of PD. Deep brain stimulation (DBS) of the subthalamic nucleus (STN) has demonstrable success in improving motor symptoms in PD. The study by Zheng et al. helps to explain the neurological bases of clinical differences between the two motor subtypes of PD. Using optogenetic strategies, Xie et al. demonstrate that STN manipulation exerts behavioral effects at the level of locomotion and abnormal involuntary movements in 6-OHDA treated rats. Mazumder et al. provide evidence that DBS in humans does not exert its therapeutic benefit through minimizing neuronal cell loss, changes in astroglial cell numbers, or levels of alpha-synuclein. These studies work to highlight the circuitry involved in DBS.

Secreted amyloid precursor protein alpha (sAPPα) is a cleavage product of APP and is involved in modulating learning and memory. Previous studies proposed that it has the potential as a therapy for preventing, delaying, or even reversing Alzheimer's disease (AD). Peppercorn et al. identified a set of genes affected by sAPPα, which will aid further investigation into the mechanism of action of this neuroprotective protein. The excitatory amino acid transporter 2 (EAAT2) also appears to be a promising therapeutic target for AD. EAAT2 is the main glutamatergic transporter in the human brain and is a key regulator of normal glutamatergic metabolism and maintenance of the excitatory/inhibitory balance and network function. The systematic review by Wood et al. demonstrates that while the findings implicate EAAT2 expressional and functional alterations as key processes in AD progression, they also highlight the need for further studies to characterize EAAT2's involvement in normal physiology and disease in human tissue and to identify compounds that can act as EAAT2 neuromodulators.

Cheng et al. explored the pathophysiological mechanism of freezing of gait (FOG) in multiple system atrophy (MSA) using RS-fMRI and found that FOG is associated with centrality of the impaired thalamus network. The examination of behavioral associations and thalamocortical connectivity suggests that the non-motor circuit plays a compensatory role in MSA.

By retrospectively analyzing DTI parameters Huang et al. report that different neuroanatomical structures are affected differently by idiopathic normal pressure hydrocephalus (INPH) related to their positions in neuronal networks and characteristics, which affects the presentation of clinical symptoms and the prognosis of shunt surgery.

A systematic review by Yap et al. on spinocerebellar ataxia type 3 (SCA3) highlights the importance of evaluating the progressive changes regarding functional connectivity of the cerebellar-cerebral neuronal networks in patients. Importantly, the clinical data show that rather than individual brain regions, the connectivity between different brain regions in distributed networks may be responsible for motor and neurocognitive function in SCA3.

Recently the focus has shifted toward therapeutics which target multiple aspects of neurodegeneration to ensure future treatment success, and the targeting of specific neuronal networks offers many potential therapeutic targets (Brichta et al., 2013; Cao et al., 2018; Stoker and Barker, 2020; Ferguson et al., 2022; Mead et al., 2022). Drug designs have also shifted from treating neurodegenerative diseases at later stages of disease progression to focusing on preventive strategies at early stages of disease development (Cao et al., 2018; Stoker and Barker, 2020; Ferguson et al., 2022). Targeting neuronal dysfunction at early stages of these disorders might offer novel and more effective therapeutic options, and understanding the neuronal network dysfunction in neurodegenerative disorders will open new insights into the fundamental processes of brain circuit function and remodeling to help uncover the etiology of these intractable neurological disorders.

In conclusion, this collection of reviews and original research for this Research Topic provides new perspectives on neuronal network changes and insights toward the value of tools which can be applied to studying neurodegeneration.

Author contributions

All authors listed have made a substantial, direct, and intellectual contribution to the work and approved it for publication.

Funding

We acknowledge funding support from the Alzheimer's New Zealand Charitable Trust (370836), Alzheimer's Zealand (3718869), and Freemasons New Zealand (3719321) to AK. AP was supported by the National Health and Medical Research Council to AP (APP1160412). FP-O was supported by Pappit-UNAM (IG200521) and by CONACyT (A1-S-7540).

Acknowledgments

We deeply thank all the authors and reviewers for their contribution to this Research Topic.

Conflict of interest

The authors declare that the research was conducted in the absence of any commercial or financial relationships that could be construed as a potential conflict of interest.

Publisher's note

All claims expressed in this article are solely those of the authors and do not necessarily represent those of their affiliated organizations, or those of the publisher, the editors and the reviewers. Any product that may be evaluated in this article, or claim that may be made by its manufacturer, is not guaranteed or endorsed by the publisher.

References

Ahmed, R. M., Devenney, E. M., Irish, M., Ittner, A., Naismith, S., Ittner, L. M., et al. (2016). Neuronal network disintegration: common pathways linking neurodegenerative diseases. *J Neurol. Neurosurg. Psychiatry* 87, 1234–1241. doi: 10.1136/jnnp-2014-308350

Brichta, L., Greengard, P., and Flajolet, M. (2013). Advances in the pharmacological treatment of Parkinson's disease: targeting neurotransmitter systems. *Trends Neurosci.* 36, 543–554. doi: 10.1016/j.tins.2013.06.003

Cao, J., Hou, J., Ping, J., and Cai, D. (2018). Advances in developing novel therapeutic strategies for Alzheimer's disease. *Mol. Neurodegener.* 13, 64. doi: 10.1186/s13024-018-0299-8

Chopade, P., Chopade, N., Zhao, Z., Mitragotri, S., Liao, R., and Chandran Suja, V. (2023). Alzheimer's and Parkinson's disease therapies in the clinic. *Bioeng. Transl. Med.* 8, e10367. doi: 10.1002/btm2.10367

Elbasiouny, S. M. (2022). Motoneuron excitability dysfunction in ALS: pseudo-mystery or authentic conundrum? *J. Physiol.* 600, 4815–4825. doi: 10.1113/JP283630

Ferguson, M. W., Kennedy, C. J., Palpagama, T. H., Waldvogel, H. J., Faull, R. L. M., and Kwakowsky, A. (2022). Current and possible future therapeutic options for Huntington's disease. *J. Cent. Nerv. Syst. Dis.* 14, 11795735221092517. doi: 10.1177/11795735221092517

Giguere, N., Burke Nanni, S., and Trudeau, L. E. (2018). On cell loss and selective vulnerability of neuronal populations in Parkinson's disease. *Front. Neurol.* 9, 455. doi: 10.3389/fneur.2018.00455

Govindpani, K., Calvo-Flores Guzman, B., Vinnakota, C., Waldvogel, H. J., Faull, R. L., and Kwakowsky, A. (2017). Towards a better understanding of GABAergic remodeling in Alzheimer's disease. *Int. J. Mol. Sci.* 18, 1813. doi: 10.3390/ijms18081813

Kwakowsky, A., Calvo-Flores Guzman, B., Govindpani, K., Waldvogel, H. J., and Faull, R. L. (2018). Gamma-aminobutyric acid A receptors in Alzheimer's disease: highly localized remodeling of a complex and diverse signaling pathway. *Neural Regen. Res.* 13, 1362–1363. doi: 10.4103/1673-5374.235240

Mead, R. J., Shan, N., Reiser, H. J., Marshall, F., and Shaw, P. J. (2022). Amyotrophic lateral sclerosis: a neurodegenerative disorder poised for successful therapeutic translation. *Nat. Rev. Drug Discov.* 1–28. doi: 10.1038/s41573-022-00612-2

Palop, J. J., Chin, J., and Mucke, L. (2006). A network dysfunction perspective on neurodegenerative diseases. *Nature* 443, 768–773. doi: 10.1038/nature05289

Revi, M. (2020). Alzheimer's disease therapeutic approaches. *Adv. Exp. Med. Biol.* 1195, 105–116. doi: 10.1007/978-3-030-3263 3-3_15

Stoker, T. B., and Barker, R. A. (2020). Recent developments in the treatment of Parkinson's disease. *F1000Res* 9, F1000 Faculty Rev-862. doi: 10.12688/f1000research.25634.1

Surmeier, D. J., Obeso, J. A., and Halliday, G. M. (2017). Selective neuronal vulnerability in Parkinson's disease. *Nat. Rev. Neurosci.* 18, 101–113. doi: 10.1038/nrn.2016.178

Wang, Z. T., Zhang, C., Wang, Y. J., Dong, Q., Tan, L., and Yu, J. T. (2020). Selective neuronal vulnerability in Alzheimer's disease. *Ageing Res. Rev.* 62, 101114. doi: 10.1016/j.arr.2020.101114

Yeung, J. H. Y., Walby, J. L., Palpagama, T. H., Turner, C., Waldvogel, H. J., Faull, R. L. M., et al. (2021). Glutamatergic receptor expression changes in the Alzheimer's disease hippocampus and entorhinal cortex. *Brain Pathol.* 31, e13005. doi: 10.1111/bpa.13005

frontiers in Neuroscience

ORIGINAL RESEARCH
published: 17 December 2021
doi: 10.3389/fnins.2021.794046

Preliminary Exploration of the Sequence of Nerve Fiber Bundles Involvement for Idiopathic Normal Pressure Hydrocephalus: A Correlation Analysis Using Diffusion Tensor Imaging

Wenjun Huang[1†], Xuhao Fang[2†], Shihong Li[1], Renling Mao[2], Chuntao Ye[1], Wei Liu[1] and Guangwu Lin[1]*

[1] Department of Radiology, Huadong Hospital Affiliated to Fudan University, Shanghai, China, [2] Department of Neurosurgery, Huadong Hospital Affiliated to Fudan University, Shanghai, China

OPEN ACCESS

Edited by:
Andrea Kwakowsky,
The University of Auckland,
New Zealand

Reviewed by:
Benito de Celis Alonso,
Meritorious Autonomous University of Puebla, Mexico
Jiu Chen,
Nanjing Medical University, China

***Correspondence:**
Guangwu Lin
lingw01000@163.com

[†] These authors have contributed equally to this work

Specialty section:
This article was submitted to Neurodegeneration, a section of the journal Frontiers in Neuroscience

Received: 13 October 2021
Accepted: 24 November 2021
Published: 17 December 2021

Citation:
Huang W, Fang X, Li S, Mao R, Ye C, Liu W and Lin G (2021) Preliminary Exploration of the Sequence of Nerve Fiber Bundles Involvement for Idiopathic Normal Pressure Hydrocephalus: A Correlation Analysis Using Diffusion Tensor Imaging. Front. Neurosci. 15:794046. doi: 10.3389/fnins.2021.794046

The study preliminarily explored the sequence and difference of involvement in different neuroanatomical structures in idiopathic normal pressure hydrocephalus (INPH). We retrospectively analyzed the differences in diffusion tensor imaging (DTI) parameters in 15 ROIs [including the bilateral centrum semiovale (CS), corpus callosum (CC) (body, genu, and splenium), head of the caudate nucleus (CN), internal capsule (IC) (anterior and posterior limb), thalamus (TH), and the bilateral frontal horn white matter hyperintensity (FHWMH)] between 27 INPH patients and 11 healthy controls and the correlation between DTI indices and clinical symptoms, as evaluated by the INPH grading scale (INPHGS), the Mini-Mental State Examination (MMSE), and the timed up and go test (TUG-t), before and 1 month after shunt surgery. Significant differences were observed in DTI parameters from the CS (p_{FA1} = 0.004, p_{ADC1} = 0.005) and the genu (p_{FA2} = 0.022; p_{ADC2} = 0.001) and body (p_{FA3} = 0.003; p_{ADC3} = 0.002) of the CC between the groups. The DTI parameters from the CS were strongly correlated with the MMSE score both pre-operatively and post-operatively. There was association between apparent diffusion coefficient (ADC) values of anterior and posterior limbs of the IC and MMSE. The DTI parameters of the head of the CN were correlated with motion, and the ADC value was significantly associated with the MMSE score. The FA value from TH correlated with an improvement in urination after shunt surgery. We considered that different neuroanatomical structures are affected differently by disease due to their positions in neural pathways and characteristics, which is further reflected in clinical symptoms and the prognosis of shunt surgery.

Keywords: idiopathic normal pressure hydrocephalus (INPH), diffusion tensor imaging (DTI), white matter (WM), central gray matter, dementia, gait disorder, incontinence

INTRODUCTION

Idiopathic normal pressure hydrocephalus (INPH), first described by Salomón Hakim in 1965 (2016), is a chronic communicating hydrocephalus syndrome characterized by normal cerebrospinal fluid (CSF) pressure (70–200 mm H_2O) and clinical symptoms including cognitive impairment, gait disorder, and incontinence (2016). Patients with INPH may experience different combinations and varying degrees of these typical clinical symptoms (Adams et al., 1965). It is known that the clinical symptoms of INPH can be improved by shunt surgery (Nakajima et al., 2021), but this invasive operation has uncertain efficacy and may incur some complications. Thus, understanding the neuropathological mechanisms underlying INPH might help us better select patients for surgery and predict its outcomes.

Diffusion tensor imaging (DTI), a high-resolution magnetic resonance imaging (MRI) technique combining 2D diffusion-weighted images to produce a 3D diffusion image showing the movement of water molecules in brain tissue (Siasios et al., 2016), is widely used to detect and quantify changes in white matter. White matter changes can be quantitatively measured by fractional anisotropy (FA) and the apparent diffusion coefficient (ADC), which can be used to identify small structural changes and determine the structural integrity and interstitial space of brain tissue (Le Bihan et al., 2001; Basser and Jones, 2002; Kanno et al., 2011). The ADC value is a general, quantitative measure of diffusion changes. The FA value, indicating the directivity of the ADC, reflects not only fiber microstructural damage, such as axonal degeneration or ischemic demyelination, but also the compression of white matter fibers caused by ventricular dilation, resulting in changes in fiber density and diffusion direction (Kanno et al., 2011; Kim et al., 2011). The FA value may be affected simultaneously by two different pathological processes: neural degeneration, which could decrease FA and ventricular dilation, which could increase FA (Sarica et al., 2021).

For INPH, most theories propose that ventricle dilation leads to tension and compression of the periventricular white matter, resulting in interstitial edema and progressive axonal degeneration and gliosis. On the other hand, different parts of nerve fibers are affected differently by ventricular dilation, which leads to vary changes in diffusion characteristics of different parts and different macroscopic effects (Sarica et al., 2021). Most previous studies have focused on white matter in different regions of the brain and explored differences in the influence of different white matter tracts on INPH (Kang et al., 2016; Siasios et al., 2016; Tsai et al., 2018; Younes et al., 2019). However, no definite conclusion has been drawn on the developmental sequence of related white matter injuries.

We hypothesized that in the same course of disease, the damage to different neuroanatomical structures are varied, which may be related to the location of the nerve fiber bundles and neural pathways and their own characteristics.

MATERIALS AND METHODS

Patients

This study was approved by the Institutional Review Board of Huadong Hospital affiliated with Fudan University (Approval number: 2017K027). Informed consent was obtained from the participants before recruitment.

The study retrospectively included twenty-seven patients referred to the Department of Neurology, Huadong Hospital affiliated with Fudan University, between August 2016 and August 2020. The subjects who fulfilled the diagnostic criteria for confirmed INPH according to Experts consensus on diagnosis and treatment of normal pressure hydrocephalus in China (2016). The criteria for confirmed INPH were as follows: (1) age over 60 years; (2) at least one of the triad of symptoms (gait disturbance, dementia, and urinary incontinence) with insidious progression for more than 6 months; (3) ventricular dilatation (Evans' index $>$ 0.3); (4) CSF pressure $<$200 mm H_2O; (5) the absence of other diseases that may account for such symptoms; and (6) a positive outcome from the CSF tap test and shunt surgery. The exclusion criteria for INPH were as follows: (1) cerebral infarction and dementia caused by recent heavy drinking, hospitalization for severe mental illness and other clear causes; and (2) secondary normal pressure hydrocephalus. The inclusion criteria for healthy elderly individuals were as follows: (1) age over 60 years; (2) no gait disorder, cognitive impairment or urination disorder, and normal MMSE score; (3) conventional cerebral MRI showing no abnormality; and (4) no active neurological, systemic or psychiatric diseases.

Clinical Assessment

All subjects underwent detailed clinical examinations by two neurosurgeons, which involved the INPH grading scale (INPHGS), the Mini-Mental State Examination (MMSE) and, for INPH patients, and the timed up and go test (TUG-t), before shunt surgery and 1 month after shunt surgery.

The INPHGS is a clinician-rated scale used to assess the severity of INPH symptoms (cognitive impairment, gait disturbance, and urinary disturbance are each evaluated on a scale from 0 to 4) that provides a reliable and effective evaluation though interviews with patients and caregivers (Nakajima et al., 2021). The total score can be used as an index, together with the evaluation points for the MMSE and TUG-t.

A lumbar tap removing 30 ml of CSF was performed on all INPH patients. After the tap, all patients were re-evaluated using the INPHGS and the TUG test. The following criteria were used to identify positive outcome: improvement of one point or more on the INPHGS or more than 10% improvement in time on the TUG test (Kang et al., 2016). A shunt valve was inserted in the lumbar subarachnoid space in all the patients who underwent a lumboperitoneal (LP) shunt procedure.

Magnetic Resonance Imaging Methodology and Data Analysis

All MRI examinations were performed with a 3T MRI system (MAGNETOM Prisma, Siemens AG) prior to any

treatment. DTI data were obtained from all participants along 10 gradient-encoding directions with b values 0 and 1,000 s/mm^2, a field-of-view (FOV) of 220 mm × 220 mm with 56 slices, a slice thickness of 2 mm with a 0.6 mm gap, an acquired resolution of 1.15 mm × 1.15 mm × 2.00 mm, a reconstructed resolution of 0.57 mm × 0.57 mm × 2.00 mm, an echo time (TE) of 78 ms, and a repetition time (TR) of 4,600 ms. The ADC and FA values were calculated using the NUMARIS/4 Siemens AG (syngo MR E11). Regions of interests (ROIs) were manually drawn on DTI images with b-values of 0 using a program developed in house and produced by Siemens AG.

The Placement of Regions of Interests

The thalamic radiation, a round-trip fiber connecting the thalamus and the cortex, travels between the thalamus, caudate and lenticulate nuclei through the centum semiovale and radiates into the cerebral cortex in a fan shape. The superior and centroparietal thalamic radiations connect the frontal and parietal lobes with the ventral thalamic nuclei through the anterior and posterior limbs of the internal capsule (IC). In another way, the anatomical structure of superior thalamus radiation is close to the and diffuses around the lateral ventricle wall, so it could be affected by ventriculomegaly. The corpus callosum (CC) is adjacent to the lateral ventricle and is greatly affected by dilation of the lateral ventricle. The corticospinal tract (CST) arises from the frontal cortex and passes through the centum semiovale toward the posterior limb of the IC.

According to the above, fifteen ROIs were manually placed along the right and left centrum semiovale (CS), CC (body, genu, and splenium), right and left frontal horn white matter hyperintensity (FHWMH), right and left head of the caudate nucleus (CN), right and left IC (anterior and posterior limb), and right and left thalamus (TH) (**Figure 1**). All ROIs were delineated by an experienced neuroradiologist.

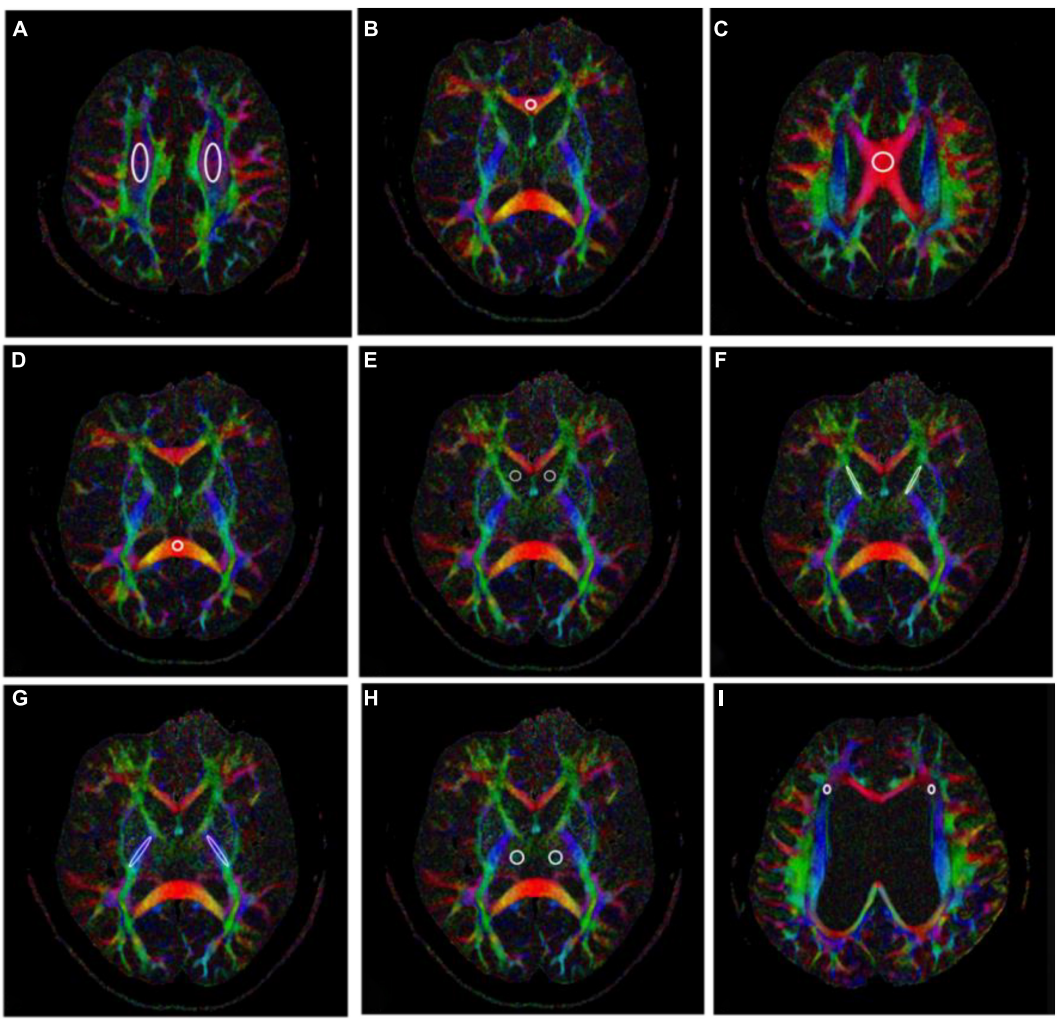

FIGURE 1 | Fifteen regions of interests (ROIs) placed along the right and left centrum semiovale (CS) **(A)**, genu of the corpus callosum (CC) **(B)**, body of the CC **(C)**, splenium of the CC **(D)**, right and left head of the caudate nucleus (CN) **(E)**, right and left anterior limb of the internal capsule (IC) **(F)**, right and left posterior limb of the IC **(G)**, right and left thalamus **(H)**, and right and left frontal horn white matter hyperintensity (FHWMH) **(I)**.

Statistical Analyses

Statistical analyses were conducted using the Statistical Package for Social Science, version 24.0 (SPSS, Chicago, IL, United States).

Clinical symptom statistics are expressed as the median (quartile). We compared the data between the INPH and control groups and between measurements made pre-operatively and 1 month post-operatively with the Mann-Whitney *U* test.

We used an independent-samples *t*-test to compare DTI parameters (FA and ADC) for the 15 ROIs between patients with INPH and healthy controls. An independent-samples *t*-test was also used to investigate any differences between the right and left hemispheres in these parameters. We considered the voxels to be independent of each other; therefore, no multiple comparison correction was performed. The results were deemed to be significant at a value of $p < 0.05$.

Spearman's correlation coefficient was used to estimate the relationship between pre-operative DTI parameters and the changes between the pre-operative and post-operative clinical measures.

RESULTS

Patient's Characteristics

The 27 INPH patients [twenty-one males and six females with a median age of 74 (range 66–89) years] with symptom duration 30.48 (20.82–40.14) months and 11 healthy controls [four males and seven females with a median age of 68.36 (range 64–75) years] constituted the final sample for analysis. There were remarkable differences between the groups in their INPHGS, MMSE, and TUG-t scores. Furthermore, all INPH patients showed notable improvement in clinical measures (INPHGS, MMSE, and TUG-t) 1 month after shunting ($p < 0.001$). Evans' index in patients with INPH was significantly higher than that in normal elderly patients before surgery ($p1 < 0.001$). and there was no significant change 1 month after shunt ($p2 > 0.05$). The evaluation results are displayed in **Table 1**.

Clinical Assessment Comparison

The differences between the pre-operative INPH and the healthy control clinical assessment (INPHGS, MMSE, and TUG-t) scores were significant ($p1 < 0.001$). Significant improvement was observed in the gait and urination assessments, as seen in the comparison between the pre-operative and post-operative INPH group scores ($p2 < 0.001$). The cognitive improvement was less significant than that of the improvements in gait and urination but still indicated statistical significance ($p2' < 0.05$). There was no significant change in the Evans index after shunt surgery ($p2'' > 0.05$) (**Table 1**).

Diffusion Tensor Imaging Parameter Comparison Between Pre-operative Idiopathic Normal Pressure Hydrocephalus Patients and Healthy Controls

There was no significant difference in the DTI parameters between the bilateral hemispheres in either group. Therefore, we took the mean value of the DTI parameters of the left and right hemispheres for the following intergroup and intragroup comparative analyses.

Regarding the FA value, compared with the healthy controls, the pre-operative INPH patients demonstrated a significant decrease in the CS, the genu and body of CC, and the anterior and posterior limbs of the IC ($p = 0.004$, 0.022, 0.003, 0.037, and 0.025, respectively). However, compared with the healthy controls, the pre-operative INPH patients demonstrated a significant increase in the ADC value in the same areas ($p = 0.005$, 0.001, 0.002, 0.037, and 0.010, respectively) as well as in the splenium of the CC and the head of the CN ($p = 0.001$ and 0.009, respectively) (**Table 2**).

TABLE 1 | Clinical measures of the idiopathic normal pressure hydrocephalus (INPH) patients obtained pre-operatively and 1 month post-operatively and of the healthy controls.

	INPH (n = 27)		Healthy control, HC (n = 11)	$P1$-value	$P2$-value
	Pre-operative	1 month post-operative		Pre vs. HC	Pre vs. post
Age (average, range)	75.07 (66–89)		68.36 (64–75)	0.008	
Sex (male/female)	21/6		4/7	0.015*	
Symptom duration (average, range)	30.48 (20.82–40.14)				
Evans' index	0.323 ± 0.046	0.320 ± 0.019	0.256 ± 0.033	<0.001**	0.665
INPHGS					
Gait	3.00 (0)	2.00 (0)	0 (0)	<0.001**	<0.001**
Cognition	3 (1)	2 (1)	0 (1)	<0.001**	0.002**
Urination	3 (1)	1 (1)	0 (0)	<0.001**	<0.001**
Total	8 (2)	5 (2)	0 (1)	<0.001**	<0.001**
Mini-Mental State Examination (MMSE)	18.15 ± 7.03	23 (5)	29 (1)	<0.001**	0.027*
Timed up and go test (TUG-t)	21.64 (8.72)	15.78 (8.13)	8.96 (1.89)	<0.001**	0.001**

Values denote the mean ± standard deviation or median (quartile).
*Significant differences are marked with *p < 0.05 and **p < 0.01.*

TABLE 2 | Comparison of the diffusion tensor imaging (DTI) parameters (FA and ADC) between the pre-operative idiopathic normal pressure hydrocephalus (INPH) patients and healthy controls.

DTI parameters	ROIs	Pre-operative INPH	Healthy control	*P*-value
FA	CS	0.385 ± 0.139	0.492 ± 0.043	0.004**
	Genu of CC	0.670 ± 0.120	0.861 ± 0.038	0.022*
	Body of CC	0.712 ± 0.136	0.849 ± 0.037	0.003**
	Splenium of CC	0.742 ± 0.156	0.894 ± 0.053	0.06
	FHWMH	0.200 ± 0.048	0.179 ± 0.024	0.24
	Head of CN	0.220 ± 0.033	0.198 ± 0.023	0.092
	Anterior limb of IC	0.584 ± 0.154	0.781 ± 0.052	0.037*
	Posterior limb of IC	0.746 ± 0.112	0.850 ± 0.031	0.025*
	Thalamus	0.314 ± 0.069	0.305 ± 0.041	0.162
ADC	CS	0.772 ± 0.240	0.438 ± 0.011	0.005**
	Genu of CC	0.622 ± 0.141	0.409 ± 0.016	0.001**
	Body of CC	0.626 ± 0.161	0.414 ± 0.021	0.002**
	Splenium of CC	0.571 ± 0.162	0.383 ± 0.024	0.001**
	FHWMH	0.863 ± 0.115	0.830 ± 0.071	0.069
	Head of CN	0.633 ± 0.084	0.573 ± 0.024	0.009**
	Anterior limb of IC	0.560 ± 0.177	0.373 ± 0.047	0.037*
	Posterior limb of IC	0.514. ± 0.084	0.395 ± 0.019	0.010*
	Thalamus	0.642 ± 0.092	0.541 (0.053)	0.074

*Values denote the mean ± standard deviation or median (quartile). Significant differences are marked with *p < 0.05 and **p < 0.01.*

Relationship Between Pre-operative Diffusion Tensor Imaging Parameters and Clinical Symptoms

Pre-operative Clinical Assessment

We performed Spearman correlation analysis between the pre-operative DTI parameters and pre-operative clinical scores of all INPH patients and obtained varying degrees of correlation for the different comparisons. The mean FA of the bilateral CS demonstrated a strong and expressively significant correlation with the MMSE score ($r = 0.659$, $p < 0.001$), a moderate, negative and almost significant correlation with the INPHGS total score ($r = -0.369$, $p = 0.058$), and strong, negative and borderline significant negative correlations with the INPHGS cognitive score and the TUG-t score ($r1 = -0.327$, $p1 = 0.096$ and $r2 = -0.323$, $p2 = 0.100$, respectively) (**Figure 2**).

The ADC value in the CS had a strong, negative and significant correlation with the MMSE score ($r = -0.579$, $p = 0.002$) and an almost significant correlation with the TUG-t score ($r = 0.337$, $p = 0.085$). Similarly, in the posterior limb of the IC and the thalamus, the FA values were moderately correlated with the MMSE and TUG-t scores ($r1 = 0.314$, $p1 = 0.111$; $r2 = 0.326$, $p2 = 0.097$), but these differences were not statistically significant (**Figures 2**, **3**).

Spearman correlation analysis also revealed a moderately significant correlation between the FA value in the splenium of the CC and the INPHGS urination score ($r = 0.424$, $p = 0.027$) and an almost significant correlation between the FA value in the head of the CN and motor function (the INPHGS gait score) ($r = -0.379$, $p = 0.051$) (**Figure 2**).

There was a negative, nearly significant correlation between the ADC in the head of the CN ($r = -0.357$, $p = 0.068$) and in anterior limb of IC ($r = -0.326$, $p = 0.097$) and the MMSE score and a strong, negative and significant correlation between the ADC in the posterior limb of the IC and the MMSE score ($r = -0.468$, $p = 0.014$). The ADC for the splenium of the CC and the thalamus was correlated with both the TUG-t ($r = 0.356$, $p = 0.069$) and INPHGS gait scores ($r = -0.379$, $p = 0.051$), respectively. However, these correlations did not reach statistical significance (**Figure 3**).

There were no significant correlations between the DTI metrics in the body of the CC and FHWMH with any of the clinical evaluation scores.

One-Month Post-operative Clinical Assessment

Both FA ($r = -0.625$, $p < 0.001$) and ADC ($r = 0.530$, $p = 0.004$) in the CS had strong significant correlations with the change in the MMSE score post-operatively. In the thalamus, the Spearman correlations for changes in the clinical assessment scores after shunt surgery vs. FA were also analyzed, revealing strong and significant correlations in ΔINPHGS—urination ($r = -0.516$, $p = 0.006$), ΔINPHGS—total ($r = -0.474$, $p = 0.012$), and ΔTUG-t ($r = -0.469$, $p = 0.014$) (**Figures 4**, **5**).

A negative and significant correlation was also revealed between the ADC in the head of the CN and ΔTUG-t ($r = -0.382$, $p = 0.050$). The other correlations involving the ADC in this region were weaker, but moderate, almost significant correlations were observed with ΔINPHGS—gait ($r = -0.338$, $p = 0.085$) and ΔMMSE ($r = 0.359$, $p = 0.066$). None of the remaining correlations were significant (**Figure 5**).

DISCUSSION

This study compared the differences in DTI parameters (FA and ADC values) between INPH patients and normal elderly individuals and analyzed the correlation between pre-operative DTI parameters and pre-operative clinical scores and their post-operative changes in INPH patients. We aimed to clarify the locations where white matter or central gray matter were affected by INPH and the sequence of white matter fiber bundle involvement over the course of disease progression to explore the possible mechanism underlying the occurrence and changes in clinical symptoms in patients and establish a foundation for promoting a window for disease diagnosis and improving the evaluation of the pre-operative prognosis.

Diffusion tensor imaging can be used to evaluate the integrity of the white matter pathway by measuring the preferred direction of water diffusion in white matter fiber bundles. FA values (reflecting the degree of anisotropy) and ADC values (presenting the degree of diffusion) were defined for quantitative evaluation of nerve injury (Bouziane et al., 2019; Spotorno et al., 2019). Among them, the heterogeneity of FA value may be related to the coexistence of two different pathological processes: neural degeneration (decreasing FA), and ventricular dilation (increase FA) (Sarica et al., 2021).

FIGURE 2 | Correlations between fractional anisotropy (FA) value and pre-operative clinical evaluation score. The numbers in the cell represent *r* values.

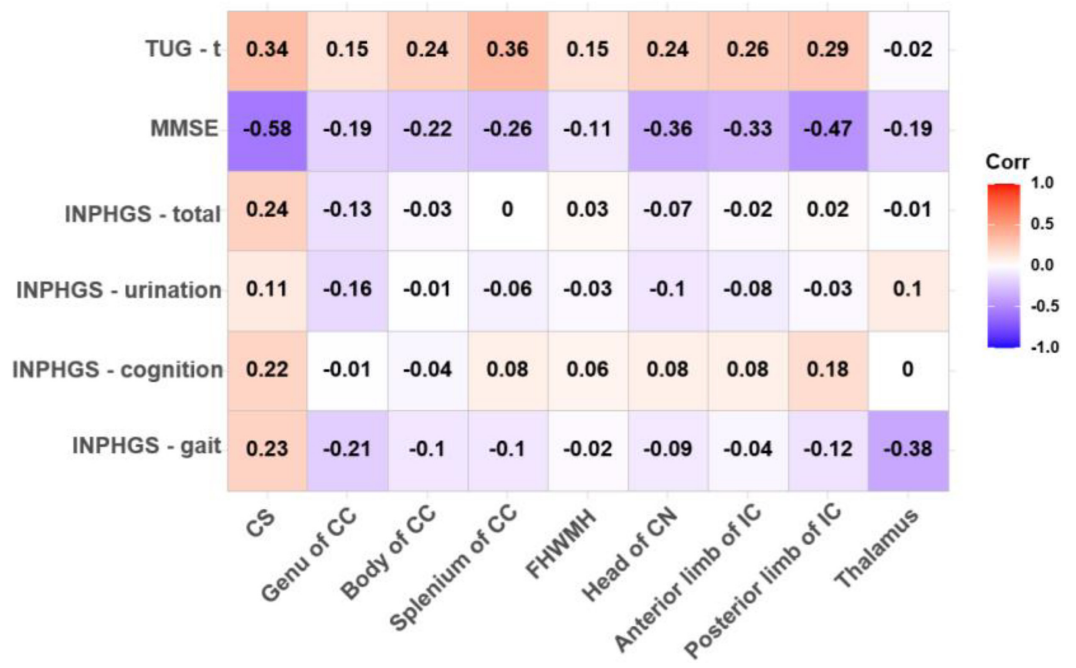

FIGURE 3 | Correlations between apparent diffusion coefficient (ADC) value and pre-operative clinical evaluation score. The numbers in the cell represent *r* values.

In this study, it was found that the FA and ADC values of the white matter in the investigated regions of INPH patients were different from those of healthy elderly individuals except for those of the FHWMH and thalamus, with the differences in the CS being the most substantial. We also found that compared with healthy elderly participants, INPH patients had significantly lower FA values but significantly increased ADC values for the CS and the anterior and posterior limbs of the IC. Due to abnormal CSF circulation, the lateral ventricle and the Sylvian fissure dilate, and the latter resists the pressure of

FIGURE 4 | Correlation between fractional anisotropy (FA) value and changes in clinical evaluation score post-operatively. The numbers in the cell represent *r* values.

FIGURE 5 | Correlation between apparent diffusion coefficient (ADC) value and changes in clinical evaluation score post-operatively. The numbers in the cell represent *r* values.

lateral ventricle dilation, so the ventricle dilates mainly along the *Z*-axis (which is perpendicular to the bi-commissural line). We hypothesize that the white matter in the CS is subjected to externally induced mechanical stress first (Silverberg et al., 2015; Yamada et al., 2019; Younes et al., 2019). As the disease progresses, prolonged compression of the white matter fibers leads to interstitial edema and progressive axonal loss (Younes et al., 2019), resulting in a decrease in the FA value and an increase in the ADC value. It has also been proposed that the increased ADC value of the CS is mainly due to stretching effect of enlarged ventricle along the *Z*-axis on CST, which reduces the tortuosity of nerve tract (Hattori et al., 2011; Sarica et al., 2021) and the

diffusion coefficient increases with increased water diffusivity parallel to these fibers.

In addition, we found that the FA value in the CS was significantly positively correlated with the pre-operative MMSE score and negatively correlated with the improvement of the post-operative MMSE score. ADC values in the CS and anterior and posterior limbs of the IC were correlated with the pre-operative and post-operative MMSE scores. The CS and the anterior and posterior limbs of the IC are involved in the subfrontal cortical pathway. As a key node of the subfrontal cortical pathway crossed by interhemispheric, projection and association fibers, the CS is thought to be a region more responsible for chronic neuropsychiatric symptoms than other regions (Beppu et al., 2010) and may be a critical region leading to the occurrence of cognitive impairment (Skiöld et al., 2010; Zhang et al., 2011; Blasel et al., 2012). We hypothesized that a lower FA value indicateded a lower degree of white matter involvement, and it was easier to recover to the normal neuroanatomical structure after shunt surgery, thus the corresponding impaired cognitive function could be improved more easily. Regarding the correlation analysis, we showed that the ADC value of the CS was moderately correlated with the TUG score before the shunt operation. The CST starts from the precentral motor area *via* the CS and the anterior two-thirds of the posterior limb of the IC to the pedunculus cerebri and then runs down to the pons, the medulla oblongata and spinal cord, mainly controlling body movement (Park et al., 2008). Given the findings of a study on the localization of body movement in the CST (Seo et al., 2012), we considered that the white matter DTI parameters in this region are probably closely related to the motor function of the lower limbs.

Alzheimer's disease (AD) pathology, the presence of amyloid-β (Aβ) at the brain, has been found in 25–60% of patients with INPH (Elobeid et al., 2015; Abu Hamdeh et al., 2018). It has been found that the deposition of Aβ in brain tissue affects resting state functional connectivity and thus clinical symptoms (Khoo et al., 2016; Bommarito et al., 2021), and that the CS is more susceptible to the deposition of Aβ than other regions of the white matter (Charidimou et al., 2014). We concluded that the CS may be a very important region with early involvement in the disease progression of INPH. As CSF is pathologically redistributed, the ventricular system first expands along the *Z*-axis. The resulting long-term pressure increase reduces the compliance of the upper brain tissue and limits the arterial pulse, leading to dysfunction of the brain lymphatic system (Yokota et al., 2019), which further aggravates the CSF circulation disorder. Combined with external mechanical pressure and internal metabolic abnormalities, such as decreased removal of hazardous substances (Silverberg et al., 2015), changes in the CS, which is first involved in the CST and the subfrontal cortical pathways, lead to reduced pathway connectivity and impaired integrity of the cognitive and motor networks. The most important clinical symptoms, gait and cognitive impairment, may be caused by early damage to the white matter in the CS, followed by damage involving the downstream nerve fibers along the white matter fibers (Selemon and Goldman-Rakic, 1985).

In this study, it was found that the FA and ADC values in the head of the CN in the INPH group were slightly higher than those in the control group, and they were found to be correlated with the gait and MMSE scores in both pre-operative and post-operative evaluations. Osuka et al. (2010) showed that the FA value of the CN in patients with hydrocephalus was significantly higher than that in normal elderly people and in those with obvious brain atrophy. In the brain, the FA value is affected by the diameter, density and range of nerve fiber myelin formation (Rose et al., 2012). The CN retains a relatively normal extracellular space after compression due to its stronger compression characteristics, which makes it less affected by edema (Torvik and Stenwig, 1977; Del Bigio and Bruni, 1988; DeVito et al., 2007). This may be the reason why the CN is relatively unaffected in the early stage of INPH and why the decrease in the FA value for the CN is delayed. As a part of the striatum, the head of the CN plays an important role in motor, cognitive and goal-oriented behavior (Robbins and Everitt, 1996; Middleton and Strick, 2000; Mestres-Missé et al., 2012). The anterior and middle parts of the CN connect to the prefrontal cortex, and the posterior part connects to the motor cortex, contributing to the formation of the cognitive circuit (Goldman and Nauta, 1977; Selemon and Goldman-Rakic, 1985; Lehéricy et al., 2004). Different parts of the CN are connected by longitudinal fibers, which help to integrate different cognitive functions with varying degrees of complexity (Kotz et al., 2013). Based on the above, we speculated that due to its downstream location in the nerve fiber bundle and its own characteristics, the CN sustains damage later and to a lesser degree than to other brain structures during the development of the disease. As the disease progresses, a progressive decrease in the FA value and the volume of the CN may be accompanied by a significant increase in gait and cognitive impairment.

We also found that the improvement in urination and the TUG-t score of patients after shunt surgery was significantly correlated with the thalamic FA value. Extensive white matter fiber connections between the thalamus and frontal lobes may form the neuroanatomical basis for disease progression (Black et al., 2009; Back et al., 2011; Griffanti et al., 2018). In terms of metabolism, intracranial CSF redistribution and local N-acetyl aspartate increases are associated with the decreased blood supply to the thalamus, resulting in subsequent axonal degeneration (Lundin et al., 2011). In our study, we did not find a significant correlation between thalamic DTI parameters and pre-operative clinical symptoms, which may be related to the course of disease and the degree to which the thalamus tolerates metabolic injury. The thalamus is located downstream of nerve fiber tracts and anatomically on both sides of the third ventricle. Since expansion of the third ventricle is not obvious in INPH, the mechanical pressure on the thalamus is presumed to be slight. On the other hand, due to the change in neuroplasticity and the improved efficiency of neural conductivity, the FA value of the thalamus increases in the early stage of INPH to compensate for the corresponding neural function (Mole et al., 2016; Tsai et al., 2018). Thus, we believe that damage to the thalamus mainly stems from damaged upstream white matter fibers and their intrinsic characteristics.

This study has some limitations. The first is that this was a cross-sectional study with a small sample size, so that these results should be interpreted cautiously. Further studies are needed to confirm our results. In addition, previous studies have shown that with the growth of age, FA value has a downward trend, and ADC value has a rising trend. Although ROI analysis is easy to perform, does not require third-party software and is suitable for clinical studies, there is a certain degree of subjectivity in how the ROI is outlined. Additionally, we did not subgroup the patients with diagnosed INPH according to the course of disease, so we were unable to clarify the differences in white matter integrity of different neural anatomical structures under different courses of disease. Finally, we did not conduct a review of the DTI metrics for the patients after the shunt operation, so we were unable to understand the changes in the post-operative white matter microstructure of the patients.

CONCLUSION

We consider the sequence of involvement and degree of injury of different neural anatomical structures in the development of INPH disease to be caused by the coordination of three factors: external mechanical stress, the location of the nerve fiber bundle of the structure and the internal characteristics of the structure. The white matter in the CS sustains damage earliest and is most significantly affected, followed by the thalamus and the CN. When we analyzed each case in detail, we also found that the patients with the most severe pre-operative clinical symptoms and the longest course of disease had significantly lower FA values in the CS than the other patients, while there was no significant difference in the FA values from the head of the CN and the thalamus.

DATA AVAILABILITY STATEMENT

The raw data supporting the conclusions of this article will be made available by the authors, without undue reservation.

ETHICS STATEMENT

The studies involving human participants were reviewed and approved by the Institutional Review Board of Huadong Hospital affiliated with Fudan University (Approval number: 2017K027). Written informed consent for participation was not required for this study in accordance with the national legislation and the institutional requirements.

AUTHOR CONTRIBUTIONS

WH, XF, SL, RM, CY, WL, and GL made a substantial contribution to the concept and design, acquisition of data or analysis, and interpretation of data. WH, XF, and SL drafted the manuscript and revised it critically for relevant intellectual content. WH and XF performed the MR examination and follow-up of patients. GL and RM were responsible for funding acquisition. All the authors approved the final version of the manuscript.

FUNDING

This study was funded by the National Natural Science Foundation of China (81771816 to GL) and Shanghai municipal population and family planning commission (201740003 to RM).

REFERENCES

Abu Hamdeh, S., Virhammar, J., Sehlin, D., Alafuzoff, I., Cesarini, K. G., and Marklund, N. (2018). Brain tissue Aβ42 levels are linked to shunt response in idiopathic normal pressure hydrocephalus. *J. Neurosurg.* 130, 121–129. doi: 10.3171/2017.7.Jns171005

Adams, R. D., Fisher, C. M., Hakim, S., Ojemann, R. G., and Sweet, W. H. (1965). Symptomatic occult hydrocephalus with "Normal" cerebrospinal-fluid pressure.A treatable syndrome. *N. Engl. J. Med.* 273, 117–126. doi: 10.1056/nejm196507152730301

Back, S. A., Kroenke, C. D., Sherman, L. S., Lawrence, G., Gong, X., Taber, E. N., et al. (2011). White matter lesions defined by diffusion tensor imaging in older adults. *Ann. Neurol.* 70, 465–476. doi: 10.1002/ana.22484

Basser, P. J., and Jones, D. K. (2002). Diffusion-tensor MRI: theory, experimental design and data analysis - a technical review. *NMR Biomed.* 15, 456–467. doi: 10.1002/nbm.783

Beppu, T., Nishimoto, H., Ishigaki, D., Fujiwara, S., Yoshida, T., Oikawa, H., et al. (2010). Assessment of damage to cerebral white matter fiber in the subacute phase after carbon monoxide poisoning using fractional anisotropy in diffusion tensor imaging. *Neuroradiology* 52, 735–743. doi: 10.1007/s00234-009-0649-x

Black, S., Gao, F., and Bilbao, J. (2009). Understanding white matter disease: imaging-pathological correlations in vascular cognitive impairment. *Stroke* 40, S48–S52. doi: 10.1161/strokeaha.108.537704

Blasel, S., Pilatus, U., Magerkurth, J., von Stauffenberg, M., Vronski, D., Mueller, M., et al. (2012). Metabolic gray matter changes of adolescents with anorexia nervosa in combined MR proton and phosphorus spectroscopy. *Neuroradiology* 54, 753–764. doi: 10.1007/s00234-011-1001-9

Bommarito, G., Van De Ville, D., Frisoni, G. B., Garibotto, V., Ribaldi, F., Stampacchia, S., et al. (2021). Alzheimer's disease biomarkers in idiopathic normal pressure hydrocephalus: linking functional connectivity and clinical outcome. *J. Alzheimer's Dis.* 83, 1717–1728. doi: 10.3233/jad-210534

Bouziane, C., Filatova, O. G., Schrantee, A., Caan, M. W. A., Vos, F. M., and Reneman, L. (2019). White matter by diffusion MRI following methylphenidate treatment: a randomized control trial in males with attention-deficit/hyperactivity disorder. *Radiology* 293, 186–192. doi: 10.1148/radiol.2019182528

Charidimou, A., Jaunmuktane, Z., Baron, J. C., Burnell, M., Varlet, P., Peeters, A., et al. (2014). White matter perivascular spaces: an MRI marker in pathology-proven cerebral amyloid angiopathy? *Neurology* 82, 57–62. doi: 10.1212/01.wnl.0000438225.02729.04

Del Bigio, M. R., and Bruni, J. E. (1988). Periventricular pathology in hydrocephalic rabbits before and after shunting. *Acta Neuropathol.* 77, 186–195. doi: 10.1007/bf00687430

DeVito, E. E., Salmond, C. H., Owler, B. K., Sahakian, B. J., and Pickard, J. D. (2007). Caudate structural abnormalities in idiopathic normal pressure hydrocephalus. *Acta Neurol. Scand.* 116, 328–332. doi: 10.1111/j.1600-0404.2007.00906.x

Elobeid, A., Laurell, K., Cesarini, K. G., and Alafuzoff, I. (2015). Correlations between mini-mental state examination score, cerebrospinal fluid biomarkers, and pathology observed in brain biopsies of patients with normal-pressure hydrocephalus. *J. Neuropathol. Exp. Neurol.* 74, 470–479. doi: 10.1097/nen.0000000000000191

Experts consensus on diagnosis and treatment of normal pressure hydrocephalus in China (2016 edition). *Zhonghua yi Xue za Zhi* 96, 1635–1638.

Goldman, P. S., and Nauta, W. J. (1977). An intricately patterned prefronto-caudate projection in the rhesus monkey. *J. Comp. Neurol.* 72, 369–386. doi: 10.1002/cne.901710305

Griffanti, L., Jenkinson, M., Suri, S., Zsoldos, E., Mahmood, A., Filippini, N., et al. (2018). Classification and characterization of periventricular and deep

white matter hyperintensities on MRI: a study in older adults. *Neuroimage* 170, 174–181. doi: 10.1016/j.neuroimage.2017.03.024

Hattori, T., Yuasa, T., Aoki, S., Sato, R., Sawaura, H., Mori, T., et al. (2011). Altered microstructure in corticospinal tract in idiopathic normal pressure hydrocephalus: comparison with Alzheimer disease and Parkinson disease with dementia. *AJNR Am. J. Neuroradiol.* 32, 1681–1687. doi: 10.3174/ajnr.A2570

Kang, K., Yoon, U., Choi, W., and Lee, H. W. (2016). Diffusion tensor imaging of idiopathic normal-pressure hydrocephalus and the cerebrospinal fluid tap test. *J. Neurol. Sci.* 364, 90–96. doi: 10.1016/j.jns.2016.02.067

Kanno, S., Abe, N., Saito, M., Takagi, M., Nishio, Y., and Hayashi, A. (2011). White matter involvement in idiopathic normal pressure hydrocephalus: a voxel-based diffusion tensor imaging study. *J. Neurol.* 258, 1949–1957. doi: 10.1007/s00415-011-6038-5

Khoo, H. M., Kishima, H., Tani, N., Oshino, S., Maruo, T., Hosomi, K., et al. (2016). Default mode network connectivity in patients with idiopathic normal pressure hydrocephalus. *J. Neurosurg.* 124, 350–358. doi: 10.3171/2015.1.Jns141633

Kim, M. J., Seo, S. W., Lee, K. M., Kim, S. T., Lee, J. I., Nam, D. H., et al. (2011). Differential diagnosis of idiopathic normal pressure hydrocephalus from other dementias using diffusion tensor imaging. *AJNR Am. J. Neuroradiol.* 32, 1496–1503. doi: 10.3174/ajnr.A2531

Kotz, S. A., Anwander, A., Axer, H., and Knösche, T. R. (2013). Beyond cytoarchitectonics: the internal and external connectivity structure of the caudate nucleus. *PLoS One* 8:e70141. doi: 10.1371/journal.pone.0070141

Le Bihan, D., Mangin, J. F., Poupon, C., Clark, C. A., Pappata, S., Molko, N., et al. (2001). Diffusion tensor imaging: concepts and applications. *J. Magn. Reson. Imaging* 13, 534–546. doi: 10.1002/jmri.1076

Lehéricy, S., Ducros, M., Krainik, A., Francois, C., Van de Moortele, P. F., Ugurbil, K., et al. (2004). 3-D diffusion tensor axonal tracking shows distinct SMA and pre-SMA projections to the human striatum. *Cereb. Cortex* 14, 1302–1309. doi: 10.1093/cercor/bhh091

Lundin, F., Tisell, A., Dahlqvist Leinhard, O., Tullberg, M., Wikkelsö, C., Lundberg, P., et al. (2011). Reduced thalamic N-acetylaspartate in idiopathic normal pressure hydrocephalus: a controlled 1H-magnetic resonance spectroscopy study of frontal deep white matter and the thalamus using absolute quantification. *J. Neurol. Neurosurg. Psychiatry* 82, 772–778. doi: 10.1136/jnnp.2010.223529

Mestres-Missé, A., Turner, R., and Friederici, A. D. (2012). An anterior-posterior gradient of cognitive control within the dorsomedial striatum. *Neuroimage* 62, 41–47. doi: 10.1016/j.neuroimage.2012.05.021

Middleton, F. A., and Strick, P. L. (2000). Basal ganglia and cerebellar loops: motor and cognitive circuits. *Brain Res. Brain Res. Rev.* 31, 236–250. doi: 10.1016/s0165-0173(99)00040-5

Mole, J. P., Subramanian, L., Bracht, T., Morris, H., Metzler-Baddeley, C., and Linden, D. E. (2016). Increased fractional anisotropy in the motor tracts of Parkinson's disease suggests compensatory neuroplasticity or selective neurodegeneration. *Eur. Radiol.* 26, 3327–3335. doi: 10.1007/s00330-015-4178-1

Nakajima, M., Yamada, S., Miyajima, M., Ishii, K., Kuriyama, N., Kazui, H., et al. (2021). Guidelines for management of idiopathic normal pressure hydrocephalus (Third Edition): endorsed by the Japanese society of normal pressure hydrocephalus. *Neurol. Med. Chirurg.* 61, 63–97. doi: 10.2176/nmc.st.2020-0292

Osuka, S., Matsushita, A., Yamamoto, T., Saotome, K., Isobe, T., Nagatomo, Y., et al. (2010). Evaluation of ventriculomegaly using diffusion tensor imaging: correlations with chronic hydrocephalus and atrophy. *J. Neurosurg.* 112, 832–839. doi: 10.3171/2009.7.Jns09550

Park, J. K., Kim, B. S., Choi, G., Kim, S. H., Choi, J. C., and Khang, H. (2008). Evaluation of the somatotopic organization of corticospinal tracts in the internal capsule and cerebral peduncle: results of diffusion-tensor MR tractography. *Korean J. Radiol.* 9, 191–195. doi: 10.3348/kjr.2008.9.3.191

Robbins, T. W., and Everitt, B. J. (1996). Neurobehavioural mechanisms of reward and motivation. *Curr. Opin. Neurobiol.* 6, 228–236. doi: 10.1016/s0959-4388(96)80077-8

Rose, S., Pannek, K., Bell, C., Baumann, F., Hutchinson, N., Coulthard, A., et al. (2012). Direct evidence of intra- and interhemispheric corticomotor network degeneration in amyotrophic lateral sclerosis: an automated MRI structural connectivity study. *Neuroimage* 59, 2661–2669. doi: 10.1016/j.neuroimage.2011.08.054

Sarica, A., Quattrone, A., Mechelli, A., Vaccaro, M. G., Morelli, M., and Quattrone, A. (2021). Corticospinal tract abnormalities and ventricular dilatation: a transdiagnostic comparative tractography study. *Neuroimage Clin.* 32:102862. doi: 10.1016/j.nicl.2021.102862

Selemon, L. D., and Goldman-Rakic, P. S. (1985). Longitudinal topography and interdigitation of corticostriatal projections in the rhesus monkey. *J. Neurosci.* 5, 776–794. doi: 10.1523/jneurosci.05-03-00776.1985

Seo, J. P., Chang, P. H., and Jang, S. H. (2012). Anatomical location of the corticospinal tract according to somatotopies in the centrum semiovale. *Neurosci. Lett.* 523, 111–114. doi: 10.1016/j.neulet.2012.06.053

Siasios, I., Kapsalaki, E. Z., Fountas, K. N., Fotiadou, A., Dorsch, A., Vakharia, K., et al. (2016). The role of diffusion tensor imaging and fractional anisotropy in the evaluation of patients with idiopathic normal pressure hydrocephalus: a literature review. *Neurosurg. Focus* 41:E12. doi: 10.3171/2016.6.Focus16192

Silverberg, G. D., Miller, M. C., Pascale, C. L., Caralopoulos, I. N., Agca, Y., Agca, C., et al. (2015). Kaolin-induced chronic hydrocephalus accelerates amyloid deposition and vascular disease in transgenic rats expressing high levels of human APP. *Fluids Barriers CNS* 12:2. doi: 10.1186/2045-8118-12-2

Skiöld, B., Horsch, S., Hallberg, B., Engström, M., Nagy, Z., Mosskin, M., et al. (2010). White matter changes in extremely preterm infants, a population-based diffusion tensor imaging study. *Acta Paediatr.* 99, 842–849. doi: 10.1111/j.1651-2227.2009.01634.x

Spotorno, N., Hall, S., Irwin, D. J., Rumetshofer, T., Acosta-Cabronero, J., Deik, A. F., et al. (2019). Diffusion tensor MRI to distinguish progressive supranuclear palsy from α-Synucleinopathies. *Radiology* 293, 646–653. doi: 10.1148/radiol.2019190406

Torvik, A., and Stenwig, A. E. (1977). The pathology of experimental obstructive hydrocephalus. Electron microscopic observations. *Acta Neuropathol.* 38, 21–26. doi: 10.1007/bf00691271

Tsai, P. H., Chen, Y. C., Chiang, S. W., Huang, T. Y., Chou, M. C., Liu, H. S., et al. (2018). Changes in sensorimotor-related thalamic diffusion properties and cerebrospinal fluid hydrodynamics predict gait responses to tap test in idiopathic normal-pressure hydrocephalus. *Eur. Radiol.* 28, 4504–4513. doi: 10.1007/s00330-018-5488-x

Yamada, S., Ishikawa, M., Yamaguchi, M., and Yamamoto, K. (2019). Longitudinal morphological changes during recovery from brain deformation due to idiopathic normal pressure hydrocephalus after ventriculoperitoneal shunt surgery. *Sci. Rep.* 9:17318. doi: 10.1038/s41598-019-53888-7

Yokota, H., Vijayasarathi, A., Cekic, M., Hirata, Y., Linetsky, M., Ho, M., et al. (2019). Diagnostic performance of glymphatic system evaluation using diffusion tensor imaging in idiopathic normal pressure hydrocephalus and mimickers. *Curr. Gerontol. Geriatr. Res.* 2019:5675014. doi: 10.1155/2019/5675014

Younes, K., Hasan, K. M., Kamali, A., McGough, C. E., Keser, Z., Hasan, O., et al. (2019). Diffusion tensor imaging of the superior thalamic radiation and cerebrospinal fluid distribution in idiopathic normal pressure hydrocephalus. *J. Neuroimaging* 29, 242–251. doi: 10.1111/jon.12581

Zhang, B., Wen, C. Y., Wang, L., and Zhang, X. (2011). Functional MRI and cognition assessment in subcortical ischemic vascular disease. *Zhonghua Nei Ke Za Zhi* 50, 411–415.

Conflict of Interest: The authors declare that the research was conducted in the absence of any commercial or financial relationships that could be construed as a potential conflict of interest.

Publisher's Note: All claims expressed in this article are solely those of the authors and do not necessarily represent those of their affiliated organizations, or those of the publisher, the editors and the reviewers. Any product that may be evaluated in this article, or claim that may be made by its manufacturer, is not guaranteed or endorsed by the publisher.

frontiers in Aging Neuroscience

ORIGINAL RESEARCH
published: 28 March 2022
doi: 10.3389/fnagi.2022.853029

Internetwork Connectivity Predicts Cognitive Decline in Parkinson's and Is Altered by Genetic Variants

Xiangyu Wei[1,2†], Qian Shen[1,3†], Irene Litvan[4†], Mingxiong Huang[1,3†], Roland R. Lee[1,3†] and Deborah L. Harrington[1,4†]*

[1] Research and Radiology Services, VA San Diego Healthcare System, San Diego, CA, United States, [2] Revelle College, University of California San Diego, La Jolla, CA, United States, [3] Department of Radiology, University of California San Diego, La Jolla, CA, United States, [4] Department of Neurosciences, University of California San Diego, La Jolla, CA, United States

OPEN ACCESS

Edited by:
Alessandro Martorana,
University of Rome Tor Vergata, Italy

Reviewed by:
Carme Uribe,
University of Toronto, Canada
Mehrafarin Ramezani,
University of Calgary, Canada
Seok Jong Chung,
Yonsei University, South Korea

***Correspondence:**
Deborah L. Harrington
dharrington@health.ucsd.edu

†ORCID:
Xiangyu Wei
orcid.org/0000-0002-8774-5296
Qian Shen
orcid.org/0000-0001-5637-4720
Irene Litvan
orcid.org/0000-0002-3485-3445
Mingxiong Huang
orcid.org/0000-0002-1025-1298
Roland R. Lee
orcid.org/0000-0001-5628-4151
Deborah L. Harrington
orcid.org/0000-0001-9658-9080

Specialty section:
This article was submitted to Neurocognitive Aging and Behavior, a section of the journal Frontiers in Aging Neuroscience

Received: 12 January 2022
Accepted: 02 March 2022
Published: 28 March 2022

Citation:
Wei X, Shen Q, Litvan I, Huang M, Lee RR and Harrington DL (2022) Internetwork Connectivity Predicts Cognitive Decline in Parkinson's and Is Altered by Genetic Variants. Front. Aging Neurosci. 14:853029. doi: 10.3389/fnagi.2022.853029

In Parkinson's disease (PD) functional changes in the brain occur years before significant cognitive symptoms manifest yet core large-scale networks that maintain cognition and predict future cognitive decline are poorly understood. The present study investigated internetwork functional connectivity of visual (VN), anterior and posterior default mode (aDMN, pDMN), left/right frontoparietal (LFPN, RFPN), and salience (SN) networks in 63 cognitively normal PD (PDCN) and 43 healthy controls who underwent resting-state functional MRI. The functional relevance of internetwork coupling topologies was tested by their correlations with baseline cognitive performance in each group and with 2-year cognitive changes in a PDCN subsample. To disentangle heterogeneity in neurocognitive functioning, we also studied whether α-synuclein (SNCA) and microtubule-associated protein tau (MAPT) variants alter internetwork connectivity and/or accelerate cognitive decline. We found that internetwork connectivity was largely preserved in PDCN, except for reduced pDMN-RFPN/LFPN couplings, which correlated with poorer baseline global cognition. Preserved internetwork couplings also correlated with domain-specific cognition but differently for the two groups. In PDCN, stronger positive internetwork coupling topologies correlated with better cognition at baseline, suggesting a compensatory mechanism arising from less effective deployment of networks that supported cognition in healthy controls. However, stronger positive internetwork coupling topologies typically predicted greater longitudinal decline in most cognitive domains, suggesting that they were surrogate markers of neuronal vulnerability. In this regard, stronger aDMN-SN, LFPN-SN, and/or LFPN-VN connectivity predicted longitudinal decline in attention, working memory, executive functioning, and visual cognition, which is a risk factor for dementia. Coupling strengths of some internetwork topologies were altered by genetic variants. PDCN carriers of the SNCA risk allele showed amplified anticorrelations between the SN and the VN/pDMN, which supported cognition in healthy controls, but strengthened pDMN-RFPN connectivity, which maintained visual memory longitudinally. PDCN carriers of the MAPT risk allele showed greater longitudinal decline in working memory and increased VN-LFPN connectivity, which in turn predicted greater decline in visuospatial processing.

Collectively, the results suggest that cognition is maintained by functional reconfiguration of large-scale internetwork communications, which are partly altered by genetic risk factors and predict future domain-specific cognitive progression.

Keywords: Parkinson's disease, internetwork functional connectivity, cognition, MAPT, SNCA, genetic variants, resting state fMRI, independent component analyses

INTRODUCTION

Cognitive decline is common in early stages of Parkinson's disease (PD), but diversity exists in the domains affected suggesting that patterns of neurodegeneration differ amongst people. The pathophysiological underpinnings of cognitive changes are complex, involving multiple neurotransmitter systems (Gratwicke et al., 2015) and large-scale brain networks (Tessitore et al., 2019), which may be vulnerable to genetic variants that carry different risks for neurocognitive progression including α-synuclein (SNCA) (Sampedro et al., 2018a; Ramezani et al., 2021) and microtubule-associated protein tau (MAPT) (Williams-Gray et al., 2009; Morley et al., 2012; Sampedro et al., 2018b). Knowledge about the pathophysiology behind cognitive changes in PD is largely based on people who already show mild cognitive impairment (MCI). Yet changes in the brain occur years before cognitive symptoms manifest (Harrington et al., 2020, 2021). As optimal treatments depend on early detection, markers of brain dysfunction that predate MCI and foreshadow the evolution of cognitive decline are sorely needed.

Across neurological disorders, intrinsic functional connectivity during resting-state fMRI (rsfMRI) is altered within core large-scale functional networks that can be identified using independent component analyses (ICA), a data-driven technique. The default mode network (DMN) is associated with internally generated cognitive states including memory retrieval, and was called a task-negative network as activity is often suppressed during task-evoked fMRI (Di and Biswal, 2014). Task-positive intrinsic networks include the salience network (SN), which controls attentional capture, internetwork switching, and inhibition (Uddin, 2015), and the left and right frontoparietal networks (LFPN, RFPN), which govern working memory and executive control (Grady et al., 2016). Although intrinsic connectivity disturbances within these and other large-scale networks have been studied in cognitively normal PD (PDCN) (Tessitore et al., 2012; Amboni et al., 2015; Baggio et al., 2015; Gorges et al., 2015; Peraza et al., 2017; Hou et al., 2021), findings are mixed likely due to diverse criteria for cognitive impairment and small samples of some studies.

Less attention has been paid to large-scale internetwork communications in PDCN, despite their role in integrating and segregating different processing resources to support cognition (Bressler and Menon, 2010). In a non-demented PD cohort, SN-RFPN and DMN-RFPN couplings were, respectively, reduced and increased relative to controls (Putcha et al., 2015). Visual network (VN) internetwork couplings were also reduced in a mixed PDCN/MCI cohort (Hou et al., 2021), in alignment with visual cognition disturbances in PD (Weil et al., 2016). However, little is known about potential large-scale internetwork disturbances in PDCN. Seed-based approaches, which measure the strength of connectivity between regions of interest, suggest that FPN regional couplings with DMN, dorsal attention (DAN), and/or VN regions are altered in PDCN (Baggio et al., 2015; Klobusiakova et al., 2019), yet normal in a mixed PDCN/MCI cohort (Campbell et al., 2020). The strength of FPN-DMN and FPN-VN regional couplings also increased over 1 year in PDCN and PD-MCI cohorts (Klobusiakova et al., 2019). Altogether, it appears that aberrant FPN internetwork communications may be a prominent feature of PD, despite discrepancies in interacting networks, which could be linked to different analytic techniques (Koch et al., 2010; Badea et al., 2017). The cognitive relevance of internetwork couplings, however, has received scant attention in PDCN.

The present study investigated internetwork intrinsic functional connectivity in PDCN and healthy adults in core networks including the DMN, LFPN, RFPN, and SN. As the DMN is composed of subsystems that capture the heterogeneous nature of self-generated thoughts (Andrews-Hanna et al., 2014b), we studied the anterior DMN (aDMN), which supports self-generated executive, conceptual, and semantic processes relevant to PD (Harrington et al., 2020, 2021), and the posterior DMN (pDMN) which supports episodic and autobiographical memory, and associative or constructive processes. VN internetwork connectivity was studied as well since disturbances in visual cognition are a marker of future dementia (Williams-Gray et al., 2013). The functional relevance of internetwork coupling topologies was tested by their correlations with baseline cognitive functioning. We also examined whether internetwork coupling topologies predicted 2-year changes in cognition in a PDCN subsample. To unravel heterogeneity in neurocognitive functioning, we examined whether genetic variants modulated internetwork connectivity and accelerated cognitive decline. We predicted that SNCA expression would alter SN internetwork connectivity owing to accumulation of α-synuclein in the insula (Christopher et al., 2014). Tau expression was expected to alter internetwork topologies comprised of frontal and posterior cortices (FPN, DMN, VN), which are modulated by MAPT variants (Nombela et al., 2014; Harrington et al., 2021).

MATERIALS AND METHODS

Participants

Participants were 63 PDCN who met the PD United Kingdom Brain Bank Criteria and 43 age, sex and education matched healthy controls. Exclusion criteria included neurological diagnoses other than PD, psychiatric diagnoses, history of alcohol or substance abuse, metal in the head, positive MRI findings, use of anticholinergics or cognitive medications, and

cognitive complaints. PD volunteers with tremors or dyskinesias that might cause head motion were excluded. Volunteers were excluded if they met the Movement Disorders Society Level II criteria for PD-MCI (Litvan et al., 2012). MCI was defined as > 1.5 standard deviations below the control group mean on at least two tests in single or different domains and the absence of cognitive complaints. There were six *de novo* PD, five taking dopamine agonist monotherapy, 26 taking levodopa monotherapy, and 26 taking levodopa combination therapy. Testing was conducted while on medication to minimize motion artifact during scanning. The Institutional Review Board at the VA San Diego Healthcare System approved the study. All subjects signed written informed consent.

Neuropsychological Assessments

Participants were administered tests of premorbid intelligence (Wechsler Test of Adult Reading) and the Montreal Cognitive Assessment (MoCA), a dementia screening tool. **Table 1** summaries the comprehensive test battery used to screen for MCI (Level II criteria), which contained two tests for each of five domains including 1) attention and working memory (Color-Word Naming, CWN; Adaptive Digit Ordering, DOT), executive functioning (Category Switching, SWA; Color-Word Inhibition, CWINH), visual and verbal memory (California Verbal Learning Test, CVLT; Brief Visuospatial Memory Test, BVMT), visual cognition, which measured visuospatial processing (Judgment of Line Orientation, JLOT) and visual organization (Hooper Visual Organization Test, HVOT), and semantic language, which measured confrontation naming (Boston Naming Test, BNT) and semantic fluency (Category Fluency, CAT). Approximately 2-years post-baseline testing, the same test battery was administered to a subsample of 40 PDCN, but not control participants. For this follow-up visit, alternative forms of the tests were used.

Table 1 shows that the groups did not differ in demographics, premorbid intelligence, or MoCA scores. Although some participants in both groups had scores that were lower than the traditional cutoff score of 26 for probable MCI, this cutoff leads to a high percentage of false positives (Weintraub et al., 2015; Carson et al., 2018; Faust-Socher et al., 2019). Indeed, many people with lower MoCA scores (22–25) show normal neuropsychological testing, and people with high MoCA scores (26–30) can show MCI on neuropsychological testing (Rosenblum et al., 2020). That said, no participant with lower MoCA scores exhibited MCI using comprehensive neuropsychological testing, which is the gold standard. The PDCN group had significantly lower scores than controls on verbal and visual memory long delay free recall (CVLT; BVMT) and both tests of visual cognition (JLOT; HVOT). This indicates a decline at the group level, but individual participants did not exhibit cognitive decline indicative of MCI.

TABLE 1 | Demographic, clinical, and cognitive characteristics.

	PD (n = 63)	HC (n = 43)	p	η_p^2
Age (years)	65.4 (6.4)	64.1 (8.5)	0.37	0.01
Education (years)	17.0 (2.1)	17.0 (2.1)	0.88	0.00
Sex (% females)	41.30%	44.20%	0.77	
Handedness (% right-handed)	82.50%	88.40%	0.58	
Wechsler test of adult reading	44.5 (5.0)	45.6 (3.8)	0.23	0.01
Montreal Cognitive Assessment (MoCA)	26.9 (2.3)	27.6 (2.0)	0.08	0.03
Disease duration (years)	4.6 (3.8)			
Levodopa dosage equivalence†	908.1 (654.0)			
UPDRS Part III	23.1 (11.3)			
Head motion				
Maximum rotation (degrees)	0.30 (016)	0.29 (0.19)	0.82	0.00
Maximum translation (mm)	0.58 (0.16)	0.55 (0.16)	0.31	0.01
Mean rotation (degrees)	0.10 (0.06)	0.09 (0.05)	0.25	0.01
Mean translation (mm)	0.22 (0.06)	0.21 (0.06)	0.21	0.02
Genetic variants				
SNCArs356219 AA:AG:GG	14:34:15	15:24:4	0.11	
MAPTrs242557 GG:GA:AA	30:25:8	13:22:8	0.20	
Attention and working memory				
Adaptive Digit Ordering (DOT)	6.5 (1.9)	6.6 (2.2)	0.70	0.00
DKEFS Color + Word Naming (CWN)	21.5 (4.4)	21.8 (4.5)	0.70	0.00
Executive functioning (DKEFS)				
Category switching (accuracy) (SWA)	13.5 (2.8)	13.3 (3.1)	0.72	0.00
Color-Word Inhibition (CWINH)	59.2 (12.9)	56.2 (11.3)	0.22	0.01
Memory (long delay free recall)				
California Verbal Learning Test 2 (CVLT)	9.0 (3.4)	11.3 (3.0)	0.001	0.11
Brief Visuospatial Memory Test-Revised (BVMT)	8.3 (2.5)	9.9 (1.9)	0.001	0.11
Visual cognition				
Judgment of Line Orientation (JLOT)	25.4 (2.9)	26.9 (2.7)	0.008	0.07
Hooper Visual Organization (HVOT)	25.4 (2.3)	26.9 (1.7)	0.001	0.10
Semantic language				
Boston Naming (BNT)	57.6 (2.6)	58.3 (1.7)	0.12	0.02
DKEFS Category Fluency (CAT)	43.2 (8.4)	44.2 (9.1)	0.55	0.00

Tabled values are raw score means (standard deviations). Group differences were tested using ANOVA and Pearson chi-square statistics (sex, handedness, SNCA, MAPT). UPDRS, Movement Disorder Society Unified Parkinson's Disease Rating Scale; DKEFS, Delis Kaplan Executive Function System.

†*Levodopa dosage equivalence was calculated using the method of Tomlinson (Tomlinson et al., 2010). Data are based on 57 participants who were taking dopaminergic therapy.*

Genotyping

Oragene-500 kits[1] were used to collect whole saliva samples (2 mL). TaqMan assays were used to genotype SNCA and MAPT polymorphisms relevant to PD (Compta et al., 2011; Nalls et al., 2011; Zhang et al., 2018). MAPTrs242557 codes the intra-H1 variation in transcriptional activity. The A allele associated with higher tau transcription levels than the G allele (Compta et al., 2011; Chen et al., 2017). SNCA rs356219 codes variations in α-synuclein levels. The G allele is linked to higher transformed plasma α-synuclein levels (Emelyanov et al., 2018).

Imaging Protocols

Imaging was conducted on a GE MR750 Discovery 3 Tesla system equipped with a Nova Medical 32-channel head coil. Head motion was limited by foam pads inserted between the head and the coil. High-resolution T1-weighted anatomical images maximized differentiation of the white and gray matter boundary

[1]https://www.dnagenotek.com

(3D spoiled gradient-recalled at steady state, minimum full TE, 3.5 ms; TR, 2,852 ms; TI, 1,000 ms; 8° flip angle; 0.8-mm slices, acquisition matrix = 512). The rsfMRI images used a high spatial and temporal resolution multiband accelerated gradient EPI sequence (slice thickness = 2 mm; TR = 800 ms; TE = 35 ms; flip angle = 52°; acquisition matrix = 104; axial slices = 72; multiband factor = 8; echo spacing = 0.612 ms; band width = 4807.69 Hz/Px), which has greater sensitivity and specificity than conventional single-band EPI protocols (Tomasi et al., 2016). Three rsfMRI runs were acquired, each lasting 5 min and 35 s. The first 12.8 s were removed to allow magnetization to stabilize to a steady state. To correct geometric distortions, a pair of gradient EPI sequences with anterior and posterior reversed gradients (TR = 8,500 ms; TE = 70.6 ms; isotropic voxels = 2 mm; flip angle = 90°; echo spacing = 0.612 ms) were acquired before rsfMRI runs.

Image Preprocessing

Functional images were preprocessed using FSL 6.4[2] and Analysis of Functional Imaging 20.0.[3] First a field map was computed from the pair of anterior and posterior reversed gradient sequences. Then it was applied to rsfMRI data to correct geometric distortions using FSL TOPUP. Each subject's distortion corrected data from three rsfMRI runs were concatenated. Additional preprocessing included motion correction using FSL MCFLIRT, high pass temporal filtering, spatial smoothing [6 mm full width half maximum (FWHM) filter] and registration to T1-weighted images. Data were transformed to MNI atlas space and carefully checked for normalization accuracy. **Table 1** shows that there were no group differences in maximum or mean rotation and translation head movements.

Independent Components Analysis

Preprocessed images were analyzed with MELODIC using a temporal concatenation spatial ICA approach (Beckmann and Smith, 2004). For each subject, 25 temporally and spatially coherent patterns were extracted, clustered at the group level, and then visually inspected for their correspondence to well-characterized networks of interest. Spatial cross-correlation was also performed to cross-validate extracted ICs with resting-state ICN templates (Smith et al., 2009; Laird et al., 2011). Six components of interest were chosen including the VN, aDMN, pDMN, LFPN, RFPN, and SN.

Dual regression analysis was conducted on the six components. First, each component was used as a mask to extract a subject and component-specific mean time course, which describes the temporal dynamics and synchrony of each component network. The time courses were then fed into a linear model against individual rsfMRI data to obtain subject-specific maps of each component (Beckmann et al., 2009; Nickerson et al., 2017). To validate that each component network was expressed in both the PD and control groups, voxelwise one sample t-tests were performed for each group using FSL randomize (5,000 permutations) with familywise error (FWE) correction for multiple comparisons ($p < 0.05$) (Nichols and Holmes, 2002). Brain regions with significant p-values in both groups in each component network were combined to form a mask to test for group differences in intra-network connectivity (FSL randomize, 5,000 permutations, $p < 0.05$, FWE corrected).

The main analyses focused on group differences in internetwork connectivity. To compute the strength of internetwork functional connectivity, Pearson correlations were performed between the subject-specific time-courses of all possible network pairs, which were extracted from the dual regression analysis for each network. A Fisher z-transformation was applied to the correlation coefficients to obtain a standardized z score of internetwork connectivity for each subject.

Brain Structure

To determine if internetwork couplings in the PD group were related to brain atrophy, cortical thickness and volume were analyzed using FreeSurfer 5.3.[4] Individual subject's cortical folding patterns were inflated, registered to a standard spherical surface template, and smoothed with 10 mm FWHM Gaussian kernel to improve the signal-to-noise ratio and reduce local variations across subjects (Fjell et al., 2009). Tests of group differences in thickness and volume (age as a nuisance variable) were conducted across the continuous cortical surface using the FreeSurfer QDEC application and the false discovery rate (FDR, $q < 0.05$) adjustment for multiple comparisons. Group differences were also tested for subcortical volumes of interest (bilateral caudate, putamen, and hippocampus), which were adjusted for total intracranial volume.

Statistical Analyses

In total, 15 internetwork coupling topologies were studied. Group differences in internetwork connectivity were tested using independent t-tests with bias-corrected accelerated bootstrapping (1,000 iterations) to reliability estimate connectivity distributions. P-values were uncorrected due to the large number of internetwork pairs and hence, the results should be cautiously interpreted. For multiple regression analyses, stepwise models entered sets of internetwork connections as the predictors of cognitive variables and genetic variants. First, we analyzed VN internetwork connections with all other networks (aDMN, pDMN, LFPN, RFPN, SN), as the VN has been poorly studied in PD despite disturbances in visual cognition (Weil et al., 2016), which correlate with occipital thinning (Garcia-Diaz et al., 2018). Second, aDMN internetwork couplings with other networks (pDMN, LFPN, RFPN, SN) were analyzed as this subnetwork regulates internally generated executive and semantic processes, which may interact with processing in other networks to support of cognition. Third, we examined pDMN couplings with core task-positive networks (LFPN, RFPN, SN). Fourth, couplings amongst task-positive networks were studied (LFPN-RFPN, LFPN-SN, RPFN-SN) given their roles in attention, working memory, and cognitive flexibility (Seeley et al., 2007), which are relevant to PD. All cognitive variables were converted to age adjusted residuals

[2]http://www.fmrib.ox.ac.uk/fsl/

[3]https://afni.nimh.nih.gov/

[4]http://surfer.nmr.mgh.harvard.edu

owing to associations of some variables with age, but not educational level.

For each group, stepwise multiple regressions were performed to identify internetwork couplings that best predicted cognition on tests of global cognition (MoCA), attention (CWN) and working memory (DOT), executive function (SWA, CWINH), visuospatial cognition (JLOT, HVOT), visual and verbal episodic memory (BVMT, CVLT), and semantic cognition (BNT, CAT). Longitudinal changes in cognition were studied in 40 PDCN participants who were retested 24.5 months post baseline (SD = 3.2, minimum = 19.9, maximum = 32.8). Longitudinal changes in age adjusted residuals were calculated using simple discrepancy scores (score at time 1—score at time 2). FDR correction was applied to all uncorrected p-values from the analyses of both baseline and longitudinal changes in cognition.

ANOVAs with bias-corrected accelerated bootstrapping tested for the effect of gene variants on (1) baseline cognitive variables for each group and (2) longitudinal changes in cognition in the PDCN subsample. To test for internetwork connectivity predictors of gene expression, stepwise multiple regressions tested for sets of internetwork couplings that predicted SNCA and MAPT expression (FDR adjusted).

RESULTS

Group Differences in Brain Morphometry

Group differences in cortical thickness and volume were non-significant. Independent t-tests (bias-corrected, bootstrapped) also failed to show group differences in left and right putamen, caudate, and hippocampus volumes (FDR adjusted). Due to the lack of manifested atrophy in the PDCN group relative to controls, gray matter was not used as a covariate in subsequent analyses.

Group Differences in Intra-Network Connectivity

Figure 1A displays the components of interest from the group ICA analyses. **Supplementary Table 1** lists the main regions comprising each component. Each of the six components was significantly expressed in the PDCN and control groups (one sample t-tests, $p < 0.05$). **Figure 1B** displays the results from between-group voxelwise comparisons of intra-network connectivity (two sample t-tests; $p < 0.05$). Only LFPN intra-network couplings were stronger in PDCN (z = 6.8, SD = 3.7) than controls (z = 4.7, SD = 2.8) [$F(1, 104) = 10.5$, $p < 0.002$, $\eta_p^2 = 0.09$]. In the PDCN group, aberrant LFPN intra-network coherence (z scores) did not correlate with baseline or longitudinal changes in cognition.

Group Differences in Internetwork Connectivity

Independent t-tests (bootstrapped) tested for group differences in internetwork connectivity. **Table 2** shows that internetwork couplings were stronger in the control than the PDCN group for the pDMN-LFPN [$t_{(1,\ 104)} = 2.0$, $p = 0.047$, $d = 0.40$], pDMN-RFPN [$t_{(1,\ 104)} = 2.41$, $p = 0.018$, $d = 0.48$], and at a subthreshold level of significance, the LFPN-RFPN [$t_{(1,\ 104)} = 1.96$, $p = 0.053$, $d = 0.39$]. Nonetheless, the findings should be cautiously interpreted as uncorrected p-values did not survive FDR correction. In the PDCN group, LFPN internetwork couplings did not correlate with aberrant LFPN intra-network coherence (z scores).

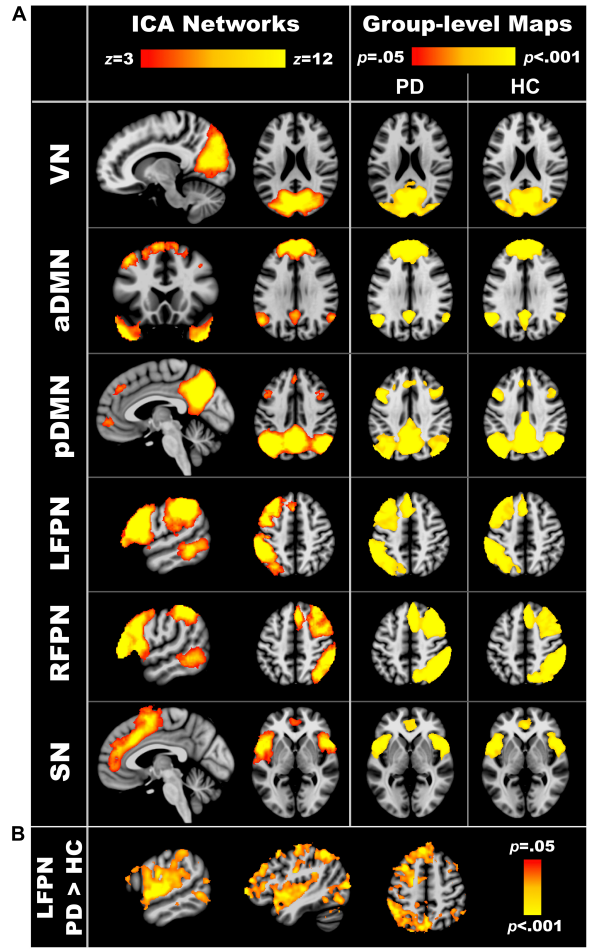

FIGURE 1 | Resting-state networks of interest. **(A)** The left column displays the spatial maps obtained from independent component analyses of the entire sample. The right column shows the group level maps derived from the dual regression analyses. To validate that each of the six component networks were expressed in both the PD and healthy control groups, voxelwise one sample t-tests were performed separately for each group using familywise error (FWE) correction for multiple comparisons ($p < 0.05$). **(B)** Significant group differences in intra-network connectivity of the LFPN ($p < 0.05$, FWE corrected). VN, visual network; aDMN, anterior default mode network; pDMN, posterior default mode network; LFPN, left frontoparietal network; RFPN, right frontoparietal network; SN, salience network.

Internetwork Connectivity Associations With Baseline Cognition

Figure 2 displays the results from the stepwise multiple regressions, which tested for sets of internetwork couplings that

TABLE 2 | Group differences in internetwork functional connectivity.

	PDCN (n = 63)	Controls (n = 43)	p	Cohen's d
Visual network				
VN-aDMN	−1.9 (3.9)	−1.7 (3.8)	0.80	0.05
VN-pDMN	2.8 (4.8)	2.0 (3.3)	0.40	0.17
VN-LFPN	−0.5 (4.3)	−0.3 (3.7)	0.73	0.07
VN-RFPN	2.4 (3.3)	3.3 (3.1)	0.13	0.30
VN-SN	−1.6 (3.4)	−1.2 (3.5)	0.59	0.11
Anterior default mode network				
aDMN-pDMN	2.4 (3.6)	2.7 (3.8)	0.73	0.07
aDMN-LFPN	2.2 (4.1)	1.4 (3.5)	0.26	0.22
aDMN-RFPN	1.2 (3.4)	1.5 (3.6)	0.74	0.07
aDMN-SN	1.3 (3.4)	0.5 (3.6)	0.27	0.22
Posterior default mode network				
pDMN-LFPN	2.0 (4.0)	3.5 (3.1)	**0.047**	0.40
pDMN-RFPN	1.0 (2.9)	2.4 (3.0)	**0.018**	0.48
pDMN-SN	−3.1 (3.7)	−3.0 (3.4)	0.92	0.02
Frontoparietal network				
LFPN-RFPN	2.5 (4.5)	4.1 (3.8)	0.053	0.39
LFPN-SN	1.8 (3.2)	0.9 (3.2)	0.14	0.29
RFPN-SN	0.3 (3.4)	0.6 (3.3)	0.67	0.09

Tabled values are Fisher z score means (standard deviations). Group differences were tested using independent t-tests with bias-corrected accelerated bootstrapping (1,000 iterations). Nominally significant p-values (bold) were not significant after FDR correction.
VN, visual network; aDMN, anterior default mode network; pDMN, posterior default mode network; LFPN, left frontoparietal network; RFPN, right frontoparietal network; SN, salience network.

best predicted baseline cognitive changes in each group separately (top) and longitudinal cognitive changes in the PDCN subsample (bottom). Graphs are shown only for results that survived FDR correction. **Figure 3** (top) provides a circular visualization of the baseline results.

Global Cognition

In PDCN stronger positive pDMN-LFPN (r = 0.36) and pDMN-RFPN couplings ($r_{xy.z}$ = 0.28) predicted better MoCA scores [F(2, 58) = 7.2, $p < 0.002$, q = 0.006, R = 0.45] (one outlier omitted). In controls stronger positive aDMN-SN couplings predicted better MoCA scores [F(1, 41) = 6.5, $p < 0.015$, q = 0.02, R = 0.37].

Attention and Working Memory

In PDCN stronger positive aDMN-pDMN couplings predicted better attention (CWN) [F(1, 61) = 4.9, $p < 0.03$, q = 0.045, R = 0.27], whereas in controls stronger positive VN-SN couplings predicted better attention [F(1, 41) = 5.6, $p < 0.02$, q = 0.03, R = 0.35]. In PDCN stronger positive aDMN-pDMN (r = 0.28) and aDMN-LFPN ($r_{xy.z}$ = 0.25) couplings predicted better working memory (DOT) [F(2, 60) = 4.7, $p < 0.01$, q = 0.019, R = 0.37], whereas in controls stronger positive VN-SN couplings predicted better working memory [F(1, 41) = 10.0, $p < 0.003$, q = 0.008, R = 0.44].

Executive

Internetwork couplings in PDCN did not predict executive functioning. In controls stronger positive pDMN-SN [F(1, 41) = 5.9, $p < 0.02$, q = 0.03, R = 0.35] and aDMN-LFPN [F(1, 41) = 8.7, $p < 0.005$, q = 0.01, R = 0.42] couplings correlated with poorer category switching accuracy (VFSWA). Stronger positive pDMN-SN couplings also correlated with poorer inhibitory control (CWINH) [F(1, 41) = 5.2, $p < 0.029$, q = 0.04, R = 0.33].

Episodic Memory

In PDCN stronger positive LFPN-SN couplings predicted better verbal memory (CVLT) [F(1, 61) = 11.3, $p < 0.001$, q = 0.002, R = 0.40]. In controls stronger positive pDMN-SN couplings predicted poorer verbal [F(1, 41) = 7.4, $p < 0.01$, q = 0.02, R = 0.39] and visual memory (BVMT) [F(1, 41) = 5.3, $p < 0.026$, q = 0.039, R = 0.34].

Visual Cognition

In PDCN stronger positive VN-RFPN couplings predicted better visuospatial processing (JLOT) [F(1, 61) = 11.4, $p < 0.001$, q = 0.004, R = 0.40]. In controls stronger positive pDMN-LFPN couplings predicted poorer visual organization (HVOT) [F(1, 41) = 5.0, $p < 0.03$, q = 0.047, R = 0.33].

Semantic Language

In PDCN stronger positive aDMN-RFPN [F(1, 61) = 7.5, $p < 0.008$, q = 0.01, R = 0.33] and RFPN-SN couplings [F(1, 61) = 5.4, $p < 0.024$, q = 0.037, R = 0.29] predicted poorer object naming (BNT). Internetwork connectivity did not predict semantic cognition in controls.

Internetwork Connectivity Predictors of Longitudinal Changes in Cognition

Supplementary Table 2 details the demographic and clinical characteristics of 40 PDCN participants who completed longitudinal neuropsychological testing. At the follow-up testing, no patient had a clinical diagnosis of dementia. Only eight patients (20%) exhibited MCI (> −1.5 SD on two or more tests), all of whom showed multidomain cognitive impairment. The number of months between baseline and follow-up testing did not correlate with longitudinal changes of any cognitive variable ($p > 0.20$ to $p < 0.96$). Paired t-tests (bootstrapped) showed significantly poorer follow-up performance on the SWA, CWINH, HVOT, and CAT (**Table 3**). Subthreshold trends for longitudinal decline were observed for CWN, JLOT, and DOT.

Stepwise multiple regressions tested for sets of internetwork couplings that best predicted longitudinal changes in cognition as measured by age adjusted simple discrepancy scores (score at time 1—score at time 2). Positive discrepancy scores signify cognitive decline at the follow-up visit, except for the CWINH wherein negative discrepancy scores signify cognitive decline at the follow-up visit. **Figure 2** (bottom) shows graphs of significant results and **Figure 3** (bottom) displays a circular visualization of the findings.

Attention and Working Memory

Stronger positive aDMN-LFPN couplings predicted greater decline in attention (CWN) [F(1, 38) = 6.8, $p < 0.01$, q = 0.017, R = 0.39]. Stronger positive aDMN-SN couplings predicted

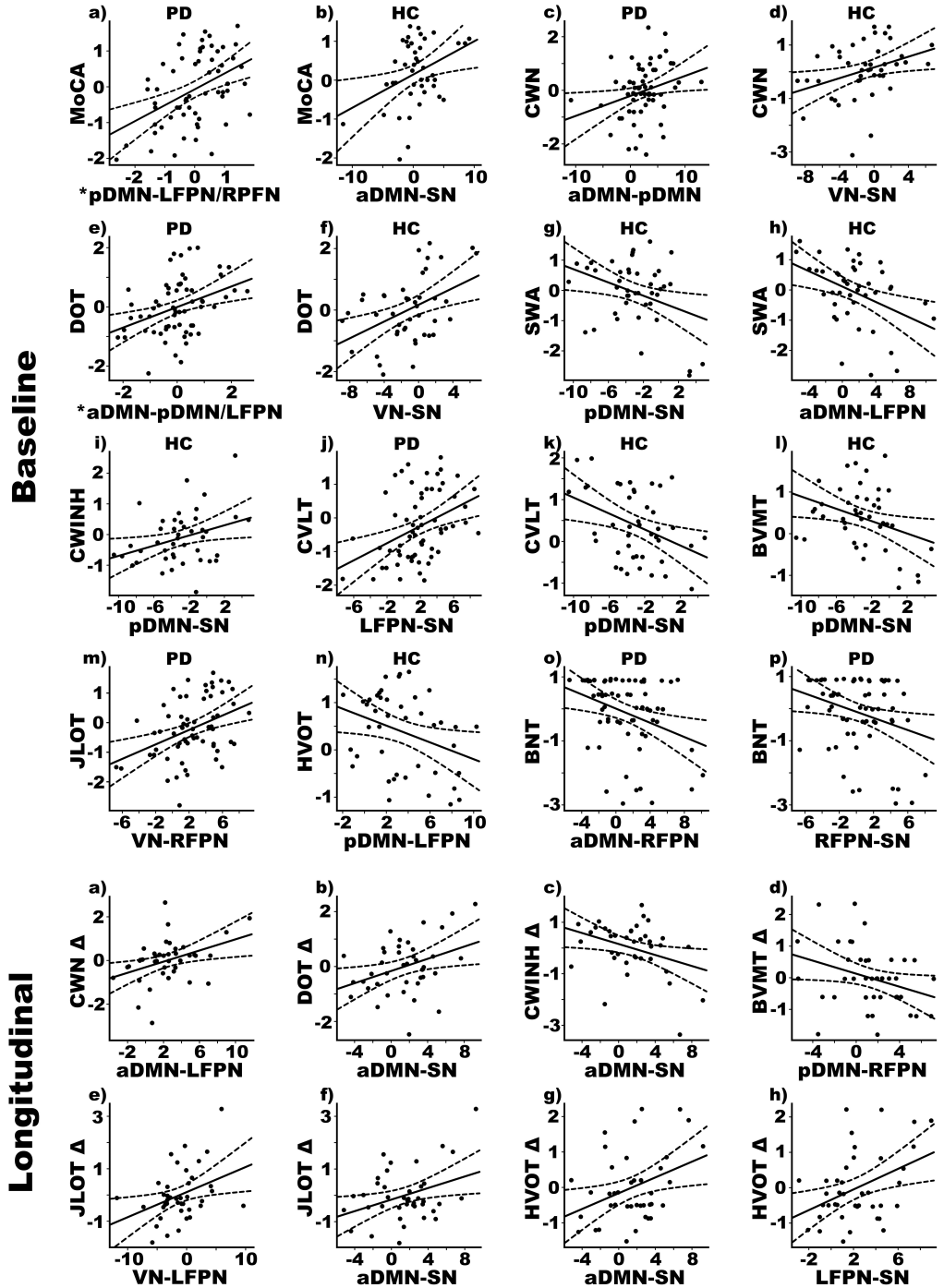

FIGURE 2 | Relationships between cognition and internetwork coupling topologies in PD and healthy control (HC) groups. Scatterplots display the best-fitting linear regression line (solid line) and 95% conference intervals (dotted lines) for significant correlations between age adjusted cognitive measures (*y*-axis) and internetwork connectivity topologies (*x*-axis). Top four rows show relationships with baseline cognitive functioning. Bottom two rows show relationships with 2-year changes in cognition, calculated using age-adjusted simple discrepancy scores designated by Δ (score at time 1—score at time 2). Positive discrepancy scores signify cognitive decline at the follow-up visit, except for the CWINH for which negative discrepancy scores signify cognitive decline. *Predicted values from the regression of internetwork connectivity onto MoCA scores are plotted for pDMN-LFPN and pDMN-RFPN couplings [Σ intercept + ($beta_{pDMN-LFPN}$ * pDMN-LFPN score) + ($beta_{pDMN-RFPN}$ * pDMN-RFPN score) = Σ–0.33 + (0.08 * pDMN-LFPN score) + (0.10 * pDMN-RFPN score)]. For DOT scores, predicted values are plotted for aDMN-pDMN and aDMN-LFPN couplings [Σ intercept + ($beta_{aDMN-pDMN}$ * aDMN-pDMN score) + ($beta_{aDMN-LFPN}$ * aDMN-LFPN score) = Σ–0.34 + (0.09 * aDMN-pDMN score) + (0.06 * aDMN-LFPN score)]. BNT, Boston Naming Test; BVMT, Brief Visuospatial Memory Test; CVLT, California Verbal Learning Test; CWINH, Color-Word Inhibition; CWN, Color Word Naming; DOT, Adaptive Digit Ordering; HVOT, Hooper Visual Organization Test; JLOT, Judgment of Line Orientation; MoCA, Montreal Cognitive Assessment; SWA, Category Switching.

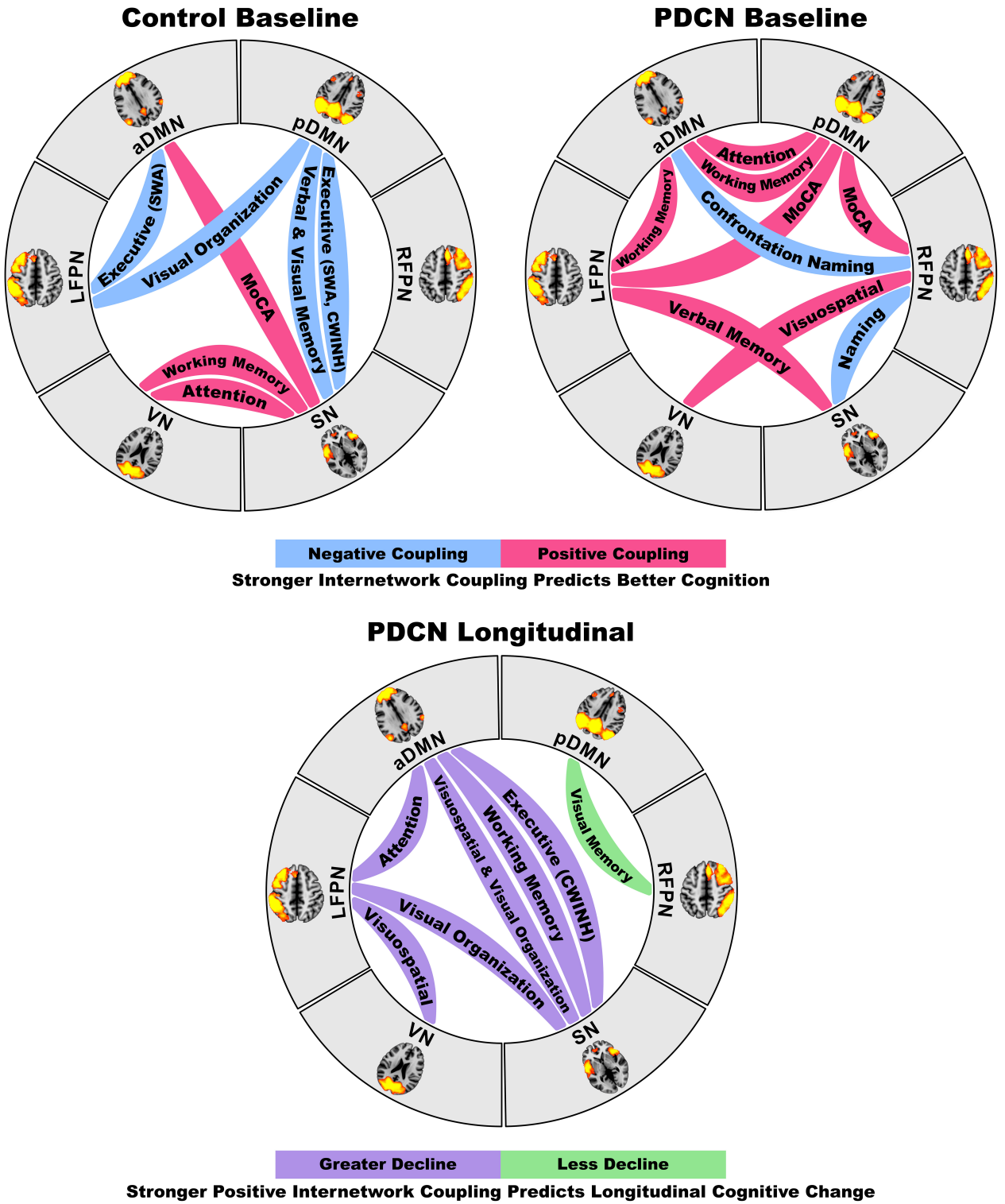

FIGURE 3 | Circular visualization of internetwork functional coupling topologies as they predict baseline and longitudinal declines in cognition. The top circular layouts depict the correlations between internetwork coupling topologies and baseline domain-specific cognitive performance in the healthy control and PDCN groups. Blue lines designate stronger negative (anticorrelated) couplings and red lines designate stronger positive couplings were correlated with better cognition. The bottom circular layout shows that stronger positive internetwork couplings predict greater longitudinal decline (purple lines) for most cognitive domains, but less longitudinal decline in visual memory. These neurocognitive relationships are graphed in **Figure 2**.

TABLE 3 | Longitudinal changes in cognition in a PDCN subsample.

	Visit 1	Visit 2	*p*	d±
Montreal Cognitive Assessment (MoCA)	27.0 (2.5)	26.7 (3.0)	0.43	0.13
Attention and working memory				
Adaptive Digit Ordering (DOT)	6.7 (1.9)	6.2 (2.7)	0.12	0.26
DKEFS Color + Word Naming (CWN)	21.9 (4.3)	20.9 (4.4)	0.08	0.29
Executive (DKEFS)				
Category switching (accuracy) (SWA)	13.6 (2.9)	11.5 (5.0)	**0.009**	0.49
Color-Word Inhibition (CWINH)	59.2 (14.2)	64.1 (22.5)	**0.04**	0.39
Memory (long delay free recall)				
California Verbal Learning Test 2 (CVLT)	9.5 (3.3)	8.8 (5.2)	0.26	0.18
Brief Visuospatial Memory Test-Revised (BVMT)	8.7 (2.5)	8.6 (3.0)	0.84	0.03
Visual cognition				
Judgment of Line Orientation (JLOT)	25.4 (2.6)	24.3 (4.5)	0.08	0.31
Hooper Visual Organization HVOT)	25.7 (2.5)	24.2 (3.6)	**0.006**	0.52
Semantic language				
Boston naming (BNT)	57.8 (2.6)	57.9 (3.0)	0.86	0.03
DKEFS Category Fluency (CAT)	43.9 (8.6)	38.8 (9.2)	**0.001**	0.60

Tabled values are raw score means (standard deviations) from a subsample of 40 PDCN participants. Longitudinal changes between baseline (Visit 1) and follow-up testing (Visit 2) were analyzed using paired t-tests with bias corrected accelerated bootstrapping (1,000 iterations). Follow-up testing occurred a mean of 24.5 months (SD = 3.4) post-baseline testing: Significant p values in bold.
DKEFS, Delis Kaplan Executive Function System.
±Cohen's d.

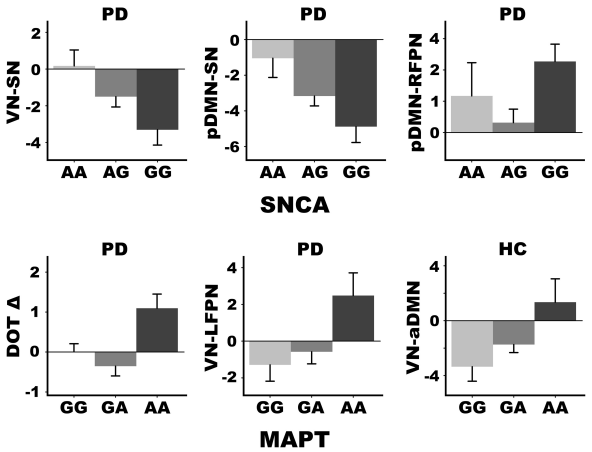

FIGURE 4 | SNCA and MAPTrs242557 mediation of internetwork coupling topologies and longitudinal change in working memory. SNCA expression altered connectivity strength in the PDCN group only but was not associated with baseline or longitudinal changes in cognition. MAPT variants altered connectivity strength of different internetwork topologies in the PDCN and healthy control (HC) groups. Moreover, only PDCN A homozygotes exhibited longitudinal decline in working memory (DOT Δ) as measured by age adjusted simple discrepancy scores (score at time 1—score at time 2) wherein positive scores signify cognitive decline. Means and standard error bars are plotted.

greater decline in working memory (DOT) [$F(1, 38) = 5.8$, $p < 0.02$, $q = 0.027$, $R = 0.36$].

Executive

Stronger positive aDMN-SN couplings predicted greater decline in inhibitory control (CWINH) [$F(1, 38) = 5.3$, $p < 0.027$, $q = 0.04$, $R = 0.35$].

Episodic Memory

Stronger anticorrelated pDMN-RFPN couplings predicted greater decline in visual episodic memory (BVMT) [$F(1, 38) = 4.2$, $p < 0.047$, $q = 0.05$, $R = 0.32$].

Visual Cognition

Stronger positive VN-LFPN [$F(1, 38) = 6.0$, $p < 0.019$, $q = 025$, $R = 0.37$] and aDMN-SN couplings [$F(1, 38) = 5.7$, $p < 0.023$, $q = 0.035$, $R = 0.36$] predicted greater decline in visuospatial processing (JLOT). Stronger positive aDMN-SN [$F(1, 38) = 5.9$, $p < 0.02$, $q = 0.03$, $R = 0.37$] and LFPN-SN couplings [$F(1, 38) = 7.5$, $p < 0.01$, $q = 0.015$, $R = 0.41$] predicted greater decline in visual-organization (HVOT).

Genetic Associations With Internetwork Connectivity and Cognitive Decline

Stepwise multiple regression analyses tested for sets of internetwork couplings that predicted SNCA and MAPT variants, separately for each group. **Figure 4** graphs the significant results (FDR corrected). SNCA was not related to internetwork connectivity in healthy controls. In PDCN, stronger anticorrelated VN-SN couplings were observed in homozygous G carriers (high α-synuclein activity) than A carriers [$F(1, 61) = 8.4$, $p < 0.005$, $q = 0.04$, $R = 0.35$]. SNCA expression also was predicted by pDMN-SN ($r = -0.36$) and pDMN-RFPN ($r_{xy.z} = 0.30$) couplings [$F(2, 60) = 7.9$, $p < 0.001$, $q = 0.01$, $R = 0.46$]. Here, pDMN-SN anticorrelations were stronger in homozygous G than A carriers, whereas stronger positive pDMN-RFPN couplings were observed in homozygous G relative to A carriers. MAPT was related to internetwork connectivity in both groups. In PDCN stronger positive VN-LFPN couplings were observed in homozygote A carriers (high tau activity) than G carriers [$F(1, 61) = 4.2$, $p < 0.004$, $q = 0.02$, $R = 0.26$]. In controls stronger anticorrelated VN-aDMN couplings were found in G homozygotes (lower tau activity) than A carriers [$F(1, 41) = 8.6$, $p < 0.005$, $q = 0.03$, $R = 0.42$].

ANOVAs tested for genetic associations with (1) age adjusted cognitive measures at baseline in each group and (2) longitudinal changes (age adjusted simple discrepancy scores) in the PDCN subsample. Carriers of different SNCA or MAPT allele types did not differ demographically (age, educational level, gender) in either group or in clinical characteristics (disease duration, levodopa dosage equivalence). SNCA and MAPT variants were not associated with baseline cognitive measures in either group or longitudinal cognitive changes in the PDCN subsample, with one exception. **Figure 4** shows that MAPT homozygous A carriers exhibited working memory (DOT) decline at follow-up testing, whereas working memory was preserved in G carriers [$F(2, 37) = 4.9$, $p < 0.01$, $q = 0.05$, $\eta_p^2 = 0.21$].

DISCUSSION

Internetwork connectivity was largely preserved in PDCN, except for reduced pDMN-RFPN/LFPN couplings, which correlated

with poorer baseline global cognition. This finding may reflect a weakened role of the FPN in regulating flexible interactions with the DMN to integrate processing resources (Spreng et al., 2010) needed to achieve diverse demands of global cognition tests. Preserved internetwork interactions in PDCN also correlated with cognition, but in a different manner for each group. In PDCN, stronger positive internetwork coupling topologies were beneficial for most, but not all, cognitive functions at baseline. This dominant neurocognitive pattern was compatible with a compensatory mechanism that may arise owing to less effective integration between other networks that normally support cognition. Indeed, different internetwork coupling topologies correlated with cognition in healthy controls. Notably, stronger positive internetwork coupling topologies also predicted greater 2-year longitudinal declines in most cognitive domains in PDCN, suggesting they may signify neurodegeneration and portend future neurocognitive progression (Cabeza et al., 2018). Heterogeneity in internetwork connectivity strength was also related to genetic variants. Higher α-synuclein was associated with reduced SN-VN/pDMN interactions and amplified RFPN-pDMN couplings, which longitudinally preserved visual memory in PDCN. In contrast, higher tau expression accelerated longitudinal working memory decline and increased VN-LFPN connectivity, which in turn predicted greater decline in visuospatial processing, a risk factor for PD dementia (Williams-Gray et al., 2013). These results could not be attributed to brain atrophy, which did not differ between groups, nor aberrant LFPN intra-network coherence, which did not correlate with internetwork connectivity.

Distinct Internetwork Topologies Predict Baseline Cognition in Cognitively Normal PD and Controls

Cognition is supported through integration and segregation (anticorrelated) of processing resources from large-scale networks (Spreng et al., 2010), which are regulated by the FPN and SN (Sridharan et al., 2008; Grady et al., 2016). In our study both groups showed positive pDMN-LFPN/RFPN couplings, albeit significantly reduced in PDCN. However, stronger pDMN-FPN couplings were beneficial for MoCA performance only in PDCN, in agreement with favorable effects of cooperative DMN-FPN communications on diverse cognitive processes (Fornito et al., 2012; Utevsky et al., 2014; Marek and Dosenbach, 2018). Cooperative FPN communications with the pDMN, which is associated with episodic memory and interrelated associative or constructive processes (Hassabis and Maguire, 2007; Andrews-Hanna et al., 2014a), may support MoCA performances especially on tests related to posterior cortical functions (e.g., visuoconstruction, memory encoding and recollection). In controls, however, positive aDMN-SN interactions benefitted MoCA performance. The aDMN consists of prefrontal and anterior temporal cortices that regulate executive, and conceptual/semantic processes (Wood and Grafman, 2003; Andrews-Hanna et al., 2014b), whereas the SN governs attention capture, internetwork switching, and inhibition. Thus, aDMN-SN communications are well suited to foster multidomain cognitive control (Sridharan et al., 2008). This coupling topology was not deployed in PDCN, possibly owing to emerging SN pathology (Christopher et al., 2015). Thus, global cognition in PDCN appears to be maintained via functional reconfiguration of internetwork communications, driven by pathological changes that cause shifts in processing load to other networks.

This conclusion aligns with our finding that internetwork connectivity correlated with domain-specific cognition differently in each group. We discovered that stronger aDMN-pDMN and aDMN-pDMN/LFPN couplings in PDCN were, respectively, favorable for attention (CWN) and working memory (DOT). The CWN test is a speeded test that requires selective attention to colors or words, whereas the DOT engages executive functions, as digit strings of increasing length must be mentally reorganized into their ascending order for recall. Both tests may benefit from stronger aDMN-pDMN connectivity owing to overlapping endogenous control and mnemonic processes, whereas favorable influences of strengthened aDMN-LFPN connectivity on the DOT aligns with LFPN control of executive components of working memory. By comparison, in healthy controls better attention and working memory both correlated with stronger VN-SN connectivity. The SN is known to drive switching between the DMN and FPN (Goulden et al., 2014). By inference, our finding may suggest that healthy adults deploy the SN to enlist VN resources to support visual attention and memory. VN-SN communications may not be effectively deployed in PDCN, perhaps owing to declining visual cognition (Weil et al., 2016), which we observed in our study, and/or emerging pathology that renders the anterior insula and anterior cingulate cortex vulnerable (Christopher et al., 2014).

Internetwork connectivity was not related to executive functioning in the PDCN group. However, stronger positive LFPN-SN and VN-RFPN couplings were compensatory, respectively, predicting better baseline verbal memory and visuospatial cognition, which exhibited decline in PDCN. In controls, however, stronger anticorrelated pDMN-SN couplings predicted better executive functioning (category switching and inhibition) and verbal/visual memory, consistent with another study (Putcha et al., 2016). Stronger anticorrelated aDMN-LFPN couplings also predicted better category switching, whereas stronger anticorrelated pDMN-LFPN couplings correlated with better visual organization. Thus, in controls segregation of task-negative and positive networks was favorable for many cognitive functions, ostensibly due to reduced competition between processes that can interfere with performance (Kelly et al., 2008).

While strengthened positive internetwork coupling topologies in PDCN typically exerted favorable influences on cognition, an exception was the BNT (confrontation naming), a measure of semantic recollection that requires generating names of common and uncommon pictures. Semantic recollection is highly relevant to PD since early decline in object naming predicts later dementia (Williams-Gray et al., 2013). We found that stronger positive aDMN-RFPN and RFPN-SN couplings in PDCN were detrimental for naming. Outwardly this finding was unexpected as integration of executive/semantic (aDMN) and attention (SN) resources with RFPN visual processing

resources might foster object naming. For the BNT, however, common object names are automatically retrieved whereas uncommon object names require attentional control (Hoffman et al., 2015). One speculation is that communications of the RFPN with attention and executive/semantic networks may be amplified in patients who have difficulty finding names due to failed automatic retrieval of semantic details, which could be a sign of impoverished representations of semantic content. This proposal is compatible with a task-activated fMRI study of semantic recollection (Harrington et al., 2021). We found that stronger connectivity of a semantic hub and the caudate with regions comprising the dorsal attention, executive, and/or language systems correlated with poorer BNT performance in PDCN. These results suggested the possibility that patients with poorer naming may allocate more attention and executive resources to support covert verbal strategic searches needed to find names that cannot be retrieved automatically (Harrington et al., 2021).

Internetwork Topologies Predict Future Cognitive Decline in Cognitively Normal PD

At 2 years post-baseline, the PDCN subsample showed significant decline in executive functioning, visual organization, and semantic fluency, with subthreshold trends for decline in attention, working memory and visuospatial processing. Greater cognitive decline for most domains, except visual episodic memory, was predicted by strengthened positive internetwork couplings. Thus, strengthened internetwork couplings, even those exerting compensatory influences on baseline cognition, foreshadowed future cognitive progression, indicating they signify neuropathology. This proposal aligns with the positive correlation between increased cortical connectivity and glucose consumption (FDG-PET) (Tomasi et al., 2013; Passow et al., 2015), which indicates a metabolic cost for hyperconnectivity that may in turn signify neuronal vulnerability. Indeed, cognitively normal people at genetic risk for Alzheimer's initially exhibit hyperactivation in the brain relative to people not at genetic risk, but activation declines longitudinally together with the emergence of episodic memory dysfunction (Rao et al., 2015).

Some internetwork topologies predicted different facets of cognition at baseline and longitudinally, likely because general processing resources are shared across domains, some of which are more vulnerable to cognitive progression (Salthouse, 2017; Tucker-Drob et al., 2019). For example, stronger positive aDMN-LFPN and LFPN-SN, respectively, predicted greater deterioration in attention and visual organization, but better baseline working memory and visual memory. In most instances, predictors of longitudinal cognitive decline did not correlate with baseline cognition. Notably, greater decline in attention, working memory, executive, visuospatial, and visual organization functions were predicted by stronger positive aDMN-SN/LFPN and LFPN-SN couplings. Amplified internetwork couplings of these networks likely foreshadow longitudinal cognitive decline across multiple domains, owing to frontostriatal vulnerabilities driven by dopaminergic loss and SN pathology (Christopher et al., 2014). Our results contrast with a seed-based approach in which increased SN-DMN regional couplings in a PD cohort unscreened for MCI predicted conversion to dementia 10 years later (Aracil-Bolanos et al., 2021). While DMN-SN coupling strength did not correlate with PDCN cognition in our study, increased pDMN-SN connectivity was maladaptive for executive functioning and episodic memory in healthy controls, consistent with these results.

Stronger positive VN-LFPN couplings also predicted greater decline in visuospatial processing. Interestingly, VN-FPN connectivity increased over 1 year in a mixed PDCN/PDMCI cohort, but not healthy controls (Klobusiakova et al., 2019), and did not correlate with cognition. Our finding indicates this internetwork coupling topology is an early signature of high-level visual disturbances in PD (Weil et al., 2016), which is of keen interest as early visuospatial decline is a risk for MCI and dementia (Williams-Gray et al., 2013; Hong et al., 2014; Hobson and Meara, 2015; Garcia-Diaz et al., 2018; Chung et al., 2020; Ohdake et al., 2020).

The above results sharply contrasted with our finding that stronger positive pDMN-RFPN couplings predicted preserved visual episodic memory longitudinally, even though performance was poorer in PDCN relative to controls at baseline. Thus, integration of pDMN memory resources with RFPN visual processing resources appears to maintain visual memory over 2 years. Interestingly, in a PDCN/PDMCI cohort the strength of DMN-FPN couplings increased over 1 year but did not correlate with cognition (Klobusiakova et al., 2019). The latter finding may be due to the short follow-up period, which could minimize changes. However, our results also demonstrate the importance of distinguishing between left and right FPN internetwork couplings as they correlated differently with cognitive tests that emphasize verbal and visual processes.

α-Synuclein and Microtubule-Associated Protein Tau Alter Cognition and Internetwork Connectivity

The SNCA rs356219 polymorphism codes for α-synuclein levels, with the G risk allele associated with higher transformed plasma α-synuclein (Mata et al., 2010; Emelyanov et al., 2018), reduced striatal binding potential (Huertas et al., 2017), and increased risk for PD (Goris et al., 2007; Trotta et al., 2012; Zhang et al., 2018). Although SNCA does not predict dementia outcome over 10 years (Williams-Gray et al., 2013), its association with cognitive decline is controversial, especially in PDCN. In our study, SNCA did not mediate baseline or longitudinal changes in cognition, consistent with some studies (Mata et al., 2014; Huertas et al., 2017), but not others (Campelo et al., 2017; Luo et al., 2019). Yet another SNCA risk variant (rs894280) predicted poorer attention and visuospatial processing (Ramezani et al., 2021). Correspondingly, higher baseline CSF α-synuclein levels also predicted faster longitudinal deterioration in visuospatial working memory and verbal memory (Stewart et al., 2014) and processing speed (Hall et al., 2015). Our discrepant results may

be related to studying a PDCN cohort wherein cognition is intact relative to cohorts not screened for MCI.

Nonetheless, we found for the first time that SNCA mediated the strength of functional connectivity between large-scale networks, but only in PDCN. This finding is compatible with the SNCA risk variant's role in modifying the effect of CSF α-synuclein levels on brain structure by accelerating cortical thinning throughout frontal and posterior cortical areas (Sampedro et al., 2018a). In our study, homozygous G carriers showed marked anticorrelated SN-VN and SN-pDMN couplings relative to A carriers. As these topologies were associated with cognition only in healthy controls, our results suggest that the SNCA risk variant amplifies segregation between the SN and the VN/pDMN, rendering their deployment less effective for cognition. Thus, accumulation of α-synuclein pathology (Christopher et al., 2015) may diminish flexible SN internetwork switching (Goulden et al., 2014), thereby dampening internetwork communications. Interestingly, homozygous G carriers also exhibited stronger positive pDMN-RFPN couplings relative to A carriers. This internetwork topology was favorable for baseline MoCA scores and predicted preserved visual episodic memory longitudinally. Still, more tightly coupled compensatory pDMN-RFPN communications in GG carriers may occur at a metabolic cost (Tomasi et al., 2013; Passow et al., 2015), such that over longer periods of time compensation might diminish as neurodegeneration increases and cognitive deficits emerge (Reuter-Lorenz and Park, 2014). This prospect aligns with a report of 2-year increases in CSF α-synuclein levels only in PD patients with longer disease durations (> 5 years) (Hall et al., 2016). Thus, longer follow-up periods may be needed to better characterize the trajectory of neurocognitive progression in carriers of risk and protective SNCA alleles.

MAPT had independent effects on internetwork communications and cognitive decline. The MAPT H1 haplotype promotes tau aggregation, which may interact with α-synuclein in Lewy body formation (Colom-Cadena et al., 2013). Higher tau transcription in PD appears to accelerate cognitive decline in early years of PD and is the strongest genetic marker of dementia conversion (Williams-Gray et al., 2013). In our study, H1 tau transcription levels had no effect on baseline cognition, consistent with some studies of the MAPT H1/H2 diplotype (Mata et al., 2014; Paul et al., 2016) but not others (Morley et al., 2012; Nombela et al., 2014). For the first time, we found working memory decline was strongly mediated by the A risk allele, which is associated with higher plasma tau levels (Chen et al., 2017), whereas working memory was preserved in G carriers. Correspondingly, tau deposition in older adults is found in large-scale brain networks including the FPN (Jones et al., 2017), which supports working memory. We also found group differences in MAPT-mediated internetwork coupling topologies. In PDCN, homozygous A carriers exhibited stronger positive VN-LFPN couplings whereas G carriers showed negative couplings. Importantly, stronger positive VN-LFPN couplings predicted greater longitudinal decline in visuospatial processing, another risk factor for the later MCI and dementia. These findings partly agree with the effect of the MAPT H1 haplotype on longitudinal volume loss in *de novo* PD, largely in the frontal cortex (Sampedro et al., 2018b), which is an element of the LFPN. The results are also compatible with reports that MAPT variants alter activation and functional connectivity of the parietal cortex, which is an element of both the VN and LFPN. Specifically, PD carriers of the MAPT H1 haplotype showed reduced left parietal and bilateral caudate activation relative to non-risk carriers when performing a mental rotation task (Nombela et al., 2014). Correspondingly, during a semantic recollection task PDCN carriers of the MAPT A risk allele showed stronger left parietal connectivity with the bilateral caudate, which was unfavorable for cognition, but diminished frontal connectivity with parietal areas, which supported compensation (Harrington et al., 2021). Altogether, our finding aligns with the vulnerability of occipital and frontoparietal cortices to tau deposition (Robakis et al., 2016; Jones et al., 2017), and implicates increased tau activity in the acceleration of visuospatial decline. In contrast, healthy control homozygote A carriers showed stronger positive VN-aDMN couplings whereas G carriers showed negative couplings, suggesting that tau deposition in occipital cortex may also drive aberrant VN internetwork communications in older adults.

Limitations

Limitations include that testing patients on medication therapy could mask functional abnormalities and affect performance on neuropsychological tests. Head motion artifact, however, can be elevated off medication, which has detrimental influences especially on low frequency rsfMRI signals. Completion of a lengthy neuropsychological test battery can also be challenging for patients after overnight withdrawal from medication therapy. From a practical standpoint it is also important to understand brain functioning and cognition in daily life as influenced by medication therapy. Second, the inclusion of six *de novo* PDCN patients increased the heterogeneity within the cohort, which could add variability to the functional connectivity measures. Despite this limitation, internetwork coupling topologies remained sensitive to cognitive and genetic variables, likely owing in part to the improved temporal resolution of our multiband fMRI protocol (Tomasi et al., 2016). Third, neurocognitive correlations were medium in magnitude, likely owing to the more restricted ranges on behavioral variables in a PDCN cohort, which may partly relate to the use of compensatory strategies that maintain cognition (Reuter-Lorenz and Park, 2014). Fourth, although our sample size was large, the statistical power for tests of genetic variants would be improved with larger samples. Even so, medium effect sizes were found for MAPT and SNCA effects on internetwork connectivity and a very large effect size was observed for MAPT prediction of working memory decline. Fifth, although our longitudinal analyses controlled for aging effects, it would be desirable to collect the same neuropsychological data longitudinally in elder controls to better gauge the rate of disease-related cognitive progression. Lastly, our analyses were constrained to six core large-scale networks, but other networks should also be considered to fully characterize internetwork communications that predict domain-specific cognitive progression.

CONCLUSION

Our results show that cognition in PDCN is maintained by functional reconfiguration of internetwork communications, possibly driven by underlying pathology that causes a shift in processing resources to other networks. We demonstrated for the first time that stronger positive internetwork coupling topologies exerted mainly compensatory influences on baseline cognition in PDCN, but predicted longitudinal changes in most cognitive domains, suggesting that they are surrogate markers of neuronal vulnerability. Strengthened aDMN-SN, LFPN-SN, and/or LFPN-VN interactions predicted longitudinal decline in visual cognition, a risk factor for future MCI and dementia, and declines in attention, executive functioning, and working memory, which are processes shared across multiple cognitive domains. Coupling strengths of some internetwork topologies were altered by genetic variants. The main findings showed that higher α-synuclein weakened internetwork communications of the SN that supported cognition in healthy controls, whereas higher tau increased VN-LFPN connectivity, which in turn predicted greater longitudinal visuospatial decline, a risk factor for dementia. Notably, the tau risk variant also accelerated longitudinal decline in working memory, whereas the protective allele prevented working memory decline. Still, internetwork coupling topologies did not predict longitudinal change in semantic fluency, which was robust in the PDCN group and is also a risk factor for MCI and dementia (Compta et al., 2013; Williams-Gray et al., 2013; Hobson and Meara, 2015). This is likely because our ICA analyses did not expose a temporal-parietal network, for which key hubs (angular gyrus, temporal pole) modulate semantic fluency in PDCN (Harrington et al., 2021). Collectively, these novel findings emphasize the prognostic value of large-scale internetwork connectivity in predicting domain-specific cognitive decline and the distinct modulatory influences of SNCA and MAPT, which partly explain heterogeneity in neurocognition. Future investigations into the roles of other genetic variants in neurocognitive functioning would be of great interest, given the paucity of studies concerning genetic modifiers of functional connectivity in PDCN.

DATA AVAILABILITY STATEMENT

The data that support the findings of this study are available on reasonable request from the corresponding author. The data are not publicly available due to privacy or ethical restrictions imposed the U.S. Department of Veteran Affairs. Genetic variant data from this study are deposited in dbSNP (https://www.ncbi.nlm.nih.gov/SNP/snp_viewTable.cgi?handle=COGNITIONPD).

ETHICS STATEMENT

The studies involving human participants were reviewed and approved by the Institutional Review Board at the VA San Diego Healthcare System. The patients/participants provided their written informed consent to participate in this study.

AUTHOR CONTRIBUTIONS

XW wrote the first draft of the manuscript and performed the neuroimaging analyses. QS supervised and assisted with the neuroimaging analyses and acquired MRI data. RL reviewed brain MRIs. XW, IL, QS, MH, and RL contributed critical content to the manuscript revision. DH conceived and designed the study, performed statistical analyses, and wrote the final manuscript. All authors read and approved the submitted version.

FUNDING

This work was supported by the U.S. Department of Veterans Affairs (Grant/Award Nos. 101-CX000146 and 101-CX000499).

ACKNOWLEDGMENTS

We thank Vida Sadeghi, Michael Widdowson, Cailey Grembowski, Jaqueline Hernandez-Lucas, and Avleen Walia for their technical support. We also thank the University of California San Diego Center for Aids Research for their analyses of genetic polymorphisms.

SUPPLEMENTARY MATERIAL

The Supplementary Material for this article can be found online at: https://www.frontiersin.org/articles/10.3389/fnagi.2022.853029/full#supplementary-material

REFERENCES

Amboni, M., Tessitore, A., Esposito, F., Santangelo, G., Picillo, M., Vitale, et al. (2015). Resting-state functional connectivity associated with mild cognitive impairment in Parkinson's disease. *J. Neurol.* 262, 425–434. doi: 10.1007/s00415-014-7591-5

Andrews-Hanna, J. R., Saxe, R., and Yarkoni, T. (2014a). Contributions of episodic retrieval and mentalizing to autobiographical thought: evidence from functional neuroimaging, resting-state connectivity, and fMRI meta-analyses. *Neuroimage* 91, 324–335. doi: 10.1016/j.neuroimage.2014.01.032

Andrews-Hanna, J. R., Smallwood, J., and Spreng, R. N. (2014b). The default network and self-generated thought: component processes, dynamic control, and clinical relevance. *Ann. N. Y. Acad. Sci.* 1316, 29–52. doi: 10.1111/nyas.12360

Aracil-Bolanos, I., Sampedro, F., Pujol, J., Soriano-Mas, C., Gonzalez-de-Echavarri, J. M., Kulisevsky, J., et al. (2021). The impact of dopaminergic treatment over cognitive networks in Parkinson's disease: Stemming the tide? *Hum. Brain Mapp.* 42, 5736–5746. doi: 10.1002/hbm.25650

Badea, L., Onu, M., Wu, T., Roceanu, A., and Bajenaru, O. (2017). Exploring the reproducibility of functional connectivity alterations in Parkinson's disease. *PLoS One* 12:e0188196. doi: 10.1371/journal.pone.0188196

Baggio, H. C., Segura, B., Sala-Llonch, R., Marti, M. J., Valldeoriola, F., Compta, Y., et al. (2015). Cognitive impairment and resting-state network connectivity in Parkinson's disease. *Hum. Brain Mapp.* 36, 199–212. doi: 10.1002/hbm.22622

Beckmann, C. F., Mackay, C. E., Filippini, N., and Smith, S. M. (2009). Group comparison of resting-state FMRI data using multi-subject ICA and dual regression. *Neuroimage* 47(Suppl. 1), S148. doi: 10.1016/S1053-8119(09)71511-3

Beckmann, C. F., and Smith, S. M. (2004). Probabilistic independent component analysis for functional magnetic resonance imaging. *IEEE Transact. Med. Imaging* 23, 137–152. doi: 10.1109/TMI.2003.822821

Bressler, S. L., and Menon, V. (2010). Large-scale brain networks in cognition: emerging methods and principles. *Trends Cogn. Sci.* 14, 277–290. doi: 10.1016/j.tics.2010.04.004

Cabeza, R., Albert, M., Belleville, S., Craik, F. I. M., Duarte, A., Grady, C. L., et al. (2018). Maintenance, reserve and compensation: the cognitive neuroscience of healthy ageing. *Nat. Rev. Neurosci.* 19, 701–710. doi: 10.1038/s41583-018-0068-2

Campbell, M. C., Jackson, J. J., Koller, J. M., Snyder, A. Z., Kotzbauer, P. T., and Perlmutter, J. S. (2020). Proteinopathy and longitudinal changes in functional connectivity networks in Parkinson disease. *Neurology* 94, e718–e728. doi: 10.1212/WNL.0000000000008677

Campelo, C. L. C., Cagni, F. C., de Siqueira Figueredo, D., Oliveira, L. G. Jr., Silva-Neto, A. B., Macedo, et al. (2017). Variants in SNCA Gene Are Associated with Parkinson's Disease Risk and Cognitive Symptoms in a Brazilian Sample. *Front. Aging Neurosci.* 9:198. doi: 10.3389/fnagi.2017.00198

Carson, N., Leach, L., and Murphy, K. J. (2018). A re-examination of Montreal Cognitive Assessment (MoCA) cutoff scores. *Int. J. Geriatr. Psychiatr.* 33, 379–388. doi: 10.1002/gps.4756

Chen, J., Yu, J. T., Wojta, K., Wang, H. F., Zetterberg, H., Blennow, K., et al. (2017). Genome-wide association study identifies MAPT locus influencing human plasma tau levels. *Neurology* 88, 669–676. doi: 10.1212/WNL.0000000000003615

Christopher, L., Duff-Canning, S., Koshimori, Y., Segura, B., Boileau, I., Chen, R., et al. (2015). Salience network and parahippocampal dopamine dysfunction in memory-impaired Parkinson disease. *Ann. Neurol.* 77, 269–280. doi: 10.1002/ana.24323

Christopher, L., Koshimori, Y., Lang, A. E., Criaud, M., and Strafella, A. P. (2014). Uncovering the role of the insula in non-motor symptoms of Parkinson's disease. *Brain* 137, 2143–2154. doi: 10.1093/brain/awu084

Chung, S. J., Lee, H. S., Kim, H. R., Yoo, H. S., Lee, Y. H., Jung, J. H., et al. (2020). Factor analysis-derived cognitive profile predicting early dementia conversion in PD. *Neurology* 95, e1650–e1659. doi: 10.1212/WNL.0000000000010347

Colom-Cadena, M., Gelpi, E., Marti, M. J., Charif, S., Dols-Icardo, O., Blesa, R., et al. (2013). MAPT H1 haplotype is associated with enhanced alpha-synuclein deposition in dementia with Lewy bodies. *Neurobiol. Aging* 34, 936–942. doi: 10.1016/j.neurobiolaging.2012.06.015

Compta, Y., Ezquerra, M., Munoz, E., Tolosa, E., Valldeoriola, F., Rios, J., et al. (2011). High cerebrospinal tau levels are associated with the rs242557 tau gene variant and low cerebrospinal beta-amyloid in Parkinson disease. *Neurosci. Lett.* 487, 169–173. doi: 10.1016/j.neulet.2010.10.015

Compta, Y., Pereira, J. B., Rios, J., Ibarretxe-Bilbao, N., Junque, C., Bargallo, N., et al. (2013). Combined dementia-risk biomarkers in Parkinson's disease: a prospective longitudinal study. *Parkinsonism Relat. Disord.* 19, 717–724. doi: 10.1016/j.parkreldis.2013.03.009

Di, X., and Biswal, B. B. (2014). Modulatory interactions between the default mode network and task positive networks in resting-state. *PeerJ.* 2:e367. doi: 10.7717/peerj.367

Emelyanov, A., Kulabukhova, D., Garaeva, L., Senkevich, K., Verbitskaya, E., Nikolaev, M., et al. (2018). SNCA variants and alpha-synuclein level in CD45+ blood cells in Parkinson's disease. *J. Neurol. Sci.* 395, 135–140. doi: 10.1016/j.jns.2018.10.002

Faust-Socher, A., Duff-Canning, S., Grabovsky, A., Armstrong, M. J., Rothberg, B., Eslinger, P. J., et al. (2019). Responsiveness to Change of the Montreal Cognitive Assessment, Mini-Mental State Examination, and SCOPA-Cog in Non-Demented Patients with Parkinson's Disease. *Dement Geriatr. Cogn. Disord* .47, 187–197. doi: 10.1159/000496454

Fjell, A. M., Westlye, L. T., Amlien, I., Espeseth, T., Reinvang, I., Raz, N., et al. (2009). High consistency of regional cortical thinning in aging across multiple samples. *Cereb. Cortex* 19, 2001–2012. doi: 10.1093/cercor/bhn232

Fornito, A., Harrison, B. J., Zalesky, A., and Simons, J. S. (2012). Competitive and cooperative dynamics of large-scale brain functional networks supporting recollection. *Proc. Natl. Acad. Sci. U.S.A* 109, 12788–12793. doi: 10.1073/pnas.1204185109

Garcia-Diaz, A. I., Segura, B., Baggio, H. C., Uribe, C., Campabadal, A., Abos, A., et al. (2018). Cortical thinning correlates of changes in visuospatial and visuoperceptual performance in Parkinson's disease: A 4-year follow-up. *Parkinsonism Relat. Disord.* 46, 62–68. doi: 10.1016/j.parkreldis.2017.11.003

Gorges, M., Muller, H. P., Lule, D., Pinkhardt, E. H., Ludolph, A. C., and Kassubek, J. (2015).). To rise and to fall: functional connectivity in cognitively normal and cognitively impaired patients with Parkinson's disease. *Neurobiol. Aging* 36, 1727–1735. doi: 10.1016/j.neurobiolaging.2014.12.026

Goris, A., Williams-Gray, C. H., Clark, G. R., Foltynie, T., Lewis, S. J., Brown, J., et al. (2007). Tau and alpha-synuclein in susceptibility to, and dementia in, Parkinson's disease. *Ann. Neurol.* 62, 145–153.

Goulden, N., Khusnulina, A., Davis, N. J., Bracewell, R. M., Bokde, A. L., McNulty, J. P., et al. (2014). The salience network is responsible for switching between the default mode network and the central executive network: replication from DCM. *Neuroimage* 99, 180–190. doi: 10.1016/j.neuroimage.2014.05.052

Grady, C., Sarraf, S., Saverino, C., and Campbell, K. (2016). Age differences in the functional interactions among the default, frontoparietal control, and dorsal attention networks. *Neurobiol. Aging* 41, 159–172. doi: 10.1016/j.neurobiolaging.2016.02.020

Gratwicke, J., Jahanshahi, M., and Foltynie, T. (2015). Parkinson's disease dementia: a neural networks perspective. *Brain* 138, 1454–1476. doi: 10.1093/brain/awv104

Hall, S., Surova, Y., Ohrfelt, A., Blennow, K., Zetterberg, H., and Hansson, O. (2016). Longitudinal Measurements of Cerebrospinal Fluid Biomarkers in Parkinson's Disease. *Mov. Disord.* 31, 898–905. doi: 10.1002/mds.26578

Hall, S., Surova, Y., Ohrfelt, A., Zetterberg, H., Lindqvist, D., and Hansson, O. (2015). CSF biomarkers and clinical progression of Parkinson disease. *Neurology* 84, 57–63. doi: 10.1212/WNL.0000000000001098

Harrington, D. L., Shen, Q., Sadeghi, V., Huang, M., Litvan, I., Wei, X., et al. (2021). Semantic Recollection in Parkinson's Disease: Functional Reconfiguration and MAPT Variants. *Front. Aging Neurosci.* 13:727057. doi: 10.3389/fnagi.2021.727057

Harrington, D. L., Shen, Q., Vincent Filoteo, J., Litvan, I., Huang, M., Castillo, G. N., et al. (2020). Abnormal distraction and load-specific connectivity during working memory in cognitively normal Parkinson's disease. *Hum. Brain Mapp.* 41, 1195–1211. doi: 10.1002/hbm.24868

Hassabis, D., and Maguire, E. A. (2007). Deconstructing episodic memory with construction. *Trends Cogn. Sci.* 11, 299–306. doi: 10.1016/j.tics.2007.05.001

Hobson, P., and Meara, J. (2015). Mild cognitive impairment in Parkinson's disease and its progression onto dementia: a 16-year outcome evaluation of the Denbighshire cohort. *Int. J. Geriatr. Psychiatr.* 30, 1048–1055.

Hoffman, P., Binney, R. J., and Lambon Ralph, M. A. (2015). Differing contributions of inferior prefrontal and anterior temporal cortex to concrete and abstract conceptual knowledge. *Cortex* 63, 250–266. doi: 10.1016/j.cortex.2014.09.001

Hong, J. Y., Sunwoo, M. K., Chung, S. J., Ham, J. H., Lee, J. E., Sohn, Y. H., et al. (2014). Subjective cognitive decline predicts future deterioration in cognitively normal patients with Parkinson's disease. *Neurobiol. Aging* 35, 1739–1743. doi: 10.1016/j.neurobiolaging.2013.11.017

Hou, Y., Wei, Q., Ou, R., Zhang, L., Yuan, X., Gong, Q., et al. (2021). Different resting-state network disruptions in newly diagnosed drug-naive Parkinson's disease patients with mild cognitive impairment. *BMC Neurol.* 21:327. doi: 10.1186/s12883-021-02360-z

Huertas, I., Jesus, S., Garcia-Gomez, F. J., Lojo, J. A., Bernal-Bernal, I., Bonilla-Toribio, M., et al. (2017). Genetic factors influencing frontostriatal dysfunction and the development of dementia in Parkinson's disease. *PLoS One* 12:e0175560. doi: 10.1371/journal.pone.0175560

Nalls, M. A., Plagnol, V., Hernandez, D. G., Sharma, M., et al. (2011). Imputation of sequence variants for identification of genetic risks for Parkinson's disease: a meta-analysis of genome-wide association studies. *Lancet* 377, 641–649. doi: 10.1016/S0140-6736(10)62345-8

Jones, D. T., Graff-Radford, J., Lowe, V. J., Wiste, H. J., Gunter, J. L., Senjem, M. L., et al. (2017). Tau, amyloid, and cascading network failure across the Alzheimer's disease spectrum. *Cortex* 97, 143–159. doi: 10.1016/j.cortex.2017.09.018

Kelly, A. C., Uddin, L. Q., Biswal, B. B., Castellanos, F. X., and Milham, M. P. (2008). Competition between functional brain networks mediates behavioral variability. *Neuroimage* 39, 527–537. doi: 10.1016/j.neuroimage.2007.08.008

Klobusiakova, P., Marecek, R., Fousek, J., Vytvarova, E., and Rektorova, I. (2019). Connectivity Between Brain Networks Dynamically Reflects Cognitive Status of Parkinson's Disease: A Longitudinal Study. *J. Alzheimers. Dis.* 67, 971–984. doi: 10.3233/JAD-180834

Koch, W., Teipel, S., Mueller, S., Buerger, K., Bokde, A. L., Hampel, H., et al. (2010). Effects of aging on default mode network activity in resting state fMRI: does the method of analysis matter? *Neuroimage* 51, 280–287. doi: 10.1016/j.neuroimage.2009.12.008

Laird, A. R., Fox, P. M., Eickhoff, S. B., Turner, J. A., Ray, K. L., McKay, D. R., et al. (2011). Behavioral interpretations of intrinsic connectivity networks. *J. Cogn. Neurosci.* 23, 4022–4037. doi: 10.1162/jocn_a_00077

Litvan, I., Goldman, J. G., Troster, A. I., Schmand, B. A., Weintraub, D., Petersen, R. C., et al. (2012). Diagnostic criteria for mild cognitive impairment in Parkinson's disease: Movement Disorder Society Task Force guidelines. *Mov. Disord.* 27, 349–356. doi: 10.1002/mds.24893

Luo, N., Li, Y., Niu, M., Zhou, L., Yao, M., Zhu, L., et al. (2019). Variants in the SNCA Locus Are Associated With the Progression of Parkinson's Disease. *Front. Aging Neurosci.* 11:110. doi: 10.3389/fnagi.2019.00110

Marek, S., and Dosenbach, N. U. (2018). The frontoparietal network: function, electrophysiology, and importance of individual precision mapping. *Dialog. Clin. Neurosci.* 20, 133–140. doi: 10.31887/DCNS.2018.20.2/smarek

Mata, I. F., Leverenz, J. B., Weintraub, D., Trojanowski, J. Q., Hurtig, H. I., Van Deerlin, V. M., et al. (2014). APOE. *MAPT, and SNCA genes and cognitive performance in Parkinson disease. JAMA Neurol.* 71, 1405–1412. doi: 10.1001/jamaneurol.2014.1455

Mata, I. F., Shi, M., Agarwal, P., Chung, K. A., Edwards, K. L., Factor, S. A., et al. (2010). SNCA variant associated with Parkinson disease and plasma alpha-synuclein level. *Arch. Neurol.* 67, 1350–1356. doi: 10.1001/archneurol.2010.279

Morley, J. F., Xie, S. X., Hurtig, H. I., Stern, M. B., Colcher, A., and Horn, S. (2012). Genetic influences on cognitive decline in Parkinson's disease. *Mov. Disord.* 27, 512–518. doi: 10.1002/mds.24946

Nichols, T. E., and Holmes, A. P. (2002). Nonparametric permutation tests for functional neuroimaging: a primer with examples. *Hum. Brain Mapp.* 15, 1–25. doi: 10.1002/hbm.1058

Nickerson, L. D., Smith, S. M., Öngür, D., and Beckmann, C. F. (2017). Using dual regression to investigate network shape and amplitude in functional connectivity analyses. *Front. Neurosci.* 11:115. doi: 10.3389/fnins.2017.00115

Nombela, C., Rowe, J. B., Winder-Rhodes, S. E., Hampshire, A., Owen, A. M., Breen, D. P., et al. (2014). Genetic impact on cognition and brain function in newly diagnosed Parkinson's disease: ICICLE-PD study. *Brain* 137, 2743–2758. doi: 10.1093/brain/awu201

Ohdake, R., Kawabata, K., Watanabe, H., Hara, K., Ogura, A., Kato, T., et al. (2020). Individual changes in visual performance in non-demented Parkinson's disease patients: a 1-year follow-up study. *J. Neural Transm.* 127, 1387–1397. doi: 10.1007/s00702-020-02248-1

Passow, S., Specht, K., Adamsen, T. C., Biermann, M., Brekke, N., Craven, A. R., et al. (2015). Default-mode network functional connectivity is closely related to metabolic activity. *Hum. Brain Mapp.* 36, 2027–2038. doi: 10.1002/hbm.22753

Paul, K. C., Rausch, R., Creek, M. M., Sinsheimer, J. S., Bronstein, J. M., Bordelon, Y., et al. (2016). APOE, MAPT, and COMT and Parkinson's Disease Susceptibility and Cognitive Symptom Progression. *J. Parkinsons. Dis.* 6, 349–359. doi: 10.3233/JPD-150762

Peraza, L. R., Nesbitt, D., Lawson, R. A., Duncan, G. W., Yarnall, A. J., Khoo, T. K., et al. (2017). Intra- and inter-network functional alterations in Parkinson's disease with mild cognitive impairment. *Hum. Brain Mapp.* 38, 1702–1715. doi: 10.1002/hbm.23499

Putcha, D., Ross, R. S., Cronin-Golomb, A., Janes, A. C., and Stern, C. E. (2015). Altered intrinsic functional coupling between core neurocognitive networks in Parkinson's disease. *Neuroimage Clin.* 7, 449–455. doi: 10.1016/j.nicl.2015.01.012

Putcha, D., Ross, R. S., Cronin-Golomb, A., Janes, A. C., and Stern, C. E. (2016). Salience and Default Mode Network Coupling Predicts Cognition in Aging and Parkinson's Disease. *J. Int. Neuropsychol. Soc.* 22, 205–215. doi: 10.1017/S1355617715000892

Ramezani, M., Mouches, P., Yoon, E., Rajashekar, D., Ruskey, J. A., Leveille, E., et al. (2021). Investigating the relationship between the SNCA gene and cognitive abilities in idiopathic Parkinson's disease using machine learning. *Sci. Rep.* 11:4917. doi: 10.1038/s41598-021-84316-4

Rao, S. M., Bonner-Jackson, A., Nielson, K. A., Seidenberg, M., Smith, J. C., Woodard, J. L., et al. (2015). Genetic risk for Alzheimer's disease alters the five-year trajectory of semantic memory activation in cognitively intact elders. *Neuroimage* 111, 136–146. doi: S1053-8119(15)00112-3

Reuter-Lorenz, P. A., and Park, D. C. (2014). How does it STAC up? Revisiting the scaffolding theory of aging and cognition. *Neuropsychol* 24, 355–370. doi: 10.1007/s11065-014-9270-9

Robakis, D., Cortes, E., Clark, L. N., Vonsattel, J. P., Virmani, T., Alcalay, R. N., et al. (2016). The effect of MAPT haplotype on neocortical Lewy body pathology in Parkinson disease. *J. Neural. Transm.* 123, 583–588. doi: 10.1007/s00702-016-1552-3

Rosenblum, S., Meyer, S., Gemerman, N., Mentzer, L., Richardson, A., Israeli-Korn, S., et al. (2020). The Montreal Cognitive Assessment: Is It Suitable for Identifying Mild Cognitive Impairment in Parkinson's Disease? *Mov. Disord. Clin. Pract.* 7, 648–655. doi: 10.1002/mdc3.12969

Salthouse, T. A. (2017). Shared and unique influences on age-related cognitive change. *Neuropsychology* 31, 11–19. doi: 10.1037/neu0000330

Sampedro, F., Marin-Lahoz, J., Martinez-Horta, S., Pagonabarraga, J., and Kulisevsky, J. (2018a). Cortical Thinning Associated with Age and CSF Biomarkers in Early Parkinson's Disease Is Modified by the SNCA rs356181 Polymorphism. *Neurodegener. Dis.* 18, 233–238. doi: 10.1159/000493103

Sampedro, F., Marin-Lahoz, J., Martinez-Horta, S., Pagonabarraga, J., and Kulisevsky, J. (2018b). Early Gray Matter Volume Loss in MAPT H1H1 de Novo PD Patients: A Possible Association With Cognitive Decline. *Front. Neurol.* 9:394. doi: 10.3389/fneur.2018.00394

Seeley, W. W., Menon, V., Schatzberg, A. F., Keller, J., Glover, G. H., Kenna, H., et al. (2007). Dissociable intrinsic connectivity networks for salience processing and executive control. *J. Neurosci* 27, 2349–2356. doi: 10.1523/JNEUROSCI.5587-06.2007

Smith, S. M., Fox, P. T., Miller, K. L., Glahn, D. C., Fox, P. M., Mackay, C. E., et al. (2009). Correspondence of the brain's functional architecture during activation and rest. *Proc. Natl. Acad. Sci.* 106, 13040–13045. doi: 10.1073/pnas.0905267106

Spreng, R. N., Stevens, W. D., Chamberlain, J. P., Gilmore, A. W., and Schacter, D. L. (2010). Default network activity, coupled with the frontoparietal control network, supports goal-directed cognition. *Neuroimage* 53, 303–317. doi: S1053-8119(10)00860-8

Sridharan, D., Levitin, D. J., and Menon, V. (2008). A critical role for the right fronto-insular cortex in switching between central-executive and default-mode networks. *Proc. Natl. Acad. Sci. U S A* 105, 12569–12574. doi: 10.1073/pnas.0800005105

Stewart, T., Liu, C., Ginghina, C., Cain, K. C., Auinger, P., Cholerton, B., et al. (2014). Cerebrospinal fluid alpha-synuclein predicts cognitive decline in Parkinson disease progression in the DATATOP cohort. *Am. J. Pathol.* 184, 966–975. doi: 10.1016/j.ajpath.2013.12.007

Tessitore, A., Cirillo, M., and De Micco, R. (2019). Functional Connectivity Signatures of Parkinson's Disease. *J. Parkinsons Dis.* 9, 637–652. doi: 10.3233/JPD-191592

Tessitore, A., Esposito, F., Vitale, C., Santangelo, G., Amboni, M., and Russo, A. (2012). Default-mode network connectivity in cognitively unimpaired patients with Parkinson disease. *Neurology* 79, 2226–2232. doi: WNL.0b013e31827689d6

Tomasi, D., Shokri-Kojori, E., and Volkow, N. D. (2016). High-Resolution Functional Connectivity Density: Hub Locations, Sensitivity, Specificity, Reproducibility, and Reliability. *Cereb. Cortex* 26, 3249–3259. doi: 10.1093/cercor/bhv171

Tomasi, D., Wang, G. J., and Volkow, N. D. (2013). Energetic cost of brain functional connectivity. *Proc Natl Acad Sci U S A* 110, 13642–13647. doi: 10.1073/pnas.1303346110

Tomlinson, C. L., Stowe, R., Patel, S., Rick, C., Gray, R., and Clarke, C. E. (2010). Systematic review of levodopa dose equivalency reporting in Parkinson's disease. *Mov. Disord.* 25, 2649–2653. doi: 10.1002/mds.23429

Trotta, L., Guella, I., Solda, G., Sironi, F., Tesei, S., and Canesi, M. (2012). SNCA and MAPT genes: Independent and joint effects in Parkinson disease in the

Italian population. *Parkinsonism Relat. Disord.* 18, 257–262. doi: 10.1016/j.parkreldis.2011.10.014

Tucker-Drob, E. M., Brandmaier, A. M., and Lindenberger, U. (2019). Coupled cognitive changes in adulthood: A meta-analysis. *Psychol. Bull.* 145, 273–301. doi: 10.1037/bul0000179

Uddin, L. Q. (2015). Salience processing and insular cortical function and dysfunction. *Nat. Rev. Neurosci.* 16, 55–61. doi: 10.1038/nrn3857

Utevsky, A. V., Smith, D. V., and Huettel, S. A. (2014). Precuneus is a functional core of the default-mode network. *J. Neurosci.* 34, 932–940. doi: 10.1523/JNEUROSCI.4227-13.2014

Weil, R. S., Schrag, A. E., Warren, J. D., Crutch, S. J., Lees, A. J., and Morris, H. R. (2016). Visual dysfunction in Parkinson's disease. *Brain* 139, 2827–2843. doi: 10.1093/brain/aww175

Weintraub, D., Simuni, T., Caspell-Garcia, C., Coffey, C., Lasch, S., Siderowf, A., et al. (2015). Cognitive performance and neuropsychiatric symptoms in early, untreated Parkinson's disease. *Mov. Disord.* 30, 919–927. doi: 10.1002/mds.26170

Williams-Gray, C. H., Evans, J. R., Goris, A., Foltynie, T., Ban, M., Robbins, T. W., et al. (2009). The distinct cognitive syndromes of Parkinson's disease: 5 year follow-up of the CamPaIGN cohort. *Brain* 132(Pt 11), 2958–2969. doi: 10.1093/brain/awp245

Williams-Gray, C. H., Mason, S. L., Evans, J. R., Foltynie, T., Brayne, C., Robbins, T. W., et al. (2013). The CamPaIGN study of Parkinson's disease: 10-year outlook in an incident population-based cohort. *J. Neurol. Neurosurg. Psychiatr.* 84, 1258–1264. doi: 10.1136/jnnp-2013-305277

Wood, J. N., and Grafman, J. (2003). Human prefrontal cortex: processing and representational perspectives. *Nat. Rev. Neurosci.* 4, 139–147. doi: 10.1038/nrn1033

Zhang, Y., Shu, L., Sun, Q., Pan, H., Guo, J., and Tang, B. (2018). A Comprehensive Analysis of the Association Between SNCA Polymorphisms and the Risk of Parkinson's Disease. *Front. Mol. Neurosci.* 11:391. doi: 10.3389/fnmol.2018.00391

Conflict of Interest: The authors declare that the research was conducted in the absence of any commercial or financial relationships that could be construed as a potential conflict of interest.

Publisher's Note: All claims expressed in this article are solely those of the authors and do not necessarily represent those of their affiliated organizations, or those of the publisher, the editors and the reviewers. Any product that may be evaluated in this article, or claim that may be made by its manufacturer, is not guaranteed or endorsed by the publisher.

frontiers | Frontiers in Neuroscience

ORIGINAL RESEARCH
published: 19 April 2022
doi: 10.3389/fnins.2022.797127

A Multi-Scale Computational Model of Levodopa-Induced Toxicity in Parkinson's Disease

Vignayanandam Ravindernath-Jayashree Muddapu[1†], *Karthik Vijayakumar*[2], *Keerthiga Ramakrishnan*[2] *and V. Srinivasa Chakravarthy*[1*]

[1] Department of Biotechnology, Bhupat and Jyothi Mehta School of Biosciences, Indian Institute of Technology Madras, Chennai, India, [2] Department of Biotechnology, Rajalakshmi Engineering College, Chennai, India

OPEN ACCESS

Edited by:
Sean Austin O. Lim,
DePaul University, United States

Reviewed by:
David J. Gabrieli,
University of Pennsylvania, United States
Romina Vuono,
University of Kent, United Kingdom

***Correspondence:**
V. Srinivasa Chakravarthy
schakra@ee.iitm.ac.in

†Present address:
Vignayanandam Ravindernath-Jayashree Muddapu, Blue Brain Project, École Polytechnique Fédérale de Lausanne (EPFL), Geneva, Switzerland

Specialty section:
This article was submitted to Neurodegeneration, a section of the journal Frontiers in Neuroscience

Received: 18 October 2021
Accepted: 15 March 2022
Published: 19 April 2022

Citation:
Muddapu VR-J, Vijayakumar K, Ramakrishnan K and Chakravarthy VS (2022) A Multi-Scale Computational Model of Levodopa-Induced Toxicity in Parkinson's Disease. Front. Neurosci. 16:797127. doi: 10.3389/fnins.2022.797127

Parkinson's disease (PD) is caused by the progressive loss of dopaminergic cells in substantia nigra pars compacta (SNc). The root cause of this cell loss in PD is still not decisively elucidated. A recent line of thinking has traced the cause of PD neurodegeneration to metabolic deficiency. Levodopa (L-DOPA), a precursor of dopamine, used as a symptom-relieving treatment for PD, leads to positive and negative outcomes. Several researchers inferred that L-DOPA might be harmful to SNc cells due to oxidative stress. The role of L-DOPA in the course of the PD pathogenesis is still debatable. We hypothesize that energy deficiency can lead to L-DOPA-induced toxicity in two ways: by promoting dopamine-induced oxidative stress and by exacerbating excitotoxicity in SNc. We present a systems-level computational model of SNc-striatum, which will help us understand the mechanism behind neurodegeneration postulated above and provide insights into developing disease-modifying therapeutics. It was observed that SNc terminals are more vulnerable to energy deficiency than SNc somas. During L-DOPA therapy, it was observed that higher L-DOPA dosage results in increased loss of terminals in SNc. It was also observed that co-administration of L-DOPA and glutathione (antioxidant) evades L-DOPA-induced toxicity in SNc neurons. Our proposed model of the SNc-striatum system is the first of its kind, where SNc neurons were modeled at a biophysical level, and striatal neurons were modeled at a spiking level. We show that our proposed model was able to capture L-DOPA-induced toxicity in SNc, caused by energy deficiency.

Keywords: Parkinson's disease, levodopa, dopamine, substance P, striatum, substantia nigra pars compacta

INTRODUCTION

Levodopa (L-DOPA), a precursor of dopamine (DA), is used as a symptom-relieving treatment for Parkinson's disease (PD) (Poewe et al., 2010). The usage of L-DOPA for PD is still debated due to its side effects with long-term treatment (Thanvi and Lo, 2004; Fahn, 2005; Lipski et al., 2011). Several

researchers suggested that L-DOPA might be harmful to SNc cells by a mechanism that probably involves oxidative stress (Pardo et al., 1995; Carvey et al., 1997; Takashima et al., 1999). However, several others proposed that L-DOPA might not accentuate neurodegeneration of SNc neurons (Jenner and Brin, 1998; Fahn et al., 2004; Fahn, 2005; Billings et al., 2019) and sometimes acts as a neuroprotective agent (Fahn, 2005; Schapira, 2008; Shimozawa et al., 2019) or promotes recovery of dopaminergic markers in the striatum (Murer et al., 1998, 1999). After several studies, it is still not clear why L-DOPA is not toxic in the case of nonparkinsonian human subjects and healthy animals and toxic in PD models of rodents (Fahn, 1997; Ziv et al., 1997; Agid, 1998; Müller et al., 2004; Weiner, 2006; Lipski et al., 2011; Olanow and Obeso, 2011; Paoletti et al., 2019). The beneficial or toxic effects of L-DOPA need to be investigated with more thorough experiments performed at preclinical and clinical levels.

Almost all neurodegenerative diseases have a characteristic loss of a certain special type of cells that are vulnerable to death due to metabolic deficiency (Fu et al., 2018; Muddapu et al., 2020). PD is characterized by loss of dopaminergic neurons in the substantia nigra pars compacta (SNc), which results in cardinal symptoms, such as tremor, rigidity, bradykinesia, and postural instability (Goldman and Postuma, 2014). The root cause of SNc cell loss in PD is still not decisively elucidated. Recent studies have proposed that PD is described to be resulting from the metabolic deficiency in SNc (Connolly et al., 2014; Pacelli et al., 2015; Muddapu et al., 2019; Muddapu and Chakravarthy, 2020). The vulnerable cells of SNc are projection neurons with large axonal arbors of complex morphologies, requiring a tremendous amount of energy to maintain information processing activities (Bolam and Pissadaki, 2012; Pissadaki and Bolam, 2013; Giguère et al., 2019; Muddapu et al., 2020). Due to substantial energy requirements, SNc neurons exhibit higher basal metabolic rates and higher oxygen consumption rates, which result in oxidative stress (Pacelli et al., 2015). With the help of computational models, Muddapu and co-workers have recently suggested that the excitotoxic loss of SNc cells might be due to energy deficiency occurring at different levels of neural hierarchy—systems, cellular and subcellular (Muddapu et al., 2019; Muddapu and Chakravarthy, 2020, 2021).

In this article, we investigated using computational modeling, the hypothesis that L-DOPA-induced toxicity can occur in two ways: by promoting DA-induced oxidative stress (autoxidation-relevant; Pardo et al., 1995; Walkinshaw and Waters, 1995; Carvey et al., 1997; Melamed et al., 1998; Takashima et al., 1999; Borah and Mohanakumar, 2010) or by exacerbating excitotoxicity in SNc (autoxidation-irrelevant; Pardo et al., 1993; Cheng et al., 1996; Blomeley and Bracci, 2008; Blomeley et al., 2009; Thornton and Vink, 2015), or by both the mechanisms, which might be precipitated by energy deficiency. To investigate our hypothesis, we propose a multiscale computational model of L-DOPA-induced toxicity in SNc, which will help us understand the mechanism behind neurodegeneration due to L-DOPA and give insights into developing disease-modifying therapeutics.

MATERIALS AND METHODS

The proposed model of L-DOPA-induced toxicity (LIT) consists of the cortico-basal ganglia system. We modeled a part of the basal ganglia system, comprising the following nuclei: SNc, striatum (STR), subthalamic nucleus (STN), and globus pallidus externa (GPe). Within the SNc, we separately considered SNc soma (cell body) and SNc terminal (bouton) that make contact with striatal neurons. The medium spiny neurons (MSNs) in the striatum are classified into two types based on the DA receptor present, namely, D1 and D2-types. In the proposed LIT model, we considered only D1-type MSNs because they only project GABAergic inputs to SNc neurons (Gerfen, 1985). Within the striatum, we modeled D1-type receptor-expressing MSNs of two subtypes: (1) D1-MSNs that release GABA only [D1-MSN (G)] [GABAergic (G) only] and (2) D1-MSNs that co-release GABA and substance P [D1-MSN (GS)] [GABAergic (G), and substance P (S)]. The pyramidal neurons in the cortex are classified into three types: regular spiking (RS), intrinsic (inactivating) bursting, and non-inactivating bursting neurons. The regular spiking neurons are further subdivided into fast-adapting and slow-adapting types of neurons (Degenetais, 2002). The time-averaged firing rate of all neuronal types varies widely, ranging from < 1 *Hz* up to several tens of hertz (Griffith and Horn, 1966; Koch and Fuster, 1989). The spontaneous firing rates of all pyramidal cortical neuronal types are as follows: fast-adapting RS (0.62 ± 0.75 *Hz*), slow-adapting RS (0.90 ± 1.23 *Hz*), intrinsic bursting (3.1 ± 2.6 *Hz*) , and non-inactivating bursting (2.8 ± 3.2 *Hz*) (Degenetais, 2002). In the cortex (CTX), the fast-adapting RS pyramidal neurons are modeled. Neurons in each nucleus are arranged as a two-dimensional lattice (**Figure 1**). The simulations were performed by numerical integration using MATLAB (RRID:SCR_001622) with a time step of 0.1*ms*.

Glucose and oxygen inputs to SNc cells were reduced to implement energy deficiency conditions in the proposed model. As the number of SNc neurons under energy deficiency increases, the dopaminergic tone to the striatum decreases due to SNc terminal loss. The dopamine deficiency leads to lesser excitation of MSN neurons by pyramidal neurons in the cortex; as a result, SNc neurons get disinhibited. Disinhibition from MSN leads to overactivity of SNc neurons, resulting in SNc neurons degeneration due to excitotoxicity.

To examine L-DOPA's role in the degeneration of SNc neurons in PD, we administered L-DOPA after a certain percentage of SNc neuronal loss due to energy deficiency and investigated how L-DOPA changes the course of SNc cell loss.

Izhikevich (Spiking) Neuron Model (STN, GPe, MSN, and CTX)

The Izhikevich neuron models can exhibit biologically realistic firing patterns at a relatively low computational expense (Izhikevich, 2003). The proposed model of LIT consists of MSN [D1-MSN (G) and D1-MSN (GS)], STN, GPe, and CTX. These nuclei are modeled as Izhikevich spiking neuron models arranged in the form of two-dimensional lattices (**Figure 1**). Based on the anatomical data of the rat basal ganglia (**Supplementary Material 1**), the neuronal population

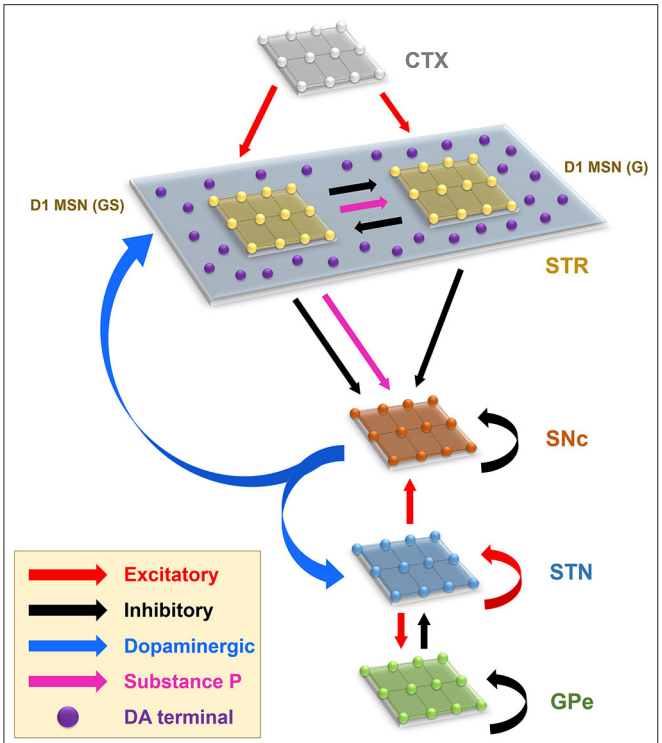

FIGURE 1 | Model architecture of the levodopa-induced toxicity. CTX, cortex; STR, striatum; D1 MSN (GS), D1-type medium spiny neuron (GABAergic and Substance P); D1 MSN (G), D1-type medium spiny neuron (GABAergic); SNc, substantia nigra pars compacta; STN, subthalamic nucleus; GPe, globus pallidus externa; DA, dopamine.

sizes in the model were selected (Oorschot, 1996; Arbuthnott and Wickens, 2007). The Izhikevich parameters for MSN were adapted from Humphries et al. (2009); for STN and GPe, they were adapted from Michmizos and Nikita (2011) and Mandali et al. (2015), respectively, and those of CTX were adapted from Izhikevich (2003), all given in **Supplementary Material 2**. The external bias current (I^x) was adjusted to match the firing rate of nuclei with published data (Tripathy et al., 2015).

The Izhikevich neuron model of STN, GPe, CTX, and MSN neurons consists of two variables: membrane potential (v^x) and membrane recovery variable (u^x):

$$C^x * \frac{d(v_{ij}^x)}{dt} = \varphi_1 - u_{ij}^x + I_{ij}^x + I_{ij}^{syn} \quad (1)$$

$$\frac{d(u_{ij}^x)}{dt} = a(b * \varphi_2 - u_{ij}^x) \quad (2)$$

$$if\ x = STN\ or\ GPe\ or\ CTX,\ \ then \quad (3)$$

$$\varphi_1 = 0.04(v_{ij}^x)^2 + 5v_{ij}^x + 140$$

$$\varphi_2 = v_{ij}^x$$

$$if\ x = MSN,\ \ then \quad (4)$$

$$\varphi_1 = k^x\left(v_{ij}^x - v_r^x\right)\left(v_{ij}^x - v_t^x\right)$$

$$\varphi_2 = \left(v_{ij}^x - v_r^x\right)$$

Resetting:

$$if\ \ v_{ij}^x \geq v_{peak}^x,\ \ then \qquad \left\{\begin{matrix} v_{ij}^x \leftarrow c \\ u_{ij}^x \leftarrow u_{ij}^x + d \end{matrix}\right\} \quad (5)$$

where, v_{ij}^x, u_{ij}^x, I_{ij}^x, and$I_{ij}^{syn}$are the membrane potential, the membrane recovery variable, the external bias current, and the total synaptic current received to neuron x at the location (i, j), respectively; v_t^x and v_r^x are the threshold and resting potentials, respectively; $k^x$is the membrane constant, C^x is the membrane capacitance, $\{a, b, c, d\}$ are Izhikevich parameters; v_{peak}^x is the maximum membrane voltage set to neuron with x being GPe or CTX or STN or MSN neuron.

Biophysical Neuron Model (SNc Soma)

The biophysical neuronal model of SNc in the proposed LIT model was adapted from Muddapu and Chakravarthy (2021). The detailed biophysical model of SNc neuron consists of soma and terminal, which includes cellular and molecular processes, such as ion channels (including active ion pumps and ion exchangers), a calcium buffering mechanism (calcium-binding proteins, calcium sequestration organelles, such as endoplasmic reticulum and mitochondria), an energy metabolism (glycolysis and oxidative phosphorylation), DA turnover processes (synthesis, storage, release, reuptake, and metabolism), molecular pathways involved in PD pathology (reactive oxygen species (ROS) formation and alpha-synuclein aggregation), and apoptotic pathways. The dynamics of SNc membrane potential $\left(v^{SNc}\right)$ is given as,

$$\frac{d(v_{ij}^{SNc})}{dt} = \frac{F * v_{cyt}}{C^{SNc} * \mathcal{A}_{pmu}} * \left[J_{m,Na} + 2 * J_{m,Ca} + J_{m,K} + J_{inp}\right] \quad (6)$$

where F is the Faraday's constant, C^{SNc} is the SNc membrane capacitance, v_{cyt} is the cytosolic volume, $\mathcal{A}_{pmu}$ is the cytosolic area, $J_{m,Na}$ is the sodium membrane ion flux, $J_{m,Ca}$ is the calcium membrane ion flux, $J_{m,K}$ is the potassium membrane ion flux, J_{inp} is the overall input current flux. The detailed information about the SNc neuron model is provided in **Supplementary Material 3**.

Biochemical Dopamine Terminal Model (SNc Terminal)

The biochemical DA terminal of SNc in the proposed LIT model was adapted from Muddapu and Chakravarthy (2021). The biochemical model of DA terminal consists of DA turnover processes, energy metabolism, and molecular pathways involved in PD pathology. The terminal is divided into two compartments, namely, intracellular (cytoplasmic and vesicular) and extracellular compartments. The DA dynamics in the extracellular compartment ($[DA_e]$) was modeled as,

$$\frac{d([DA_e])}{dt} = J_{rel} - J_{DAT} - J_{eda}^o \quad (7)$$

where, J_{rel} represents the flux of calcium-dependent DA release from the DA terminal, J_{DAT} represents the unidirectional flux

of DA translocated from the extracellular compartment (ECS) into the intracellular compartment (cytosol) *via* DA plasma membrane transporter (DAT), and J^{o}_{eda} represents the outward flux of DA degradation, which clears DA from ECS.

The DA dynamics in the intracellular compartment ($[DA_i]$) was modeled as

$$\frac{d([DA_i])}{dt} = \frac{d([DA_c])}{dt} + \frac{d([DA_v])}{dt} \tag{8}$$

where $[DA_c]$ and $[DA_v]$ refer to the DA concentrations in the cytosolic and vesicular compartments, respectively.

The DA dynamics in the cytosolic compartment ($[DA_c]$) is given by,

$$\frac{d([DA_c])}{dt} = J_{DAT} - J_{VMAT} - J^{o}_{cda} + J_{ldopa} \tag{9}$$

where, J_{DAT} represents the unidirectional flux of DA translocated from ECS into the cytosol through DAT, J_{VMAT} represents the flux of DA into vesicle through vesicular monoamine transporters (VMAT), J^{o}_{ida} represents the outward flux of DA degradation, which clears DA from the cytosol, and J_{ldopa} represents the flux of synthesized cytosol DA from levodopa, which is induced by calcium.

The DA dynamics in the vesicular compartment ($[DA_v]$) is given by,

$$\frac{d([DA_v])}{dt} = J_{VMAT} - J_{rel} \tag{10}$$

where, J_{rel} represents the flux of calcium-dependent DA release from the DA terminal and J_{VMAT} represents the flux of DA stored into a vesicle.

Based on the membrane activity, the DA turnover and other molecular processes were modulated in the terminal. The modulation of neuronal activity on the terminal was carried on by calcium dynamics, where calcium modulates DA synthesis and release. The calcium-induced synthesis of DA is given as,

$$J_{ldopa} = f([Ca_i]) \tag{11}$$

The calcium-induced release of DA is given as,

$$J_{rel} = f([Ca_i]) \tag{12}$$

where $[Ca_i]$ is the intracellular calcium concentration in the DA terminal. Detailed information about the SNc terminal model was provided in **Supplementary Material 4**.

Synaptic Connections

The synaptic connectivity among different neuronal populations was modeled as a standard single exponential model of postsynaptic currents (Humphries et al., 2009) as follows:

$$\tau_{Recep} * \frac{d(h^{x\to y}_{ij})}{dt} = -h^{x\to y}_{ij} + S^{x}_{ij}(t) \tag{13}$$

$$I^{x\to y}_{ij}(t) = W_{x\to y} * h^{x\to y}_{ij}(t) * (v^{y}_{ij}(t) - E_{Recep}) \tag{14}$$

The N-Methyl-D-aspartic Acid (NMDA) current was regulated by voltage-dependent magnesium channels, which were modeled as,

$$B_{ij}(v_{ij}) = \frac{1}{1 + \left(\frac{[Mg^{2+}]}{3.57} * e^{-0.062 * v^{y}_{ij}(t)}\right)} \tag{15}$$

where, $h^{x\to y}_{ij}$ is the gating variable for the synaptic current from x to y, τ_{Recep} is the decay constant for the synaptic receptor, S^{x}_{ij} is the spiking activity of neuron x at time t, $W_{x\to y}$ is the synaptic weight from neuron x to y, v^{y}_{ij} is the membrane potential of the neuron y for the neuron at the location (i, j), E_{Recep} is the receptor-associated synaptic potential ($Recep$ = NMDA/AMPA/GABA), and $\left[Mg^{2+}\right]$ is the magnesium ion concentration. The time constants of gamma-amino butyric acid (GABA), alpha-amino-3-hydroxy-5-methyl-4-isoxazole propionic acid (AMPA), and NMDA in GPe, CTX, MSN, SNc, and STN were chosen from Götz et al. (1997) as given in **Supplementary Material 2**.

To accommodate extensive axonal arborization of SNc neurons (Bolam and Pissadaki, 2012), we considered one-to-many projections from SNc soma to SNc terminals (**Supplementary Material 5**). The connectivity patterns among different neuronal populations were given in **Supplementary Material 5**.

Total Synaptic Current Received by Each Neuron Type

SNc

The total synaptic current received by an *SNc* neuron at the lattice position (i,j) is the summation of the glutamatergic input from the *STN* neurons, considering both *NMDA* and *AMPA* receptor activation, comprising the GABAergic inputs from the $D1-MSN\ (GS)$ and $D1-MSN\ (G)$ neurons and the lateral GABAergic current from other *SNc* neurons.

$$\begin{aligned} I^{SNcsyn}_{ij} = {} & F_{STN\to SNc} * \left(I^{NMDA\to SNc}_{ij} + I^{AMPA\to SNc}_{ij}\right) \\ & + \left(F_{D1-MSN\ (G)\to SNc} * I^{D1-MSN(G)\to SNc}_{ij}\right) \\ & + \left(F_{D1-MSN\ (GS)\to SNc} * I^{D1-MSN(GS)\to SNc}_{ij}\right) + I^{GABAlat}_{ij} \end{aligned} \tag{16}$$

where $I^{NMDA\to SNc}_{ij}$ and $I^{AMPA\to SNc}_{ij}$ are the glutamatergic currents corresponding to *NMDA* and *AMPA* receptors activation, respectively; $I^{D1-MSN(G)\to SNc}_{ij}$ and $I^{D1-MSN(GS)\to SNc}_{ij}$ are the GABAergic inputs from the $D1-MSN\ (G)$ and $D1-MSN\ (GS)$ neurons, respectively; $I^{GABAlat}_{ij}$ is the lateral GABAergic current from other *SNc* neurons; $F_{STN\to SNc}$ is the scaling factor in the glutamatergic current from the *STN* neuron; $F_{D1-MSN\ (G)\to SNc}$ is the scaling factor in the GABAergic current from $D1-MSN\ (G)$ neuron; $F_{D1-MSN\ (GS)\to SNc}$ is the scaling factor in the GABAergic current from the $D1-MSN\ (GS)$ neuron.

GPe

The total synaptic current received by a *GPe* neuron at the lattice position (i,j) is the summation of the glutamatergic input

from the *STN* neurons, considering both *NMDA* and *AMPA* receptors activation and the lateral GABAergic current from other *GPe* neurons.

$$I_{ij}^{GPesyn} = I_{ij}^{NMDA\rightarrow GPe} + I_{ij}^{AMPA\rightarrow GPe} + I_{ij}^{GABAlat} \quad (17)$$

where $I_{ij}^{NMDA\rightarrow GPe}$ and $I_{ij}^{AMPA\rightarrow GPe}$ are the glutamatergic currents from the *STN* neuron, considering both *NMDA* and *AMPA* receptors activation, respectively; $I_{ij}^{GABAlat}$ is the lateral GABAergic current from other *GPe* neurons.

STN

The total synaptic current received by an *STN* neuron at the lattice position (i,j) is the summation of the GABAergic input from the *GPe* neurons and the lateral glutamatergic input from other *STN* neurons, considering both *NMDA* and *AMPA* receptors activation.

$$I_{ij}^{STNsyn} = I_{ij}^{GABA\rightarrow STN} + I_{ij}^{NMDAlat} + I_{ij}^{AMPAlat} \quad (18)$$

where $I_{ij}^{GABA\rightarrow STN}$ is the GABAergic current from the *GPe* neuron; $I_{ij}^{NMDAlat}$ and $I_{ij}^{AMPAlat}$ are the lateral glutamatergic currents from other *STN* neurons, considering both *NMDA* and *AMPA* receptors activation, respectively.

D1-MSN (GS)

The total synaptic current received by a $D1-MSN\ (GS)$ neuron at the lattice position (i,j) is the summation of the GABAergic input from the $D1-MSN\ (G)$ neurons and the glutamatergic input from *CTX* neurons, considering both *NMDA* and *AMPA* receptors activation.

$$I_{ij}^{D1-MSN(GS)syn} = I_{ij}^{GABA\rightarrow D1-MSN(GS)} + I_{ij}^{NMDA\rightarrow D1-MSN(GS)} + I_{ij}^{AMPA\rightarrow D1-MSN(GS)} \quad (19)$$

where $I_{ij}^{GABA\rightarrow D1-MSN(GS)}$ is the GABAergic current from the $D1-MSN(G)$ neuron, $I_{ij}^{NMDA\rightarrow D1-MSN(GS)}$, and $I_{ij}^{AMPA\rightarrow D1-MSN(GS)}$ are the glutamatergic currents from *CTX* neurons, considering both *NMDA* and *AMPA* receptors activation, respectively.

D1-MSN (G)

The total synaptic current received by a $D1-MSN\ (G)$ neuron at the lattice position (i,j) is the summation of the GABAergic input from the $D1-MSN\ (GS)$ neurons and the glutamatergic input from *CTX* neurons, considering both *NMDA* and *AMPA* receptor activation.

$$I_{ij}^{D1-MSN(G)syn} = I_{ij}^{GABA\rightarrow D1-MSN(G)} + I_{ij}^{NMDA\rightarrow D1-MSN(G)} + I_{ij}^{AMPA\rightarrow D1-MSN(G)} \quad (20)$$

where $I_{ij}^{GABA\rightarrow D1-MSN(G)}$ is the GABAergic current from the $D1-MSN(GS)$ neuron, and $I_{ij}^{NMDA\rightarrow D1-MSN(G)}$, and $I_{ij}^{AMPA\rightarrow D1-MSN(G)}$ are the glutamatergic currents from *CTX* neurons, considering both *NMDA* and *AMPA* receptors activation, respectively.

Lateral Connections

The lateral connections in SNc, STN, and GPe were modeled as Gaussian neighborhoods (Muddapu et al., 2019),

$$w_{ij,pq}^{m\rightarrow m} = A_m * e^{\frac{-d_{ij,pq}^2}{R_m^2}} \quad (21)$$

$$d_{ij,pq}^2 = (i-p)^2 + (j-q)^2 \quad (22)$$

where $w_{ij,pq}^{m\rightarrow m}$ is the lateral connection weight of neuron type m at the location (i,j), $d_{ij,pq}$ is the distance from the center neuron (p,q), R_m is the variance of Gaussian, and A_m is the strength of lateral synapse, $m = GPe\ or\ STN\ or\ SNc$.

The connections within SNc and GPe populations were considered inhibitory and within STN as excitatory (Muddapu et al., 2019) (**Figure 1**). No lateral connections were considered for both the MSNs and CTX populations. The lateral currents in the STN and GPe were modeled similar to Equations 13–15 and in the case of SNc, which was modeled as,

$$H_\infty = \frac{1}{1+e^{\left(\frac{-\left(v_{ij}^x-\theta_g-\theta_g^H\right)}{\sigma_g^H}\right)}} \quad (23)$$

$$\frac{d(s_{ij}^{x\rightarrow y})}{dt} = \alpha * \left(1-s_{ij}^{x\rightarrow y}\right) * H_\infty - \beta * s_{ij}^{x\rightarrow y} \quad (24)$$

$$I_{ij}^{x\rightarrow y}(t) = W_{x\rightarrow y} * s_{ij}^{x\rightarrow y *} \left(v_{ij}^y(t) - E_{GABA}\right) \quad (25)$$

where $I_{ij}^{x\rightarrow y}$ is the synaptic current from neuron x to y, $W_{x\rightarrow y}$ is the synaptic conductance from neurons x to y, v_{ij}^x and v_{ij}^y are the membrane potential of the neurons x and y, respectively, for the neuron at the location (i, j), E_{GABA} is the GABAergic receptor potential, and $s_{ij}^{x\rightarrow y}$ is the synaptic gating variable for the neuron. The parametric values of α, β, θ_g, θ_g^H, σ_g^H were adapted from Rubin and Terman (2004) and given in **Supplementary Material 6**.

Neuromodulatory Effect on the Neuronal Populations

The effect of neuromodulators, such as DA and substance P (SP), in the proposed LIT model was modeled based on Buxton et al. (2017) and Muddapu et al. (2019), respectively.

Dopaminergic Modulation

DA-modulated lateral connection strength in SNc, STN, and GPe populations. As the DA level increases, the lateral connection strength in SNc and GPe increases, whereas, in the case of STN, it decreases (Kreiss et al., 1997). DA-modulation of lateral connection strength was modeled as,

$$A^{STN} = s_{\max}^{STN} * e^{\left(-cd_{stn} * DA_s(t)\right)} \quad (26)$$

$$A^{GPe} = s_{\min}^{GPe} * e^{\left(cd_{gpe} * DA_s(t)\right)} \quad (27)$$

$$A^{SNc} = s_{\min}^{SNc} * e^{\left(cd_{snc} * DA_s(t)\right)} \quad (28)$$

where $s_{\max}^{STN}$, $s_{\min}^{GPe}$, and $s_{\min}^{SNc}$ are lateral connection strengths at the basal spontaneous activity of the population without any external dopaminergic influence in *STN*, *GPe*, and *SNc*, respectively. cd_{stn}, cd_{gpe}, and cd_{snc} were the factors by which DA affects the lateral connections in *STN*, *GPe*, and *SNc* populations, respectively, and $DA_s\,(t)$ is the instantaneous DA level, the spatial average DA concentration of all the terminals. All parameter values are given in **Supplementary Material 6**.

The post-synaptic effect of DA in SNc, STN, and GPe was modeled similar to Muddapu et al. (2019),

$$W_{x\to y} = \left(1 - cd2{*}DA_s\,(t)\right){*}w_{x\to y} \tag{29}$$

where $w_{x\to y}$ is the synaptic weight ($STN \to GPe$, $GPe \to STN$, $STN \to STN$, $GPe \to GPe$, $STN \to SNc$, $SNc \to SNc$, $MSN \to SNc$), $cd2$ is the parameter that affects the post-synaptic current, and $DA_s(t)$ is the instantaneous DA level.

The effect of DA in the MSN population occurs on both synaptic and intrinsic ion channels (Surmeier et al., 2007). The cortical inputs to MSN were modulated by DA as similar to Humphries et al. (2009),

$$I_{DA}^{x}\,(t) = I_{CTX\to MSN}^{x}\,(t) * \left(1 + \left(\frac{\beta_{DA}}{\alpha_{DA}^{y}}\right){*}DA_s\,(t)\right) \tag{30}$$

where $I_{CTX\to MSN}^{x}$ is the synaptic current from *CTX* to *MSN* (where $x = NMDA\ or\ AMPA$), $DA_s\,(t)$ is the instantaneous DA level, α_{DA}^{y} is the DA effect on the y neuron [where $y = D1-MSN\,(GS)\ or\ D1-MSN\,(G)$)], and β_{DA} was adapted from Humphries et al. (2009).

In addition to modulating cortical afferent connections, DA also has effects on the intrinsic ion channels (Humphries et al., 2009), which was modeled in the Izhikevich neuron model as,

$$v_r^{DA} = v_r^{MSN}{*}\left(1 + K^{MSN}{*}\left(\frac{DA_s\,(t)}{\alpha_{DA}^{y}}\right)\right) \tag{31}$$

$$d_{msn}^{DA} = d_{msn}{*}\left(1 - L^{MSN}{*}\left(\frac{DA_s\,(t)}{\alpha_{DA}^{y}}\right)\right) \tag{32}$$

where v_r^{DA} and d_{msn}^{DA} are the DA-modulated resting potential and after-spike reset value of *MSN*, respectively, v_r^{MSN}, and d_{msn} are the resting potentials and after-spike reset value of *MSN*, respectively, $DA_s\,(t)$ is the instantaneous DA level; α_{DA}^{y} is the DA effect on the y neuron [where $y = D1-MSN\,(GS)\ or\ D1-MSN\,(G)$)], and K^{MSN} and L^{MSN} were adapted from Humphries et al. (2009).

Substance P Modulation

SP modulates excitatory afferent connections of SNc (soma) and D1 MSN (G) in the proposed LIT model (**Figure 1**). It was observed that SP modulates the glutamatergic afferents of MSNs directly (Blomeley and Bracci, 2008) or indirectly (Blomeley et al., 2009) by co-release of SP by GABAergic D1 MSNs (Reiner et al., 2010; Buxton et al., 2017). In the proposed LIT model, we modeled SP-modulation of glutamatergic afferents of the D1 MSN (G) population by the D1 MSN (GS) population similar to Buxton et al. (2017). It was observed that SP and tachykinin NK1 receptor (NK1-R) are highly expressed within the SNc (Mantyh et al., 1984; Sutoo et al., 1999; Ribeiro-da-Silva and Hökfelt, 2000; Lessard and Pickel, 2005; Thornton and Vink, 2015). SP-containing striatal neurons project to dopaminergic neurons where SP potentiates the release of striatal DA (Brimblecombe and Cragg, 2015; Thornton and Vink, 2015). It was reported that a DA-dependent decrease in SP levels was observed in the basal ganglia regions (Sivam, 1991; Thornton et al., 2010; Thornton and Vink, 2015). Therefore, there is a feedback regulation between DA and SP, which helps maintain DA homeostasis (Thornton et al., 2010; Thornton and Vink, 2015). In the proposed LIT model, we assumed that SP modulates STN glutamatergic inputs to SNc such that increased SP levels lead to excitation of SNc, which, in turn, enhances the striatal DA level, modeled similar to Buxton et al. (2017). Also, we incorporated SP-DA feedback regulation (SDFR) in SP-modulation in the proposed LIT model. The SP-modulation of glutamatergic inputs to D1 MSN (G) and SNc along with SDFR was given as,

$$I_{ij}^{x\to y}\,(t) = W_{x\to y}{*}h_{ij}^{x\to y}\,(t){*}NSP{*}SDFR{*}\left(v_{ij}^{y}\,(t) - E_{Recep}\right) \tag{33}$$

$$NSP = \left(1 + w_{sp}{*}N_{ij}^{sp}\left(t - \tau_d^{sp}\right)\right) \tag{34}$$

$$N_{ij}^{sp}\,(t) = \beta_{sp}{*}\left[1 - e^{\left(\frac{-A_{ij}^{sp}(t)}{\lambda_{sp}}\right)^{b_{sp}}}\right] \tag{35}$$

$$A_{ij}^{sp}\,(t) = \left[e^{\left(\frac{-S_{ij}^{x}(t)}{\tau_f^{sp}}\right)} - e^{\left(\frac{-S_{ij}^{x}(t)}{\tau_r^{sp}}\right)}\right] \tag{36}$$

$$SDFR = (1 - DA_s\,(t)) \tag{37}$$

where $h_{ij}^{x\to y}$is the gating variable for the synaptic current from x to y, $W_{x\to y}$ is the synaptic weight from neurons x to y, S_{ij}^{x} is the spiking activity of neuron x at time t, v_{ij}^{y} is the membrane potential of the neuron y for the neuron at the location (i, j), E_{Recep} is the receptor-associated synaptic potential ($Recep$ = NMDA/AMPA), τ_d^{sp} is the fixed time delay between MSN activity and the onset of neuropeptide effect, β_{sp} is the gain factor, N_{ij}^{sp} is the modulatory effect of SP, w_{sp} is the influence of SP on $w_{STN\to SNc}$, A_{ij}^{sp} is the amplitude of SP released, which is induced by spiking activity $\left(S_{ij}^{x}\right)$, $DA_s\,(t)$ is the instantaneous DA level, b_{sp} and λ_{sp} were adapted from Buxton et al. (2017) and given in **Supplementary Material 6**.

Neurodegeneration of SNc Neurons

Calcium plays a dual role in living organisms as a survival factor or a ruthless killer (Orrenius et al., 2003). For the survival of neurons, minimal (physiological) levels of glutamate stimulation are required. Under normal conditions, calcium concentration within a cell is tightly regulated by pumps, transporters, calcium-binding proteins, endoplasmic reticulum (ER), and mitochondria

(Wojda et al., 2008; Surmeier et al., 2011). Due to prolonged calcium influx driven by excitotoxicity, the calcium homeostasis within the cell is disturbed, which results in cellular imbalance, leading to the activation of apoptotic pathways (Bano and Ankarcrona, 2018). The SNc soma undergoes degeneration when a calcium build-up inside the cell becomes high, resulting in calcium loading inside ER and mitochondria, which leads to ER-stress-induced and mitochondrial-induced apoptosis, respectively (Malhotra and Kaufman, 2011). In the proposed LIT model, we incorporate a mechanism of programmed cell death, whereby an SNc neuron under high stress (high calcium levels) kills itself. The stress in a given SNc neuron was observed by monitoring the intracellular calcium concentrations in the cytoplasm, ER, and mitochondria.

The SNc neuron undergoes ER-stress-induced apoptosis when calcium levels in ER cross a certain threshold (ER_{thres}). Under such conditions, the particular SNc neuron gets eliminated as follows,

$$if \quad Ca_{ij}^{ER}(t) > ER_{thres}, \quad then \quad v_{ij}^{SNc}(t) = 0 \tag{38}$$

where Ca_{ij}^{ER} is the calcium concentration in the ER, ER_{thres} is the calcium concentration threshold after which ER-stress-induced apoptosis gets initiated $\left(ER_{thres} = 2.15\,x\,10^{-3}\ mM\right)$, and v_{ij}^{SNc} is the membrane voltage of the neuron at the lattice position $\left(i,j\right)$.

The ER calcium concentration ($[Ca_{er}]$) dynamics is given by,

$$\frac{d([Ca_{er}])}{dt} = \frac{\beta_{er}}{\rho_{er}} * \left(J_{serca,er} - J_{ch,er} - J_{leak,er}\right) \tag{39}$$

where β_{er} is the ratio of free calcium to total calcium concentration in the ER, ρ_{er} is the volume ratio between the ER and cytosol, $J_{serca,er}$ is the calcium buffering flux by ER uptake of calcium through SERCA, $J_{ch,er}$ is the calcium efflux from ER by CICR mechanism, and $J_{leak,er}$ is the calcium leak flux from ER. The detailed information about the calcium dynamics in ER was provided in **Supplementary Material 8**.

The SNc neuron undergoes mitochondria-induced apoptosis when calcium levels in mitochondria cross a certain threshold (MT_{thres}). Then, that particular SNc neuron will be eliminated as follows,

$$if \quad Ca_{ij}^{MT}(t) > MT_{thres}, \quad then \quad v_{ij}^{SNc}(t) = 0 \tag{40}$$

where Ca_{ij}^{MT} is the calcium concentration in mitochondria, MT_{thres} is the calcium concentration threshold beyond which mitochondria-induced apoptosis gets initiated ($MT_{thres} = 0.0215\ mM$), and v_{ij}^{SNc} is the membrane voltage of neurons at the lattice position $\left(i,j\right)$.

The MT calcium concentration ($[Ca_{mt}]$) dynamics is given by,

$$\frac{d([Ca_{mt}])}{dt} = \frac{\beta_{mt}}{\rho_{mt}} * \left(J_{mcu,mt} - J_{out,mt}\right) \tag{41}$$

where β_{mt} is the ratio of free calcium to total calcium concentration in the ER, ρ_{mt} is the volume ratio between the MT and cytosol, $J_{mcu,mt}$ is the calcium buffering flux by MT uptake of calcium through MCUs, and $J_{out,mt}$ is the calcium efflux from MT through sodium-calcium exchangers, mPTPs, and non-specific leak flux. The detailed information about the calcium dynamics in MT is provided in **Supplementary Material 8**.

When calcium concentration in ER crosses a certain threshold, there is an efflux of excess calcium from ER out into the cytoplasm, which activates calpain and proapoptotic factors through the cytochrome-c-independent apoptotic pathway. Similarly, when calcium concentration in MT crosses a certain threshold, excess calcium in MT results in the formation of mitochondrial transition pores (MTPs). Proapoptotic cytochrome-c is released from MT through MTPs, which triggers cytochrome-c-dependent apoptosis. In the proposed modeling study, when the apoptotic signal gets activated from either of the pathways in a particular neuron, we formulated an approach wherein that particular neuron was eliminated by making $v_{ij}^{SNc}(t) = 0$ from the time t till the end of the simulation.

Terminal Degeneration of SNc Neurons

DA is the primary contributor to the oxidative stress in the neuron (Luo and Roth, 2000; Lotharius et al., 2005; Miyazaki and Asanuma, 2008). To evade oxidative stress, SNc neurons tightly regulate the DA turnover processes (Guo et al., 2018). It was inferred that methamphetamine-induced dopaminergic nerve terminal loss (Ricaurte et al., 1982, 1984; Cadet et al., 2003; Ares-Santos et al., 2014) is precipitated by oxidative stress (De Vito and Wagner, 1989) by enhancing cytoplasmic DA levels (Larsen et al., 2002; Mark et al., 2004). In the proposed LIT model, the oxidative stress in the SNc terminals was observed by monitoring intracellular ROS concentration. The SNc terminal is eliminated when ROS levels in the terminal cross a certain threshold (ROS_{thres}) as follows,

$$if \quad \left[ROS_{ij}^{T}\right](t) > ROS_{thres}, \quad then \quad Ca_{ij}^{T}(t) = 0 \tag{42}$$

where ROS_{ij}^{T} is the ROS concentration in the SNc terminal, ROS_{thres} is the ROS concentration threshold above which oxidative stress-induced terminal degeneration gets initiated ($ROS_{thres} = 0.0147\ mM$); Ca_{ij}^{T} is the calcium concentration of the SNc terminal at the lattice position $\left(i,j\right)$.

The ROS concentration in the SNc terminal was given as,

$$\frac{d(\left[ROS_{ij}^{T}\right])}{dt} = J_{leak} + J_{env} + J_{dopa} - J_{cat} - J_{dox} \tag{43}$$

where J_{leak} is the flux of oxidative stress due to mitochondrial leakage, J_{env} is the flux of external oxidative stress (includes environmental toxins, inflammatory responses, etc.), J_{dopa} is the flux of oxidative stress due to excess cytoplasmic dopamine, J_{cat} is the catabolizing flux of ROS by a catalase enzyme, and J_{dox} is the flux of the GSH-dependent ROS-scavenging pathway. The detailed information about the ROS formation is provided in **Supplementary Material 9**.

When the ROS level crosses a certain threshold, excess ROS triggers degeneration of the terminal. In the proposed modeling study, when the ROS level crosses the threshold

in a particular terminal, we formulate an approach wherein that particular terminal was eliminated by making $Ca_{ij}^{T}(t) = 0$ from the time t till the end of the simulation since calcium plays an important role in the function of the terminal.

Neuroprotective Strategies

Levodopa Therapy

To alleviate PD symptoms, the most potent drug, L-DOPA, a precursor of DA, is typically administrated (Jankovic and Aguilar, 2008). During medication, serum L-DOPA is taken up from the blood into the extracellular fluid compartment by aromatic L-amino acid transporter by competing with other amino acids (Camargo et al., 2014; Figura et al., 2018). L-DOPA, thus absorbed into the bloodstream, later enters SNc terminals and gets converted to DA by aromatic L-amino acid decarboxylase (Khor and Hsu, 2007). In the proposed LIT model, serum L-DOPA uptake into the SNc terminal from the blood was modeled as a single step along with competition with other amino acids, such as tyrosine and tryptophan (Porenta and Riederer, 1982). It was described using the Michaelis-Menten equation (Chou, 1976) where serum L-DOPA competes with serum tyrosine and serum tryptophan for transporter (Reed et al., 2012) as given below:

$$V_{trans} = \frac{V_{trans}^{\max} * [LDOPA_S]}{K_m^{LDOPA_s} * \left(1 + \frac{[TYR_s]}{K_a^{TYR_s}} + \frac{[TRP_s]}{K_a^{TRP_s}}\right) + [LDOPA_S]} \quad (44)$$

where $V_{trans}^{\max}$ is the maximum flux through aromatic L-amino acid transporter, $[LDOPA_S]$ is the serum L-DOPA concentration, $K_m^{LDOPA_s}$ is the concentration of $[LDOPA_S]$ at which velocity of the transporter attained half of the maximal velocity, $[TYR_s]$ is the serum tyrosine concentration, and $[TRP_s]$ is the serum tryptophan concentration. $K_a^{TYR_s}$ is the affinity constant for $[TYR_s]$, and $K_a^{TRP_s}$ is the affinity constant for $[TRP_s]$.

L-DOPA therapy was implemented in the proposed LIT model by the following criterion,

$$[LDOPA_s]\left(N_{sc}^{z}, t\right) = \begin{cases} 0, & N_{sc}^{z}(t) > T_l^z \\ \left[LDOPA_s^{med}\right], & N_{sc}^{z}(t) \le T_l^z \end{cases} \quad (45)$$

$$T_l^z = P_z^{snc} - \left(pcl * P_z^{snc}\right) \quad (46)$$

where $[LDOPA_s]\left(N_{sc}^{z}, t\right)$ is the instantaneous serum $[LDOPA]$ concentration based on the number of surviving SNc neurons or terminals at the time $(t)\left(N_{sc}^{z}(t)\right)$, $\left[LDOPA_s^{med}\right]$ is the serum $[LDOPA]$ concentration during medication, $N_{sc}^{z}(t)$ is the instantaneous number of surviving SNc neurons or terminals, pcl is the percentage of SNc cell or terminal loss (25%) at which therapeutic intervention was employed $\left(pcl = 0.25\right)$, T_l^z represents the number of surviving SNc cells or terminals at which therapeutic intervention was employed, and P_z^{snc} is the population size of $z(z = \textit{soma or terminal})$. In the present study, therapeutic intervention is given at 25% SNc cell or terminal loss.

SP Antagonist Therapy

It was reported that SP exacerbated dopaminergic neurodegeneration in mice (Wang et al., 2014), and, therefore, administrating SP antagonists creates neuroprotection of dopaminergic neurons in PD (Thornton and Vink, 2012, 2015; Johnson et al., 2017). In the proposed LIT model, SP antagonist effect was implemented as,

$$w_{spa} = w_{sp} * \delta_{spa} \quad (47)$$

where w_{sp} is the influence of SP on $w_{STN \to SNc}$, δ_{spa} is the proportion of SP inhibition, and w_{spa} is the influence of SP on $w_{STN \to SNc}$ under SP antagonist therapy.

The SP antagonist therapy was implemented in the proposed LIT model by the following criterion,

$$\delta_{spa}\left(N_{sc}^{z}, t\right) = \begin{cases} 0, & N_{sc}^{z}(t) > T_l^z \\ \delta_{spa}^{med}, & N_{sc}^{z}(t) \le T_l^z \end{cases} \quad (48)$$

where $\delta_{spa}\left(N_{sc}^{z}, t\right)$ is the instantaneous proportion of SP inhibition based on the number of surviving SNc neurons or terminals at the time $(t)\left(N_{sc}^{z}(t)\right)$, δ_{spa}^{med} is the proportion of SP inhibition during therapy, $N_{sc}^{z}(t)$ is the instantaneous number of surviving SNc neurons or terminals, and T_l^z represents the number of surviving SNc cells or terminals at which therapeutic intervention was employed $(z = \textit{soma or terminal})$.

Glutathione Therapy

The impaired DA metabolism causes oxidative stress (ROS), leading to PD pathogenesis (Masato et al., 2019). It was reported that abnormal activity of vesicular monoamine transporter 2 (VMAT2) leads to reduced vesicular DA storage and increased cytoplasmic DA, which results in oxidative stress-induced degeneration of cell bodies (soma) and terminals (Kariya et al., 2005; Caudle et al., 2007; Pifl et al., 2014; Mingazov and Ugryumov, 2019). It was reported that glutathione (GSH) administration improves PD symptoms, but the underlying mechanism is unclear (Zeevalk et al., 2008; Hauser et al., 2009; Mischley et al., 2017). We suggest that glutathione administration might result in ROS scavenging, leading to neuroprotection (Li et al., 2015). In the proposed LIT model, the glutathione effect was implemented as,

$$\left[GSH_{gst}^{z}\right] = \left[GSH^{z}\right] + \left[GSH_{gs}^{z}\right] \quad (49)$$

where $\left[GSH_{gs}^{z}\right]$ is the GSH concentration under glutathione therapy $(z = \textit{soma or terminal})$, and $[GSH^z]$ is the GSH concentration.

The glutathione therapy was implemented in the proposed LIT model by the following criterion,

$$\left[GSH_{gs}^{z}\right]\left(N_{sc}^{z}, t\right) = \begin{cases} 0, & N_{sc}^{z}(t) > T_l^z \\ \left[GSH_{med}^{z}\right], & N_{sc}^{z}(t) \le T_l^z \end{cases} \quad (50)$$

where $\left[GSH_{gs}^{z}\right]\left(N_{sc}^{z}, t\right)$ is the instantaneous $[GSH]$ therapy based on the number of surviving SNc neurons or terminals at the

time (t) $\left(N_{sc}^{z}(t)\right)$, $N_{sc}^{z}(t)$ is the instantaneous number of surviving SNc neurons or terminals, $\left[GSH_{med}^{z}\right]$ is the $[GSH]$ concentration dosage under GSH therapy, and T_{l}^{z} represents the number of surviving SNc cells or terminals at which therapeutic intervention was employed ($z = soma\ or\ terminal$).

For statistical analysis, we have used the one-way ANOVA method to validate the significance of variance and rejected the null hypothesis when the p-value is <0.05 (Kim, 2017).

RESULTS

We investigated the Izhikevich models of the neurons of CTX, MSN, GPe, and STN, which were chosen from the literature (Humphries et al., 2009; Michmizos and Nikita, 2011; Mandali et al., 2015) for their characteristic firing patterns and other biological properties (**Figure 2**). Along with the above Izhikevich neuronal models, we also investigated the biophysical neuronal model of SNc for its characteristic responses (**Figure 3**). Next, we explored the effect of DA and SP on the network of MSN and SNc neurons and compared them with published data (**Figure 4**).

Then, we show the effect of homogeneous (**Figure 5**) and heterogeneous (**Figure 6**) energy deficit conditions on the progression of SNc soma and terminal loss. Next, we show the effect of extracellular L-DOPA on the progression of SNc soma and terminal loss under energy deficit conditions (**Figure 7**). Finally, we explored various therapeutics, such as L-DOPA, SP antagonist, and glutathione (**Figure 8**), for their neuroprotective effect on the progression of SNc soma and terminal loss under energy deficit conditions.

Characteristic Firing Response of Different Neuron Types

The response of a single neuron model of five different neuron types involved in the proposed LIT model for different external applied currents is shown in **Figure 2**. The basal firing frequency of the different neuronal types was matched with experimentally observed firing frequencies (Tripathy et al., 2014) by adjusting I_{ij}^{x} parameter, which is given in **Supplementary Material 2**.

The combined (spontaneous and stimulus-driven) firing rate of the pyramidal cortical neuron in the model was tuned by adjusting I_{ij}^{x} value, which falls in the range of $10 - 15\ Hz$ (**Figure 2A**). Similarly, the combined (spontaneous and cortical-driven) firing rate of MSN was tuned such that it falls in the range of $10 - 20\ Hz$, which was observed experimentally (Mahon et al., 2006; Pitcher et al., 2007; **Figure 2B**).

The GPe neurons exhibit an atypical firing pattern where bursts and pauses appear aperiodically in a continuous tonic high-frequency firing (Kita and Kita, 2011; Hegeman et al., 2016). In the model, we adjusted I_{ij}^{x} value such that the GPe spontaneous firing rate is $\sim\ 30\ Hz$, which falls in the range of $8 - 60\ Hz$ observed experimentally (Elias et al., 2008; Bugaysen et al., 2010; Lindahl et al., 2013; **Figure 2C**).

Unlike GPe neurons, STN neurons exhibit two distinct firing patterns experimentally: tonic pacemaking firing and phasic high-frequency bursting (Beurrier et al., 1999; Allers et al., 2003), and the STN neuronal model adapted here exhibits both types of firing patterns. In the model, we adjusted I_{ij}^{x} value such that the STN spontaneous firing rate is $\sim\ 13\ Hz$, which falls in the range of $6 - 30\ Hz$ observed experimentally (Allers et al., 2003; Lindahl et al., 2013; **Figure 2D**).

Similar to STN neurons, SNc neurons experimentally exhibit two distinct firing patterns: background or low-frequency irregular tonic firing ($3 - 8\ Hz$), and bursting or high-frequency regular phasic firing ($\sim\ 20\ Hz$) (Grace and Bunney, 1984a,b). In the model, SNc neurons spontaneously fire with a firing rate of $\sim\ \ 4\ Hz$ (**Figure 3**), which was observed experimentally, and the underlying calcium oscillation driving this spontaneous voltage oscillation was ranging in between $\sim\ 1\ x\ 10^{-4}\ mM$ and $\sim\ \ 1\ x\ 10^{-3}\ mM$, and peaks to $\sim\ \ 1\ x\ 10^{-3}\ mM$ upon arrival of the action potential (**Figure 3C**; Dedman and Kaetzel, 1997; Ben-Jonathan and Hnasko, 2001; Wojda et al., 2008). This spontaneous calcium oscillation in the SNc terminal induces dopamine release, which was in the concentration range of $(34 - 48)\ \ x\ 10^{-6}\ mM$ observed experimentally (Garris et al., 1997; **Figure 3D**). When depolarizing external current [continuous pulse ($I_{ext} = 25\ x\ 10^{-6}\ pA$) and duration ($1\ s$))] was injected, SNc neuron exhibited a bursting type of firing, which lasted for more than 1 s after the pulse was removed (**Figure 2B**, positive current), demonstrating the slow-adapting nature of SNc neuron due to an excess calcium build-up inside the neuron (**Figure 3C**, positive current; Kuznetsova et al., 2010). During the depolarizing current stimulation, SNc neurons that exhibit the property within a burst that spikes after an initial spike showed a decrease in amplitude (**Figure 3B**, positive current), which is a characteristic bursting property of SNc neurons (Grace and Bunney, 1984a). The dopamine concentration released by SNc neuron during depolarizing current stimulation peaked at $\sim$ $118\ x\ 10^{-6}\ mM$ (**Figure 3D**, positive current), which falls in the range of $(90 - 220)\ x\ 10^{-6}\ mM$ observed experimentally (Chen and Budygin, 2007). Further increase in depolarizing current amplitude increases extracellular DA release exponentially but never exceeds beyond $1\ x\ 10^{-3}\ mM$ (not shown; Gonon, 1988). When hyperpolarized external current [continuous pulse ($I_{ext} = -300\ x\ 10^{-6}\ pA$) and duration ($1\ s$))] was injected, SNc neuron exhibited quiescent state until stimulation was removed (**Figure 3B**, negative current). Due to hyperpolarized current stimulation, the calcium oscillation in SNc neuron was minimal (**Figure 3C**, negative current), which resulted in the near absence of extracellular DA (**Figure 3D**, negative current).

The lateral connections in SNc, STN, and GPe neuronal populations were studied in the previous work (Muddapu et al., 2019). To simplify the proposed LIT model, no lateral connections were considered in CTX and MSN neuronal populations.

Neuromodulatory Effect of Dopamine on MSN and SNc Neuronal Populations

DA affects both synaptic and intrinsic ion channels of MSN (Surmeier et al., 2007), and the combined (synaptic and intrinsic) effect of DA on MSN was formulated in the

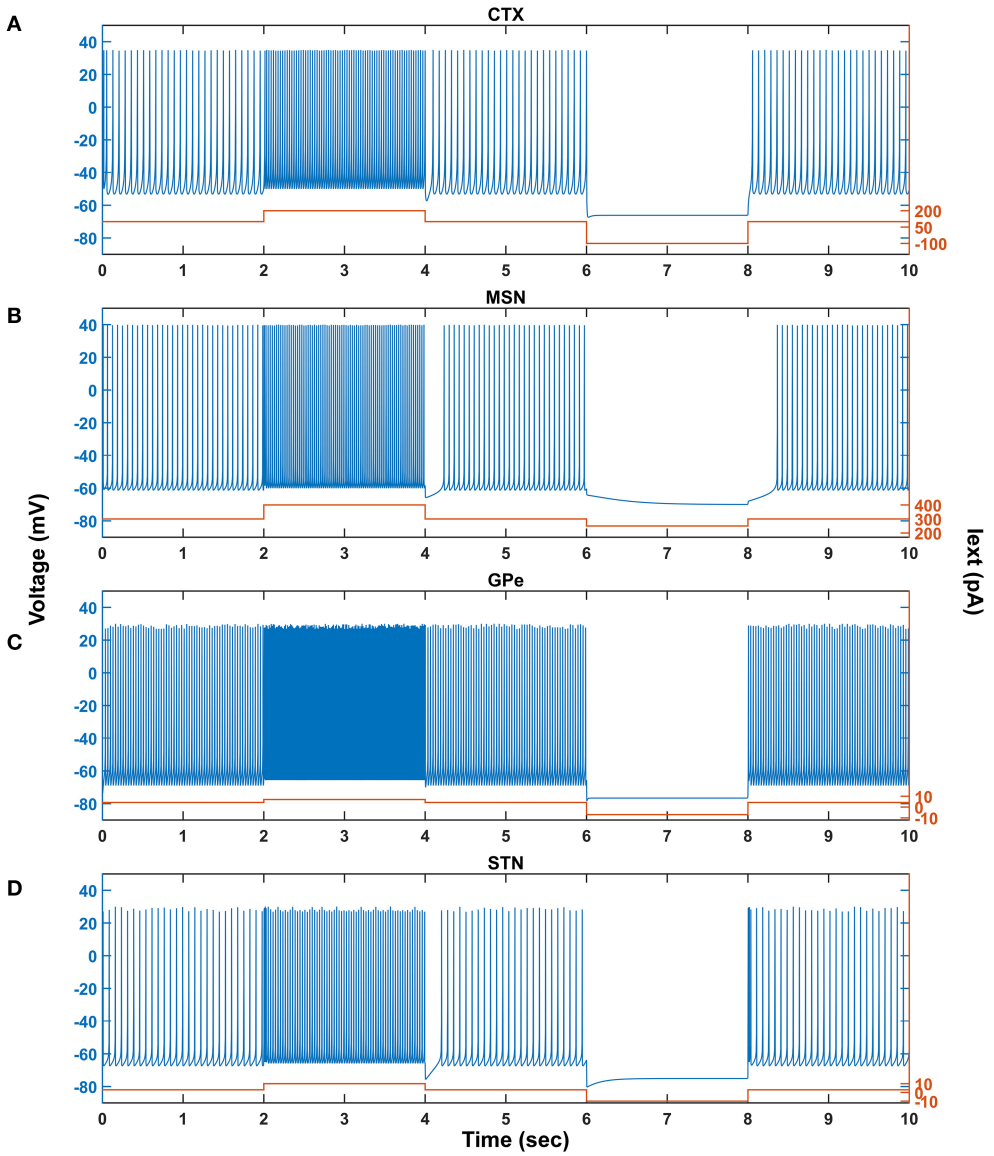

FIGURE 2 | Characteristic behavior of individual neurons from a single isolated neuron. Characteristic behavior of individual CTX **(A)**, MSN **(B)**, GPe **(C)**, and STN **(D)** neuronal types. CTX, cortex; MSN, medium spiny neuron; GPe, globus pallidus externa; STN, subthalamic nucleus; Iext, external current; pA, picoampere; mV, millivolt; sec, second.

model. As the DA levels increase, the influence of cortical glutamatergic inputs on D1-type MSN increases, resulting in monotonously increasing firing frequency (**Figure 4A**), which was consistent with experimental (Cepeda et al., 1993) and previous modeling studies (Humphries et al., 2009). In addition, SP also affects synaptic ion channels of MSN, especially glutamatergic afferents from cortical neurons (Blomeley and Bracci, 2008; Blomeley et al., 2009). As the SP levels [or SP scaling factor (W_{sp}))] increase, the influence of cortical glutamatergic inputs on D1-type MSN increases, resulting in monotonously increasing firing frequency (**Figure 4B**), which was similar to experimental (Blomeley and Bracci, 2008) and other modeling studies (Buxton et al., 2017).

DA affects both synaptic ion channels at a single neuronal level and lateral connections (Muddapu et al., 2019) at the network level of SNc neurons. As the DA level increases, the influence of synaptic and lateral connection inputs on SNc increases, resulting in monotonously decreasing firing frequency (**Figure 4C**), which was similar to experimental (Hebb and Robertson, 1999; Vandecasteele et al., 2005; Tepper and Lee, 2007; Ford, 2014) and other modeling studies (Muddapu et al., 2019). In addition, SP also affects the synaptic ion channels of SNc, especially glutamatergic afferents from STN (Brimblecombe and Cragg,

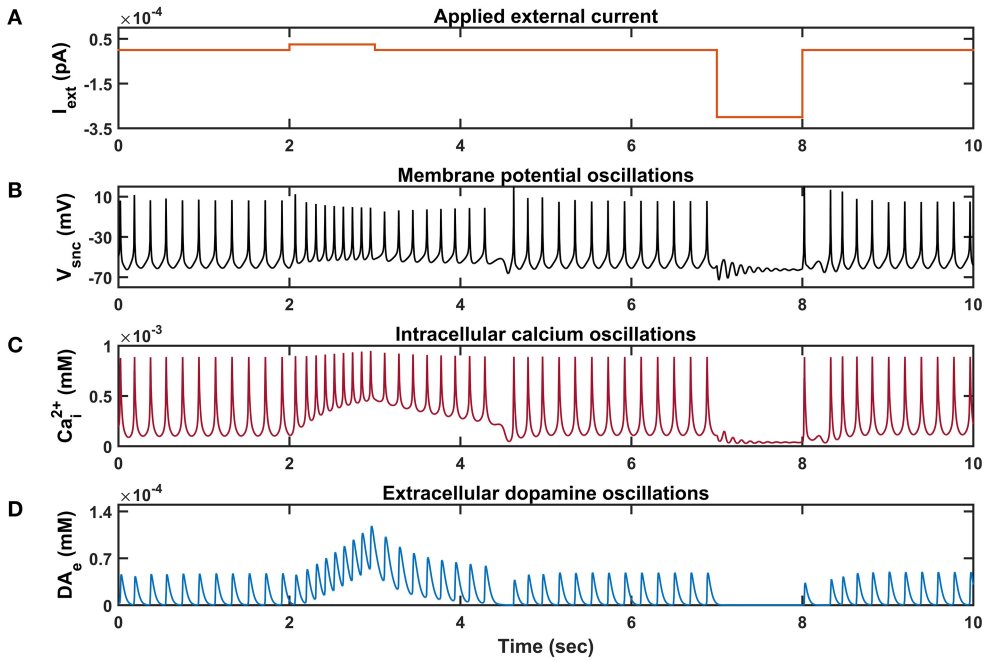

FIGURE 3 | Characteristic behavior of individual SNc neuron simulated in isolation. **(A)** Applied external current (I_{ext}), **(B)** membrane potential oscillations (V_{snc}), **(C)** intracellular calcium oscillations (Ca_i^{2+}), **(D)** extracellular dopamine concentration (DA_e). pA, picoampere; mV, millivolt; sec, second; mM, millimolar.

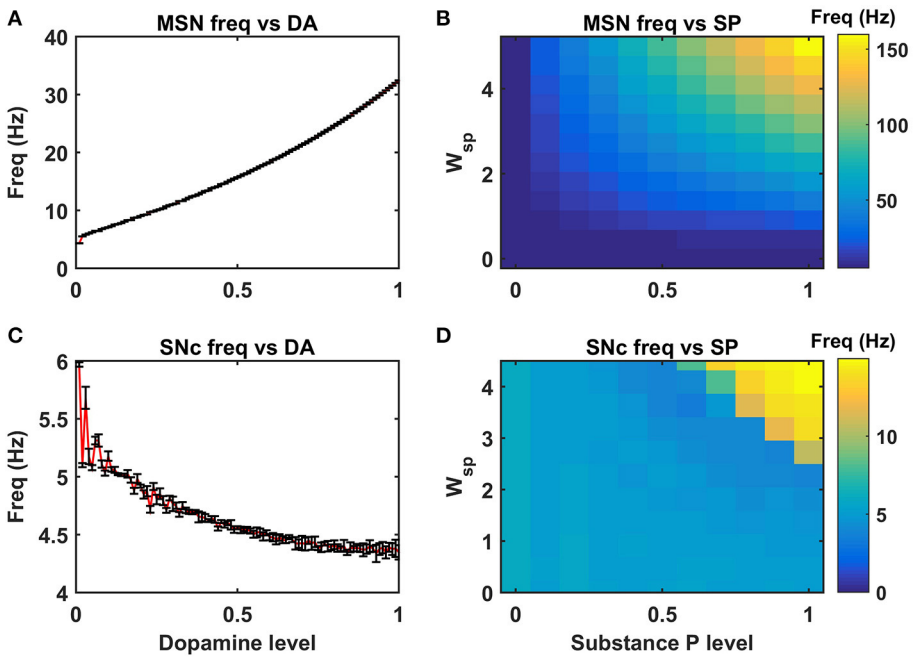

FIGURE 4 | Neuromodulatory effects of DA and SP on MSN and SNc neuronal populations. Effect of dopamine on MSN **(A)** and SNc **(C)** populations. Effect of SP on MSN **(B)** and SNc **(D)**. MSN, medium spiny neuron; DA, dopamine; Freq, frequency; SP, substance P; SNc, substantia nigra pars compacta; W_{sp}, scaling factor of SP influence; Hz, hertz.

2015; Thornton and Vink, 2015). As the SP level [or SP scaling factor (W_{sp}))] increases, the influence of STN glutamatergic inputs on SNc increases, resulting in monotonously increasing firing frequency (**Figure 4D**), which was similar to experimental

studies (Brimblecombe and Cragg, 2015). The detailed analysis of DA effect on STN and GPe neuronal populations was described in the previous work (Muddapu et al., 2019).

Energy Deficiency Occurring Similarly in SNc Somas and Terminals

To investigate energy deficiency as the possible root cause of SNc cell loss in PD, we simulated ischemic conditions by modulating glucose and oxygen inputs to the model. The ischemic condition was implemented in two scenarios, as SNc somas (in the midbrain) and terminals (in the striatum) are located far from each other: homogeneous (energy deficiency occurs similarly in somas and terminals) and heterogeneous (energy deficiency occurs differently in somas and terminals). Homogeneous energy deficiency was implemented by reducing glucose and oxygen values by the same proportions in both SNc somas and terminals. The homogeneous energy deficiency causes soma loss at 70% energy deficiency (**Figure 5A**). The soma loss at high energy deficiency can result from the threshold-like effect of STN on SNc. The influence of STN on SNc was observed by monitoring currents from STN to SNc, which showed higher positive currents after 50% of somas and terminals were in energy deficiency (**Figure 5B**). However, soma loss does not occur until 70% homogeneous energy deficiency. So, a threshold-like phenomenon exists between STN and SNc, after which the runaway effect kicks in. Contrarily, terminal loss starts with just 10% of somas and terminals in energy deficiency (**Figure 5C**). The terminal loss at low energy deficiency can result from a ROS build-up due to energy deficiency. As a result, increased ROS production in SNc terminals was observed from 10% homogeneous energy deficiency, leading to terminal degeneration (**Figure 5D**).

Energy Deficiency Occurring Differently in SNc Somas and Terminals

Heterogeneous energy deficiency was implemented by reducing glucose and oxygen values by different proportions in SNc somas and terminals. The heterogeneous energy deficiency causes soma loss at only 100% energy deficiency in terminals when the energy deficiency in somas is set at 0%, 25%, or 50% (**Figures 6A–C**). When 75% of somas were energy deficient, significant loss of soma was observed when 100% of terminals are in energy deficiency (**Figure 6D**). However, when 100% of somas were in energy deficiency, significant loss of soma was observed at all percentages of energy deficiency in terminals, and maximum loss of soma ($\sim$ 45%) was observed when 100% of terminals were in energy-deficient condition (**Figure 6E**). Contrarily, the terminal loss was observed for all non-zero percentages of energy deficiency in somas and terminals (**Figures 6F–J**). The terminal loss increases with an increase in the percentage of terminals in energy deficiency for all percentages of somas in energy deficiency (**Figures 6F–J**).

Effect of Extracellular L-DOPA

To investigate the effect of extracellular (serum) L-DOPA on SNc somas and terminal loss under energy deficiency (100% energy deficiency), we have modified extracellular L-DOPA concentration in the range from $36\ x\ 10^{-9}\ mM$ to $36\ mM$ in multiples of 10 (**Figure 7A**). At an extracellular L-DOPA concentration of zero, the percentage loss of somas and terminals was $\sim$ 75% and $\sim$ 40%, respectively, under 100% homogeneous energy deficiency. At lower concentrations of extracellular L-DOPA, ranging from $36\ x\ 10^{-9}\ mM$ to $36\ x\ 10^{-6}\ mM$, a more significant loss (average value of $\sim$ 63%) (**Figure 7A**) of SNc somas was observed when compared to SNc terminals (average value of $\sim$ 46%) (**Figure 7B**). Contrarily, at higher concentrations of extracellular L-DOPA, ranging from $36\ x\ 10^{-4}\ mM$ to $36\ mM$, more of SNc terminal loss (average value of $\sim$ 95%) (**Figure 7B**) was observed when compared to SNc somas (average value of $\sim$ 37%) (**Figure 7A**). At extracellular L-DOPA concentration of $36\ x\ 10^{-5}\ mM$, the percentage loss of SNc somas and terminals was similar, which was in the range of $50 - 60\%$, and this value of the extracellular L-DOPA concentration was observed in previous studies (Khor and Hsu, 2007; Reed et al., 2012; Cullen and Wong-Lin, 2015).

L-DOPA and Its Adjuvant Therapies

To test the hypothesis of L-DOPA-induced toxicity, we have administered a range of external L-DOPA concentrations in the model when the percentage loss of somas or terminals crosses was 25% due to energy deficiency. When external L-DOPA concentration $\left(36\ x\ 10^{-5}\ mM\right)$ administered was near the basal value (basal L-DOPA concentration was fixed at $36\ x\ 10^{-5}\ mM$), it was observed that the percentage loss of SNc somas and terminals was not altered much. When external L-DOPA concentration administered was in the range from $36\ x\ 10^{-4}\ mM$ to $36\ x\ 10^{-3}\ mM$, it was observed that the percentage loss of SNc somas was decreasing; however, the percentage loss of SNc terminals was not significantly altered. On the contrary, when administered external L-DOPA concentration was above $36\ x\ 10^{-3}\ mM$, it was observed that the percentage loss of SNc somas and SNc terminals increased (**Figures 8A,B**).

The simulation results showed that L-DOPA, indeed, induced toxicity in SNc cells at higher concentrations, which might be due to excitotoxicity or oxidative stress, or both. To evade L-DOPA toxicity in all stages of L-DOPA therapy in the case of PD, we need to understand the mechanism behind the toxicity. To do so, we co-administered two different drugs along with L-DOPA, namely, SP antagonist and glutathione (ROS scavenger), which targets overexcitation in SNc somas (by reducing SP-mediated excitatory inputs to SNc) and an ROS build-up in SNc terminals (by scavenging ROS), respectively. When SP antagonists are co-administered (with administered L-DOPA concentration fixed at $36\ x\ 10^{-4}\ mM$), it was observed that the percentage loss of SNc somas was decreasing with increasing inhibition of SP transmission (**Figure 8C**). However, there was no significant change in the percentage loss of SNc terminals across the different extents of SP transmission inhibition (**Figure 8D**). When glutathione was co-administered (with administered L-DOPA concentration fixed at $36\ x\ 10^{-4}\ mM$), it was observed that the percentage loss of SNc somas and terminals was decreasing with increasing glutathione concentration (**Figures 8E,F**).

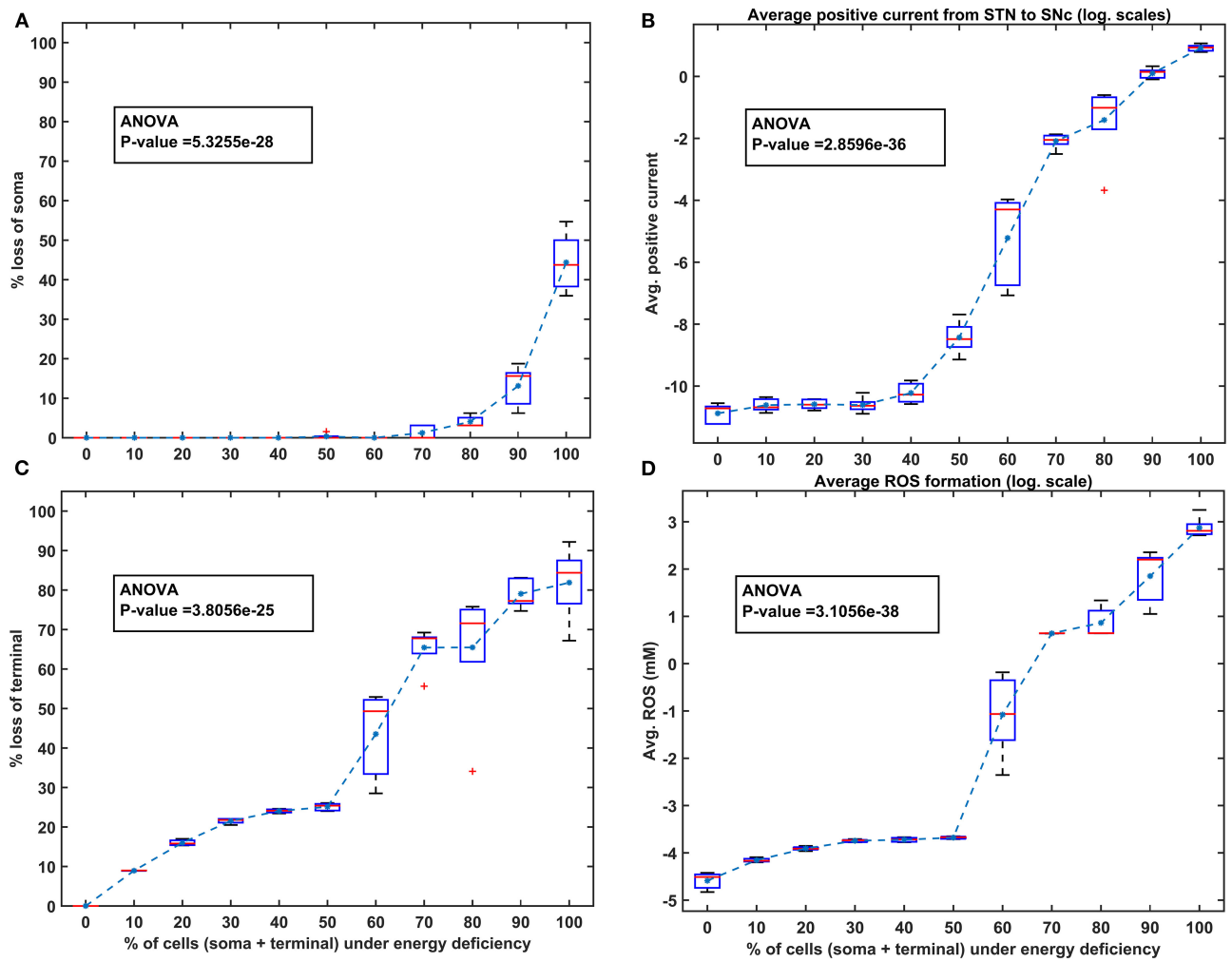

FIGURE 5 | The model response under homogeneous energy deficiency. **(A)** The percentage loss of SNc somas, **(B)** the average positive current (log. scale) from STN to SNc, **(C)** the percentage loss of SNc terminals, **(D)** the average ROS concentration (log. scale). STN, subthalamic nucleus; SNc, substantia nigra pars compacta; ROS, reactive oxygen species; mM, millimolar.

DISCUSSION

L-DOPA-Induced Toxicity Model

Site of Degeneration

This computational study aims to develop a model of SNc-striatum, which helps us understand L-DOPA-induced toxicity in SNc neurons under energy deficiency conditions. From both homogeneous and heterogeneous energy deficiency results, it suggests that SNc (axonal) terminals are more vulnerable to energy imbalance when compared to SNc cell bodies (somas), which was also observed experimentally, when an injury is initiated at axonal terminals (Burré et al., 2010; Cheng et al., 2010; Giguère et al., 2019; Wong et al., 2019). The higher positive currents from STN projections to SNc might lead to excitotoxic loss of SNc somas (**Figure 5A**), and increased ROS production might lead to increased SNc terminal loss (**Figure 5C**). DA transporters, which play a crucial role in DA neurotransmission, were depleted more in axonal terminals compared to cell bodies in early PD (Fazio et al., 2018). From these studies, it can be postulated that pathogenesis starts at axonal terminals, which are more vulnerable to energy deficiencies and, therefore, are ideal sites for developing novel disease-modifying therapeutics.

Significance of Basal Extracellular L-DOPA

The loss of SNc somas was more when compared to SNc terminals at lower concentrations of extracellular L-DOPA (**Figure 7**). This might be due to lower extracellular DA levels as a result of lower extracellular L-DOPA concentrations and lower vesicular DA levels (due to reduced packing of DA into vesicles as a result of lower energy levels), causing disinhibition of SNc somas (as a result of lesser cortical excitation of MSNs), which are already in a low energy state. Due to disinhibition and energy deficiency, SNc somas might become overactive, which leads to a calcium build-up, resulting in excitotoxic loss of SNc somas (Albin and Greenamyre, 1992; Muddapu et al., 2019).

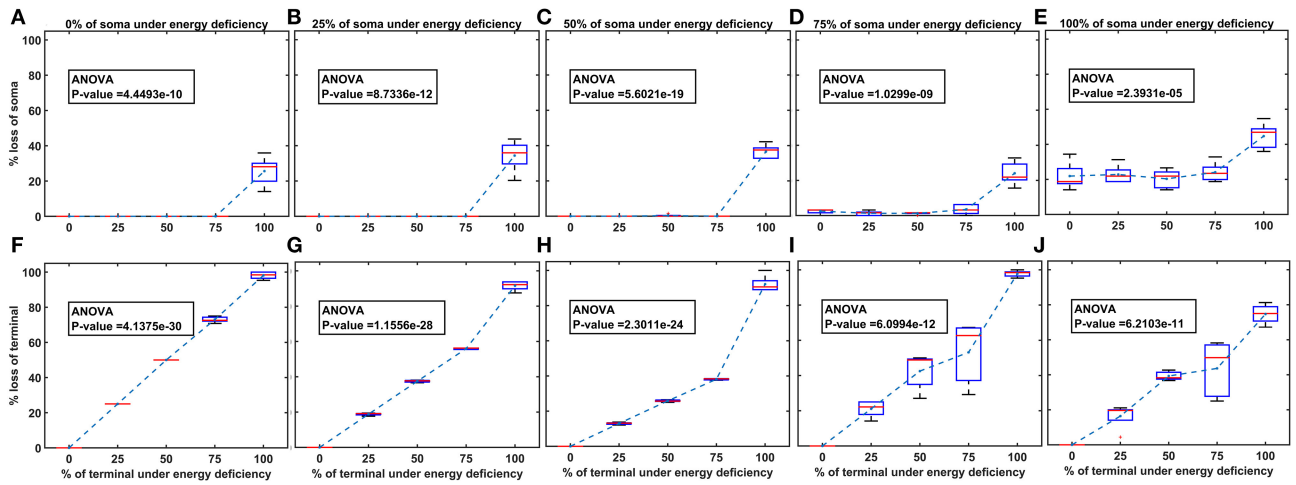

FIGURE 6 | The model response under heterogeneous energy deficiency. **(A–E)** The percentage loss of SNc somas, **(F–J)** the percentage loss of SNc terminals. SNc, substantia nigra pars compacta.

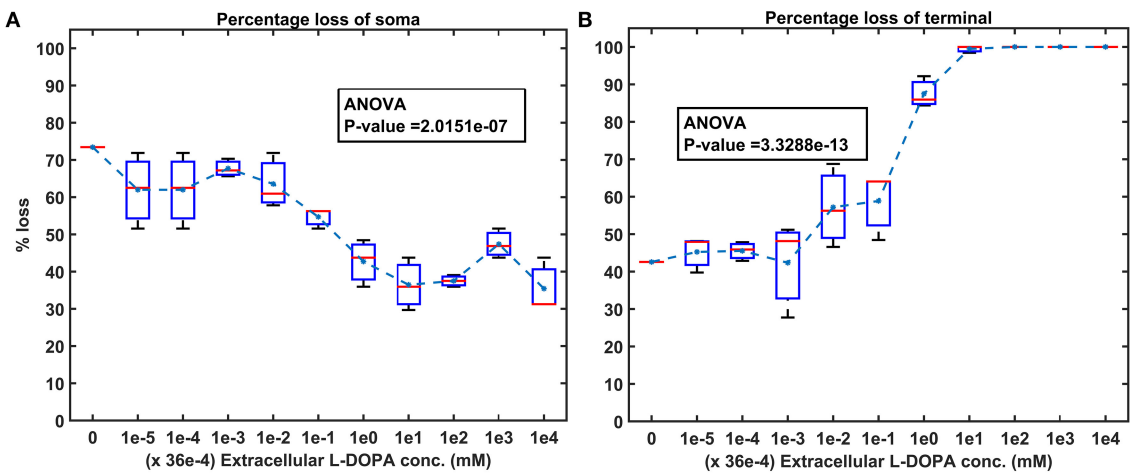

FIGURE 7 | Model response to different extracellular L-DOPA under energy deficiency. **(A)** Percentage loss of somas for various extracellular L-DOPA concentrations, **(B)** percentage loss of terminals for various extracellular L-DOPA concentrations. conc, concentration; L-DOPA, levodopa; mM, millimolar.

Contrarily, the loss of SNc terminals was more when compared to SNc somas at higher concentrations of extracellular L-DOPA (**Figure 7**). This might be due to higher cytoplasmic DA levels as a result of higher extracellular L-DOPA concentrations, lower vesicular packaging of DA (due to lower energy levels), and L-DOPA-induced stimulation of DA metabolism (Mosharov et al., 2009), resulting in DA-mediated oxidative stress in the SNc terminals (Farooqui, 2012; Morrison et al., 2012). Due to higher DA levels and energy deficiency, DA in SNc terminals causes oxidative stress, resulting in SNc terminal loss. At higher concentrations of extracellular L-DOPA, loss of SNc somas was lower compared to lower concentrations of extracellular L-DOPA as a result of the restoration of inhibitory tone from MSNs due to higher extracellular DA concentrations. The extracellular L-DOPA concentration of 36 x 10^{-5} mM was considered as basal extracellular L-DOPA concentrations in the proposed LIT model. At these values, the percentage loss of SNc somas and terminals was similar, which was observed in previous studies (Khor and Hsu, 2007; Reed et al., 2012; Cullen and Wong-Lin, 2015). Our model was able to show the significance of basal extracellular L-DOPA concentrations, which is needed to be maintained for normal functioning.

Adjuvant Therapies

When external L-DOPA concentration administered was in the range from 36 x 10^{-4} mM to 36 x 10^{-3} mM, it was observed that the percentage loss of SNc somas was decreasing, suggesting the neuroprotective benefits of L-DOPA therapy in altering or halting the progression of the SNc cell loss. However, this neuroprotective effect was not seen in the case of SNc terminals. When external L-DOPA concentration administered

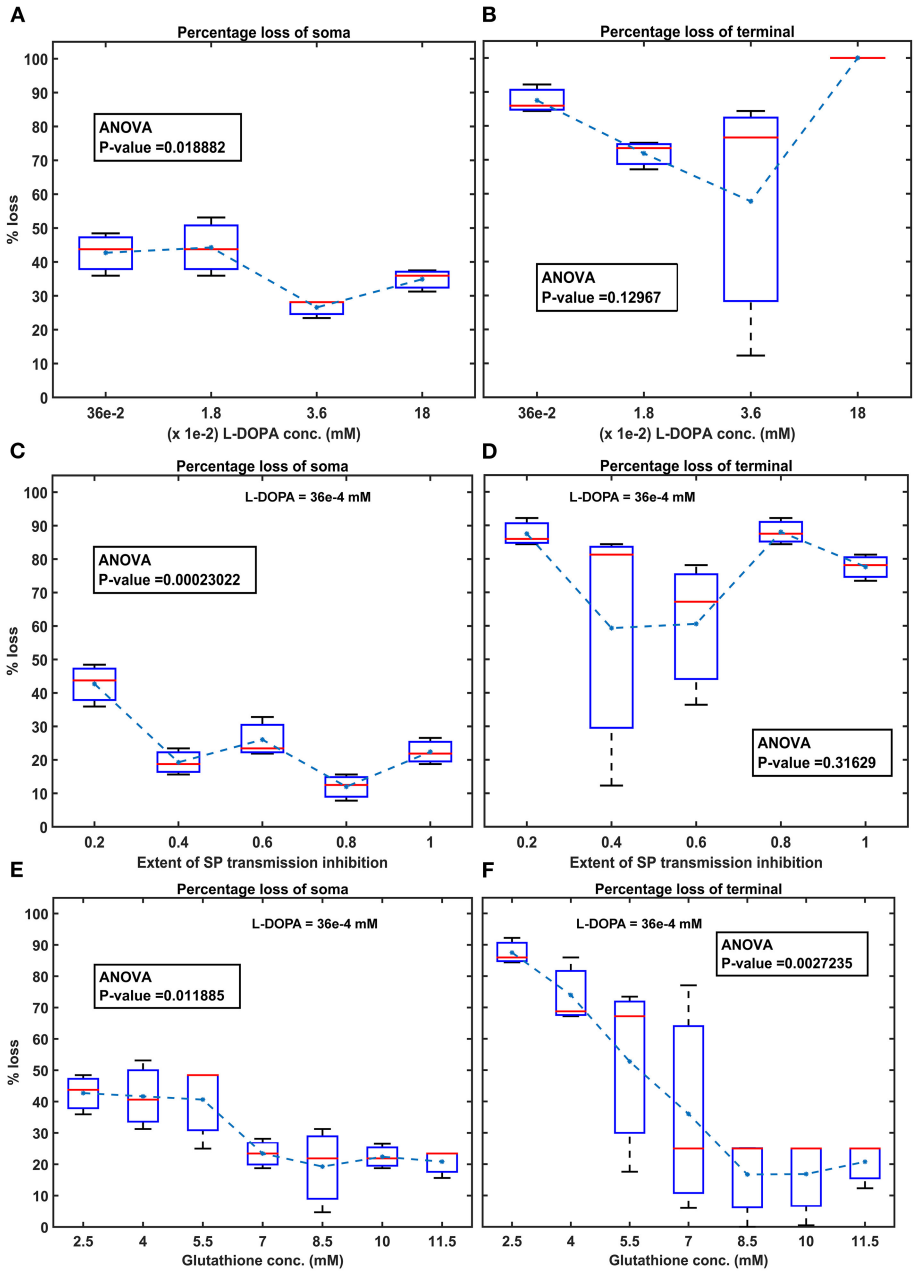

FIGURE 8 | Model response to different therapeutics under energy deficiency. **(A)** Percentage loss of somas during L-DOPA therapy, **(B)** percentage loss of terminal during L-DOPA therapy, **(C)** percentage loss of somas during SP antagonist therapy, **(D)** percentage loss of terminals during SP antagonist therapy, **(E)** percentage loss of somas during glutathione therapy, (**F**) percentage loss of terminals during glutathione therapy. All the therapeutic interventions were initiated at 25% soma or terminal loss. conc, concentration; L-DOPA, levodopa; SP, substance P; mM, millimolar; ANOVA, analysis of variance.

was above this range, the neuroprotective effect of L-DOPA therapy diminished in the case of SNc somas.

To prevent L-DOPA-induced toxicity, two different adjuvant therapies were carried on. In the first scenario, SP antagonist was co-administrated along with L-DOPA, which resulted in a further decrease in SNc soma loss, but no significant change in SNc terminal loss. From this, we can state that inhibiting excitotoxicity in SNc somas does not decrease SNc terminal loss, which suggests that excitotoxicity in SNc somas does not contribute to oxidative stress in SNc terminals in L-DOPA-induced toxicity. In the second scenario, glutathione was co-administrated along with L-DOPA, which decreased both SNc soma and terminal loss. From this, we can state that inhibiting oxidative stress in SNc terminals did reduce the loss of SNc somas, which suggests that oxidative stress in SNc terminals does contribute to excitotoxicity in SNc somas in L-DOPA-induced

toxicity. From these results, we can suggest that adjunct therapies, such as antioxidants (Pardo et al., 1993, 1995; Walkinshaw and Waters, 1995; Carvey et al., 1997; Borah and Mohanakumar, 2010; Betharia et al., 2019; Nikolova et al., 2019; Deng et al., 2020), and other potential therapies, such as D2 agonists (Asanuma et al., 2003), glycogen synthase kinase 3 inhibitors (Choi and Koh, 2018), and calcium-binding protein drugs (Isaacs et al., 1997), co-administrated along with L-DOPA, should be able to evade L-DOPA toxicity in all stages of PD.

Insights Into the Mechanism of L-DOPA-Induced Toxicity

The simulation results showed that the L-DOPA-induced toxicity in cell bodies and axonal terminals of SNc neurons was autoxidation irrelevant and autoxidation relevant, respectively. In the case of cell bodies, excess DA in the striatum due to L-DOPA therapy stimulates glutamatergic cortical inputs to MSNs, which leads to overexcitation of MSNs. The overexcited MSNs co-release SP along with GABA onto SNc neurons. SP modulates SNc glutamatergic inputs in such a way that it overexcites SNc neurons, resulting in excitotoxic neuronal loss in SNc. However, in the case of axonal terminals, excess DA in terminals due to L-DOPA therapy leads to autooxidation of DA. The autoxidation of DA results in the production of free radicals, which lead to oxidative stress in SNc axonal terminals, resulting in axonal synaptic pruning of SNc neurons. The study suggests that L-DOPA-induced toxicity occurs by two mechanisms: DA-mediated oxidative stress in axonal terminals of SNc neurons and by exacerbating STN-mediated overexcitation in cell bodies of SNc neurons.

To summarize the main outcome of the present modeling study:

- SNc (axonal) terminals are more vulnerable to energy deficiency than SNc somas.
- Basal extracellular L-DOPA concentration is needed to maintain for normal functioning of the neuron.
- Adjuvant therapies, along with L-DOPA, such as glutathione, result in evading L-DOPA-induced toxicity.
- L-DOPA-induced toxicity in cell bodies and axonal terminals of SNc neurons was autoxidation irrelevant and autoxidation relevant, respectively.

SNc Positive Feedback Loops—Scope of Vulnerability

Normal Scenario

In normal conditions, there is no SNc cell or terminal loss where SNc maintains the dopaminergic tone on its target regions, such as STN, D1-MSN(G), and D1-MSN(GS). In the first loop (**Figure 8**), normal dopaminergic tone to D1-MSN(G) results in inhibition of SNc by GABAergic projections. In the second loop (**Figure 8**), normal dopaminergic tone to D1-MSN(GS) results in inhibition of SNc by GABA and lesser excitation of SNc by SP due to DA-SP feedback (Brimblecombe and Cragg, 2015; Thornton and Vink, 2015). In the third loop (**Figure 8**), normal dopaminergic tone to STN results in lesser excitation of SNc by glutamatergic projections (Hassani et al., 1997; Magill et al., 2001; Yang et al., 2016).

Pathological Scenario

Under pathological conditions, there is an SNc cell or terminal loss where SNc fails to maintain the dopaminergic tone in its target regions, such as STN, D1-MSN(G), and D1-MSN(GS). In the first loop (**Figure 8**), DA deficiency in the striatum causes lesser excitation of D1-MSN(G) by the cortex, which, by feedback, results in disinhibition of SNc. In other words, initial DA deficiency due to SNc cell loss causes lesser excitation of D1-MSN(G), which disinhibits SNc, resulting in further SNc cell loss due to excitotoxicity, which acts as positive feedback. In the second loop, DA deficiency in the striatum causes lesser excitation of D1-MSN(GS) by the cortex, which results in disinhibition (through GABA) and further excitation of SNc (through SP, due to low DA, the effect of SP gets enhanced). Thus, the disinhibition of SNc happens in a manner similar to the first loop; however, the overexcitation of SNc happens due to the DA-SP feedback mechanism, which also acts as positive feedback. In the third loop, DA deficiency causes overexcitation of STN, which results in the overactivation of SNc. In other words, initial DA deficiency due to SNc cell loss causes overexcitation of STN, which, in turn, overexcites SNc by a positive feedback mechanism, resulting in further SNc cell loss due to excitotoxicity.

Medication Scenario—Optimal L-DOPA Dosage

In medication conditions, L-DOPA is administrated where dopaminergic tone to SNc target regions [STN, D1-MSN(G), D1-MSN(GS)] is restored. If the administrated L-DOPA dosage goes beyond a certain threshold, overexcited D1-MSN(GS) through the DA-SP feedback mechanism makes SNc hyperactive, resulting in SNc cell loss due to excitotoxicity. Along with SNc cell body loss, SNc terminals also undergo degeneration due to excess DA-causing oxidative stress. To summarize, L-DOPA-induced toxicity in SNc does not occur when L-DOPA dosage is below the threshold, which results in the survival of remaining SNc cells. However, if L-DOPA dosage goes beyond a threshold, from that point onward, the aforementioned runaway effect kicks in, leading to a progressive and irrevocable cell loss in SNc. Thus, it is evident that L-DOPA might be toxic to SNc neurons under high dosage, which triggers a runaway effect, resulting in uncontrollable SNc cell loss.

In Section Effect of Extracellular L-DOPA, we studied the effect of L-DOPA on the survivability of SNc somas and terminals under energy deficiency. Simulations have shown that the basal level of extracellular L-DOPA is required for the normal functioning of cellular processes within SNc cells. If the concentration levels go below or above this basal level, all three loops of **Figure 9** tend to operate in the pathological state, which eventually leads to SNc cell loss (**Figure 7**). In Section L-DOPA and Its Adjuvant Therapies, we studied the ability of L-DOPA therapy to alter the progression of SNc cell loss (soma and terminal) under energy deficiency. Simulations show that there exists a twilight L-DOPA dosage at which SNc cell loss was minimal (**Figures 8A,B**). At this L-DOPA dosage, all three

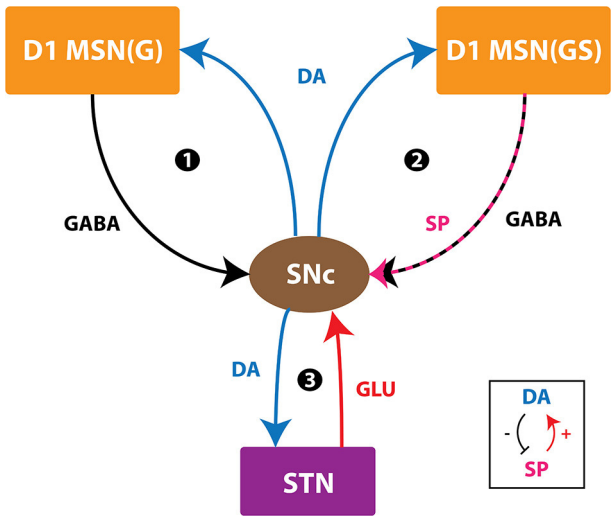

FIGURE 9 | Positive feedback loops of SNc. SNc, substantia nigra pars compacta; STN, subthalamic nucleus; D1 MSN(G), D1-type DA receptor-expressing medium spiny neuron (release GABA); D1 MSN(GS), D1-type DA receptor-expressing medium spiny neuron (co-release GABA and SP); DA, dopamine; SP, substance P; GLU, glutamate; GABA, gamma-aminobutyric acid. Inset, DA-SP feedback.

loops in **Figure 9** tend to operate in an optimal state where pathological influence from all three loops on SNc cells was minimal. If the dosage deviates from this optimal regime, all three loops (**Figure 9**) tend to operate in a pathological state. In order words, when L-DOPA dosage is very low, the overall effect (overexcitation leading to runaway effect) on SNc cells will lead to their degeneration due to excitotoxicity as a result of disinhibition (through the first loop), disinhibition, overexcitation (through the second loop), and overexcitation (through the third loop). When L-DOPA dosage is very high, its overall effect on SNc cells will eventually lead to their degeneration due to excitotoxicity: excess L-DOPA causes DA-induced oxidative stress in SNc cells, leading to loss of dopaminergic tone in SNc target nuclei. It is shown that as external L-DOPA is administered, the percentage loss of SNc somas comes down as the L-DOPA concentration increases till 36 x 10^{-3} mM; concentration levels beyond 36 x 10^{-3} mM result in diminishing neuroprotective effect of L-DOPA (**Figure 8A**).

Medication Scenario—Role of Adjuvant Drugs

We hypothesize that L-DOPA-induced toxicity in SNc cells at higher L-DOPA concentrations might be caused by excitotoxicity, oxidative stress, or both. To investigate this hypothesis and evade L-DOPA toxicity in all stages of L-DOPA therapy in PD, we need to understand the mechanism behind the toxicity. To study it *in silico*, we co-administered two different drugs along with L-DOPA - SP antagonists and glutathione. When SP antagonists were co-administered, it was observed that the percentage loss of SNc somas was decreasing with increasing inhibition of SP transmission (SP antagonist reduces SP-induced excitation in SNc; **Figure 8C**). However, there was no significant change in the percentage loss of SNc terminals (**Figure 8D**). From this, we can say that excitotoxicity in SNc soma was reduced when SP antagonist is co-administrated along with L-DOPA, which means L-DOPA-induced toxicity in SNc soma was occurring due to excitotoxicity. When glutathione was co-administered along with L-DOPA, the percentage loss of SNc somas and terminals was observed to decrease with increasing glutathione concentration (**Figures 8E,F**). From this, we can say that oxidative stress in SNc terminals was reduced when glutathione was administrated along with L-DOPA but not with SP antagonist. This means that L-DOPA-induced toxicity in SNc terminals was occurring due to oxidative stress. In addition, glutathione co-administrated with L-DOPA increases the survivability of SNc somas, which means oxidative stress in SNc terminals does contribute to excitotoxicity in SNc somas in L-DOPA-induced toxicity.

To summarize the main interpretation of the present modeling study:

- SNc neurons are involved in three positive feedback loops.
- Under energy deficiency, these positive feedback loops exacerbate the vulnerability of SNc neurons.
- Under L-DOPA medication, if the dosage goes beyond a threshold, which triggers a runaway effect, resulting in uncontrollable SNc cell loss.
- At ideal L-DOPA dosage, all positive feedback loops operate in an optimal state where pathological influence from all loops on SNc cells was minimal.
- Oxidative stress in SNc terminals does contribute to excitotoxicity in SNc somas in L-DOPA-induced toxicity. Contrarily, excitotoxicity in SNc somas does not contribute to oxidative stress in SNc terminals in L-DOPA-induced toxicity.

Limitations and Future Directions

Although the proposed model captures the exciting results of L-DOPA-induced toxicity, it is not without limitations. For example, in the proposed model, the serotonergic system was not considered, which also takes up L-DOPA and contributes to striatal DA levels (Stansley and Yamamoto, 2015; Svenningsson et al., 2015). This DA release from serotonergic terminals can even contribute to L-DOPA-induced dyskinesias (Carta et al., 2008; Carta and Tronci, 2014). Similarly, interneurons in the striatum were also not considered for simplifying the model. In the proposed model, we have considered the DA modulation on the neural activity as an immediate effect rather than a slow process. However, the effect of neuropeptide on neural activity was delayed by 40 *ms* based on previous studies (Buxton et al., 2017). In future modeling studies, we would like to incorporate the delayed DA modulation on the neural activity, which provides a more realistic effect of neuromodulators.

The ischemic condition was implemented in the proposed model by lowering glucose and oxygen levels, which can be extended by adding a blood vessel module (Cloutier et al., 2009) and varying cerebral blood flow to simulate ischemia condition more realistically. In the proposed model, stress was monitored in SNc neurons alone, which can be extended to other neuronal types in the model by monitoring stress levels, where

an intracellular calcium build-up can be a stress indicator (Bano and Ankarcrona, 2018). To do so, all neuronal types should be modeled as conductance-based models where calcium dynamics should be included. Our studies show that L-DOPA dosage plays an important role in the progression of the disease. The proposed model will be integrated with a behavioral model of cortico-basal ganglia circuitry (Muralidharan et al., 2018; Nair et al., 2022a) to show the effect of L-DOPA-induced toxicity at the behavioral level and optimize the L-DOPA dosage to achieve maximum effect on the symptoms with a minimal dosage of the drug (Nair et al., 2022b).

We suggest some experimental approaches to validate some of the predictions from our modeling study. Under induced progressive energy deficiency conditions in animal models (Puginier et al., 2019), L-DOPA administration at moderate levels can also be toxic, which needs to be studied by measuring metabolites of the DA autoxidation process. To study the effects of L-DOPA-induced toxicity in SNc somas in midbrain and SNc terminals in the striatum, similar toxin-induced animal models can be used, where oxidative stress in terminals can be examined by monitoring the levels of free radicals, and excitotoxicity in somas can be examined by monitoring calcium levels (Wong et al., 2019). By co-administering antioxidants along with L-DOPA in toxin-induced animal models (Pardo et al., 1993, 1995; Walkinshaw and Waters, 1995; Carvey et al., 1997; Borah and Mohanakumar, 2010; Betharia et al., 2019; Nikolova et al., 2019), the progression of SNc soma and terminal loss can be altered along with prolonging the "honeymoon period" of L-DOPA therapy (Holford and Nutt, 2008; Stocchi et al., 2010; Erro et al., 2016).

CONCLUSION

In conclusion, we believe that the proposed model provides significant insights into understanding the mechanisms behind L-DOPA-induced toxicity under energy deficiency conditions. From simulation results, it was shown that SNc terminals are more vulnerable to energy imbalances when compared to SNc somas. The study suggests that L-DOPA-induced toxicity occurs differently in SNc somas and terminals; in the case of SNc somas, it might be due to excitotoxicity caused by STN, and, in the case of SNc terminals, it might be due to oxidative stress caused by dopamine autoxidation. From adjuvant therapies, it was clear that co-administering antioxidants, along with L-DOPA, can be neuroprotective. Based on the aforementioned modeling efforts and some earlier ones (Muddapu et al., 2019), we are trying to understand the root cause of PD neurodegeneration as energy deficiency occurring at different neural hierarchies: subcellular, cellular, and network levels.

DATA AVAILABILITY STATEMENT

The datasets presented in this study can be found in online repositories. The names of the repository/repositories and accession number(s) can be found at: http://modeldb.yale.edu/263719 - accession: patrick.

AUTHOR CONTRIBUTIONS

VM contributed to conceptualization, model development, data curation, formal analysis, investigation, methodology, and manuscript writing. VC contributed to conceptualization, model development, data curation, formal analysis, investigation, methodology, manuscript writing, and supervision. KV and KR contributed to conceptualization and model development. All authors contributed to the article and approved the submitted version.

SUPPLEMENTARY MATERIAL

The Supplementary Material for this article can be found online at: https://www.frontiersin.org/articles/10.3389/fnins.2022.797127/full#supplementary-material

REFERENCES

Agid, Y. (1998). Levodopa: is toxicity a myth? *Neurology* 50, 858–863. doi: 10.1212/WNL.50.4.858

Albin, R. L., and Greenamyre, J. T. (1992). Alternative excitotoxic hypotheses. *Neurology* 42, 733–738. doi: 10.1212/WNL.42.4.733

Allers, K. A., Walters, J. R., and Kreiss, D. S. (2003). "Neuronal firing patterns in the subthalamic nucleus," in *The Basal Ganglia V*, eds A. M. Graybiel, M. R. Delong, and S. T. Kitai (Boston, MA: Springer US), 245–254. doi: 10.1007/978-1-4615-0179-4_25

Arbuthnott, G. W., and Wickens, J. (2007). Space, time and dopamine. *Trends Neurosci.* 30, 62–69. doi: 10.1016/j.tins.2006.12.003

Ares-Santos, S., Granado, N., Espadas, I., Martinez-Murillo, R., and Moratalla, R. (2014). Methamphetamine causes degeneration of dopamine cell bodies and terminals of the nigrostriatal pathway evidenced by silver staining. *Neuropsychopharmacology* 39, 1066–1080. doi: 10.1038/npp.2013.307

Asanuma, M., Miyazaki, I., and Ogawa, N. (2003). Dopamine- or L-DOPA-induced neurotoxicity: the role of dopamine quinone formation and tyrosinase in a model of Parkinson's disease. *Neurotox. Res.* 5, 165–176. doi: 10.1007/BF03033137

Bano, D., and Ankarcrona, M. (2018). Beyond the critical point: an overview of excitotoxicity, calcium overload and the downstream consequences. *Neurosci. Lett.* 663, 79–85. doi: 10.1016/j.neulet.2017.08.048

Ben-Jonathan, N., and Hnasko, R. (2001). Dopamine as a prolactin (PRL) inhibitor. *Endocr. Rev.* 22, 724–763. doi: 10.1210/edrv.22.6.0451

Betharia, S., Rondón-Ortiz, A. N., and Brown, D. A. (2019). Disubstituted dithiolethione ACDT exerts neuroprotective effects against 6-hydroxydopamine-induced oxidative stress in SH-SY5Y cells. *Neurochem. Res.* 44, 1878–1892. doi: 10.1007/s11064-019-02823-3

Beurrier, C., Congar, P., Bioulac, B., and Hammond, C. (1999). Subthalamic nucleus neurons switch from single-spike activity to burst-firing mode. *J. Neurosci.* 19, 599–609.

Billings, J. L., Gordon, S. L., Rawling, T., Doble, P. A., Bush, A. I., Adlard, P. A., et al. (2019). l-3,4-dihydroxyphenylalanine (l-DOPA) modulates brain iron, dopaminergic neurodegeneration and motor dysfunction in iron overload and mutant alpha-synuclein mouse models of Parkinson's disease. *J. Neurochem.* 150, 88–106. doi: 10.1111/jnc.14676

Blomeley, C., and Bracci, E. (2008). Substance P depolarizes striatal projection neurons and facilitates their glutamatergic inputs. *J. Physiol.* 586, 2143–2155. doi: 10.1113/jphysiol.2007.148965

Blomeley, C. P., Kehoe, L. A., and Bracci, E. (2009). Substance P mediates excitatory interactions between striatal projection neurons. *J. Neurosci.* 29, 4953–4963. doi: 10.1523/JNEUROSCI.6020-08.2009

Bolam, J. P., and Pissadaki, E. K. (2012). Living on the edge with too many mouths to feed: why dopamine neurons die. *Mov. Disord.* 27, 1478–1483. doi: 10.1002/mds.25135

Borah, A., and Mohanakumar, K. P. (2010). Salicylic acid protects against chronic l-DOPA-induced 6-OHDA generation in experimental model of parkinsonism. *Brain Res.* 1344, 192–199. doi: 10.1016/j.brainres.2010.05.010

Brimblecombe, K. R., and Cragg, S. J. (2015). Substance P weights striatal dopamine transmission differently within the striosome-matrix axis. *J. Neurosci.* 35, 9017–9023. doi: 10.1523/JNEUROSCI.0870-15.2015

Bugaysen, J., Bronfeld, M., Tischler, H., Bar-Gad, I., and Korngreen, A. (2010). Electrophysiological characteristics of globus pallidus neurons. *PLoS ONE* 5:e12001. doi: 10.1371/journal.pone.0012001

Burré, J., Sharma, M., Tsetsenis, T., Buchman, V., Etherton, M. R., and Südhof, T. C. (2010). α-Synuclein promotes SNARE-complex assembly *in vivo* and *in vitro*. *Science* 329, 1663–1667. doi: 10.1126/science.1195227

Buxton, D., Bracci, E., Overton, P. G., and Gurney, K. (2017). Striatal neuropeptides enhance selection and rejection of sequential actions. *Front. Comput. Neurosci.* 11:62. doi: 10.3389/fncom.2017.00062

Cadet, J. L., Jayanthi, S., and Deng, X. (2003). Speed kills: cellular and molecular bases of methamphetamine-induced nerve terminal degeneration and neuronal apoptosis. *FASEB J.* 17, 1775–1788. doi: 10.1096/fj.03-0073rev

Camargo, S. M. R., Vuille-dit-Bille, R. N., Mariotta, L., Ramadan, T., Huggel, K., Singer, D., et al. (2014). The molecular mechanism of intestinal levodopa absorption and its possible implications for the treatment of Parkinson's disease. *J. Pharmacol. Exp. Ther.* 351, 114–123. doi: 10.1124/jpet.114.216317

Carta, M., Carlsson, T., Muñoz, A., Kirik, D., and Björklund, A. (2008). Serotonin-dopamine interaction in the induction and maintenance of L-DOPA-induced dyskinesias. *Prog. Brain Res.* 172, 465–478. doi: 10.1016/S0079-6123(08)00922-9

Carta, M., and Tronci, E. (2014). Serotonin system implication in l-DOPA-induced dyskinesia: from animal models to clinical investigations. *Front. Neurol.* 5:78. doi: 10.3389/fneur.2014.00078

Carvey, P. M., Pieri, S., and Ling, Z. D. (1997). Attenuation of levodopa-induced toxicity in mesencephalic cultures by pramipexole. *J. Neural Transm.* 104, 209–228. doi: 10.1007/BF01273182

Caudle, W. M., Richardson, J. R., Wang, M. Z., Taylor, T. N., Guillot, T. S., McCormack, A. L., et al. (2007). Reduced vesicular storage of dopamine causes progressive nigrostriatal neurodegeneration. *J. Neurosci.* 27, 8138–8148. doi: 10.1523/JNEUROSCI.0319-07.2007

Cepeda, C., Buchwald, N. A., and Levine, M. S. (1993). Neuromodulatory actions of dopamine in the neostriatum are dependent upon the excitatory amino acid receptor subtypes activated. *Proc. Natl. Acad. Sci. U. S. A.* 90, 9576–9580. doi: 10.1073/pnas.90.20.9576

Chen, K. C., and Budygin, E. A. (2007). Extracting the basal extracellular dopamine concentrations from the evoked responses: re-analysis of the dopamine kinetics. *J. Neurosci. Methods* 164, 27–42. doi: 10.1016/j.jneumeth.2007.03.020

Cheng, H. C., Ulane, C. M., and Burke, R. E. (2010). Clinical progression in Parkinson disease and the neurobiology of axons. *Ann. Neurol.* 67, 715–725. doi: 10.1002/ana.21995

Cheng, N. N., Maeda, T., Kume, T., Kaneko, S., Kochiyama, H., Akaike, A., et al. (1996). Differential neurotoxicity induced by L-DOPA and dopamine in cultured striatal neurons. *Brain Res.* 743, 278–283. doi: 10.1016/S0006-8993(96)01056-6

Choi, H., and Koh, S.-H. (2018). Understanding the role of glycogen synthase kinase-3 in L-DOPA-induced dyskinesia in Parkinson's disease. *Expert Opin. Drug Metab. Toxicol.* 14, 83–90. doi: 10.1080/17425255.2018.1417387

Chou, T.-C. (1976). Derivation and properties of Michaelis-Menten type and Hill type equations for reference ligands. *J. Theor. Biol.* 59, 253–276. doi: 10.1016/0022-5193(76)90169-7

Cloutier, M., Bolger, F. B., Lowry, J. P., and Wellstead, P. (2009). An integrative dynamic model of brain energy metabolism using *in vivo* neurochemical measurements. *J. Comput. Neurosci.* 27, 391–414. doi: 10.1007/s10827-009-0152-8

Connolly, N. M. C., Dussmann, H., Anilkumar, U., Huber, H. J., and Prehn, J. H. M. (2014). Single-cell imaging of bioenergetic responses to neuronal excitotoxicity and oxygen and glucose deprivation. *J. Neurosci.* 34, 10192–10205. doi: 10.1523/JNEUROSCI.3127-13.2014

Cullen, M., and Wong-Lin, K. (2015). Integrated dopaminergic neuronal model with reduced intracellular processes and inhibitory autoreceptors. *IET Syst. Biol.* 9, 245–258. doi: 10.1049/iet-syb.2015.0018

De Vito, M. J., and Wagner, G. C. (1989). Methamphetamine-induced neuronal damage: a possible role for free radicals. *Neuropharmacology* 28, 1145–1150. doi: 10.1016/0028-3908(89)90130-5

Dedman, J. R., and Kaetzel, M. A. (1997). Chapter 22: the role of intracellular calcium as a regulatory signal. *Princ. Med. Biol.* 7, 515–530. doi: 10.1016/S1569-2582(97)80130-4

Degenetais, E. (2002). Electrophysiological properties of pyramidal neurons in the rat prefrontal cortex: an *in vivo* intracellular recording study. *Cereb. Cortex* 12, 1–16. doi: 10.1093/cercor/12.1.1

Deng, H., Jia, Y., Pan, D., and Ma, Z. (2020). Berberine alleviates rotenone-induced cytotoxicity by antioxidation and activation of PI3K/Akt signaling pathway in SH-SY5Y cells. *Neuroreport* 31, 41–47. doi: 10.1097/WNR.0000000000001365

Elias, S., Ritov, Y., and Bergman, H. (2008). Balance of increases and decreases in firing rate of the spontaneous activity of basal ganglia high-frequency discharge neurons. *J. Neurophysiol.* 100, 3086–3104. doi: 10.1152/jn.90714.2008

Erro, R., Picillo, M., Vitale, C., Amboni, M., Moccia, M., Santangelo, G., et al. (2016). The non-motor side of the honeymoon period of Parkinson's disease and its relationship with quality of life: a 4-year longitudinal study. *Eur. J. Neurol.* 23, 1673–1679. doi: 10.1111/ene.13106

Fahn, S. (1997). Levodopa-induced neurotoxicity: does it represent a problem for the treatment of Parkinson's disease? *CNS Drugs* 8, 376–393. doi: 10.2165/00023210-199708050-00004

Fahn, S. (2005). Does levodopa slow or hasten the rate of progression of Parkinson's disease? *J. Neurol.* 252, iv37–iv42. doi: 10.1007/s00415-005-4008-5

Fahn, S., Oakes, D., Shoulson, I., Kieburtz, K., Rudolph, A., Lang, A., et al. (2004). Levodopa and the progression of Parkinson's Disease. *N. Engl. J. Med.* 351, 2498–2508. doi: 10.1056/NEJMoa033447

Farooqui, T. (2012). "Dopamine-mediated oxidative stress associated with neurodegeneration in Parkinson's disease," in *Molecular Aspects of Neurodegeneration and Neuroprotection*, ed T. Farooqui (Sharjah: Bentham Science Publishers), 62–71. doi: 10.2174/978160805092511101010062

Fazio, P., Svenningsson, P., Cselényi, Z., Halldin, C., Farde, L., and Varrone, A. (2018). Nigrostriatal dopamine transporter availability in early Parkinson's disease. *Mov. Disord.* 33, 592–599. doi: 10.1002/mds.27316

Figura, M., Kuśmierska, K., Bucior, E., Szlufik, S., Koziorowski, D., Jamrozik, Z., et al. (2018). Serum amino acid profile in patients with Parkinson's disease. *PLoS ONE* 13:e0191670. doi: 10.1371/journal.pone.0191670

Ford, C. P. (2014). The role of D2-autoreceptors in regulating dopamine neuron activity and transmission. *Neuroscience* 282, 13–22. doi: 10.1016/j.neuroscience.2014.01.025

Fu, H., Hardy, J., and Duff, K. E. (2018). Selective vulnerability in neurodegenerative diseases. *Nat. Neurosci.* 21, 1350–1358. doi: 10.1038/s41593-018-0221-2

Garris, P. A., Christensen, J. R., Rebec, G. V., and Wightman, R. M. (1997). Real-time measurement of electrically evoked extracellular dopamine in the striatum of freely moving rats. *J. Neurochem.* 68, 152–161. doi: 10.1046/j.1471-4159.1997.68010152.x

Gerfen, C. R. (1985). The neostriatal mosaic. I. compartmental organization of projections from the striatum to the substantia nigra in the rat. *J. Comp. Neurol.* 236, 454–476. doi: 10.1002/cne.902360404

Giguère, N., Delignat-Lavaud, B., Herborg, F., Voisin, A., Li, Y., Jacquemet, V., et al. (2019). Increased vulnerability of nigral dopamine neurons after expansion of their axonal arborization size through D2 dopamine receptor conditional knockout. *PLoS Genet.* 15:e1008352. doi: 10.1371/journal.pgen.1008352

Goldman, J. G., and Postuma, R. (2014). Premotor and nonmotor features of Parkinson's disease. *Curr. Opin. Neurol.* 27, 434–441. doi: 10.1097/WCO.0000000000000112

Gonon, F. G. (1988). Nonlinear relationship between impulse flow and dopamine released by rat midbrain dopaminergic neurons as studied by *in vivo* electrochemistry. *Neuroscience* 24, 19–28.

Götz, T., Kraushaar, U., Geiger, J., Lübke, J., Berger, T., and Jonas, P. (1997). Functional properties of AMPA and NMDA receptors expressed in identified types of basal ganglia neurons. *J. Neurosci.* 17, 204–15.

Grace, A. A., and Bunney, B. S. (1984a). The control of firing pattern in nigral dopamine neurons: burst firing. *J. Neurosci.* 4, 2877–2890.

Grace, A. A., and Bunney, B. S. (1984b). The control of firing pattern in nigral dopamine neurons: single spike firing. *J. Neurosci.* 4, 2866–2876.

Griffith, J. S., and Horn, G. (1966). An analysis of spontaneous impulse activity of units in the striate cortex of unrestrained cats. *J. Physiol.* 186, 516–534. doi: 10.1113/jphysiol.1966.sp008053

Guo, J., Zhao, X., Li, Y., Li, G., and Liu, X. (2018). Damage to dopaminergic neurons by oxidative stress in Parkinson's disease (Review). *Int. J. Mol. Med.* 41, 1817–1825. doi: 10.3892/ijmm.2018.3406

Hassani, O. K., François, C., Yelnik, J., and Féger, J. (1997). Evidence for a dopaminergic innervation of the subthalamic nucleus in the rat. *Brain Res.* 749, 88–94.

Hauser, R. A., Lyons, K. E., McClain, T., Carter, S., and Perlmutter, D. (2009). Randomized, double-blind, pilot evaluation of intravenous glutathione in Parkinson's disease. *Mov. Disord.* 24, 979–983. doi: 10.1002/mds.22401

Hebb, M. O., and Robertson, H. A. (1999). Identification of a subpopulation of substantia nigra pars compacta ?- aminobutyric acid neurons that is regulated by basal ganglia activity. *J. Comp. Neurol.* 416, 30–44. doi: 10.1002/(SICI)1096-9861(20000103)416:1<30::AID-CNE4>3.0.CO;2-2

Hegeman, D. J., Hong, E. S., Hernández, V. M., and Chan, C. S. (2016). The external globus pallidus: progress and perspectives. *Eur. J. Neurosci.* 43, 1239–1265. doi: 10.1111/ejn.13196

Holford, N., and Nutt, J. G. (2008). Disease progression, drug action and Parkinson's disease: why time cannot be ignored. *Eur. J. Clin. Pharmacol.* 64, 207–216. doi: 10.1007/s00228-007-0427-9

Humphries, M. D., Lepora, N., Wood, R., and Gurney, K. (2009). Capturing dopaminergic modulation and bimodal membrane behaviour of striatal medium spiny neurons in accurate, reduced models. *Front. Comput. Neurosci.* 3:26. doi: 10.3389/neuro.10.026.2009

Isaacs, K. R., Wolpoe, M. E., and Jacobowitz, D. M. (1997). Calretinin-immunoreactive dopaminergic neurons from embryonic rat mesencephalon are resistant to levodopa-induced neurotoxicity. *Exp. Neurol.* 146, 25–32. doi: 10.1006/exnr.1997.6530

Izhikevich, E. M. (2003). Simple model of spiking neurons. *IEEE Trans. Neural Netw.* 14, 1569–1572. doi: 10.1109/TNN.2003.820440

Jankovic, J., and Aguilar, L. G. (2008). Current approaches to the treatment of Parkinson's disease. *Neuropsychiatr. Dis. Treat.* 4, 743–757. doi: 10.2147/ndt.s2006

Jenner, P. G., and Brin, M. F. (1998). Levodopa neurotoxicity: experimental studies versus clinical relevance. *Neurology* 50, S39–43. doi: 10.1212/wnl.50.6_suppl_6.s39

Johnson, M. B., Young, A. D., and Marriott, I. (2017). The therapeutic potential of targeting substance P/NK-1R interactions in inflammatory CNS disorders. *Front. Cell. Neurosci.* 10, 1–14. doi: 10.3389/fncel.2016.00296

Kariya, S., Takahashi, N., Hirano, M., and Ueno, S. (2005). Increased vulnerability to L-DOPA toxicity in dopaminergic neurons from VMAT2 heterozygote knockout mice. *J. Mol. Neurosci.* 27, 277–279. doi: 10.1385/JMN:27:3:277

Khor, S.-P., and Hsu, A. (2007). The pharmacokinetics and pharmacodynamics of levodopa in the treatment of Parkinson's disease. *Curr. Clin. Pharmacol.* 2, 234–243. doi: 10.2174/157488407781668802

Kim, T. K. (2017). Understanding one-way ANOVA using conceptual figures. *Kor. J. Anesthesiol.* 70, 22–26. doi: 10.4097/KJAE.2017.70.1.22

Kita, H., and Kita, T. (2011). Role of striatum in the pause and burst generation in the globus pallidus of 6-OHDA-treated rats. *Front. Syst. Neurosci.* 5:42. doi: 10.3389/fnsys.2011.00042

Koch, K. W., and Fuster, J. M. (1989). Unit activity in monkey parietal cortex related to haptic perception and temporary memory. *Exp. Brain Res.* 76, 292–306. doi: 10.1007/BF00247889

Kreiss, D. S., Mastropietro, C. W., Rawji, S. S., and Walters, J. R. (1997). The response of subthalamic nucleus neurons to dopamine receptor stimulation in a rodent model of Parkinson's disease. *J. Neurosci.* 17, 6807–6819.

Kuznetsova, A. Y., Huertas, M. A., Kuznetsov, A. S., Paladini, C. A., and Canavier, C. C. (2010). Regulation of firing frequency in a computational model of a midbrain dopaminergic neuron. *J. Comput. Neurosci.* 28, 389–403. doi: 10.1007/s10827-010-0222-y

Larsen, K. E., Fon, E. A., Hastings, T. G., Edwards, R. H., and Sulzer, D. (2002). Methamphetamine-induced degeneration of dopaminergic neurons involves autophagy and upregulation of dopamine synthesis. *J. Neurosci.* 22, 8951–8960. doi: 10.1523/JNEUROSCI.22-20-08951.2002

Lessard, A., and Pickel, V. M. (2005). Subcellular distribution and plasticity of neurokinin-1 receptors in the rat substantia nigra and ventral tegmental area. *Neuroscience* 135, 1309–1323. doi: 10.1016/j.neuroscience.2005.07.025

Li, X.-Y., Mei, G.-H., Dong, Q., Zhang, Y., Guo, Z.-L., Su, J.-J., et al. (2015). Enhanced neuroprotective effects of coadministration of tetrandrine with glutathione in preclinical model of Parkinson's disease. *Parkinsons. Dis.* 2015:931058. doi: 10.1155/2015/931058

Lindahl, M., Kamali Sarvestani, I., Ekeberg, O., and Kotaleski, J. H. (2013). Signal enhancement in the output stage of the basal ganglia by synaptic short-term plasticity in the direct, indirect, and hyperdirect pathways. *Front. Comput. Neurosci.* 7:76. doi: 10.3389/fncom.2013.00076

Lipski, J., Nistico, R., Berretta, N., Guatteo, E., Bernardi, G., and Mercuri, N. B. (2011). L-DOPA: a scapegoat for accelerated neurodegeneration in Parkinson's disease? *Prog. Neurobiol.* 94, 389–407. doi: 10.1016/j.pneurobio.2011.06.005

Lotharius, J., Falsig, J., Van Beek, J., Payne, S., Dringen, R., Brundin, P., et al. (2005). Progressive degeneration of human mesencephalic neuron-derived cells triggered by dopamine-dependent oxidative stress is dependent on the mixed-lineage kinase pathway. *J. Neurosci.* 25, 6329–6342. doi: 10.1523/JNEUROSCI.1746-05.2005

Luo, Y., and Roth, G. S. (2000). The roles of dopamine oxidative stress and dopamine receptor signaling in aging and age-related neurodegeneration. *Antioxid. Redox Signal.* 2, 449–460. doi: 10.1089/15230860050192224

Magill, P. J., Bolam, J. P., and Bevan, M. D. (2001). Dopamine regulates the impact of the cerebral cortex on the subthalamic nucleus-globus pallidus network. *Neuroscience* 106, 313–330. doi: 10.1016/S0306-4522(01)00281-0

Mahon, S., Vautrelle, N., Pezard, L., Slaght, S. J., Deniau, J.-M., Chouvet, G., et al. (2006). Distinct patterns of striatal medium spiny neuron activity during the natural sleep-wake cycle. *J. Neurosci.* 26, 12587–12595. doi: 10.1523/JNEUROSCI.3987-06.2006

Malhotra, J. D., and Kaufman, R. J. (2011). ER stress and its functional link to mitochondria: role in cell survival and death. *Cold Spring Harb. Perspect. Biol.* 3:a004424. doi: 10.1101/cshperspect.a004424

Mandali, A., Rengaswamy, M., Chakravarthy, V. S., and Moustafa, A. A. (2015). A spiking Basal Ganglia model of synchrony, exploration and decision making. *Front. Neurosci.* 9:191. doi: 10.3389/fnins.2015.00191

Mantyh, P. W., Maggio, J. E., and Hunt, S. P. (1984). The autoradiographic distribution of kassinin and substance K binding sites is different from the distribution of substance P binding sites in rat brain. *Eur. J. Pharmacol.* 102, 361–364. doi: 10.1016/0014-2999(84)90269-3

Mark, K. A., Soghomonian, J. J., and Yamamoto, B. K. (2004). High-dose methamphetamine acutely-activates the striatonigral pathway to increase striatal glutamate and mediate long-term dopamine toxicity. *J. Neurosci.* 24, 11449–11456. doi: 10.1523/JNEUROSCI.3597-04.2004

Masato, A., Plotegher, N., Boassa, D., and Bubacco, L. (2019). Impaired dopamine metabolism in Parkinson's disease pathogenesis. *Mol. Neurodegener.* 14, 1–21. doi: 10.1186/s13024-019-0332-6

Melamed, E., Offen, D., Shirvan, A., Djaldetti, R., Barzilai, A., and Ziv, I. (1998). Levodopa toxicity and apoptosis. *Ann. Neurol.* 44, S149–S154. doi: 10.1002/ana.410440722

Michmizos, K. P., and Nikita, K. S. (2011). "Addition of deep brain stimulation signal to a local field potential driven Izhikevich model masks the pathological firing pattern of an STN neuron," in *2011 Annual International Conference of the IEEE Engineering in Medicine and Biology Society* (Boston, MA: IEEE), 7290–7293. doi: 10.1109/IEMBS.2011.6091700

Mingazov, E. R., and Ugryumov, M. V. (2019). Molecular markers of dopamine transport in nigrostriatal dopaminergic neurons as an index of neurodegeneration and neuroplasticity. *Neurochem. J.* 13, 43–48. doi: 10.1134/S181971241901015X

Mischley, L. K., Lau, R. C., Shankland, E. G., Wilbur, T. K., and Padowski, J. M. (2017). Phase IIb study of intranasal glutathione in Parkinson's disease. *J. Parkinsons. Dis.* 7, 289–299. doi: 10.3233/JPD-16 1040

Miyazaki, I., and Asanuma, M. (2008). Dopaminergic neuron-specific oxidative stress caused by dopamine itself. *Acta Med. Okayama* 62, 141–150. doi: 10.18926/AMO/30942

Morrison, B. E., Marcondes, M. C. G., Nomura, D. K., Sanchez-Alavez, M., Sanchez-Gonzalez, A., Saar, I., et al. (2012). Cutting edge: IL-13Rα1 expression in dopaminergic neurons contributes to their oxidative stress–mediated loss following chronic peripheral treatment with lipopolysaccharide. *J. Immunol.* 189, 5498–5502. doi: 10.4049/jimmunol.1102150

Mosharov, E. V., Larsen, K. E., Kanter, E., Phillips, K. A., Wilson, K., Schmitz, Y., et al. (2009). Interplay between cytosolic dopamine, calcium, and α-synuclein causes selective death of substantia nigra neurons. *Neuron* 62, 218–229. doi: 10.1016/J.NEURON.2009.01.033

Muddapu, V. R., and Chakravarthy, V. S. (2020). A multi-scale computational model of excitotoxic loss of dopaminergic cells in Parkinson's disease. *Front. Neuroinform.* 14:34. doi: 10.3389/FNINF.2020.00034

Muddapu, V. R., and Chakravarthy, V. S. (2021). Influence of energy deficiency on the subcellular processes of Substantia Nigra Pars Compacta cell for understanding Parkinsonian neurodegeneration. *Sci. Rep.* 11:9. doi: 10.1038/s41598-021-81185-9

Muddapu, V. R., Dharshini, S. A. P., Chakravarthy, V. S., and Gromiha, M. M. (2020). Neurodegenerative diseases – is metabolic deficiency the root cause? *Front. Neurosci.* 14:213. doi: 10.3389/fnins.2020.00213

Muddapu, V. R., Mandali, A., Chakravarthy, V. S., and Ramaswamy, S. (2019). A computational model of loss of dopaminergic cells in Parkinson's disease due to glutamate-induced excitotoxicity. *Front. Neural Circuits* 13:11. doi: 10.3389/fncir.2019.00011

Müller, T., Hefter, H., Hueber, R., Jost, W. H., Leenders, K. L., Odin, P., et al. (2004). Is levodopa toxic? *J. Neurol. Suppl.* 251, 44–46. doi: 10.1007/s00415-004-1610-x

Muralidharan, V., Mandali, A., Balasubramani, P. P., Mehta, H., Srinivasa Chakravarthy, V., and Jahanshahi, M. (2018). "A cortico-basal ganglia model to understand the neural dynamics of targeted reaching in normal and Parkinson's conditions," in *Computational Neuroscience Models of the Basal Ganglia*, eds V. S. Chakravarthy and A. A. Moustafa (Singapore: Springer Singapore), 167–195. doi: 10.1007/978-981-10-8494-2_10

Murer, M. G., Dziewczapolski, G., Menalled, L. B., García, M. C., Agid, Y., Gershanik, O., et al. (1998). Chronic levodopa is not toxic for remaining dopamine neurons, but instead promotes their recovery, in rats with moderate nigrostriatal lesions. *Ann. Neurol.* 43, 561–575. doi: 10.1002/ana.410430504

Murer, M. G., Raisman-Vozari, R., and Gershanik, O. (1999). Levodopa in Parkinson's disease: neurotoxicity issue laid to rest? *Drug Saf.* 21, 339–352. doi: 10.2165/00002018-199921050-00001

Nair, S. S., Muddapu, V. R., and Chakravarthy, V. S. (2022a). A multiscale, systems-level, neuropharmacological model of cortico-basal ganglia system for arm reaching under normal, Parkinsonian, and Levodopa medication conditions. *Front. Comput. Neurosci.* 15:122. doi: 10.3389/fncom.2021.756881

Nair, S. S., Muddapu, V. R. J., Sriram, M., Aditya, R., Gupta, R., and Chakravarthy, S. (2022b). "Is there a better way to assess Parkinsonian motor symptoms?—experimental and modelling approach," in *Techniques for Assessment of Parkinsonism for Diagnosis and Rehabilitation*, eds S. P. Arjunan and D. K. Kumar (Singapore: Springer Singapore), 151–167. doi: 10.1007/978-981-16-3056-9_10

Nikolova, G., Karamalakova, Y., and Gadjeva, V. (2019). Reducing oxidative toxicity of L-dopa in combination with two different antioxidants: an essential oil isolated from Rosa Damascena Mill., and vitamin C. *Toxicol. Rep.* 6, 267–271. doi: 10.1016/j.toxrep.2019.03.006

Olanow, C. W., and Obeso, J. A. (2011). Levodopa toxicity and Parkinson disease: still a need for equipoise. *Neurology* 77, 1416–1417. doi: 10.1212/WNL.0b013e318232ac0a

Oorschot, D. E. (1996). Total number of neurons in the neostriatal, pallidal, subthalamic, and substantia nigral nuclei of the rat basal ganglia: a stereological study using the cavalieri and optical disector methods. *J. Comp. Neurol.* 366, 580–599. doi: 10.1002/(SICI)1096-9861(19960318)366:4<580::AID-CNE3>3.0.CO;2-0

Orrenius, S., Zhivotovsky, B., and Nicotera, P. (2003). Regulation of cell death: the calcium-apoptosis link. *Nat. Rev. Mol. Cell Biol.* 4, 552–565. doi: 10.1038/nrm1150

Pacelli, C., Giguère, N., Bourque, M. J., Lévesque, M., Slack, R. S., and Trudeau, L. É. (2015). Elevated mitochondrial bioenergetics and axonal arborization size are key contributors to the vulnerability of dopamine neurons. *Curr. Biol.* 25, 2349–2360. doi: 10.1016/j.cub.2015.07.050

Paoletti, F. P., Tambasco, N., and Parnetti, L. (2019). Levodopa treatment in Parkinson's disease: earlier or later? *Ann. Transl. Med.* 7, S189–S189. doi: 10.21037/atm.2019.07.36

Pardo, B., Mena, M. A., Casarejos, M. J., Paíno, C. L., and De Yébenes, J. G. (1995). Toxic effects of L-DOPA on mesencephalic cell cultures: protection with antioxidants. *Brain Res.* 682, 133–143. doi: 10.1016/0006-8993(95)00341-M

Pardo, B., Mena, M. A., Fahn, S., and de Yébenes, J. G. (1993). Ascorbic acid protects against levodopa-induced neurotoxicity on a catecholamine-rich human neuroblastoma cell line. *Mov. Disord.* 8, 278–284. doi: 10.1002/mds.870080305

Pifl, C., Rajput, A., Reither, H., Blesa, J., Cavada, C., Obeso, J. A., et al. (2014). Is Parkinson's disease a vesicular dopamine storage disorder? Evidence from a study in isolated synaptic vesicles of human and nonhuman primate striatum. *J. Neurosci.* 34, 8210–8218. doi: 10.1523/JNEUROSCI.5456-13.2014

Pissadaki, E. K., and Bolam, J. P. (2013). The energy cost of action potential propagation in dopamine neurons: clues to susceptibility in Parkinson's disease. *Front. Comput. Neurosci.* 7:13. doi: 10.3389/fncom.2013.00013

Pitcher, T. L., Wickens, J. R., and Reynolds, J. N. J. (2007). Differences in striatal spiny neuron action potentials between the spontaneously hypertensive and Wistar-Kyoto rat strains. *Neuroscience* 146, 135–142. doi: 10.1016/j.neuroscience.2007.01.003

Poewe, W., Antonini, A., Zijlmans, J. C., Burkhard, P. R., and Vingerhoets, F. (2010). Levodopa in the treatment of Parkinson's disease: an old drug still going strong. *Clin. Interv. Aging* 5, 229–238. doi: 10.2147/cia.s6456

Porenta, G., and Riederer, P. (1982). A mathematical model of the dopaminergic synapse: stability and sensitivity analyses, and simulation of Parkinson's disease and aging processes. *Cybern. Syst.* 13, 257–274. doi: 10.1080/01969728208927705

Puginier, E., Bharatiya, R., Chagraoui, A., Manem, J., Cho, Y. H., Garret, M., et al. (2019). Early neurochemical modifications of monoaminergic systems in the R6/1 mouse model of Huntington's disease. *Neurochem. Int.* 128, 186–195. doi: 10.1016/J.NEUINT.2019.05.001

Reed, M. C., Nijhout, H. F., and Best, J. A. (2012). Mathematical insights into the effects of levodopa. *Front. Integr. Neurosci.* 6, 1–24. doi: 10.3389/fnint.2012.00021

Reiner, A., Hart, N. M., Lei, W., and Deng, Y. (2010). Corticostriatal projection neurons - dichotomous types and dichotomous functions. *Front. Neuroanat.* 4, 1–15. doi: 10.3389/fnana.2010.00142

Ribeiro-da-Silva, A., and Hökfelt, T. (2000). Neuroanatomical localisation of substance P in the CNS and sensory neurons. *Neuropeptides* 34, 256–271. doi: 10.1054/npep.2000.0834

Ricaurte, G. A., Guillery, R. W., Seiden, L. S., Schuster, C. R., and Moore, R. Y. (1982). Dopamine nerve terminal degeneration produced by high doses of methylamphetamine in the rat brain. *Brain Res.* 235, 93–103. doi: 10.1016/0006-8993(82)90198-6

Ricaurte, G. A., Seiden, L. S., and Schuster, C. R. (1984). Further evidence that amphetamines produce long-lasting dopamine neurochemical deficits by destroying dopamine nerve fibers. *Brain Res.* 303, 359–364. doi: 10.1016/0006-8993(84)91221-6

Rubin, J. E., and Terman, D. (2004). High frequency stimulation of the subthalamic nucleus eliminates pathological thalamic rhythmicity in a computational model. *J. Comput. Neurosci.* 16, 211–235. doi: 10.1023/B:JCNS.0000025686.47117.67

Schapira, A. H. V. (2008). The clinical relevance of levodopa toxicity in the treatment of Parkinson's disease. *Mov. Disord.* 23:22146. doi: 10.1002/mds.22146

Shimozawa, A., Fujita, Y., Kondo, H., Takimoto, Y., Terada, M., Sanagi, M., et al. (2019). Effect of l-dopa/benserazide on propagation of pathological α-synuclein. *Front. Neurosci.* 13, 1–8. doi: 10.3389/fnins.2019.00595

Sivam, S. P. (1991). Dopamine dependent decrease in enkephalin and substance P levels in basal ganglia regions of postmortem Parkinsonian brains. *Neuropeptides* 18, 201–207. doi: 10.1016/0143-4179(91)90148-C

Stansley, B., and Yamamoto, B. (2015). L-Dopa and brain serotonin system dysfunction. *Toxics* 3, 75–88. doi: 10.3390/toxics3010075

Stocchi, F., Jenner, P., and Obeso, J. A. (2010). When do levodopa motor fluctuations first appear in Parkinson's disease. *Eur. Neurol.* 63, 257–266. doi: 10.1159/000300647

Surmeier, D. J., Ding, J., Day, M., Wang, Z., and Shen, W. (2007). D1 and D2 dopamine-receptor modulation of striatal glutamatergic signaling in striatal medium spiny neurons. *Trends Neurosci.* 30, 228–235. doi: 10.1016/j.tins.2007.03.008

Surmeier, D. J., Guzman, J. N., Sanchez-Padilla, J., and Goldberg, J. A. (2011). The origins of oxidant stress in parkinson's disease and therapeutic strategies. *Antioxidants Redox Signal.* 14, 1289–1301. doi: 10.1089/ars.2010.3521

Sutoo, D., Yabe, K., and Akiyama, K. (1999). Quantitative imaging of substance P in the human brain using a brain mapping analyzer. *Neurosci. Res.* 35, 339–346. doi: 10.1016/S0168-0102(99)00101-7

Svenningsson, P., Rosenblad, C., Arvidsson, K. A. E., Wictorin, K., Keywood, C., Shankar, B., et al. (2015). Eltoprazine counteracts l-DOPA-induced dyskinesias in Parkinson's disease: a dose-finding study. *Brain* 138, 963–973. doi: 10.1093/brain/awu409

Takashima, H., Tsujihata, M., Kishikawa, M., and Freed, W. J. (1999). Bromocriptine protects dopaminergic neurons from levodopa-induced toxicity by stimulating D2receptors. *Exp. Neurol.* 159, 98–104. doi: 10.1006/exnr.1999.7122

Tepper, J. M., and Lee, C. R. (2007). GABAergic control of substantia nigra dopaminergic neurons. *Prog. Brain Res.* 160, 189–208. doi: 10.1016/S0079-6123(06)60011-3

Thanvi, B. R., and Lo, T. C. N. (2004). Long term motor complications of levodopa: clinical features, mechanisms, and management strategies. *Postgrad. Med. J.* 80, 452–458. doi: 10.1136/pgmj.2003.013912

Thornton, E., Tran, T. T. B., and Vink, R. (2010). A substance P mediated pathway contributes to 6-hydroxydopamine induced cell death. *Neurosci. Lett.* 481, 64–67. doi: 10.1016/j.neulet.2010.06.057

Thornton, E., and Vink, R. (2012). Treatment with a substance P receptor antagonist is neuroprotective in the intrastriatal 6-hydroxydopamine model of early Parkinson's disease. *PLoS ONE* 7:e34138. doi: 10.1371/journal.pone.0034138

Thornton, E., and Vink, R. (2015). Substance P and its tachykinin NK1 receptor: a novel neuroprotective target for Parkinson's disease. *Neural Regen. Res.* 10, 1403–1405. doi: 10.4103/1673-5374.165505

Tripathy, S. J., Burton, S. D., Geramita, M., Gerkin, R. C., and Urban, N. N. (2015). Brain-wide analysis of electrophysiological diversity yields novel categorization of mammalian neuron types. *J. Neurophysiol.* 113, 3474–3489. doi: 10.1152/jn.00237.2015

Tripathy, S. J., Savitskaya, J., Burton, S. D., Urban, N. N., and Gerkin, R. C. (2014). NeuroElectro: a window to the world's neuron electrophysiology data. *Front. Neuroinform.* 8:40. doi: 10.3389/fninf.2014.00040

Vandecasteele, M., Glowinski, J., and Venance, L. (2005). Electrical Synapses between dopaminergic neurons of the substantia nigra pars compacta. *J Neurosci* 25, 291–298. doi: 10.1523/Jneurosci.4167-04.2005

Walkinshaw, G., and Waters, C. M. (1995). Induction of apoptosis in catecholaminergic PC12 cells by L-DOPA. Implications for the treatment of Parkinson's disease. *J. Clin. Invest.* 95, 2458–2464. doi: 10.1172/JCI117946

Wang, Q., Chu, C.-H., Qian, L., Chen, S.-H., Wilson, B., Oyarzabal, E., et al. (2014). Substance P exacerbates dopaminergic neurodegeneration through neurokinin-1 receptor-independent activation of microglial NADPH oxidase. *J. Neurosci.* 34, 12490–12503. doi: 10.1523/JNEUROSCI.2238-14.2014

Weiner, W. J. (2006). Levodopa–toxic or neuroprotective? *Nat. Clin. Pract. Neurol.* 2, 518–519. doi: 10.1038/ncpneuro0293

Wojda, U., Salinska, E., and Kuznicki, J. (2008). Calcium ions in neuronal degeneration. *IUBMB Life* 60, 575–590. doi: 10.1002/iub.91

Wong, Y. C., Luk, K., Purtell, K., Burke Nanni, S., Stoessl, A. J., Trudeau, L., et al. (2019). Neuronal vulnerability in Parkinson disease: should the focus be on axons and synaptic terminals? *Mov. Disord.* 34, 1406–1422. doi: 10.1002/mds.27823

Yang, C., Yan, Z., Zhao, B., Wang, J., Gao, G., Zhu, J., et al. (2016). D2 dopamine receptors modulate neuronal resonance in subthalamic nucleus and cortical high-voltage spindles through HCN channels. *Neuropharmacology* 105, 258–269. doi: 10.1016/j.neuropharm.2016.01.026

Zeevalk, G. D., Razmpour, R., and Bernard, L. P. (2008). Glutathione and Parkinson's disease: is this the elephant in the room? *Biomed. Pharmacother.* 62, 236–249. doi: 10.1016/j.biopha.2008.01.017

Ziv, I., Zilkha-Falb, R., Offen, D., Shirvan, A., Barzilai, A., and Melamed, E. (1997). Levodopa induces apoptosis in cultured neuronal cells—a possible accelerator of nigrostriatal degeneration in Parkinson's disease? *Mov. Disord.* 12, 17–23. doi: 10.1002/mds.870120105

Conflict of Interest: The authors declare that the research was conducted in the absence of any commercial or financial relationships that could be construed as a potential conflict of interest.

Publisher's Note: All claims expressed in this article are solely those of the authors and do not necessarily represent those of their affiliated organizations, or those of the publisher, the editors and the reviewers. Any product that may be evaluated in this article, or claim that may be made by its manufacturer, is not guaranteed or endorsed by the publisher.

frontiers | Frontiers in Neuroscience

ORIGINAL RESEARCH
published: 17 May 2022
doi: 10.3389/fnins.2022.848821

Bidirectional Optogenetic Modulation of the Subthalamic Nucleus in a Rodent Model of Parkinson's Disease

Caroline Xie[1], *John Power*[2] *and Asheeta A. Prasad*[1,3]*

[1] School of Psychology, University of New South Wales, Sydney, NSW, Australia, [2] Department of Physiology and Translational Neuroscience Facility, School of Medical Sciences, University of New South Wales, Sydney, NSW, Australia, [3] Faculty of Medicine and Health, School of Medical Sciences, University of Sydney, Sydney, NSW, Australia

Parkinson's disease (PD) is a neurodegenerative disorder characterized by a range of motor symptoms. Treatments are focused on dopamine replacement therapy or deep brain stimulation (DBS). The subthalamic nucleus (STN) is a common target for DBS treatment of PD. However, the function of the STN in normal conditions and pathology is poorly understood. Here, we show in rats that optogenetic modulation of STN neuronal activity exerts bidirectional control of motor function, where inhibition of the STN increases movement and STN activation decreases movement. We also examined the effect of bidirectional optogenetic manipulation STN neuronal activity under dopamine depleted condition using the bilateral rodent 6-hydroxydopamine (6-OHDA) model of Parkinson's disease. Optogenetic inhibition of the STN in the absence of dopamine had no impact on motor control yet STN excitation led to pronounced abnormal involuntary movement. Administration of levodopa rescued the abnormal involuntary movements induced by STN excitation. Although dopamine and STN dysfunction are well established in PD pathology, here we demonstrate simultaneous STN over activity and loss of dopamine lead to motor deficits. Moreover, we show the dysfunction of the STN is dependent on dopamine. This study provides evidence that the loss of dopamine and the over activity of the STN are key features of PD motor deficits. These results provide insight into the STN pathology in PD and therapeutic mechanism of targeting the STN for the treatment for PD.

Keywords: Parkinson's disease, subthalamic nucleus, optogenetics, 6-hydroxydopamine, motor symptoms

OPEN ACCESS

Edited by:
Hua Feng,
Army Medical University, China

Reviewed by:
Robert LeMoyne,
Northern Arizona University, United States
Clémentine Bosch-Bouju,
Institut Polytechnique de Bordeaux, France

***Correspondence:**
Asheeta A. Prasad
asheeta.prasad@unsw.edu.au

Specialty section:
This article was submitted to Neurodegeneration, a section of the journal Frontiers in Neuroscience

Received: *05 January 2022*
Accepted: *31 March 2022*
Published: *17 May 2022*

Citation:
Xie C, Power J and Prasad AA (2022) Bidirectional Optogenetic Modulation of the Subthalamic Nucleus in a Rodent Model of Parkinson's Disease. Front. Neurosci. 16:848821. doi: 10.3389/fnins.2022.848821

HIGHLIGHTS

- Our study shows direct role of STN in bidirectional regulation of motor control, where increase in STN activity decreases movement and inhibition of STN increases movement.
- Motor functions regulated by STN are dependent on dopamine.
- Administration of levodopa rescued the motor deficits induced by STN activation in the neurotoxin PD rodent model.
- The combination of the traditionally applied neurotoxin rodent model with optogenetics provides relevant rodent model for assessing pharmacotherapies for PD motor symptoms.

INTRODUCTION

Parkinson's disease (PD) is a complex neurological disorder with pathological hallmarks of dopamine loss and hyperactivity of the subthalamic nucleus (STN) (Levy et al., 2000). Links between STN and PD were clearly demonstrated in a non-human primate model of PD study where motor deficits were reversed by STN lesions (Bergman et al., 1994). Moreover, deep brain stimulation (DBS) of the STN has been a successful treatment for PD patients for over 30 years (Limousin and Foltynie, 2019). Interestingly, post-mortem human brain studies in PD cases show no significant changes in the number of neurons in the STN (Hardman et al., 1997). The primary pathology in the clinical studies have found increased firing rates of the STN in PD patient's correlating with severity of motor deficits (Levy et al., 2000).

The STN was anatomically identified in humans by Jules Bernard Luys (Parent, 2002). Its distinctive biconvex morphology is shared across humans and rodents (Hardman et al., 1997; Alkemade et al., 2019; Wallén-Mackenzie et al., 2020). STN is part of the basal ganglia and executes motor function as part of the indirect striatal pathway with inputs from the globus pallidus or the hyper direct pathway with inputs from the cerebral cortex (Gerfen, 1992). The emergence of optogenetic technologies to stimulate and inhibit specific neuronal populations with high temporal precision has revolutionised our understanding of striatal pathways components. For example, temporal optogenetic activation of striatal D2 receptor expressing neurons (indirect pathway) decreases movement (Kravitz et al., 2010). Activation of parvalbumin terminals in the STN arising from the GP and direct optogenetic inhibition of STN neurons promotes movement (Pamukcu et al., 2020). These optogenetic studies provide insight in specific neurons and pathways in motor regulation.

However, the effect of DBS on individual components of the striatal pathways in pathology remains unclear. In the absence of dopamine, other pre-clinical PD studies have activated striatal neurons to induce dyskinesia (Kravitz et al., 2010; Hernández et al., 2017). However, direct optogenetic inhibition of STN neurons in the unilateral neurotoxin rodent PD model had no effect on motor control (dyskinesia); instead motor dysfunction was rescued by activation of the hyper-direct pathway (Gradinaru et al., 2009). In clinical cases, pathologies of the STN and dopamine loss co-exist it is difficult to determine if one precedes the other and their independent contributions in motor dysfunction. We hypothesise that STN dysfunction is dependent on dopamine. To address the contribution of STN functions in motor control in normal and PD motor pathology, here we examined both STN activation and inhibition in normal and dopamine lesion rats.

MATERIALS AND METHODS

Subjects

Adult male Long Evans (Randwick, UNSW) weighing between 300 and 350 g at the time of surgery. Rats were housed in a colony room maintained on 12:12 h light/dark cycle (lights on at 7.00 a.m.) in ventilated racks in groups of four. Food and water were available *ad libitum*. All procedures were approved by the Animal Care and Ethics Committee at The University of New South Wales and conducted in accordance with the NIH Guide for the Care and Use of Laboratory Animals. The procedures were designed to minimise the number of animals used.

Surgeries

Stereotaxic surgeries was done as previously described in Prasad et al. (2020). Briefly, rats were anesthetized *via* intraperitoneal injection with a mixture of 1.3 ml/kg ketamine anesthetic (Ketapex; Apex Laboratories, Sydney, Australia) at a concentration of 100 mg/ml and 0.3 ml/kg of the muscle relaxant xylazine (Rompun; Bayer, Sydney, Australia) at a concentration of 20 mg/ml. Rats received a subcutaneous injection of 0.1 ml 50 mg/ml carprofen (Pfizer, Tadworth, United Kingdom) before being placed in the stereotaxic frame (Kopf Instruments, Tujunga, CA, United States). The stereotaxic coordinates were based on a rat brain atlas (Paxinos and Watson, 2009), following flat skull coordinates relative to bregma in mm: (AP, ML, DV): STN (−3.6 AP, ±2.6 ML, −8.0 DV), STN optic fibers (−3.6 AP, ±2.6 ML, −7.5 DV), and striatum (+1.28 AP, ±3.0 ML, −5.2 DV). Optic cannulas were secured using jeweller's screws and dental cement (Vertex Dental, Netherlands). Viral vectors or 6-OHDA were infused with a 23-gauge, cone-tipped 5 μl stainless steel injector (SGE Analytical Science) using an infusion pump (UMP3 with SYS4 Micro-controller, World Precision Instruments, Inc., Sarasota, FL, United States). The needle was left in place for 10 min to allow for diffusion and reduce spread up the infusion tract. At the end of surgery, rats received intramuscular injection of 0.2 ml of 150 mg/ml solution of procaine penicillin (Benacillin; Troy Laboratories, NSW, Australia) and 0.2 ml of 100 mg/ml cephazolin sodium (AFT Pharmaceuticals, North Ryde, NSW, Australia).

Viral Vectors

AAV5-CaMKII-eYFP, AAV5-CaMKII-HA-eNpHR3.0-IRES-Eyfp, or AAV5-CaMKII-HA-eChR2-IRES-eYFP at a minimum of 2×10^{12} viral particles per ml were obtained from the UNC Vector Core, University of North Carolina. Vector volume of 300 nl (150 nl/min) was infused per hemisphere.

Drugs

6-OHDA (6-Hydroxydopamine hydrobromide; H116, Sigma-Aldrich, Australia) was dissolved with 0.02% ascorbic acid saline solution (3 μg/μl). Rats either received 12 μg (4 ul of 3 μg/μl 6-OHDA) unilaterally into the medial forebrain bundle (MFB) or 6 μg (2 ul of 3 μg/μl 6-OHDA) bilaterally into the striatum. L-dopa (25 mg/kg, methyl L-dopa hydrochloride; #D1507, Sigma-Aldrich) and benserazide (10 mg/kg, benserazide hydrochloride; # B0477000, Sigma-Aldrich) (1 ml/kg; i.*p*.), 20 min prior to test session similar to Moreira Vasconcelos et al. (2020).

Optogenetic Manipulation

LEDs and optical parameters were as previous applied in Gibson et al. (2018). Fibre optic cannulae and patch cables were fabricated from 0.39 NA, Ø400 μm core multimode optical fiber and ceramic ferrules (Thor Labs, Newton, NJ, United States). Optic cannulas on animals were attached to patch cables connected to 625 nm LEDs (Doric Lenses Inc., Quebec, Canada) or 470 nm LEDs (Doric Lenses Inc., Quebec, Canada). 625 nm light was delivered as continuous illumination (8–10 mW) and 470 nm light was delivered as trains of 20 ms light pulses (10–12 mW, 12.5 Hz) (Gibson et al., 2018).

Electrophysiological Validation of Opsins Activity

Brain slices were prepared from rats that had received (AAV5-CaMKII-HA-eNpHR3.0-IRES-eYFP or AAV5-CaMKII-HA-ChR2-IRES-eYFP) into the STN (−3.6 AP, ±2.6 ML, −8 DV) at least 6 weeks before slice preparation. Rats were deeply anesthetized with isoflurane (5%), decapitated and their brain rapidly removed and submerged in ice-cold oxygenated (95% O_2, 5%CO_2) HEPES based artificial cerebral spinal fluid [HEPES-aCSF; (in mM) 95 NaCl, 2.5 KCl, 30 $NaHCO_3$, 1.2 NaH_2PO_4, 20 HEPES, 25 glucose, 5 ascorbate, 2 thiourea, 3 sodium pyruvate, pH adjusted to 7.3–7.4 with NaOH] with low (0.5 mM) $CaCl_2$, and high (10 mM) MgSO4 for 2–3 min. Coronal slices (300 μm) were made using a vibratome (model VT1200, Leica) and then incubated for 10 min in a 30°C neural protective recovery HEPES-aCSF (NaCl was replaced by equimolar N-methyl-D-glucamine, pH adjusted to 7.3–7.4 with HCl), and then transferred to a Braincubator (Payo Scientific, #BR26021976) and maintained at 16°C in a HEPES-aCSF holding solution with 2 mM $CaCl_2$, and 2 mM $MgSO_4$.

For recordings, slices were transferred to a recording chamber and continuously perfused with standard aCSF (30°C) containing (in mM); NaCl, 124; KCl, 3; $NaHCO_3$, 26; NaH_2PO_4, 1.2; glucose, 10; $CaCl_2$, 2.5; and $MgCl_2$, 1.3. Targeted whole-cell patch-clamp recordings were made from eYFP+ STN neurons using a microscope (Zeiss Axio Examiner D1) equipped with 20× water immersion objective (1.0 NA), LED fluorescence illumination system (pE-2, CoolLED) and an EMCCD camera (iXon+, Andor Technology). Patch pipettes (3–5 MΩ) were filled with an internal solution containing 130 mM potassium gluconate, 10 mM KCl, 10 mM HEPES, 4 mM Mg_2-ATP, 0.3 mM Na_3-GTP, 0.3 mM EGTA, and 10 mM phosphocreatine disodium salt (pH 7.3 with KOH, 280–290 mOsm). Electrophysiological recordings were amplified using a Multiclamp amplifier (700B, Molecular Devices, CA, United States), filtered at 6–10 kHz, and digitized at 20 kHz with a National Instruments multifunction I/O device (PCI-6221). Recordings were controlled and analysed offline using Axograph (Axograph, Sydney, Australia).

Electrophysiological data were analysed off-line using AxoGraph. Series resistance, membrane resistance, and cell capacitance were calculated using in built routines in Axograph. ChR2 and eNpHR3.0 were stimulated using blue (470 nm) and orange light (GYR LED bandpass filtered 605/50 nm) delivered through the objective. When possible, protocols were repeated up to five times and the results averaged. Data were excluded if the series resistance was >25 MΩ or more than 100 pA was required to maintain the neuron at -60 mV. Liquid junction potentials were uncompensated.

BEHAVIOURAL PROCEDURES

Open Field

Locomotor activity was assessed in Plexiglas chambers (Med Associates; width = 43.2 cm, length = 43.2 cm, height = 30.5 cm). Movement was tracked with three 16 beam infrared arrays. Infrared beams were located on both the x- and y-axes for positional tracking of multiple motor behaviours including ambulatory distance, episodes, counts, stereotypic, resting, and vertical time. Suspended above the chamber was a camera and LED plus fiber-optic rotary joint controlled by LED driver (Doric Lenses). There were three equal segments for test sessions, a pre-stimulation period followed by optic stimulation (stimulation period) and post-stimulation. In non-lesioned rats, **Figure 2** each segment was 1 min and the case of lesioned rats each phase was reduced to 10 s to minimise the duration of severe motor symptoms. The total distance travelled and average speed were recorded using the tracking system.

Real Time Place Preference Test

Real time place preference test was assessed in a custom-made behavioural arena consisting of two plexiglass chambers (50 × 50 × 50 cm) using a protocol adapted from Stamatakis and Stuber (2012). One chamber was assigned as the stimulation side and the other non-stimulated, which was counter balanced. The rat was placed in the non-stimulated side at the onset of the experiment and each time the rat crossed to the stimulation side of the chamber, optogenetic stimulation was delivered until the rat crossed back into the non-stimulation side. The session was for 20 min and video recorded. The time spent in each chamber was scored manually.

Abnormal Involuntary Movements Scoring

Abnormal involuntary movements (AIMs) were scored according to a rat dyskinesia scale (Cenci and Lundblad, 2007). Stereotypic behaviour was classified into three subtypes; axial dystonia, limb dyskinesia, and orolingual dyskinesia. During optical stimulation, rats were assessed for each subtypes on a scale (0–4) of progressive severity. The total AIMs score for each rat was calculated by adding the individual scores of each subtype of stereotypic behaviour, hence the maximum score a rat could obtain would be 12.

Bidirectional Regulation of Motor Function With Optogenetic Manipulation of the Subthalamic Nucleus

Rats were assigned to three groups, eYFP, ChR2, and NpHR3.0, which received AAV5-CaMKII-eYFP,

AAV5-CaMKII-HA-ChR2-IRES-eYFP, and AAV5-CaMKII-HA-eNpHR3.0-IRES-eYFP bilaterally in the STN, respectively. Optic cannulas were placed 0.5 mm above the STN right above the viral injection. After a minimum of 3 weeks post-surgery, all groups test assessed for locomotor and real time place preference test during optogenetics manipulation.

Bidirectional Regulation of Subthalamic Nucleus the Bilateral 6-Hydroxydopamine Model

There were four groups; eYFP +Saline, eYFP +6-OHDA, ChR2 +6-OHDA, and NpHR3.0 +6-OHDA. All rats received bilateral injections of either saline or 6-OHDA in the striatum, followed by bilateral viral injections in the STN with AAV5-CaMKII-eYFP, AAV5-CaMKII-HA-eNpHR3.0-IRES-eYFP or AAV5-CaMKII-HA-eChR2-IRES-eYFP. Optic fibers were secured above the STN. After a minimum of 3 weeks post-surgery, all groups were assessed for motor behaviour during optogenetic manipulation.

Immunohistochemistry

At the conclusion of the experiments, rats were deeply anesthetized with sodium pentobarbital (100 mg/kg, i.*p*.) and perfused transcardially with 150 ml of 0.9% saline, containing heparin (5000 i.u/ml), followed by 400 ml of 4% paraformaldehyde in 0.1 M phosphate buffer (PB), pH 7.4. Brains were post-fixed for 1 h in the same fixative and placed in 20% sucrose solution overnight. Brains were frozen and sliced to 40 μm coronal sections using Leica CM3050 cryostat. Four serially adjacent sets from the STN and substantia nigra were obtained from each brain and stored in 0.1% sodium azide in 0.1 M PBS, pH 7.2 to assess level of dopamine loss in the SN and virus expression and cannuale placement.

To detect tyrosine hydroxylase (TH) expression, sections were washed in 0.1 M PB, followed by 50% ethanol, 50% ethanol with 3% hydrogen peroxidase, then 5% normal horse serum (NHS) in PB (30 min each). Sections were then incubated in sheep antiserum against TH (1:2000; cat. no. AB1542, Life Technologies) in a PB solution blocking buffer (2% NHS and 0.2% Triton X-10) (48 h at 4°C). The sections were then washed and incubated in biotinylated donkey anti-goat (1:1000; Jackson ImmunoResearch Laboratories) for 24 h at 4°C. Finally, the sections were incubated in avidin-biotinylated horseradish peroxidase complex (Vector Elite kit: 6 μl/ml avidin and 6 μl/ml biotin; Vector Laboratories, 2 h at room temperature), washed in PB, and then incubated (15 min) in a diaminobenzidine solution (DAB) containing 0.1% 3,3-diaminobenzidine, 0.8% D-glucose and 0.016% ammonium chloride. Immunoreactivity was catalysed by the addition of 0.2 μl/ml glucose oxidase (24 mg/ml, 307 U/mg, Sigma). Brain sections were then washed in PB pH 7.4. Sections were mounted onto gelatin-coated slides, dehydrated, cleared in histolene, and cover-slipped with Entellan (Proscitech). To quantify the extent of dopamine depletion, manual counts of TH-immunoreactive neurons were made using Adobe Photoshop software. For each rat, counting was restricted to SN of the coronal section that best matched bregma -5.20 to -5.55 of the rat brain atlas (Paxinos and Watson, 2009). Cell counts were performed blind to the experimental group.

For the detection of viral vector expression, brain sections were washed in 0.1 M PB, then 5% normal horse serum (NHS) in PB (30 min each) and then incubated in rabbit antiserum against eGFP (1:2000; cat. no. AA11122, Life Technologies) for 24 h at 4°C. The primary antibodies were diluted in blocking buffer. After washing off unbound primary antibody, sections were incubated overnight at 4°C in AlexaFluor-488 conjugate (1:1000, A11034, Invitrogen). Brain sections were then washed in PB, pH 7.4, and mounted using mounting media. eGFP-immunoreactivity was assessed to determine the extent of transfection and optic cannula placements were imaged using Olympus light microscope (BX53) at 10× magnification.

Data Analyses

Data in figures and table are represented as mean ± SEM. The criteria for inclusion in final analysis was correct AAV or tracer and/or fiber placements determined after histology. Group numbers used for analyses in each experiment are indicated under the subheadings of behavioural procedures above. Our primary behavioural dependent variables were locomotor activity. A one-way ANOVA with Bonferroni *post-hoc* test was used to compare group differences. A paired samples *t*-test was used to compare means pre and post Levodopa administration. Statistical significance was set as $p < 0.05$. All statistical procedures were performed with SPSS 27 and GraphPad Prism 7.

RESULTS

Experiment 1: Electrophysiological Validation of Opsins in the Subthalamic Nucleus

The capacity of optogenetic manipulations to modulate STN neuronal firing was validated using *in vitro* electrophysiological recordings. Targeted whole-cell patch-clamp recordings were made from eYFP+ STN neurons in brain slice prepared from rats injected with AAV-CaMKII-ChR2-eYFP or AAV-CaMKII-eNpHR3.0-eYFP (**Figure 1A**). Majority of STN neurons are glutamatergic (Schweizer et al., 2014) and the CaMKII promotor has been used for selective expression opsin constructs STN glutamatergic neurons (Gradinaru et al., 2009; Wu et al., 2020). Consistent with previous reports these neurons had depolarized membrane potentials and often fired spontaneously (Bevan and Wilson, 1999). The membrane resistance and cell capacitance were 560 ± 362 MΩ and 7.8 ± 1.7 pF (mean ± SD; $n = 6$). ChR2 expressing neurons were stimulated with trains of brief (20 ms) blue light pulses (12.5 Hz 8 s). Each light pulse evoked a rapid depolarisation that evoked 1 or more action potentials (**Figures 1B–D**; $n = 4$ neurons/2 rats). Photo-stimulation of eNpHR3.0 expressing neurons evoked a rapid hyperpolarisation that reliably supressed neuronal firing for the duration of the light (**Figure 1E**; $n = 2/2$). Together,

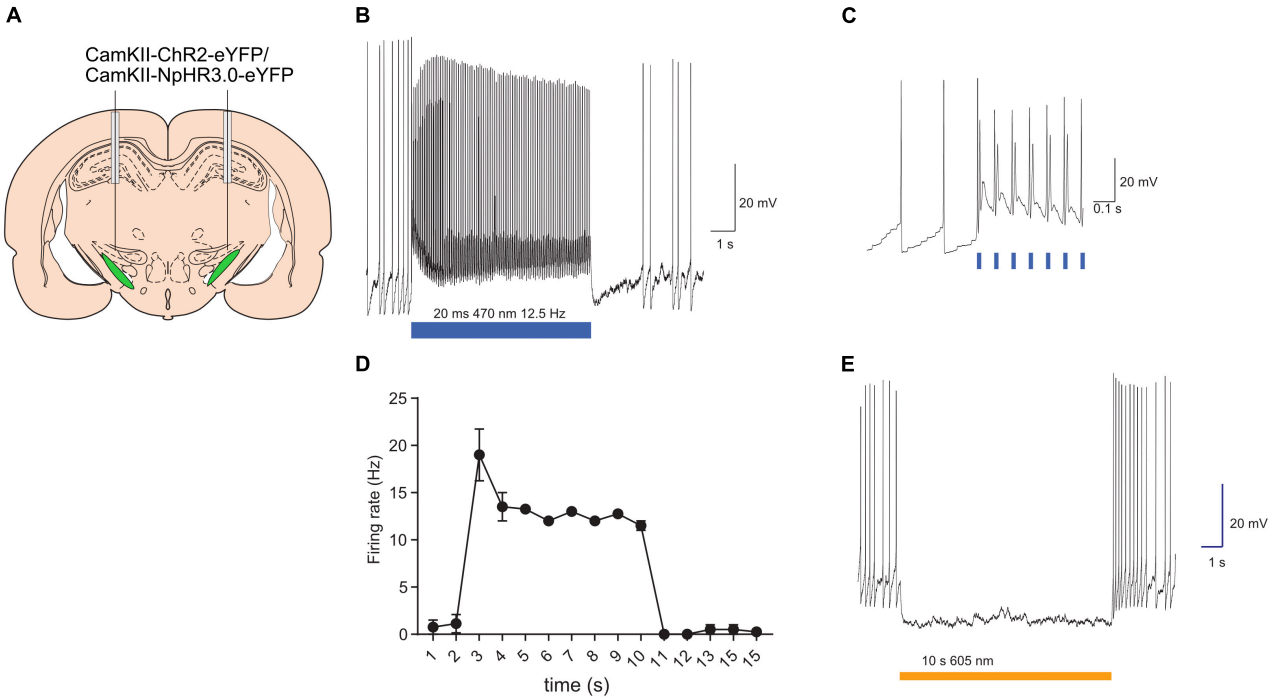

FIGURE 1 | Validation of opsins activity with *in vitro* electrophysiology. Schematic of subthalamic nucleus targeting of opsins **(A)**. Example of light-evoked excitation of ChR2-expressing neurons **(B)**. Light-evoked excitation shown on an expanded timescale to revealing synchrony between light onset and action potential generation **(C)**. Summary data plotting mean (±SEM; $n = 4$) firing frequency in presence and absence of light stimulation **(D)**. Example of light-evoked suppression of neuronal firing in eNpHR3.0-expressing neurons **(E)**. Bars indicate timing of light presentations. $^{*}p < 0.05$.

these results confirm our capacity to modulate STN neuronal activity with light.

Experiment 2: Bidirectional Optogenetic Manipulation of the Subthalamic Nucleus Induces Opposing Effects on Locomotor Activity

There were three groups, eYFP ($n = 10$), ChR2 ($n = 10$), and NpHR3.0 ($n = 11$) that received microinjections of AAV-CaMKII-eYFP, AAV-CaMKII-ChR2-eYFP, and AAV-CaMKII-eNpHR3.0-eYFP, respectively, into the STN (**Figures 2A–C**). Light was delivered *via* an optical fiber inserted dorsal to the STN. Locomotor activity was measured pre-stimulation, stimulation, and post-stimulation in a single 3-min session (one minute per phase). Locomotion measurements for ambulatory distance travelled, ambulatory episodes ambulatory counts, resting time and vertical time were recorded by MedPC open field arena software. Mean and ±SEM are reported in **Table 1**. One-way ANOVA analysis showed no group differences for ambulatory distance during pre-stimulation, $F_{(2,28)} = 0.264$, $p = 0.770$ and post-stimulation phase, $F_{(2,28)} = 1.152$, $p = 0.331$. There were significant differences between groups only during stimulation phase, $F_{(2,28)} = 16.210$, $p < 0.001$. *Post hoc* analysis showed significant difference between groups. Locomotion measurements for ambulatory distance in eYFP group was higher than and ChR2, $p = 0.002$, eYFP was lower than NpHR3.0, $p = 0.033$, and NpHR3.0 group was higher than ChR2 group, $p < 0.001$ (**Figure 2D**).

Measurements for ambulatory episodes showed no group differences for during pre-stimulation, $F_{(2,28)} = 0.425$, $p = 0.658$ and post-stimulation phase, $F_{(2,28)} = 0.179$, $p = 0.837$. There were significant differences between groups only during stimulation phase, $F_{(2,28)} = 13.900$, $p < 0.001$. *Post hoc* analysis showed significant decrease between eYFP and ChR2, $p = 0.011$, increase between eYFP and NpHR3.0, $p = 0.019$ and increase between ChR2 and NpHR3.0, $p < 0.001$ (**Figure 2E**). For ambulatory counts, there was no difference between groups during pre-stimulation, $F_{(2,28)} = 0.276$, $p = 0.761$ and post-stimulation phase, $F_{(2,28)} = 0.770$, $p = 0.473$. There were significant differences between groups only during stimulation phase, $F_{(2,28)} = 14.905$, $p < 0.001$. *Post hoc* analysis showed significant decrease between eYFP and ChR2, $p = 0.007$, increase between eYFP and NpHR3.0, $p = 0.021$ and increase ChR2 and NpHR3.0, $p < 0.001$ (**Figure 2F**). Resting time was not different between groups during pre-stimulation $F_{(2,28)} = 0.155$, $p = 0.857$ and post-stimulation phase, $F_{(2,28)} = 1.484$, $p = 0.244$. There were significant differences between groups only during stimulation phase $F_{(2,28)} = 14.346$, $p < 0.001$. *Post hoc* analysis showed significant decrease between eYFP and ChR2, $p = 0.015$, and increase between eYFP and NpHR3.0, $p = 0.011$ (**Figure 2G**). Vertical time was not significantly different across all phases, $F_{(2,28)} > 0.902$, $p > 0.503$ (**Figure 2H**). Real time place preference was expressed as the percentage of time spent in

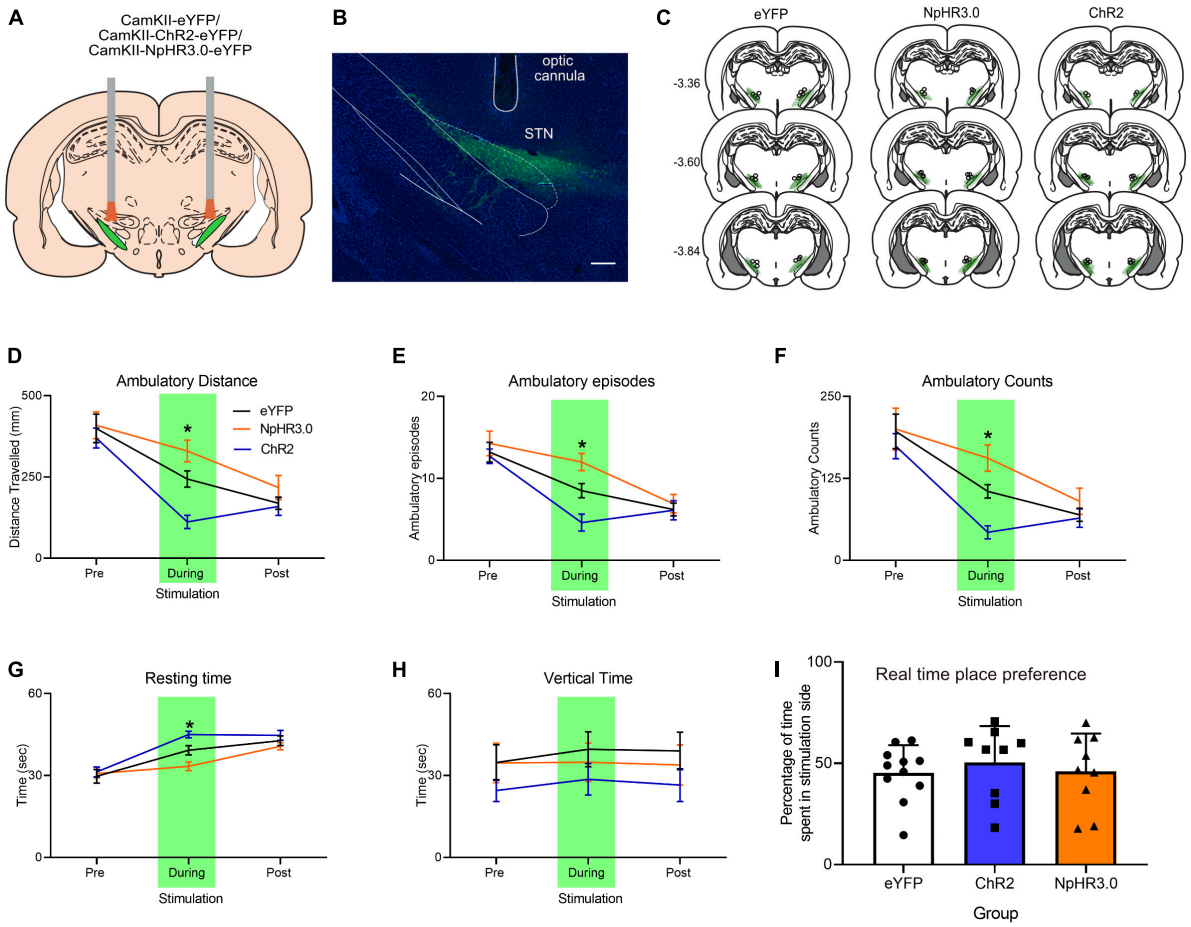

FIGURE 2 | Bidirectional regulation of motor control with optogenetic manipulation of the subthalamic nucleus. **(A)** Schematic bidirectional optogenetic manipulation subthalamic nucleus. **(B)** Representative immuno-histological image of eYFP expression in the STN and optic cannula placement, scale bar: 250 mm. **(C)** Placement of viral expression and optic cannula in the STN. Total of 3 min open field test involving pre, during, and post-stimulation periods, 1 min per phase showing **(D)** ambulatory distance, **(E)** ambulatory episodes, **(F)** ambulatory counts, **(G)** resting time, and **(H)** vertical time. **(I)** Graph showing real-time place preference. Data are expressed as mean ± SEM. *$p < 0.05$.

stimulated chamber, mean ± SEM for eYFP was 45.37% ± 4.09, ChR2 was 45.32% ± 7.75 and NpHR3.0 was 46.08% ± 6.20 (**Figure 2I**). There was no significant difference between groups, $F_{(2,28)} = 0.248$, $p = 0.782$.

Experiment 3: Bidirectional Optogenetic Manipulation of the Subthalamic Nucleus in Bilateral 6-Hydroxydopamine Lesioned Rats

We next examined the impact of optogenetic manipulation of STN neurons on motor symptoms in 6-OHDA preclinical model of PD. Dopamine neurons in the substantia nigra are most vulnerable in PD (Damier et al., 1999). Nigral neurons project to the dorsal striatum in contrast to the dopamine neurons in the ventral tegmental area which project mainly to the ventral striatum (Prensa and Parent, 2001). Lesions of the dorsolateral striatum contribute to motor regulation (Pisa, 1988). Hence, we injected 6-OHDA into the dorsal lateral region of the striatum to preferentially lesion nigral dopamine neurons.

In this experiment there were four groups. One group that received saline in the striatum and eYFP in the STN ($n = 6$). This is the saline +eYFP group and acts a control to assess changes in 6-OHDA rats. The other three groups received 6-OHDA and either eYFP ($n = 5$) ChR2 ($n = 8$) or NpHR3.0 ($n = 8$) in the STN (**Figure 3A**). The placements of optic cannula and virus expression are shown in **Figure 3B**. The extent of dopamine neuronal loss was assessed after behavioural studies. The number of TH immunoreactive neurons were significantly reduced in the 6-OHDA lesion groups compared to saline +eYFP group, $F_{(3,22)} = 18.398$, $p \leq 0.001$ (**Figures 3C,D**).

All groups were assessed for locomotor changes in the open field without stimulation for 20 min. There were no differences between groups for ambulatory distance travelled $F_{(3,22)} = 1.206$, $p = 0.331$ (**Figure 4A**). To assess the impact on locomotor upon STN stimulation, the following locomotor assay was segmented into three phases; pre-stimulation, stimulation,

TABLE 1 | Mean ± SEM of ambulatory distance, ambulatory episodes, ambulatory counts, stereotypic time, resting time and vertical time during pre-stimulation, optogenetic stimulation and post-stimulation.

	Pre-stimulation						During stimulation						Post stimulation					
	eYFP		NpHR3.0		ChR2		eYFP		NpHR3.0		ChR2		eYFP		NpHR3.0		ChR2	
	Mean	±SEM	Mean	±SEM	Mean	±SEM	Mean	±SEM	Mean	±SEM	Mean	±SEM	Mean	±SEM	Mean	±SEM	Mean	±SEM
Ambulatory Distance	399.3	43.8	408.8	41.6	370	30.8	243.7	25.1	329.9	33.4*	111.6	20.6*	168.8	18.9	217.3	37	159.1	27.7
Ambulatory Episodes	13.2	1.2	14.3	1.5	12.7	0.9	8.5	0.9	12	1.1*	4.6	1.0*	6.2	0.8	6.9	1.1	6.1	1.2
Ambulatory Counts	196.7	26.4	200.4	31.8	174.3	19.1	105.3	10.3	156.2	20.1*	42.9	10.1*	69.4	10	90.1	20	64.5	14.2
Stereotypic Time	17	1.2	20.4	0.6	17.1	1.1	15.4	1.2	19.4	1.2	12.8	1.1	13.9	1.4	15.3	0.9	12.4	1.6
Resting Time	29.7	2.5	30.7	1.6	31.3	1.8	39.3	1.7	33.4	1.6*	45	1.2*	42.8	1.8	40.7	1.3	44.7	1.8
Vertical Time	34.8	6.5	34.6	7.3	24.5	4	39.6	6.4	34.9	7	28.6	5.8	39	6.9	33.9	7.4	26.5	6

*$p < 0.05$

and post-stimulation phase. We observed that optogenetic stimulation of the PD +ChR2 induced severe motor symptoms of abnormal involuntary movements (AIMs) including twisting of the neck, tremor of the forelimbs and jaw, and inability to move voluntarily. Unlike the reduced motor responses observed during STN optogenetic activation in non-lesioned rats, under dopamine depletion activation of the STN induced severe motor symptoms including (see **Supplementary Videos**). Hence optogenetic manipulation period was reduced to 10 s in contrast to 1 min in the presence of dopamine to reduce the period of adverse impact on the rats. We found this time sufficient to detect significant deficits (see **Supplementary Videos**). For distance travelled, there was no difference between all groups during pre-stimulation, $F_{(3,22)} = 1.178$, $p = 0.341$ and post-stimulation phase, $F_{(3,22)} = 1.555$, $p = 0.229$. There was significant difference during optogenetic stimulation, $F_{(3,22)} = 7.156$, $p = 0.002$. The 6-OHDA + ChR2 group had significantly reduced movement compared other groups, $p < 0.02$, **Figure 4B**. For step counts, there was no difference between all group during pre-stimulation, $F_{(3,22)} = 0.680$, $p = 0.573$ but there was significant decrease during stimulation, $F_{(3,22)} = 14.684$, $p < 0.001$ and post-stimulation phase, $F_{(3,22)} = 3.141$, $p = 0.046$, **Figure 4C**. *Post hoc* analysis show significant difference only the 6-OHDA + ChR2 group during stimulation. In the post-stimulation phase, significantly decrease was detected between 6-OHDA + eYFP and the 6-OHDA + ChR2 group, $p = 0.035$.

Experiment 4: Application of Levodopa Rescues Motor Deficits Induced by Subthalamic Nucleus Excitation in 6-Hydroxydopamine-Lesioned Rats

The prominent motor deficits observed in only the group with dopamine loss and STN activation led us to consider the "two hit hypotheses" for PD motor symptoms where the loss of dopamine along with increase in STN activity leads to the motor dysfunction. To test this hypothesis, we thought to supplement all groups with levodopa prior to stimulating the STN. For statistical analysis paired samples *t*-test analysis was applied as AIMs was detected in the one group. Analysis demonstrated that in the presence of levodopa there was significant improvement of AIMs in the ChR2 group, $t_{(7)} = 3.451$, $p = 0.011$, **Figure 4D**. There was also no significant difference in distance travelled during pre-stimulation, stimulation or post-stimulation phases, $F_{(3,20)} < 1.706$, $p > 0.05$, **Figure 4E**. There was a significant reduction in number of steps during STN excitation between the control and ChR2 group, $F_{(1,11)} = 129.647$, $p < 0.001$. Administration of levodopa rescued the motor deficits, leading to no group difference in steps between control and ChR2 with levodopa, $F_{(1,11)} = 1.034$, $p = 0.331$, **Figure 4F**.

DISCUSSION

Therapeutical targeting of the STN *via* lesion or deep brain stimulation improves motor symptoms in PD patients (Limousin et al., 1995). A major interest in the field is to decipher the

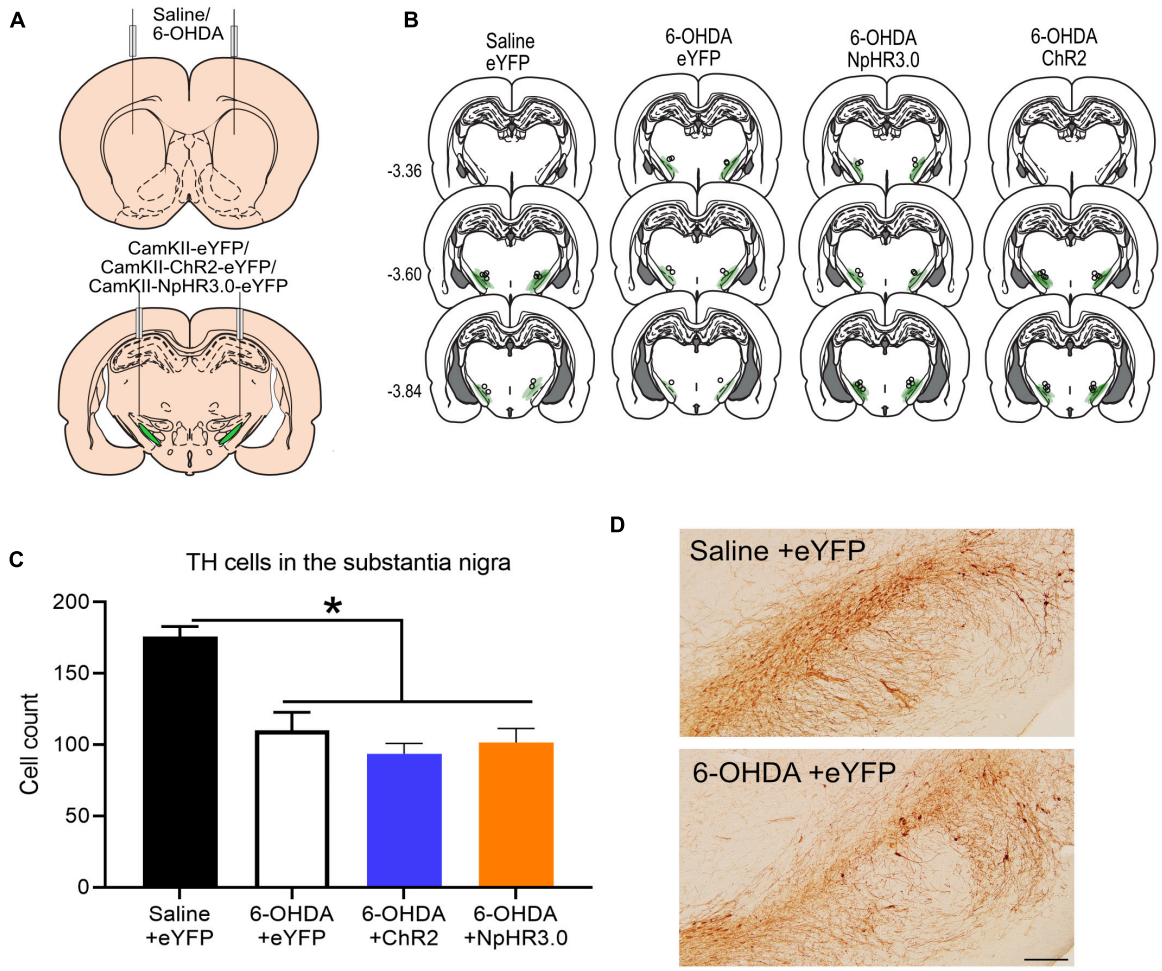

FIGURE 3 | Bidirectional regulation of subthalamic nucleus in dopamine in PD rodent model: Schematic of bilateral saline/6-OHDA administration in the striatum and optogenetic manipulation subthalamic nucleus **(A)**. Placement of viral expression and optic cannula in the STN **(B)**. Graph of tyrosine hydroxylase (TH)-immunoreactive cells in the substantia nigra in all groups **(C)**. Representative TH immunostaining from coronal sections of the substantia nigra in saline +eYFP and 6-OHDA + eYFP group. Scale bar: 200 μm **(D)**. *$p < 0.05$.

pivotal role of STN in motor control and dysfunction. To address these fundamental questions, we measured motor function while using optogenetics to selectively activate and inhibit STN neurons under normal and dopamine depleted conditions.

We found that direct inhibition of STN neurons increases locomotion, consistent with its position in striatal indirect pathway. Conversely, direct excitation of STN decreased movement in rats (**Figures 2D–H**). Similar results have been observed in mice whereby optogenetic inhibition of STN neurons induces hyperlocomotion (Schweizer et al., 2014; Guillaumin et al., 2020; Heston et al., 2020; Pamukcu et al., 2020) and direct optogenetic excitation of the STN reduces specific locomotion tasks (Guillaumin et al., 2020). These results suggest that STN neuronal activity is capable of bidirectional motor regulation within the indirect pathway and suggests that STN-DBS has an inhibitory effect on STN glutamatergic neurons.

Clinical studies show STN-DBS may impact non-motor behaviour (Bjerknes et al., 2021; Voruz et al., 2022). STN optogenetic stimulation or inhibition had no effect on the real time place preference assay (**Figure 2I**). The null effect of STN optogenetic manipulation on non-motor behaviour maybe driven using CaMKII promoter used in our study to selectively express in excitatory glutamatergic neurons (Egashira et al., 2018; Hoshino et al., 2021). Application of specific promotors such as CaMKII promoter limits manipulation of excitatory glutamatergic neurons and not effecting inhibitory neurons or passing fibers (Gradinaru et al., 2009). DBS electrical stimulation in the STN also impacts the local network, including stimulation of some STN neurons, inhibition of other STN neurons, and activation of passing fibres in the STN (Bosch et al., 2011; Dvorzhak et al., 2013). Conditional reduction of vGLUT2 neurons in the STN induces hyperlocomotion in mice without impacting limbic and cognitive functions (Schweizer et al., 2014). Together with others, our study reveals the potential of cell specific targeting of STN neurons with optogenetics technology for targeting specific behaviours akin to electrical DBS.

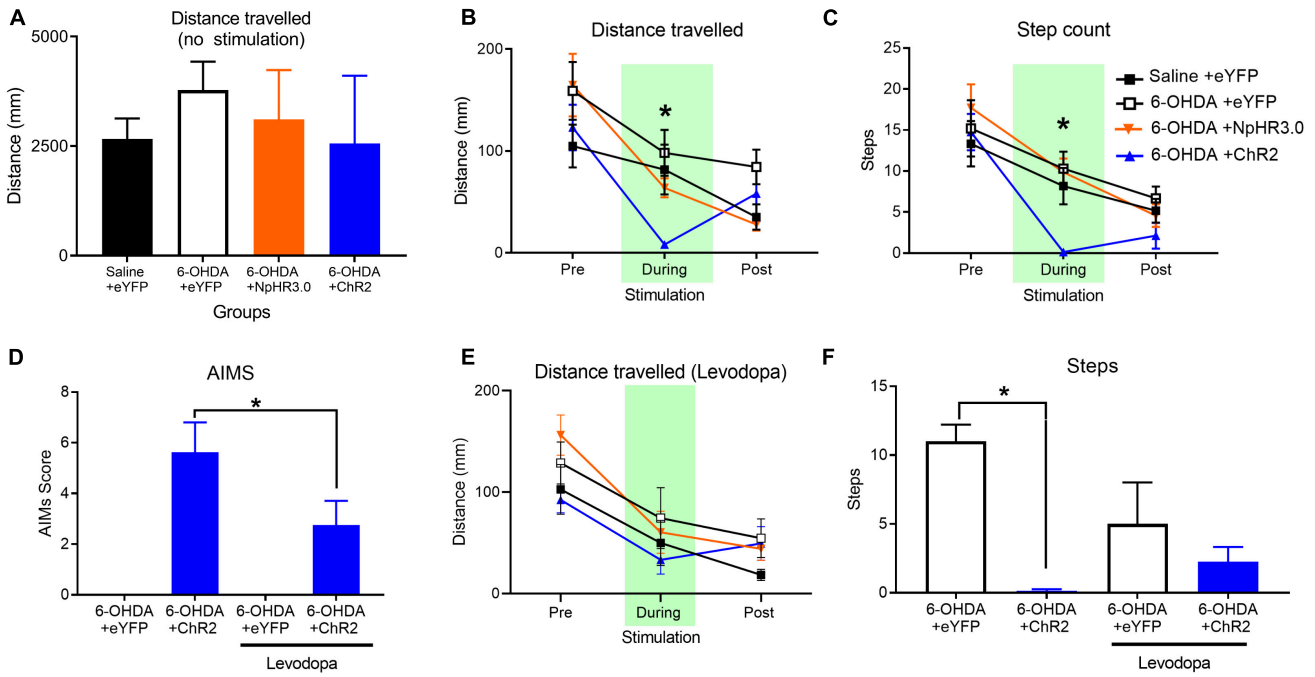

FIGURE 4 | Changes in locomotor in PD rodent model upon STN stimulation and Levodopa administration. No significant effect on groups on distance travelled during no optogenetic manipulation **(A)**. A 30 s open field test involving 10 s pre-, during and post-stimulation periods demonstrated a significant decline in distance **(B)** and step count **(C)**. Levodopa administration significantly reduced abnormal involuntary movement (AIMS) **(D)** rescues impact on distance travelled **(E)** significantly lower step count **(F)**. Data is expressed as mean ± SEM, $^*p < 0.05$.

Dopamine loss is a pathological hallmark of PD. To better understand the relationship between STN activity and motor function in PD we examined the effect of STN modulation in rats with 6-OHDA lesions. Optogenetic activation of striatal neurons (non-selective) in unilateral 6-OHDA show similar dyskinesia phenotype (Hernández et al., 2017). Here we demonstrate temporally that the increased activity of the STN with the application of optogenetics and absence of dopamine using pharmacological manipulation severely impact motor control.

Subthalamic nucleus excitation-induced motor dysfunction was dependent on the loss of dopamine as augmentation of dopamine transmission by Levodopa attenuated the STN excitation-induced motor deficits. It's unclear whether Levodopa acts on STN neurons directly or indirectly. STN neurons expresses dopamine D1 and D2 receptors (Boyson et al., 1986; Hassani et al., 1997) and focal application of dopamine agonists into the STN reduces neuronal excitability in the STN (Hassani and Féger, 1999). Our study demonstrates that STN motor function is impacted by the absences and presence of dopamine (**Figure 4**).

Methodological Considerations

A caveat of our experimental model is the sub-sequential effect of pharmacological manipulation of dopamine. It is possible that the loss of dopamine alters STN activity (Benazzouz et al., 2000). However, we included two other groups with dopamine depletion [the control group (6-OHDA + eYFP) and inhibition (6-OHDA + NpHR3.0) group] which did not display motor deficits. Albeit of the initial brain region of aberration, we show evidence that both STN and dopamine abnormalities together lead to motor deficits. This study leads to the key question of does STN pathology precede dopamine loss or if loss of dopamine induces alteration in STN activity.

CONCLUSION

Here we show the key neural pathologies of PD motor symptoms is inclusive of dopamine depletion and over activity of the STN. Serendipitously, we show a novel and robust PD animal model for assessing pharmacotherapies for PD motor symptoms. For example, the therapeutic effects of levodopa in this study sets the platform to assess other pharmacological agents for PD treatment. The pathology is temporal and reversible upon optical stimulation. The combination of the traditionally applied neurotoxin rodent model with optogenetics provides relevant rodent model to for Parkinson's motor symptoms. This model incorporates both hallmarks of PD pathology, setting a screening platform for future studies targeting STN directed treatments. Moreover, demonstrating optogenetics approach in characterizing the pathological features of PD, we can therefore develop new and improved therapeutic strategies to target STN dysfunction. Our findings demonstrate that dopamine loss and STN over activity are key features of PD motor symptoms. This draws insight to the underlying causes of PD motor

symptoms, highlighting that while the loss of dopamine is the hallmark of PD, the STN is also an integral component of PD pathology and treatment.

DATA AVAILABILITY STATEMENT

The raw data supporting the conclusions of this article will be made available by the authors, without undue reservation.

ETHICS STATEMENT

The study involving animals was reviewed and approved by the UNSW Animal Care and Ethics Committee. All studies were performed in accordance with the Animal Research Act 1985 (NSW), under the guidelines of the National Health and Medical Research Council Code for the Care and Use of Animals for Scientific Purposes in Australia (2013).

AUTHOR CONTRIBUTIONS

CX and AAP conducted behavioural and immunohistological experiments. JP carried out all electrophysiological experiments. All authors contributed to the preparation of the manuscript, contributed to the article, and approved the submitted version.

FUNDING

Preparation of this manuscript was supported by grants from the National Health and Medical Research Council of Australia to AAP (APP1160412).

SUPPLEMENTARY MATERIAL

The Supplementary Material for this article can be found online at: https://www.frontiersin.org/articles/10.3389/fnins.2022.848821/full#supplementary-material

Supplementary Video 1 | 6-OHDA +NpHR3.0: Optic stimulation at 625 nm of the subthalamic nucleus (STN) with CaMKII- NpHR3.0 opsin does not affect motor performance in 6-OHDA lesioned rats.

Supplementary Video 2 | 6-OHDA +ChR2: Optic stimulation at 470 nm of the subthalamic nucleus (STN) with CaMKII-ChR2-eYFP opsin evoked abnormal involuntary motor performance in 6-OHDA lesioned rats.

REFERENCES

Alkemade, A., de Hollander, G., Miletic, S., Keuken, M. C., Balesar, R., de Boer, O., et al. (2019). The functional microscopic neuroanatomy of the human subthalamic nucleus. *Brain Struct. Funct.* 224, 3213–3227. doi: 10.1007/s00429-019-01960-3

Benazzouz, A., Piallat, B., Ni, Z. G., Koudsie, A., Pollak, P., and Benabid, A. L. (2000). Implication of the subthalamic nucleus in the pathophysiology and pathogenesis of Parkinson's disease. *Cell Transplant* 9, 215–221. doi: 10.1177/096368970000900207

Bergman, H., Wichmann, T., Karmon, B., and DeLong, M. R. (1994). The primate subthalamic nucleus. II. Neuronal activity in the MPTP model of parkinsonism. *J. Neurophysiol.* 72, 507–520. doi: 10.1152/jn.1994.72.2.507

Bevan, M. D., and Wilson, C. J. (1999). Mechanisms underlying spontaneous oscillation and rhythmic firing in rat subthalamic neurons. *J. Neurosci.* 19, 7617–7628. doi: 10.1523/JNEUROSCI.19-17-07617.1999

Bjerknes, S., Toft, M., Brandt, R., Rygvold, T. W., Konglund, A., Dietrichs, E., et al. (2021). Subthalamic nucleus stimulation in parkinson's disease: 5-year extension study of a randomized trial. *Mov. Disord. Clin. Pract.* 9, 48–59. doi: 10.1002/mdc3.13348

Bosch, C., Degos, B., Deniau, J.-M., and Venance, L. (2011). Subthalamic nucleus high-frequency stimulation generates a concomitant synaptic excitation–inhibition in substantia nigra pars reticulata. *J. Physiol.* 589, 4189–4207. doi: 10.1113/jphysiol.2011.211367

Boyson, S. J., McGonigle, P., and Molinoff, P. B. (1986). Quantitative autoradiographic localization of the D1 and D2 subtypes of dopamine receptors in rat brain. *J. Neurosci.* 6:3177. doi: 10.1523/JNEUROSCI.06-11-03177.1986

Cenci, M. A., and Lundblad, M. (2007). Ratings of L-DOPA-induced dyskinesia in the unilateral 6-OHDA Lesion model of parkinson's disease in rats and mice. *Curr. Protocols Neurosci.* 41, 9.25.21–29.25.23. doi: 10.1002/0471142301.ns0925s41

Damier, P., Hirsch, E. C., Agid, Y., and Graybiel, A. M. (1999). The substantia nigra of the human brain: II. Patterns of loss of dopamine-containing neurons in Parkinson's disease. *Brain* 122, 1437–1448. doi: 10.1093/brain/122.8.1437

Dvorzhak, A., Gertler, C., Harnack, D., and Grantyn, R. (2013). High frequency stimulation of the subthalamic nucleus leads to presynaptic gaba(b)-dependent depression of subthalamo-nigral afferents. *PLoS One* 8:e82191. doi: 10.1371/journal.pone.0082191

Egashira, Y., Mori, Y., Yanagawa, Y., and Takamori, S. (2018). Development of lentiviral vectors for efficient glutamatergic-selective gene expression in cultured hippocampal neurons. *Sci. Rep.* 8:15156. doi: 10.1038/s41598-018-33509-5

Gerfen, C. R. (1992). The neostriatal mosaic: multiple levels of compartmental organization. *Trends Neurosci.* 15, 133–139.

Gibson, G. D., Prasad, A. A., Jean-Richard-Dit-Bressel, P., Yau, J. O. Y., Millan, E. Z., Liu, Y., et al. (2018). Distinct accumbens shell output pathways promote versus prevent relapse to alcohol seeking. *Neuron* 98, 512–520 e516. doi: 10.1016/j.neuron.2018.03.033

Gradinaru, V., Mogri, M., Thompson, K. R., Henderson, J. M., and Deisseroth, K. (2009). Optical deconstruction of parkinsonian neural circuitry. *Science* 324, 354–359. doi: 10.1126/science.1167093

Guillaumin, A., Serra, G. P., Georges, F., and Wallén-Mackenzie, Å (2020). Experimental investigation into the role of the subthalamic nucleus (STN) in motor control using optogenetics in mice. *Brain Res.* 1755:147226. doi: 10.1016/j.brainres.2020.147226

Hardman, C. D., Halliday, G. M., McRitchie, D. A., and Morris, J. G. (1997). The subthalamic nucleus in Parkinson's disease and progressive supranuclear palsy. *J. Neuropathol. Exp. Neurol.* 56, 132–142. doi: 10.1097/00005072-199702000-00003

Hassani, O. K., and Féger, J. (1999). Effects of intrasubthalamic injection of dopamine receptor agonists on subthalamic neurons in normal and 6-hydroxydopamine-lesioned rats: an electrophysiological and c-Fos study. *Neuroscience* 92, 533–543. doi: 10.1016/S0306-4522(98)00765-9

Hassani, O.-K., François, C., Yelnik, J., and Féger, J. (1997). Evidence for a dopaminergic innervation of the subthalamic nucleus in the rat. *Brain Res.* 749, 88–94. doi: 10.1016/S0006-8993(96)01167-5

Hernández, L. F., Castela, I., Ruiz-DeDiego, I., Obeso, J. A., and Moratalla, R. (2017). Striatal activation by optogenetics induces dyskinesias in the 6-hydroxydopamine rat model of Parkinson disease. *Mov. Disord.* 32, 530–537. doi: 10.1002/mds.26947

Heston, J., Friedman, A., Baqai, M., Bavafa, N., Aron, A. R., and Hnasko, T. S. (2020). Activation of subthalamic nucleus stop circuit disrupts cognitive performance. *eNeuro* 7:ENEURO.0159-20.2020. doi: 10.1523/ENEURO.0159-20.2020

Hoshino, C., Konno, A., Hosoi, N., Kaneko, R., Mukai, R., Nakai, J., et al. (2021). GABAergic neuron-specific whole-brain transduction by AAV-PHP.B incorporated with a new GAD65 promoter. *Mol. Brain* 14:33. doi: 10.1186/s13041-021-00746-1

Kravitz, A. V., Freeze, B. S., Parker, P. R., Kay, K., Thwin, M. T., Deisseroth, K., et al. (2010). Regulation of parkinsonian motor behaviours by optogenetic control of basal ganglia circuitry. *Nature* 466, 622–626. doi: 10.1038/nature09159

Levy, R., Hutchison, W. D., Lozano, A. M., and Dostrovsky, J. O. (2000). High-frequency synchronization of neuronal activity in the subthalamic nucleus of parkinsonian patients with limb tremor. *J. Neurosci.* 20, 7766–7775. doi: 10.1523/jneurosci.20-20-07766.2000

Limousin, P., and Foltynie, T. (2019). Long-term outcomes of deep brain stimulation in Parkinson disease. *Nat. Rev. Neurol.* 15, 234–242. doi: 10.1038/s41582-019-0145-9

Limousin, P., Pollak, P., Benazzouz, A., Hoffmann, D., Le Bas, J. F., Broussolle, E., et al. (1995). Effect of parkinsonian signs and symptoms of bilateral subthalamic nucleus stimulation. *Lancet* 345, 91–95. doi: 10.1016/s0140-6736(95)90062-4

Moreira Vasconcelos, C. F., da Cunha Ferreira, N. M., Hardy Lima Pontes, N., de Sousa Dos Reis, T. D., Basto Souza, R., Aragão Catunda Junior, F. E., et al. (2020). Eugenol and its association with levodopa in 6-hydroxydopamine-induced hemiparkinsonian rats: behavioural and neurochemical alterations. *Basic Clin. Pharmacol. Toxicol.* 127, 287–302. doi: 10.1111/bcpt.13425

Pamukcu, A., Cui, Q., Xenias, H. S., Berceau, B. L., Augustine, E. C., Fan, I., et al. (2020). Parvalbumin and npas1 pallidal neurons have distinct circuit topology and function. *J. Neurosci.* 40, 7855–7876. doi: 10.1523/jneurosci.0361-20.2020

Parent, A. (2002). Jules Bernard Luys and the subthalamic nucleus. *Mov. Disord.* 17, 181–185. doi: 10.1002/mds.1251

Paxinos, G., and Watson, C. (2009). *The Rat Brain In Stereotaxic Coordinates*. Cambridge, MA: Academic.

Pisa, M. (1988). Motor somatotopy in the striatum of rat: manipulation, biting and gait. *Behav. Brain Res.* 27, 21–35. doi: 10.1016/0166-4328(88)90106-4

Prasad, A. A., Xie, C., Chaichim, C., Nguyen, J. H., McClusky, H. E., Killcross, S., et al. (2020). Complementary roles for ventral pallidum cell types and their projections in relapse. *J. Neurosci.* 40, 880–893. doi: 10.1523/jneurosci.0262-19.2019

Prensa, L. A., and Parent, A. (2001). The nigrostriatal pathway in the rat: a single-axon study of the relationship between dorsal and ventral tier nigral neurons and the striosome/matrix striatal compartments. *J. Neurosci.* 21, 7247–7260. doi: 10.1523/jneurosci.21-18-07247.2001

Schweizer, N., Pupe, S., Arvidsson, E., Nordenankar, K., Smith-Anttila, C. J., Mahmoudi, S., et al. (2014). Limiting glutamate transmission in a Vglut2-expressing subpopulation of the subthalamic nucleus is sufficient to cause hyperlocomotion. *Proc. Natl. Acad. Sci. U.S.A.* 111, 7837–7842. doi: 10.1073/pnas.1323499111

Stamatakis, A. M., and Stuber, G. D. (2012). Activation of lateral habenula inputs to the ventral midbrain promotes behavioral avoidance [10.1038/nn.3145]. *Nat. Neurosci.* 15, 1105–1107. doi: 10.1038/nn.3145

Voruz, P., Pierce, J., Ahrweiller, K., Haegelen, C., Sauleau, P., Drapier, S., et al. (2022). Motor symptom asymmetry predicts non-motor outcome and quality of life following STN DBS in Parkinson's disease. *Sci. Rep.* 12:3007. doi: 10.1038/s41598-022-07026-5

Wallén-Mackenzie, Å, Dumas, S., Papathanou, M., Martis Thiele, M. M., Vlcek, B., König, N., et al. (2020). Spatio-molecular domains identified in the mouse subthalamic nucleus and neighboring glutamatergic and GABAergic brain structures. *Commun. Biol.* 3:338. doi: 10.1038/s42003-020-1028-8

Wu, H., Yan, X., Tang, D., Gu, W., Luan, Y., Cai, H., et al. (2020). Internal states influence the representation and modulation of food intake by subthalamic neurons. *Neurosci. Bull.* 36, 1355–1368. doi: 10.1007/s12264-020-00533-3

Conflict of Interest: The authors declare that the research was conducted in the absence of any commercial or financial relationships that could be construed as a potential conflict of interest.

Publisher's Note: All claims expressed in this article are solely those of the authors and do not necessarily represent those of their affiliated organizations, or those of the publisher, the editors and the reviewers. Any product that may be evaluated in this article, or claim that may be made by its manufacturer, is not guaranteed or endorsed by the publisher.

frontiers | Frontiers in Neuroscience

ORIGINAL RESEARCH
published: 26 May 2022
doi: 10.3389/fnins.2022.858524

Secreted Amyloid Precursor Protein Alpha, a Neuroprotective Protein in the Brain Has Widespread Effects on the Transcriptome and Proteome of Human Inducible Pluripotent Stem Cell-Derived Glutamatergic Neurons Related to Memory Mechanisms

Katie Peppercorn[1,2], Torsten Kleffmann[3], Owen Jones[2,4], Stephanie Hughes[1,2†] and Warren Tate[1,2†]*

[1] Department of Biochemistry, University of Otago, Dunedin, New Zealand, [2] Brain Health Research Centre, University of Otago, Dunedin, New Zealand, [3] Division of Health Sciences, Research Infrastructure Centre, University of Otago, Dunedin, New Zealand, [4] Department of Psychology, University of Otago, Dunedin, New Zealand

Secreted amyloid precursor protein alpha (sAPPα) processed from a parent human brain protein, APP, can modulate learning and memory. It has potential for development as a therapy preventing, delaying, or even reversing Alzheimer's disease. In this study a comprehensive analysis to understand how it affects the transcriptome and proteome of the human neuron was undertaken. Human inducible pluripotent stem cell (iPSC)-derived glutamatergic neurons in culture were exposed to 1 nM sAPPα over a time course and changes in the transcriptome and proteome were identified with RNA sequencing and Sequential Window Acquisition of All THeoretical Fragment Ion Spectra-Mass Spectrometry (SWATH-MS), respectively. A large subset (∼30%) of differentially expressed transcripts and proteins were functionally involved with the molecular biology of learning and memory, consistent with reported links of sAPPα to memory enhancement, as well as neurogenic, neurotrophic, and neuroprotective phenotypes in previous studies. Differentially regulated proteins included those encoded in previously identified Alzheimer's risk genes, APP processing related proteins, proteins involved in synaptogenesis, neurotransmitters, receptors, synaptic vesicle proteins, cytoskeletal proteins, proteins involved in protein and organelle trafficking, and proteins important for cell signalling, transcriptional splicing, and functions of the proteasome and lysosome. We have identified a complex set of genes affected by sAPPα, which may aid further investigation into the mechanism of how this neuroprotective protein affects memory formation and how it might be used as an Alzheimer's disease therapy.

Keywords: APP, amyloid beta (A4) precursor protein, sAPPα, human neuron, proteome, transcriptome, Alzheimer's disease, memory

OPEN ACCESS

Edited by:
Asheeta Prasad,
The University of Sydney, Australia

Reviewed by:
Irina Dudanova,
Max Planck Institute of Neurobiology (MPIN), Germany
Nigel Hooper,
The University of Manchester, United Kingdom

***Correspondence:**
Warren Tate
warren.tate@otago.ac.nz

† These authors have contributed equally to this work and share last authorship

Specialty section:
This article was submitted to Neurodegeneration, a section of the journal Frontiers in Neuroscience

Received: *20 January 2022*
Accepted: *14 March 2022*
Published: *26 May 2022*

Citation:
Peppercorn K, Kleffmann T, Jones O, Hughes S and Tate W (2022) Secreted Amyloid Precursor Protein Alpha, a Neuroprotective Protein in the Brain Has Widespread Effects on the Transcriptome and Proteome of Human Inducible Pluripotent Stem Cell-Derived Glutamatergic Neurons Related to Memory Mechanisms. Front. Neurosci. 16:858524. doi: 10.3389/fnins.2022.858524

INTRODUCTION

Learning and memory can be modulated by the brain protein, secreted amyloid precursor protein alpha (sAPPα), and so this molecule has potential for developing therapies preventing, delaying, or even reversing Alzheimer's disease (AD) (Mockett et al., 2017). To harness this potential, the mechanism of how sAPPα exerts its function of preserving and protecting memory needs to be elucidated in detail.

Secreted amyloid precursor protein alpha (also referred to in the literature as sAβPPα or APPsα) is the extracellular soluble proteolytic cleavage product of plasma membrane bound APP. APP is a synaptic adhesion molecule (SAM) associated with the formation of synaptic connections during neurodevelopment, contributing to the integration of the neural network, influencing neuronal migration, and the functional organisation of the growth cone and dendritic spines, where it is enriched (Stahl et al., 2014; Sosa et al., 2017). APP acts as a WNT receptor, binding the ligands WNT3a and WNT5a and this binding in turn regulates APP protein levels (Liu et al., 2021).

Endogenous sAPPα is released extracellularly after cleavage from APP by the membrane bound alpha secretases, A Disintegrin And Metalloproteinases (ADAM) 9, 10, and 17 (also known as TACE) (Allinson et al., 2003; Asai et al., 2003).

Exogenous sAPPα enhances memory (Meziane et al., 1998), is neuroprotective (Turner et al., 2007), neurogenic (Caille et al., 2004; Baratchi et al., 2012), and neurotrophic (Chasseigneaux et al., 2011). Recombinant sAPPα, can be produced in cultured HEK cells (Turner et al., 2007), and this protein regulates gene expression (Ryan et al., 2013), stimulates synaptic protein synthesis (Claasen et al., 2009) and enhances Long-Term Potentiation (LTP) (Mockett et al., 2019) and spatial learning (Ishida et al., 1997; Taylor et al., 2008).

Few studies have analysed gene expression in isolated neurons after exposure to sAPPα. IGF2 expression was shown to be regulated by sAPPα in human neuroblastoma cells (SHSY5Y) (Morris, 2011), and in rat hippocampal neurons (Stein et al., 2004). A gene array experiment identified a set of temporally changing differentially expressed genes in hippocampal slices (Ryan et al., 2013). Lentiviral overexpression of sAPPα in a mouse model of AD identified upregulation of neuroprotective genes (Ryan et al., 2021). sAPPα specifically upregulates Arc synthesis (Livingstone et al., 2019), and glutamate AMPA receptor synthesis and its trafficking (Livingstone et al., 2021).

Here we describe, how exogenously produced sAPPα applied extracellularly to human neurons (i^3Ns) in culture affects the cells' transcriptome and proteome.

RNA sequencing, an established technique for identifying and quantifying changes in global expression (Chu and Corey, 2012) was used alongside Sequential Window Acquisition of All THeoretical Fragment Ion Spectra-Mass Spectrometry (SWATH-MS), which is a quantitative and highly sensitive method for assessing changes in the proteome under different conditions (Gillet et al., 2012; Collins et al., 2013).

RNA sequencing detected both protein coding (30%) and non-coding transcripts (70%), which were significantly ($p \leq 0.05$) differentially expressed (minimum 1.5-fold change), indicative of a complex transcriptional and translational regulatory function of sAPPα that has not previously been described. SWATH-MS analysis of the differentially regulated proteins identified many that were related to neurological functions.

MATERIALS AND METHODS

Synthesis of Secreted Amyloid Precursor Protein Alpha

The protocol for the expression of human $sAPP\alpha^{695}$ in HEK cells in culture and secretion into the media was developed originally in the laboratory of Warren Tate (Turner et al., 2007). Briefly, HEK cells, stably transformed with the gene fragment for sAPPα, were cultured in DMEM without serum. sAPPα was expressed and secreted into the media, and the collected media (500 mL) was concentrated by precipitation with 60% (w/v) ammonium sulphate, with stirring for 1 h at 4°C followed by centrifuging at 10,000 × *g* for 45 min. The protein precipitate was resuspended in 20 mM Tris–HCl, pH 7.0 and residual salt was first removed by FPLC coupled to a HiTrap® desalting column. The post translational modifications added to sAPPα during expression in the HEK cells bind to heparin and so a Heparin Sepharose column can be used for affinity purification. The recovered protein fraction was bound to a HiTrap® heparin column and sAPPα was eluted with an increasing NaCl gradient in the buffer. Salt was again removed by FPLC with a HiTrap® desalting column. SDS-PAGE, Western blotting, and BCA assay analysis confirmed the purity, identity, and determined the concentration of the purified sAPPα respectively.

Human Cortical Neuron (i^3N) Cell Culture

This protocol was developed by the laboratory of Michael Ward (National Institute of Health, MD, United States) (Wang et al., 2017; Fernandopulle et al., 2018; **Figure 1A**). WTC11 hNGN2 inducible pluripotent stem cells (iPSC's) were cultured in Essential 8 media (Gibco) on Matrigel™ (Corning) coated plates until required for differentiation into cortical neurons, at which time they were passaged using accutase (Gibco) to obtain a single cell suspension. Cells (3×10^6) were seeded onto 100 mm Matrigel coated cell culture dishes with Induction Media (IM; DMEM), 1 × N2 supplement (Gibco), 1 × non-essential amino acids (NEAA, Gibco), 1 × GlutaMax (Gibco) supplemented with 10 μM doxycycline (dox, Sigma), and 10 μM Rho-associated protein kinase (ROCK) inhibitor Y-27632 (RI, day 3). After 24 h, nascent neuritic extensions were visible under a microscope, the media was replaced with IM + dox but without RI (day 2) and the cells were incubated for 24 h. Fresh IM + dox was applied to the cells and they were returned to the incubator for a further 24 h (day 1). After 3 days of doxycycline treatment, neurites were clearly visible under a microscope. The day 0 i^3N cells were cryo-preserved or plated onto Poly-L-ornithine coated cell culture vessels (for biochemistry, 1×10^5 cells/cm^2) or coverslips (for immunocytochemistry or electrophysiology, 5×10^4 cells/cm^2) in Cortical Media (CM); Brain Phys neuronal medium (STEMCELL Technologies), 1 × B27 supplement (Gibco), 10 ng/ml brain-derived neurotrophic factor (BDNF,

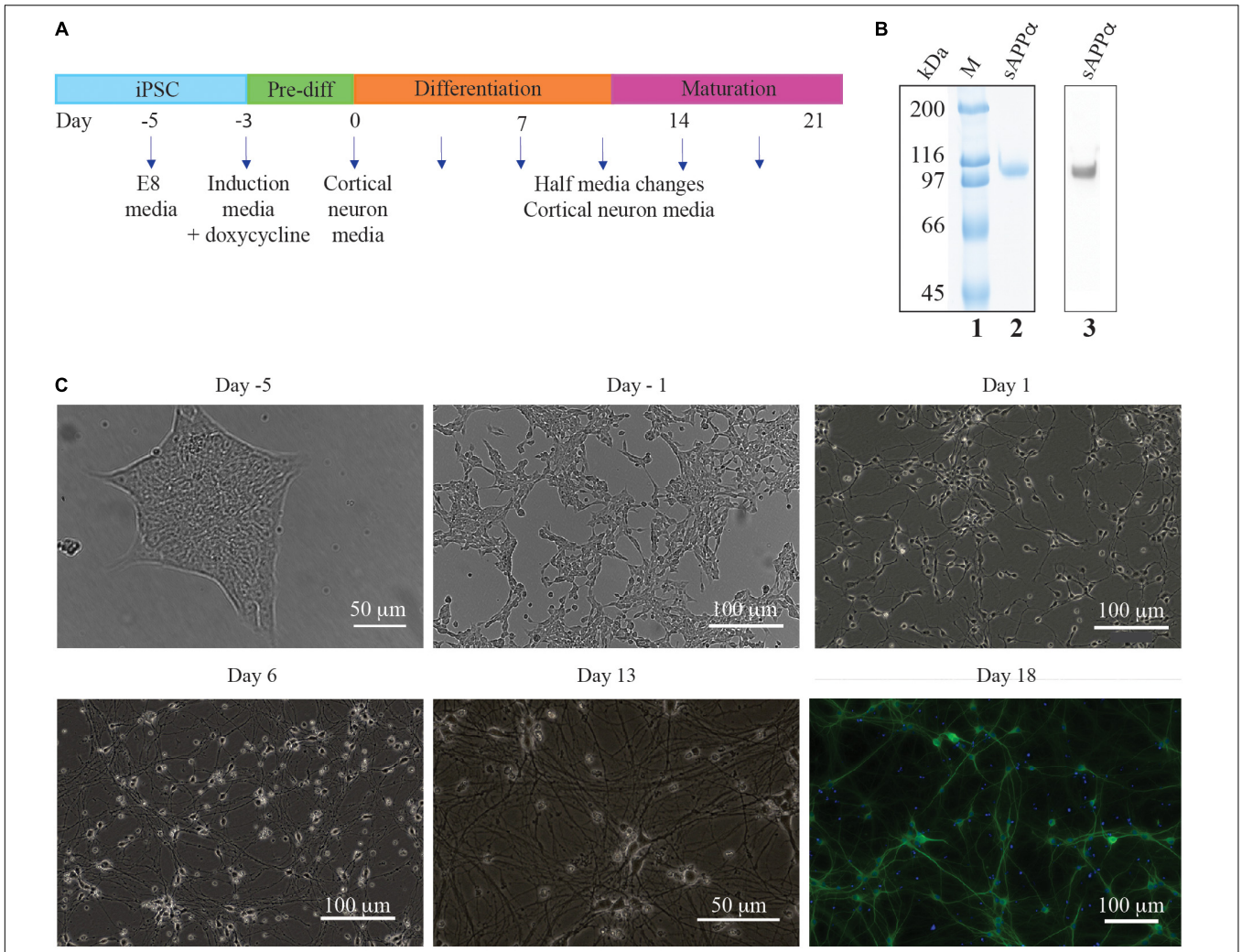

FIGURE 1 | Timeline of iPSC derived neuron generation. **(A)** E8 media until differentiation was required. Three day exposure (day −3 to day 0) to induction media containing doxycycline initiated NGN2 cortical neuron transcription factor gene expression. Cells were then cultured on poly L ornithine plates in cortical neuron media. **(B)** SDS-PAGE of purified sAPPα stained with colloidal Coomassie (lane 2) and a Western blot with N-terminal APP antibody (lane 3) which confirms the identity of sAPPα. Lane 1 has broad range protein markers (Biorad), **(C)** Brightfield photographs illustrating the generation of neurons generated from an mNGN2-iPSC colony (Day −5). Initially the iPSC colony is passaged as a single cell suspension (day −3, not shown) and after 2 days exposure to doxycycline the cells have elongated and neurites beginning to develop (day −1). After 3 days exposure to doxycycline the cells are committed to the neuron fate and are plated onto poly L ornithine plates where neurites develop further and lengthen (Day 1 and 6) and make connections with other neurons (Day 13). DIV 18 i3Ns were probed with antibodies against MAP2 (dendrite).

Pepro Tech) in PBS containing 0.1% (w/v) IgG and protease-free BSA (Gibco), 10 g/ml NT-2 (Pepro Tech) in PBS containing 0.1% (w/v) IgG and protease-free BSA, 1 µg/mL laminin (Gibco). Half media changes every 4 days for the first week were followed by weekly half media changes.

Immunocytochemistry

Characterisation of DIV 18 i^3Ns was carried out by immunocytochemistry. Cells were plated on coverslips and fixed by incubation with 300 µL 4% (v/v) paraformaldehyde (PFA, Sigma) for 15 min at room temperature. PFA was aspirated and 300 µL PBS added to the well followed by blocking by incubation with 300 µL PBS containing 3% (v/v) Normal goat serum (NGS, Invitrogen) at room temperature for 1 h. Primary antibody, MAP2 (1:1,000) (Synaptic Systems 188004), was diluted in 350 µL 3% (v/v) NGS in PBS, which contained 0.1% (v/v) Triton-X (BDH) and incubated at 4°C overnight. Antibody was removed and cells were washed three times with a 10 min incubation of 350 µL PBS, 0.1% (v/v) Triton-X. Fluorescently labelled secondary antibody anti Guinea Pig^{647} (1:1,000) (Invitrogen A21450) was diluted in 300 µL 3% (v/v) NGS in PBS, 0.1% (v/v) Triton-X and incubated at room temperature for 1 h. Three PBS-Triton-X washes removed unbound antibody and PBS was added to each well. The plates were wrapped in foil and stored at 4°C until imaging on a Fluorescent Eclipse Ti2 microscope (Nikon) attached to an

Intensilight C-HGF1 light source (Nikon) and a DS-Qi2 camera (Nikon) linked to a computer with NIS-Elements D imaging software (Nikon).

Electrophysiology

Electrophysiological characterisation of DIV18 i^3Ns was determined by single-cell electrophysiological (patch clamp) experiments to confirm that the i^3N cell culture protocol yields electrically active neurons. Coverslips housing i^3Ns were transferred to a recording chamber attached to a stage and upright microscope (Olympus BX50WI) equipped with infrared differential interference contrast optics for visualising individual cells. The cells were bathed in room temperature (24°C) artificial cerebrospinal fluid (aCSF, 124 mM NaCl, 3.2 mM KCl, 1.25 mM NaH_2PO_4, 26 mM $NaHCO_3$, 2.5 mM $CaCl_2$, 1.3 mM $MgCl_2$, and 10 mM D-glucose) saturated with carbogen [95% (v/v) O_2/5% (v/v) CO_2], flowing at 2 ml/min for the duration of the experiments. Cells were patched with thick-walled borosilicate glass recording pipettes pulled on a Flaming/Brown micropipette puller (Sutter P-97) and filled with K^+-based internal solution (135 mM K^+ gluconate, 10 mM HEPES, 4 mM ATP-Na, 0.4 mM GTP-Na_2, 10 mM phosphocreatine, 4 mM $MgCl_2$). Recordings were made using a MultiClamp 700B amplifier coupled to a Digitizer 1440A A/D board and controlled using pClamp10 software (all hardware and software from Molecular Devices). Signals were low-pass filtered at 5 KHz and digitised at 20 KHz. All patch reagents were purchased from Sigma-Aldrich. ACSF salts/sugars were purchased from Merck.

Current clamp recordings were used to elicit action potentials (indicative of electrically active, mature neurons). Cells were held at resting membrane potential (~ -70 mV) and subjected to current steps of −100 pA for 200 ms in the presence or absence of the potent and selective Na^+ channel blocker tetrodotoxin (TTX; 1 μM).

Voltage clamp recordings were obtained by clamping the neuronal membrane potential at −70 mV for a 5 min period to record spontaneous excitatory post synaptic currents (sEPSCs). The AMPA/Kainate receptor blocker NBQX (2,3-dioxo-6-nitro-7-sulfamoyl-benzo[f]quinoxaline, 10 μM) was washed in for the final minute of recording. Drugs were purchased from HelloBio ltd.

Secreted Amyloid Precursor Protein Alpha Treatment and Time Course

At DIV18 sAPPα was added to the culture media to a final concentration of 1 nM, in a reverse time course, 2 h and 30 min (for transcriptome studies) and 24, 6, and 2 h (for proteome studies) prior to harvesting the cells. This concentration of sAPPα has been shown in many of our *in vitro* published studies to be the optimum concentration for eliciting its neurological effects (for example, Ryan et al., 2013). The 0 h control cells were not exposed to sAPPα and the reverse order time course ensured all cells had the same time in culture. Cell pellets were either frozen at −80°C until required for peptide generation for mass spectrometry or lysed directly in the culture vessel for immediate RNA extraction.

Transcriptomics: RNA Sequencing

For the transcriptomics study, after media was aspirated and the cells rinsed with pre-warmed PBS, they were lysed directly in the wells of the plate by Buffer RL (350 μl) (Total RNA extraction kit, Norgen, Canada). Following 5 min incubation with swirling at room temperature the lysate was transferred to a microcentrifuge tube (2 ml), absolute ethanol added, and the solution mixed by vortexing. After centrifuging, supernatant was passed through a sterile 25-gauge needle 10× to shear the DNA, the RNA was bound to the Norgen column by centrifuging the solution for 1 min at 3,500 × *g* followed by three washes with Solution A of the kit (400 μl). Residual liquid was removed from the column by centrifuging for 2 min, and RNA was eluted with Elution Solution A (50 μl) into a fresh tube by centrifuging for 2 min at 200 × *g*, followed by 1 min at 14,000 × *g*. The RNA was stored at −80°C until use. It was treated with DNase-1 (ThermoFisher), purified (RNA clean up kit, Zymo Research) and the RNA integrity measured on a bioanalyzer (Agilent, United States). Very high-quality RNA (RIN > 9) was extracted from the human neurons by this procedure.

Nine samples of total RNA (0 h, 30 min, 2 h – each time point in triplicate) were submitted to the Otago Genomics Facility at the University of Otago (Dunedin, New Zealand) for library construction and sequencing. The libraries were prepared using TruSeq Stranded Total RNA Library Prep Gold kit (Illumina Inc., San Diego, CA, United States). All nine libraries were uniquely indexed and validated according to the manufacturer's protocol. The nine pooled libraries at equimolar concentrations were then paired end sequenced across four lanes of HiSeq 2500 flow cells using V2 Rapid chemistry (Illumina), generating 100 bp reads. The FASTQ output files were trimmed [Trimmomatic (Bolger et al., 2014)], aligned [STAR alignReads function (Dobin et al., 2013)], and mapped to the G38 human genome (Genome Reference Consortium, National Centre for Biotechnology Information, NCBI). They were merged into one read count table for statistical analysis. Two pairwise comparisons were performed, which compared the 30 min data to the 0 h data, and the 2 h data to the 0 h data, to generate tables containing ratios (fold change) showing differential expression of reads for each genomic feature. The analysis was done using limma and edgeR. The voom function of limma was used to transform count data into logCPM (count per million), estimation of mean – variance relationship in the group and thus generating a table of weights. In the next step a linear model was fitted for each gene given the series of experiments (lmFit). Moderated *t*-statistics, moderated *F*-statistic, and log-odds of differential expression were computed by empirical Bayes moderation of the standard errors toward a common value (Ritchie et al., 2015). The 100 bp reads were aligned to the human genome and, after statistical stringency was applied, a set of differentially regulated transcripts was derived compared with no treatment with sAPPα (0 time). The three biological replicates are considered too low for false discovery rate to be applied (Schurch et al., 2016) resulting in removal of valuable data (false negatives), so the unadjusted *p*-values were used for the initial selection of candidates for further investigation. Significantly ($p \leq 0.05$)

differentially expressed (1.5-fold) transcripts were grouped, and common pathways and Gene Ontology (GO) terms were sorted using the STRING functional pathway analysis[1] (version 11) and literature searching.

Proteomics: Peptide Generation

For the proteomics study, the cells were first loosened from the plate by TrypLE^{TM} Express Enzyme (Gibco, ThermoFisher) (500 μl) enzymatic digestion in each well of a 6-well plate. After rinsing with pre-warmed PBS, cells were harvested by centrifuging in an Eppendorf "lo bind" tube (1.5 ml), the pellets were snap frozen in an ethanol/dry ice bath and stored at −80°C until use.

For analysis, the frozen cell pellets from the four biological replicates of each sample at each time point were thawed in 200 μL digestion buffer [500 mM triethylammonium bicarbonate (TEAB)], 1 mM PMSF, 1 mM EDTA, 0.1% (w/v) SDS, 1% (w/v) sodium deoxycholate (SDC/DOC, Sigma), and homogenised with at least 20 grinds with a pestle creating shearing forces to break open the cells. The homogenate was vortexed for 10 s and sonicated for 1 min. After centrifuging at 16,000 × *g* for 30 min at 20°C the soluble fraction (supernatant) was retained, and contaminating DNA digested by addition of benzonase (100 U) (Sigma) followed by centrifuging at 16,000 × *g* for 30 min at 20°C. The supernatant was transferred to a 10 kDa molecular weight cut off centrifugal filter cassette unit (Amicon Ultracel – EMD Millipore), carefully avoiding the top lipid layer and the bottom pellet (DNA). Samples were further processed following the protocol for filter-aided sample processing (FASP) (Wiśniewski, 2017). In brief detergents (SDS and DOC) were depleted by washing the samples in 8 M urea in 200 mM TEAB followed by reduction and alkylation of disulphide bonds in 5 mM TCEP [Tris(2-carboxyethyl)phosphine] in 200 mM TEAB and 10 mM iodoacetamide in 200 mM TEAB, respectively. Reduced and alkylated proteins were recovered from the cassette by inversion of the filter unit placed onto a new 1.6 mL microcentrifuge tube and centrifuging. To ensure complete recovery a further 50 mL TEAB buffer was added to the filter cassette, vortex mixed, and inverted to collect the remaining protein solution by centrifugation.

The protein content of each sample was quantified with the Bradford protein quantitation assay (Bio-Rad protein assay, Bio-Rad). Peptides were generated by digesting 100 μg protein with 5 μg Trypsin (1/20th trypsin) gently vortexed and incubated overnight at 37°C. A "tryptic boost" with half the amount (2.5 μg) of the trypsin used for the overnight incubation, was added to the protein/peptide solution, gently vortexed and incubated for a further 5 h at 37°C. Peptides were purified and concentrated by Solid Phase Extraction (SPE) on Sep-Pac C18 cartridges (Waters).

Quantitative Proteomics

Proteins were identified and quantified by SWATH-MS as described in detail elsewhere (Sweetman et al., 2020). In brief an aliquot of each sample was pooled into a reference sample that was used to generate a comprehensive spectral library. The peptides of this complex reference sample were pre-fractionated into 11 fractions by high pH reverse phased fractionation on C18 cartridges (Pierce^{TM} High pH Reversed-Phase Peptide Fractionation Kit, Thermo Fischer Scientific) according to the manufacturer's protocol. Each fraction was then analysed in technical duplicates by data-dependent acquisition (DDA) mass spectrometry for protein identification using a 5600 + Triple Time-Of-Flight (TOF) mass spectrometer coupled to an Eksigent "ekspert nanoLC 415" uHPLC system (AB Sciex). For peptide quantification each individual sample was subjected to data-independent acquisition (DIA) using SWATH-MS in three technical replicates. For SWATH-MS the same instrument setup and LC-gradient settings were used as used for DDA-MS to allow an accurate alignment of the DIA peak intensities to the spectral library.

Data-dependent acquisition raw data was searched against the human reference sequence database (87,570 sequence entries, downloaded from the NCBI server[2] on 29/03/2019) using the ProteinPilot software version 4.5 (AB SCIEX). Significant peptide identifications at a false discovery rate (FDR) of ≤1% and a confidence of ≥95% were loaded into the SWATH Acquisition MicroApp 2.0 of the PeakView software (version 2.2, ABSciex) to build a spectral library. The spectral information from SWATH-MS raw data was then matched to library spectra using a time window of 12 min and a mass accuracy of 50 ppm. The intensities of the 6 strongest fragment ions from each of the 10 strongest peptides per protein that were matching the library spectra at a FDR ≤ 1% were imported into the MarkerView software (version 1.2, AB Sciex) for quantification. Intensities were normalised between the different sample runs based on the total sum of peak intensities. Unsupervised multivariate statistical analysis using principal component analysis (PCA) was then performed in the MarkerView software for sample grouping and comparison. A *t*-test of the median value of the technical replicates was carried out comparing the sAPPα group with the PBS control group, generating a dataset of proteins with significantly different relative abundances between the two groups ($p \leq 0.01$, minimum 1.5-fold change). Any proteins with a coefficient of variance over 40% of their abundance between the technical replicates were also removed from the data set. The significantly differentially expressed proteins were investigated by searching the literature and by using the STRING database (see text footnote 1) to identify functional association networks and identify potential interactions. The STRING analysis considered the differentially expressed protein lists against the three species commonly used in sAPPα research (mouse, rat databases as well as human) as some data was more enriched in the mouse and rat, and this resulted in a wider array of GO term enrichment outputs, some highly relevant to neurological function.

[1] http://string-db.org

[2] https://www.ncbi.nlm.nih.gov/

RESULTS

Secreted Amyloid Precursor Protein Alpha Production

The protein produced after expression in HEK cells in culture was highly purified to homogeneity and was identified as sAPPα by Western blotting (**Figure 1B** lane 2 – SDS polyacrylamide gel stained with Coomassie blue, and lane 3 – Western blot with an N-terminal APP antibody). The protein was larger than that theoretically derived from the amino acid sequence (72 kDa) as there are known post translational glycosylations added to the protein in human cells. The glycosylated protein has a molecular weight of ∼100 kDa. This preparation was used to determine the effect of sAPPα on the human neuron cells' transcriptome and proteome.

i^{3}N Cell Culture Characterisation

Isogenic cell cultures of human i^{3}Ns were derived from a doxycycline iPSC cell line that had been stably integrated with the neuron transcription factor neurogenin-2 (Wang et al., 2017; Fernandopulle et al., 2018). After 18 days *in vitro* these cells as shown below exhibited electrophysiological properties of glutamatergic neurons and expressed neuronal markers specific to the pre- and post-synapse, axon, and dendrites and have a morphology that is typically neuronal with long neurites projecting from a cell body.

Brightfield microscopy shows the differentiation of iPSC's into neurons (**Figure 1C**). The iPSCs grow in tight isolated colonies (day 5) but are dissociated to a single cell suspension prior to the induction of differentiation by addition of doxycycline to the culture media (day 3, not shown). The differentiating cells begin to elongate and no longer grow in colonies (day 1). Neurites (axons and dendrites) grow out from the soma (day 1) which lengthen (day 6) and form connections with other cells (day 13).

Immunocytochemistry experiments confirmed that the i^{3}Ns expressed neural markers for dendrites (MAP2) (**Figure 1C**). Previous studies from the group have shown using confocal microscopy the post synaptic protein (homer), pre-synaptic proteins (synaptophysin) and the axon marker (tau) in these cells (Basak et al., 2021). For the studies here characterisation was repeated using fluorescence microscopy and confirmed the presence of these markers

Electrophysiology Characterisation

Experiments determined that the i^{3}N were typical electrically active neurons firing Na^+ channel-dependent action potentials (**Figure 2A**) which were blocked after treatment with the sodium channel blocker TTX (**Figure 2B**). Blockade of sEPSCs by NBQX (**Figure 2C**) indicated that the currents were due to AMPA-type glutamate receptor activation i.e., these neurons form glutamatergic synapses.

RNA Sequencing

The isolated RNA from three biological replicates at each of the three time points (0, 30 min and 2 h) after incubation with 1 nM sAPPα was subjected to RNA sequencing. A total of 25,272 expressed transcripts were identified in the i^{3}N cells. Pairwise comparisons were made between both the 30 min and 2 h data against the 0 h time point data. Differentially expressed transcripts were selected if the (log 2) fold change was ±0.58 or with a *p*-value of ≤0.05. After 30 min exposure to exogenous sAPPα 645 differentially expressed transcripts were identified (**Figure 3A**), and 408 were identified after 2 h of exposure (**Figure 3B**). Biotype analysis of these transcripts revealed that 37% (30 min) and 25% (2 h) were protein coding genes, 38% (30 min) and 42% (2 h) were lncRNAs and 17% (30 min) and 25% (2 h) pseudogenes. The full lists of differentially expressed gene transcripts and their biotype at each time point are shown in **Supplementary Table 1**.

There were 241 differentially expressed protein coding transcripts at 30 min and 103 at 2 h. Differentially expressed protein coding genes from each time point were subjected to STRING functional network analysis. **Table 1** shows the GO

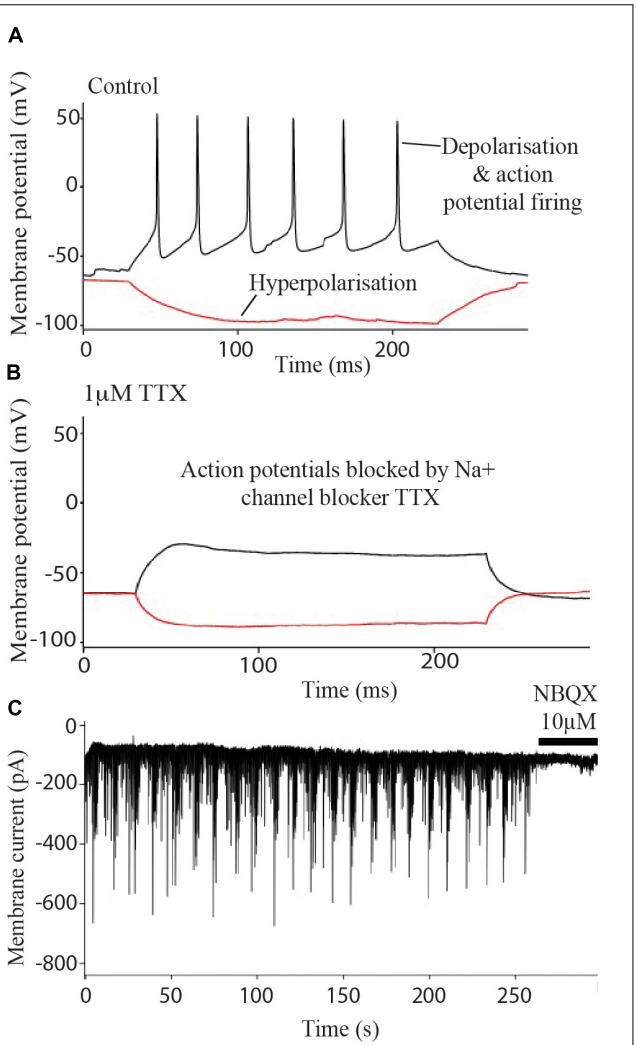

FIGURE 2 | Electrophysiology of iPSC derived neurons. Neurons fire action potentials **(A)** which are blocked after the addition of 1 μm TTX **(B)**. Excitatory post synaptic currents **(C)** are abolished after treatment with 10 μM NBQX.

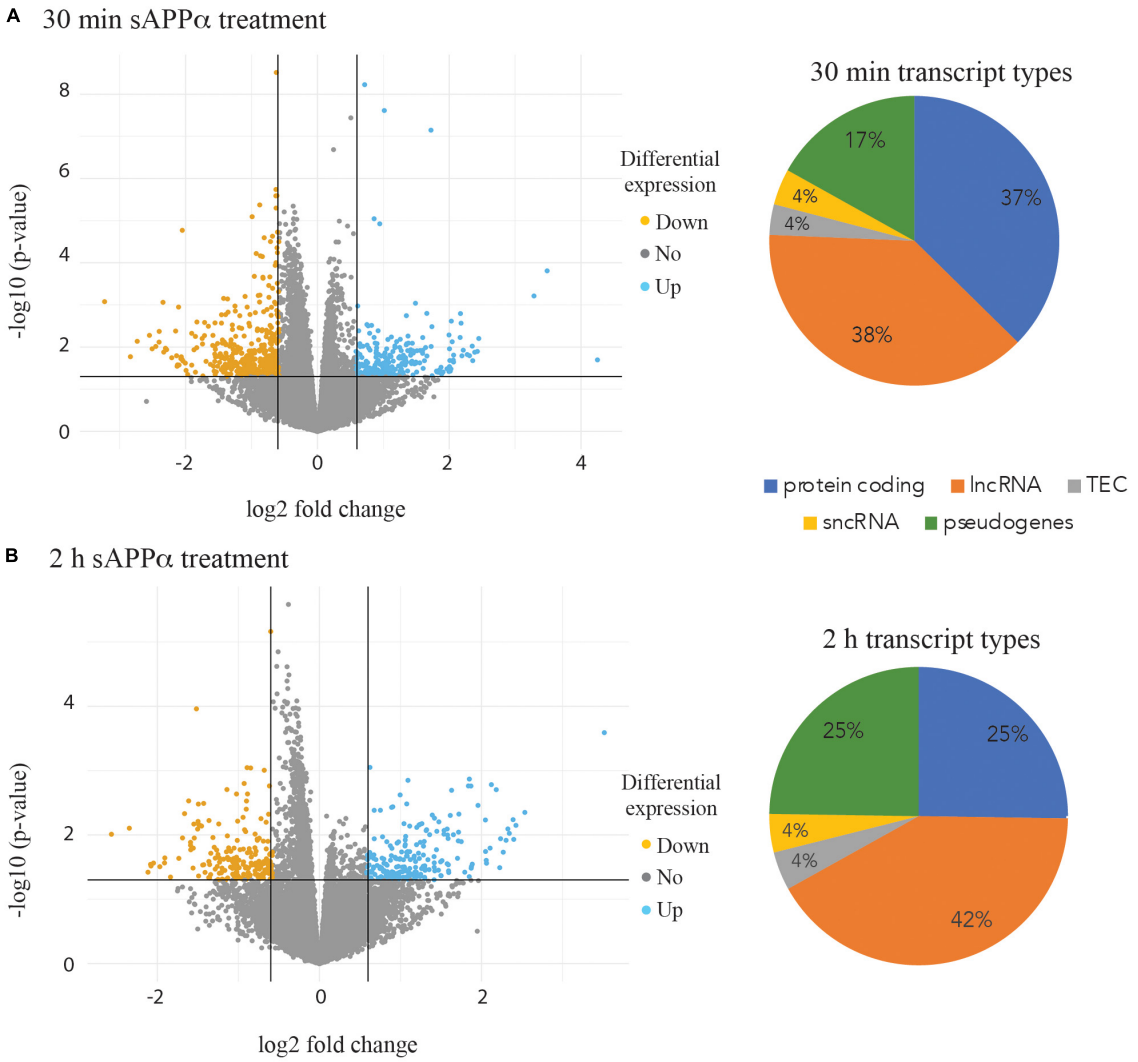

FIGURE 3 | Volcano plots highlighting differential expression of individual transcripts. Transcripts down regulated (orange points) and up regulated (blue points) are shown after 30 min **(A)** and 2 h incubation of the human neurons with 1 nM sAPPα **(B)**. Pie charts illustrating the proportion of biotypes within the group of significantly differentially expressed transcript groups in the 30 min **(A)** and 2 h **(B)** data. lncRNA – long non coding RNA, sncRNA – short non coding RNA, TEC – transcript type to be experimentally confirmed.

terms for enriched biological process, molecular function, cellular component and Uniprot Keywords within the 30 min data.

The protein coding transcripts differentially expressed at 30 min were grouped by their association with GO Pathway categories, following a STRING functional analysis.

The protein coding transcripts differentially expressed at 30 min were associated with the following GO Pathway categories.

(i) GO **Biological Functional** categories linked the differentially expressed transcripts to specific neuronal roles, including neuronal fate determination and WNT signalling. Cell signalling was a predominant class that included cell–cell signalling, cell surface signalling pathways, morphogenesis, cell communication, regulation in response to signalling, signal transduction, and calcium independent cell adhesion *via* plasma membrane adhesion molecules. (ii) GO **Molecular Function** categories included WNT binding, G protein coupled receptor binding, DNA-binding transcription activator activity, and signalling receptor binding, while (iii) GO **Cellular Component** terms indicated a large proportion of proteins affected by sAPPα were localised to the plasma membrane, cell periphery or extracellular space.

Figure 4 shows the STRING functional network diagram for protein coding genes identified as differentially expressed after 30 min and 2 h. Three individual clusters were identified by performing MCL clustering in the 30 min data (**Figure 4A**) which included a cluster of Claudin (CLDN), WNT signalling and Early Response genes.

No GO term enrichment was found after a STRING analysis of the 2 h data (**Figure 4B**).

TABLE 1 | Enrichment of GO terms in RNA sequencing data.

RNA sequencing data 30 min					
# Term ID	**Term description**	**Observed gene count**	**Background gene count**	**Strength**	**False discovery rate**
Molecular function enriched GO terms					
GO:0005109	Frizzled binding	6	39	1.11	0.0154
GO:0017147	Wnt-protein binding	5	33	1.11	0.045
GO:0001664	G protein-coupled receptor binding	16	294	0.66	0.0044
GO:0030545	Receptor regulator activity	20	536	0.5	0.0154
GO:0048018	Receptor ligand activity	18	490	0.49	0.0252
Biological Process enriched GO terms					
GO:0060070	Canonical wnt signalling pathway	8	85	0.9	0.0341
GO:0009887	Animal organ morphogenesis	29	967	0.4	0.0193
GO:0007267	Cell-cell signalling	33	1,145	0.39	0.0128
Cellular Component enriched GO term					
GO:0005886	Plasma membrane	94	5,314	0.17	0.0206
Uniprot Keywords					
KW-0879	Wnt signalling pathway	12	194	0.72	0.0028
KW-0272	Extracellular matrix	12	265	0.58	0.0255
KW-0964	Secreted	48	1,818	0.35	0.00013

A literature search of the protein coding transcripts revealed that ∼30% from both 30 min and 2 h data were involved with cell signalling, neurotransmitters, receptors and ion channels, gene transcription, actin and tubulin dynamics, ECM and cell adhesion. Additionally, the 30 min data contained eight early response genes/immediate early genes (EGR1, EGR2, FOS, KLF10, E2F8, NPAS4, BAZ2A, and CCN1).

Table 2 lists the protein encoding genes in more detail under the subheadings of (i) *early response genes and transcriptional regulators*, (ii) *cell signalling,* (iii) *neurotransmitters, receptors, and channels,* (iv) *actin and tubulin dynamics*, (v) *extracellular matrix and cell adhesion*, and (vi) *APP related proteins.* This data set indicates that sAPPα by 30 min rapidly initiates an extensive new gene expression network for the human neuron cell in culture.

Immediate early genes (IEGs) involved in memory formation were differentially expressed after 30 min and represent one of the clusters in **Figure 4A**. Early growth factor 1 (EGR 1, Zif268, Krox24) is upregulated 3.3-fold after 30 min. SNAP29 and PSD-95 are genes modulated by EGR1 and these were identified as differentially expressed in the proteome data after 24 h (Duclot and Kabbaj, 2017). A transcriptional repressor (NAB2) for EGR1 is downregulated 1.5-fold, which is consistent with the increase in EGR1 and 2 (Russo et al., 1995). Upregulated IEGs FOS and NPAS4 encode two different types of memory engrams from the same experience (Sun et al., 2020). APP promotor contains an AP1 binding site required for FOS binding potentially modulating APP transcription (Trejo et al., 1994).

WNT signalling related molecules were enriched in these data and from another cluster in **Figure 4A**. WNTs are involved during synaptic development where their expression is increased after depolarisation and NMDA receptor activation in the hippocampus, leading to dendrite development (Budnik and Salinas, 2011).

Five solute carriers were differentially expressed. These membrane proteins transport solutes across membranes and their dysregulation is implicated in neurodegenerative disease (Ayka and Şehirli, 2020). One of these, the glutamine transporter SLC7A8, is downregulated, which may impact on levels of glutamate in the neuron (Albrecht and Zielińska, 2019). Stimulation of NMDA receptors by glutamate triggers the release of Nitric Oxide, synthesised by NOS, which is downregulated here 2.6-fold. NO acts as a retrograde messenger for the induction of LTP and LTD in the hippocampus (Zorumski and Izumi, 1998). Trafficking and channel gating of AMPA receptors is regulated by TARPs like CACNG5 which is downregulated (Milstein and Nicoll, 2008).

The proadrenomedullin gene (upregulated here) generates two neuromodulatory peptides (i) AM which binds to microtubule associated proteins (MAPs) and (ii) PAMP which binds to kinesin increasing the transportation of cargo (Larráyoz and Martínez, 2012). Ablation of the ADM gene which is increased in aging mice, improves memory performance (Larrayoz et al., 2017). DARPP-32 is concentrated in dendritic spines (Blom et al., 2013) where it functions as a kinase or phosphatase inhibitor after stimulation by glutamate or dopamine (Svenningsson et al., 2004).

ADAM proteins are extracellular proteases which maintain the perinuclear net (ECM) environment required for synaptic connectivity and their dysregulation causes neurodegeneration (Gottschall and Howell, 2015). Two ADAMs are downregulated here.

Cell adhesion molecule NECTIN1 is involved with the formation of adhesive sites between cells at the synapse (Mizoguchi et al., 2002). A decrease (as seen here) in NECTIN1 level, increases the number of synapses (Honda et al., 2006). Another group of cell adhesion molecules are Claudins (CLDN). They also form a network cluster in **Figure 4A**. They form tight junctions controlling the permeability of the membrane to water and ion, Claudin-like proteins interact with actin and actin binding proteins at the synapse (Tikiyani and Babu, 2019) and Claudin family member Stargazin acts as an obligate auxiliary subunit of transmembrane

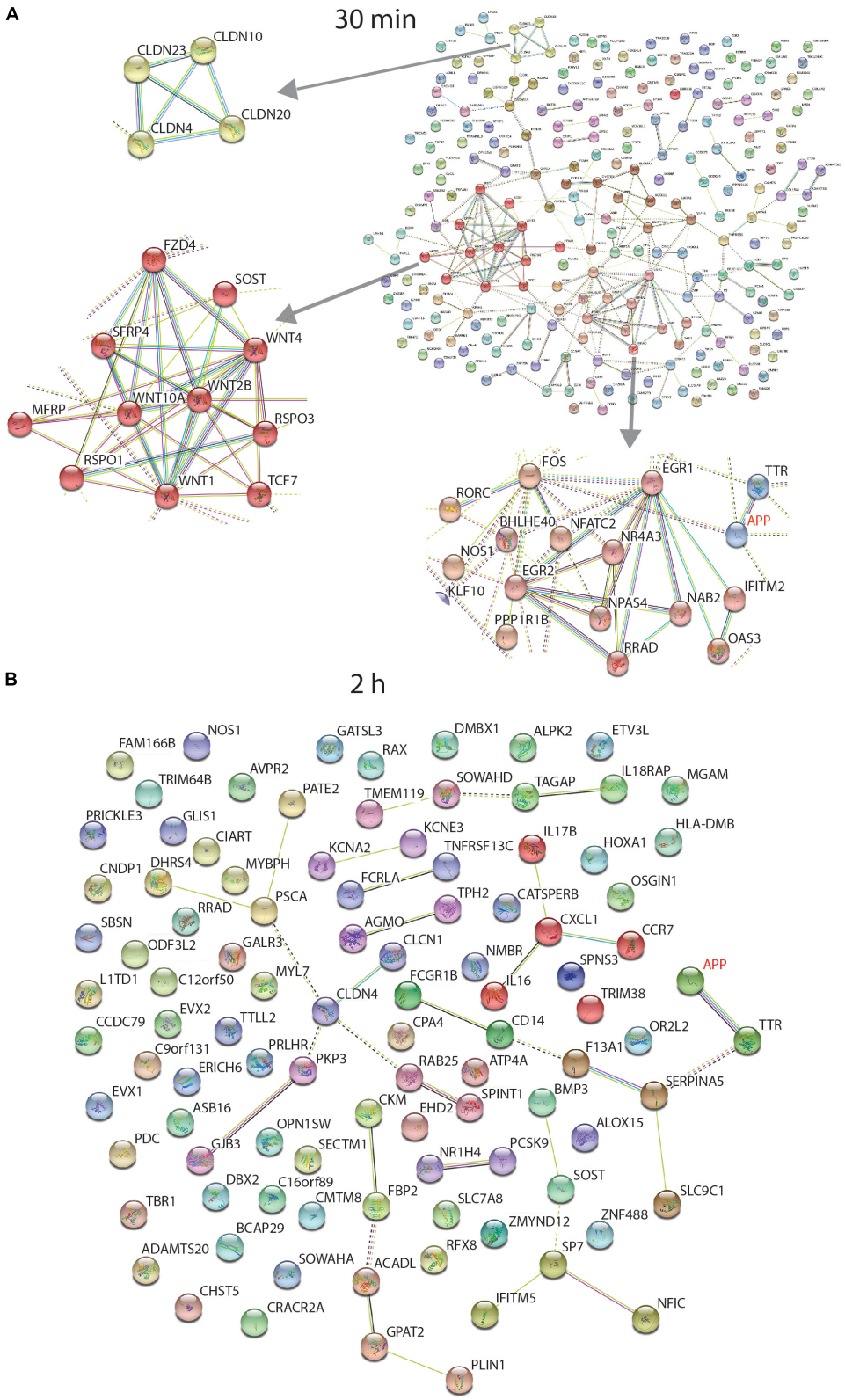

FIGURE 4 | STRING interaction network of differentially expressed protein coding genes. Data from RNA sequencing at 30 min **(A)** and 2 h **(B)**. At 30 min, incubation of the human neurons with 1 nmM sAPPα, differentially expressed transcripts were associated with enriched GO terms (coloured). There were 12 extracellular matrix proteins (purple), 48 secreted proteins (red) and 94 proteins associated with the plasma membrane (green). Three individual clusters shown at left were identified by performing MCL clustering in the 30 min data which included a cluster of Claudin (CLDN), WNT signalling and Early Response genes. The 2 h data had no enriched GO terms. Coloured proteins (nodes) are coloured representing different clusters identified after applying the Markov Clustering Algorithm (MCL) (Brohée and van Helden, 2006).

TABLE 2 | RNA sequencing data selection of protein coding genes differentially expressed after 30 min incubation with 1 nM sAPPα and their functions.

Protein coding transcripts differentially expressed at 30 min					
Gene	**Reg.**	**References**	**Gene**	**Reg.**	**References**
Early response genes and transcriptional regulators			**Receptors, channels, and transporters**		
EGR1	Up	Duclot and Kabbaj, 2017	*ARRDC4*	Down	Foot et al., 2017
EGR2	Up	Poirier et al., 2007	*SLC7A8*	Down	Albrecht and Zielińska, 2019
FOS	Up	Gandolfi et al., 2017	*SLC10A1*	Up	Ayka and Şehirli, 2020
KLF10	Down	Subramaniam et al., 2010	*SLC16A6*	Down	
E2F8	Down	Weijts et al., 2012	*SLC16A9*	Down	
NPAS4	Up	Sun et al., 2020	*SLC9C1*	Up	
BAZ2A	Down	Guetg et al., 2010	*NOS1*	Down	Paul and Ekambaram, 2011
NKX2-2	Down	Jarrar et al., 2015	*CACNG5*	Down	Milstein and Nicoll, 2008
Cell signalling			*ATP12A*	Down	Larsen et al., 2016
SPRY2	Up	Impagnatiello et al., 2001	*ATP4B*	Down	
WNT4	Down	Inaki et al., 2007	*HTR2B*	Up	Wood et al., 2011
WNT1	Down	Budnik and Salinas, 2011	*CLCN1*	Down	Chen et al., 2013
WNT10A	Down		*OTOF*	Down	Takago et al., 2018
WNT2B	Down		**Extracellular matrix and cell adhesion**		
RSPO1	Down	Jin and Yoon, 2012	*ADAMTS8*	Down	Gottschall and Howell, 2015
RSPO3	Down		*ADAMTS15*	Down	
S100A11	Down	Zhang et al., 2021	*NECTIN1*	Down	Mizoguchi et al., 2002
PLEKHA4	Down	Lenoir et al., 2015	*CLDN10*	Down	Tikiyani and Babu, 2019
PLEKHG6	Down	O'Neill et al., 2018	*CLDN20/23*	Down	
Actin and microtubule dynamics			*CLDN4*	Down	
ADM	Up	Larrayoz et al., 2017	*PCDHGA6*	Down	Weiner et al., 2005
CHAMP1	Down	Hempel et al., 2015	*PCDHGB2*	Down	
CAPN6	Down	Chen et al., 2020a	*CCN1*	Up	Chen and Lau, 2009
LIMS2	Down	Xu et al., 2016	**APP and AD related**		
DARPP-32	Up	Svenningsson et al., 2004	*SERPINC1*	Down	Sanrattana et al., 2019
–	–	–	*SERPINE1*	Down	Ho et al., 1994
–	–	–	*TTR*	Down	Li and Buxbaum, 2011
–	–	–	*CXCL1*	Up	Zhang et al., 2015

AMPA receptors that is required for glutamatergic currents (Walker et al., 2006; Wang et al., 2008). Procadherin (PCDH) family members (downregulated) are neural cadherin-like cell adhesion proteins detected in synapses and at growth cones (Weiner et al., 2005).

In summary, by 30 min of sAPPα exposure there is a differential expression of IEG's and WNT signalling molecules that will have effect on downstream genes, and genes that facilitate transport of solutes and remodelling of cellular structures like the synapse.

For the 2 h time point by contrast not only were there fewer differentially expressed protein transcripts but there was no overrepresentation of GO pathways. Nevertheless, 30 differentially expressed transcripts were common to both time points and for those downregulated this was reduced at 2 h in all cases. For the upregulated genes three genes had further enhanced upregulation at 2 h but the remainder were also reduced.

Table 3 shows a list of those differentially expressed genes at 2 h with links to neuronal function or APP, they separated into the following categories (i) *receptors, channels, and transporters*, (ii) *cell signalling*, (iii) *actin and microtubule dynamics*, and (iv) *extracellular matrix and cell adhesion*.

Some notable protein coding genes at 2 h include *ADAMTS20*, *KCNA2*, *ABSN*, and *IL17B* which may have important neural functions. In Caenorhabditis elegans gon-1, a conserved extracellular ADAMTS protease (Homologous to ADAMTS20 shown upregulated here), is required for maintaining proper synaptic morphology at the neuromuscular junction (Kurshan et al., 2014). KCNA2 (Kv1.2) is a potassium voltage gated channel involved in the induction of LTP (Hyun et al., 2015) and KCNE3 is also known as MinK-related peptide 2 which modulates potassium channels in the brain to determine firing frequency (McCrossan et al., 2003).

SBSN (Suprabasin) is involved with WNT, AKT and P38MAPK signalling (Pribyl et al., 2021) and induces sprouting during angiogenesis (Takahashi et al., 2020). Interleukins are a family of cytokines, IL16 (downregulated) induces c-fos expression and neurite outgrowth (Fenster et al., 2010). IL17B (down regulated) protein is localised to neuronal cell bodies and is linked to Charcot–Marie–Tooth (CMT) demyelinating disease (Moore et al., 2002). Another gene linked to CMT and deafness

TABLE 3 | RNA sequencing data selection of protein coding genes differentially expressed after 2 h incubation with 1 nM sAPPα and their functions.

Protein coding transcripts differentially expressed at 2 h					
Gene	**Reg.**	**References**	**Gene**	**Reg.**	**References**
Receptors, channels, and transporters			**Cell signalling**		
SLC7A8	Down	Albrecht and Zielińska, 2019	*SBSN*	Up	Pribyl et al., 2021
SLC9C1	Up	Ayka and Şehirli, 2020	*IL16*	Down	Fenster et al., 2010
NOS1	Down	Paul and Ekambaram, 2011	*IL17B*	Down	Moore et al., 2002
KCNA2	Down	Hyun et al., 2015	**Extracellular matrix and cell adhesion**		
KCNE3	Up	McCrossan et al., 2003	*CLCN1*	Down	Tikiyani and Babu, 2019
Actin and microtubule dynamics			*CLDN4*	Down	
MYBPH	Down	Hirokawa et al., 2010	*GJB3*	Down	Xia et al., 1998
CXCL1	Up	Zhang et al., 2015	*ADAMTS20*	Up	Kurshan et al., 2014

is the connexin, GJB3 (downregulated) which is a gap junction protein (Xia et al., 1998). Gap junctions are specialised cell–cell contacts that provide direct intracellular communication. They allow passive diffusion of molecules up to 1 kDa, including nutrients, metabolites (glucose), ions (K^+, Ca^{2+}) and second messengers (IP3, cAMP).

Sequential Window Acquisition of All THeoretical Fragment Ion Spectra-Mass Spectrometry

For the proteome study human iPSCs were first differentiated into glutamatergic neurons (i^3N's) as described above. Mature i^3N's were treated with 1 nM sAPPα with four biological replicates in a reverse time course for 24, 6, 2 h, or harvested immediately (0 h) so all cells had been in culture for the same time. A comparison of the differentially regulated proteins at each time point compared with the no sAPPα 0 h time control reflects the dynamic changes in protein expression and abundance that sAPPα is mediating. Cell pellets were processed to isolate proteins and generate peptides. Firstly, shotgun mass spectrometry proteomics of the pooled reference sample significantly identified 4,500 proteins, which were integrated into the spectral library. After matching the SWATH-MS spectral data against the library, 3,233 proteins were quantified at a sufficient intensity and low variability among the three technical replicates.

A PCA was carried out to assess variability in the data across all the four time points and among the four biological replicates of each time point. This showed that the four biological replicates from each time point (separately coloured) clustered together and were tightly grouped with their technical replicates. The PCA analysis showed that the biological replicates of the 0 and 2 h time points tended to group together but were clearly separated from the 6 and 24 h samples, which were themselves clustered together. This is illustrated in **Figure 5A** where the ellipses were drawn around the data sets for each time point to see how the data grouped together (four biological replicates and three technical replicates for each time point). A Venn diagram of the differentially expressed proteins (minimum 1.5-fold change, statistical stringency, $p \leq 0.01$) when compared to the untreated sample (0 h) at each time point is shown in **Figure 5B**. At 2 h, of the 21 differentially expressed proteins, 16 were differentially expressed at this time point only, and 2 were found at all time points compared with the untreated 0 h condition. At 6 h there were 115 proteins unique to this time point, and 201 shared with 24 h only, and only 2 shared with 2 h, and 2 with the other time points. There were 177 proteins uniquely differentially expressed at the 24 h time point

The median value of the technical replicates for each protein at each time point was taken to form ratio changes of 2 or 6 or 24 vs 0 h for each protein, and this is also referred to as the fold change measurement. The fold change values were converted to their log2 equivalent. A student two-tailed *t*-test was performed on the data to predict the significance (*p*-value) of the observed changes. Volcano plots were generated by plotting the −log10 *p*-value (*y*-axis) against log2 fold change (FC, *x*-axis) for each protein. The volcano plots show proteins as individual points, coloured in orange or blue if they are significantly down- or upregulated, respectively (**Figures 5C,D**). Differentially regulated proteins were initially considered for analysis if they reached a threshold of log2(FC) $\pm$ 0.58 (1.5-fold change) with a p-value $\leq$ 0.01.

For the 2 h time point there were only 11 upregulated and 8 down regulated proteins identified. These data are shown in **Supplementary Table 2**. By contrast, for the 6 vs 0 h data, there were many more differentially regulated proteins at the stringency of $p \leq 0.01$ (320, with 222 upregulated and 98 downregulated) (**Figure 5C**), and also for the 24 vs 0 h data, where there were 380 proteins identified, 265 differentially upregulated and 115 downregulated (**Figure 5D**).

The full lists of differentially regulated proteins are shown in **Supplementary Table 2** for each time point.

To find any common biological pathways or networks in which these proteins may be involved, a STRING functional network analysis was performed on the differentially expressed proteins from each time point and some of the enriched pathways are highlighted (**Figure 6**). As APP is the protein from which sAPPα is derived it was of interest to find any proteins in the data sets which had links to APP. In each case APP was added to the STRING search to determine if there are any known relationships between it and any of the differentially expressed proteins. Since sAPPα is known to influence learning and memory mechanisms, and the structure in the cell responsible for this ability is primarily the synapse, any proteins in the data set that were associated with

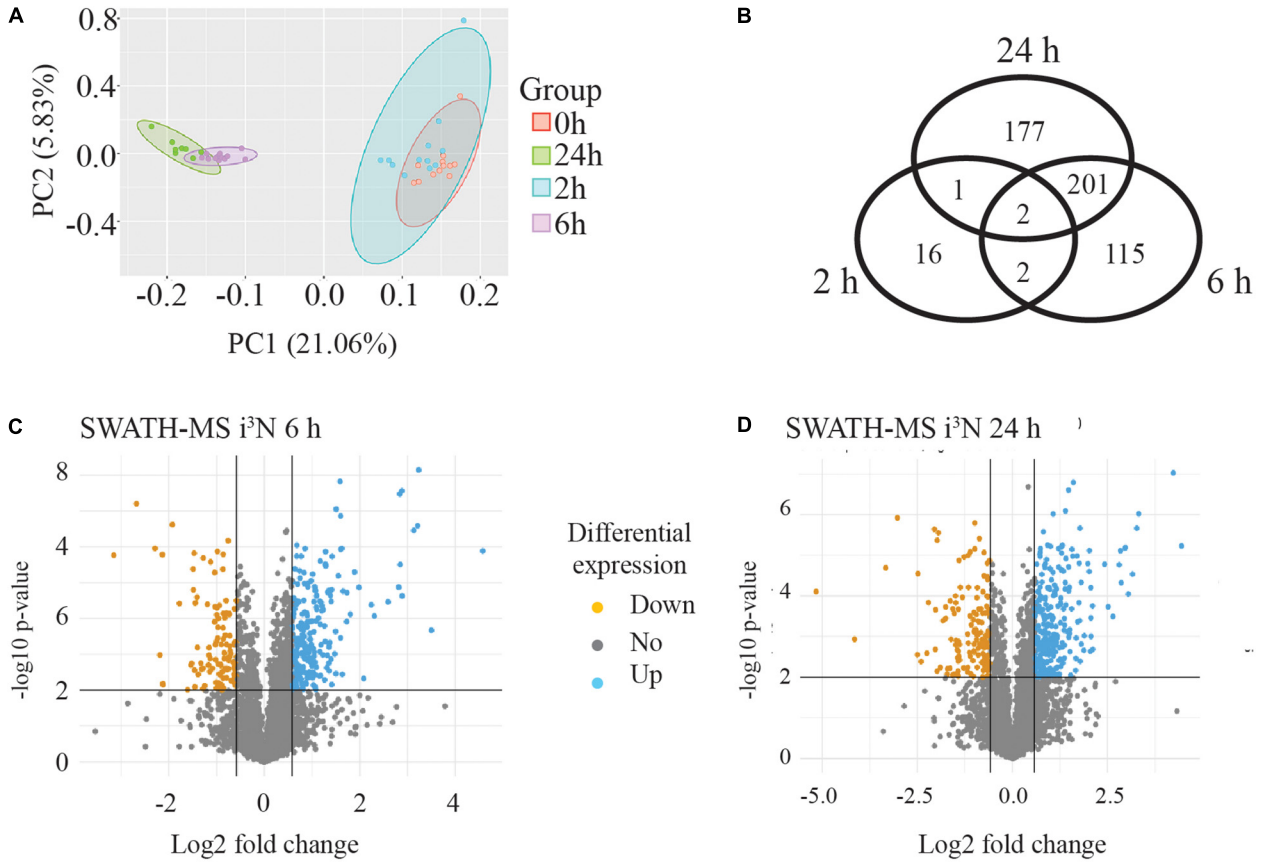

FIGURE 5 | SWATH-MS data analysis from human neurons treated with sAPPα. **(A)** PCA analysis illustrates four biological replicates and three technical replicates of the samples for each time point. The data from each time point is within an elipse. It showed that the data from 6 and 24 h data segregated from the 0 and 2 h data. **(B)** Venn diagram of significantly ($p \leq 0.01$) differentially regulated proteins revealed the number of proteins exclusive and in common to each time point compared to the zero time point. Inverse volcano plots the −log10 *p*-value (*y*-axis) against Log2 fold change (*x*-axis) at 6 h **(C)** and 24 h **(D)** to highlight any down regulated (orange point) and up regulated (blue point) proteins which meet criteria for selection of a minimum 1.5-fold change (log2 fold change ≤ -0.58 or ≥ 0.58) with *p*-value ≤ 0.01.

the neuronal projections (dendrites and axons) and the synaptic regions have been highlighted (**Figures 6A,B**).

The STRING algorithm calculates when there are enough proteins belonging to a group to be considered enriched. For example, there were 47 proteins in the neuron projection category at 24 h, but at 6 h this category was not considered enriched. A manual analysis however, compared the protein lists back to the 6 h data and noted several relevant proteins occurring in that data set as well. Supplementary tables contain the comprehensive list of enriched GO terms for 6 h (**Supplementary Table 3**) and 24 h (**Supplementary Table 4**) time point.

As illustrated in the string diagrams for the 6 h (**Supplementary Figure 1**) and 24 h (**Supplementary Figure 2**) time points, for all differentially expressed proteins there were many functional interactions within these complex patterns. Of the 320 differentially expressed proteins at 6 h (**Supplementary Figure 1**), over 80% belonged to one or more of the gene-enriched ontology groups. Of those related to neuronal functions, 15 proteins had an association with APP. Cellular compartment enrichment included many proteins that were associated with the GO terms "synapse" (42), "growth cone" (11), vesicle (112), mitochondria (65), and cytoskeleton (22). APOE and DLE4 were involved with the enriched biological process GO term "AMPA receptor clustering," and three proteins with "axon hillock." When the list of proteins was searched against the mouse database the "Axon guidance reactome pathway" was enriched with nine differentially expressed proteins. In the summary of the analysis data from the 24 h time point linked to neurological function (**Supplementary Figure 2**), APP was now linked with 20 different proteins, and GO Cellular Component terms enriched included "synapse, neuron projection, spliceosomal complex, cell junction, mitochondrial, and actin cytoskeleton." GO biological processes had highly significant categories of "modulation of excitatory post synaptic potential," "membrane biogenesis, regulation of exocytosis, regulation of actin filament polymerisation, and regulation of RNA splicing."

To tease out functionally important interactions with APP, a STRING diagram associated with "Neuronal projection" and "Synapse" GO terms were generated to observe how they

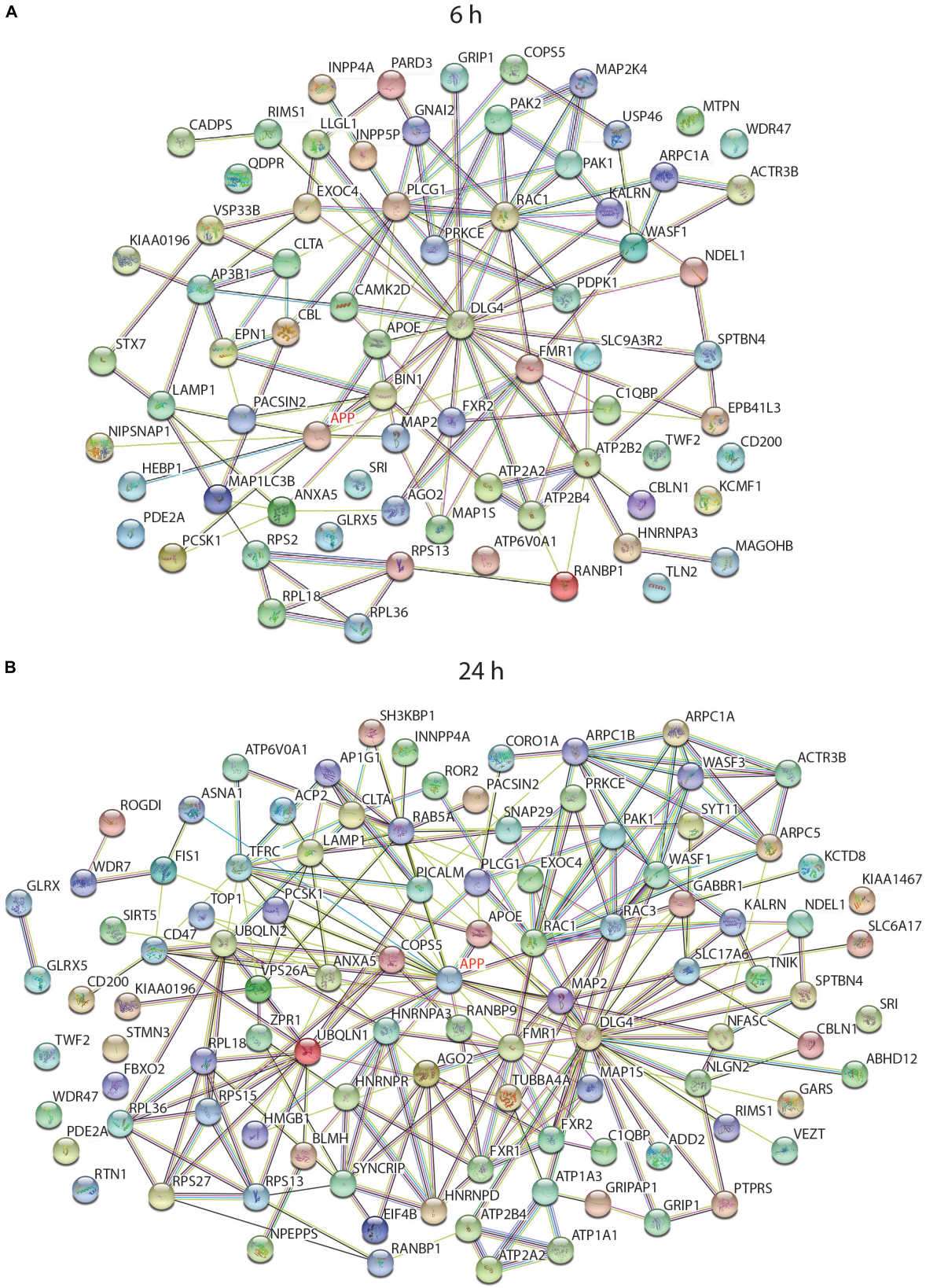

FIGURE 6 | String analysis of functional interactions of differentially regulated proteins after incubation of neurons with sAPPα. Diagram shows the significantly differentially regulated proteins, which were linked to cellular component GO terms with a neural functions and/or had a connection to APP, and their relationship to others in the 6 h **(A)** and 24 h **(B)** data set when searched against the human protein database (log2 (FC) -/+ 0.58, $p \leq 0.01$).

interacted with each other and the experimental effector protein sAPPα (as APP). This is illustrated in **Figures 6A,B** (the full list of proteins associated with each GO term is in **Supplementary Table 5**). This clearly illustrates that sAPPα can change the overall gene expression of the human neuron for functions critical to its role as a neural cell not only directly but also indirectly as it spreads out to affect many other cellular and biological functions.

The full lists of the differentially expressed proteins are shown in **Supplementary Table 2** and those proteins highlighted as having neuronal function or linked to APP or AD are shown in **Supplementary Table 6** (6, 24 h). Those related to APP included one differentially regulated protein at 2 h, 9 proteins at 6 h and 21 proteins at 24 h after sAPPα application. Of previously identified Alzheimer's risk genes (Rosenthal et al., 2012), four proteins encoded by them were differentially expressed, for example, APOE was upregulated at 6 and 24 h, and PICALM was downregulated at 24 h, BIN1 upregulated at 6 h, and SH3KBP1 was upregulated at 6 and 24 h. These are listed in more detail in **Table 4** (6 h) and **Table 5** (24 h). The references in the table describe the protein in question. Categories included in **Table 4** are (i) *synaptic vesicle*, (ii) *APP and AD related*, (iii) *neurite outgrowth and synapse*, (iv) *actin and microtubule dynamics*, (v) *neurotransmitters receptors and ion channels*, and (vi) *lysosome and proteasome*. Hence, the proteins discussed here **Table 4** (6 h) relate to GO terms with (i) neuronal functions or (ii) have known association with APP (as predicted by the STRING network analysis) or (iii) are associated with a neurological disorder.

Table 5 shows the protein differentially expressed at 24 h under the categories (i) *APP and AD related*, (ii) *neurotransmitter and ion channels*, (iii) *synaptic vesicle*, (iv) *actin and microtubule dynamics*, (v) *neurite outgrowth and synapse*, and (vi) *proteasome and lysosome*.

DISCUSSION

This study investigated how the neuroprotective protein, sAPPα, changes the gene expression profile of a human neuron in culture. The key reagent for the study was a recombinant sAPPα (Turner et al., 2007) derived from the APP^{695} isoform, which is the predominant form in the brain. We confirmed by immunocytochemistry that APP was expressed in the neurons in culture and thereby physiologically important in this human cell culture model. The isogenic human iPSC-derived glutamatergic neurons (i^3N) grown in culture for the studies expressed neuronal markers of axons, dendrites and pre and post synaptic compartments. The changes in the expression profile of the neurons in response to sAPPα was determined by discovery transcriptomics and proteomics.

Transcriptome

To access the immediate effects of sAPPα on expression at the genome the time points of 30 min and 2 h after sAPPα application were chosen, resulting in 204 and 103 differentially expressed protein coding transcripts respectively. Protein coding transcripts made up 37 and 25% of the differentially expressed transcripts at 30 min and 2 h of exposure to sAPPα, respectively – the remainder were predominantly lncRNA transcripts (∼40%). With less published literature on their functions, a preliminary investigation of how they might relate to changes in neurological functions of the neurons did not give any close linkages, and so were not further investigated here. They will be the subject of a more detailed future investigation. It found that IEGs/transcription factors were a significant feature of the 30 min transcripts. A secondary expression of a cascade of genes regulated by the transcription factors will be initiated. Previously, we have shown if an IEG (e.g., *EGR-1* or *FOS*) is expressed as an mRNA by 30 min from a stimulatory induction, then upregulation of the proteins encoded by these transcripts occurs at 1–2 h (Abraham et al., 1991; Demmer et al., 1993).

The STRING functional network analysis also revealed distinct **hubs** of transcripts that encode proteins which are functionally associated to one another according to known and predicted interactions as well as from the literature. Of these

(i) ***APP*** was directly linked to five genes and each of those genes were also linked to other genes (number in parenthesis), *CX3CL1* (2), *TTR* (3), *C3* (3), *NRGN* (1), and *FOS* (15).
(ii) ***FOS*** was the largest hub and 15 other protein encoding genes were linked to it; *SERPINE1, EGR1, EGR2, PPP1R1B, HNF1A, CCNA2, KLF10, AVPR1A, CXCL1, GHRH, NOS1, NR4A3, NPAS4, RORC*, and *NFATC2* plus *APP*.
(iii) ***EGR1*** had 13 protein encoding genes linked to it, *SERPINE1, OAS3, CXCL1, BHLHE40, GDF15, NR4A3, NPAS4, EGR2, IFITM2, RRAD, NFATC2, NAB2*, and *FOS*.
(iv) ***EGR2*** was linked to eight protein encoding genes, *EGR1, WNT1, NFATC2, NPAS4, NR4A3, RRAD, FOS*, and *NAB2*.
(v) ***WNT1***, *10A, 2* and *4* collectively were linked to 21 other protein encoding genes, *EGR2, WNT10A, WNT4, MFRP, NKX2-2, RSPO3, TCF7, ATOH1, RSPO1, LRP5L, SFRP4, FZD4, SOST, MFRP, EDAR, WNT1, WNT2B, FOXL1*, and *CYP11A1*.

The hub proteins encompass the IEG transcription factors (*FOS, EGF1*, and *EGF2*) and key signalling molecules *APP* and *WNT1*, and the connected proteins fit broadly into the following functional groups of cell signalling, actin and tubulin dynamics – cytoskeleton, early response genes and transcriptional regulators, extracellular matrix and cell adhesion, and receptors, and channels and neurotransmitters.

Proteome

The differential protein profiles measured in this study indicate that some are associated with the observed changes in gene expression of the transcription factors, that would modify the phenotype of the neurons. These long-term physiological actions of sAPPα (LTP facilitation, neurite outgrowth, neuroprotection, and gene expression) can have rapid onset (min to h) but can also be long lasting (days to months). After 2 h exposure to sAPPα in this study there were only 21 proteins differentially expressed at a stringency of $p < 0.01$ and with a fold change of 1.5 or greater compared with untreated cells (0 h). By contrast 320 and 380 differentially regulated proteins were identified at

TABLE 4 | SWATH-MS data selection of proteins differentially regulated after 6 h exposure to sAPPα.

Proteins differentially regulated after 6 h					
Protein	**Reg.**	**References**	**Protein**	**Reg.**	**References**
Synaptic vesicle			**APP and AD related**		
CLTA	Up	Redlingshöfer et al., 2020	APOE	Up	Saunders et al., 1993
BIN1	Up	De Rossi et al., 2020	CD200	Up	Varnum et al., 2015
NIPSNAP1	Down	Antonucci et al., 2016	COPS5	Up	Wang et al., 2013
RIMS1	Up	Lonart, 2002	PCSK1	Up	Maftei et al., 2019
VAPA	Up	Lindhout et al., 2019	**Actin and microtubule dynamics**		
EPN1	Down	Jakobsson et al., 2008	MAP2	Up	Johnson and Jope, 1992
SNX12	Up	Zhang et al., 2018	MAP1S	Down	Bodakuntla et al., 2019
SNX2	Up		MAP1LC3B2	Up	
STX7	Up	Mori et al., 2021	MAP2K4	Up	
EXOC4	Down	Liebl et al., 2005	MAPRE3	Up	
Neurite outgrowth and synapse			WDR47	Up	Chen et al., 2020c
CBLN1	Up	Yuzaki, 2011	CORO2A	Up	Marshall et al., 2009
PSD95	Down	Coley and Gao, 2018	CORO2B	Down	Chen et al., 2020b
TWF2	Up	Yamada et al., 2007	PACSIN2	Up	Ritter et al., 1999
SPTBN4	Down	Machnicka et al., 2014	MTA2	Down	Covington and Fuqua, 2014
WASHC5	Down	Freeman et al., 2013	ACTR3B	Down	Galloni et al., 2021
RABIF	Down	Gulbranson et al., 2017	AP3B1	Up	Li et al., 2016
RAC1	Up	Haditsch et al., 2009	ARPC1A	Up	Spence et al., 2016
RALA	Up	Li et al., 2007	KALRN	Up	Mandela and Ma, 2012
RALB	Up		PFDN1	Down	Liang et al., 2020
RANBP1	Up	Mignogna and D'Adamo, 2018	PFDN4	Up	
RANBP3	Down		PFDN6	Up	Gu et al., 2008
NDEL1	Down	Kuijpers et al., 2016	TLN2	Down	Morgan et al., 2004
AGO2	Up	Rajgor et al., 2018	**Receptors, channels, and transporters**		
IGFBPL1	Up	Guo et al., 2018	GRIP1	Up	Tan et al., 2015
CADM4	Up	Tanabe et al., 2013	INPP4A	Down	Sasaki et al., 2010
Lysosome and proteasome			SLC25A22	Up	Hu et al., 2020
USP10	up	Lim et al., 2019	SLC41A3	Down	
USP15	down	Young et al., 2019	SLC9A3R2	Up	
USP24	up		FXR2	Up	Guo et al., 2015
USP46	up		FMR1	Up	Telias, 2019
CBL	up	Zhang et al., 2020	ATP2A2	Up	Mata and Sepulveda, 2010; Larsen et al., 2016
KCMF1	down	Hong et al., 2015	ATP2B2	Down	
UBE3A	down	Vatsa and Jana, 2018	ATP2B4	Up	
–	–	–	ATP6V0A1	Up	
–	–	–	LAMP1	Up	Hwang et al., 2019

the same stringency and at 6 and 24 h, respectively. IEGs known to be involved in memory formation, which were differentially expressed after 30 min included Early Growth Factor 1 (EGR1, aka Zif268, and Krox24). SNAP 29 and PSD-95 are downstream genes modulated by EGR1 (Duclot and Kabbaj, 2017), and these were identified in our proteome profile as differentially regulated after 24 h. WNT signalling related molecules are also enriched in these data. It is interesting that APP has recently been identified as a WNT signalling receptor (Liu et al., 2021).

Proteins Related to Neurological Function at the Synapse

Synaptogenesis

The long-term aim of the focus on sAPPα is that it has potential for development as a therapeutic for AD. Proteins from four risk factor genes for AD are differentially regulated in the proteome dataset (APOE, PICALM, BINI, and SH3KBP1) (Rosenthal et al., 2012). For example, BIN 1 (upregulated) is a late onset AD risk factor gene that aids memory consolidation and regulates presynaptic neurotransmitter release (De Rossi et al., 2020). Synaptogenesis is an important component of this. Synaptogenesis involves actin nucleation and encompasses WASH/WAVE/Arp2/3 proteins/Coronins/ACTR3B/AP3B1/ARPC1A, which are all differentially regulated in our study. Arp2/3 complex is necessary for the recruitment of AMPA receptors in newly formed excitatory glutamatergic synapses (Spence et al., 2016). Coronins are actin binding proteins that can regulate actin dynamics by coordinating the activities of the actin-polymerising nucleator Arp2/3 complex (Chan et al., 2011). Interestingly, CORO2A is one of the long-lived

TABLE 5 | SWATH-MS data selection of proteins differentially regulated after 24 h of exposure to sAPPα.

Proteins differentially regulated after 24 h					
Protein	**Reg.**	**References**	**Protein**	**Reg.**	**References**
APP and AD related			**Receptors, channels, and transporters**		
SH3KBP1	Up	Rosenthal et al., 2012	SRI	Up	Genovese et al., 2020
APOE	Up	Saunders et al., 1993	GABBR1	Up	Terunuma et al., 2014
CD200	Up	Varnum et al., 2015	KCTD8	Down	Seddik et al., 2012
PICALM	Down	Zhao et al., 2015	GRIP1	Up	Tan et al., 2015
TFRC	Up	Zhou et al., 2017	GRIPAP1	Up	Chiu et al., 2017
BLMH	Down	Lefterov et al., 2000	FMR1	Up	Telias, 2019
COPS5	Up	Wang et al., 2013	FXR1	Up	Guo et al., 2015
FBXO2	Up	Atkin et al., 2014	FXR2	Up	
PCSK1	Up	Maftei et al., 2019	SLC17A6	Up	Hu et al., 2020
VPS26A	Up	Lin et al., 2015	SLC25A22	Up	
Synaptic vesicle			SLC41A3	Down	
SYT11	Up	Shimojo et al., 2019	SLC6A17	Down	
SNAP29	Up	Pan et al., 2005	ATP1A1	Up	
CLTA	Up	Redlingshöfer et al., 2020	ATP1A3	Up	Mata and Sepulveda, 2010;Larsen et al., 2016
RIMS1	Up	Lonart, 2002	ATP2A2	Up	
AP1G1	Up	Guardia et al., 2018	ATP2B4	Up	
RAB5A	Up	de Hoop et al., 1994	ATP6V0A1	Up	
WDR7	Up	Chen et al., 2020c	**Actin and microtubule dynamics**		
VAPA	Down	Lindhout et al., 2019	TUBB4A	Down	Sase et al., 2020
SNX12	Up	Zhang et al., 2018	TUBB4B	Down	Muñoz-Lasso et al., 2020
SNX2	Up		MAP2	Up	Johnson and Jope, 1992
Neurite outgrowth and synapse			MAP1S	Down	
CBLN1	Up	Yuzaki, 2011	MAPRE3	Up	Bodakuntla et al., 2019
NLGN2	Down	Katzman and Alberini, 2018	STMN3	Up	Uchida and Shumyatsky, 2015
EXOC4	Down	Liebl et al., 2005	WDR47	Up	Chen et al., 2020c
CD47	Up	Lehrman et al., 2018	CORO1A	Down	Jayachandran et al., 2014
PSD95	Down	Coley and Gao, 2018	CORO1B	Up	
AGO2	Up	Rajgor et al., 2018	CORO2A	Up	Heo et al., 2018
TWF2	Up	Yamada et al., 2007	CORO2B	Down	Chen et al., 2020b
ADD2	Up	Babic and Zinsmaier, 2011	TNIK	Down	Fu et al., 1999
NFASC	Up	Pourhoseini et al., 2021	PFDN1	Down	Liang et al., 2020
SPTBN4	Down	Machnicka et al., 2014	PFDN4	Up	
KALRN	Up	Mandela and Ma, 2012	PFDN6	Up	Gu et al., 2008
NDEL1	Down	Kuijpers et al., 2016	ACTR3B	Down	Spence et al., 2016
WASF1	Up	Derivery et al., 2009	ARPC1A	Up	
WASF3	Down		ARPC1B	Up	
WASHC5	Down	Freeman et al., 2013	ARPC5	Up	
RAC1	Up	Haditsch et al., 2009	**Proteasome and lysosome**		
RAC3	Up	de Curtis, 2019	LAMP1	Up	Hwang et al., 2019
RALA	Up	Li et al., 2007	LAMTOR1	Up	Malek et al., 2012
RALB	Up		UBQLN1	Up	Hiltunen et al., 2006
RANBP1	Up	Mignogna and D'Adamo, 2018	UBQLN2	Up	Renaud et al., 2019
RANBP3	Down		USP10	Up	Lim et al., 2019
RANBP9	Down		USP24	Up	Young et al., 2019
IGFBPL1	Up	Guo et al., 2018		–	–
PTPRS	Up	Yu et al., 2018	–	–	–

proteins (LLP) identified as having an extraordinarily long (months/years) half-life at the synapse and they are postulated to be important for long term stable memories (Heo et al., 2018). Cerebellin 1 (CBLN1, upregulated) is a synaptic organiser involved with the precise apposition of presynaptic and postsynaptic regions, essential for the

formation of functional synapses. CBLN receptors are the presynaptic, neurexin (NRX) and the post synaptic, glutamate receptor (GluD2) (Yuzaki, 2011). PSD-95 (downregulated) is a postsynaptic scaffolding protein that plays a critical role in synaptogenesis and synaptic plasticity by providing a platform for the postsynaptic clustering of crucial synaptic proteins (Coley and Gao, 2018).

Exocytotic Release of Neurotransmitters at the Synapse

Exocytosis is a critical component of the function of the synapse. NIPSNAP1 is part of the SNARE complex (downregulated at 6 h) involved in the exocytotic release of neurotransmitters during synaptic transmission (Antonucci et al., 2016). At 24 h, SNAP29, which is associated with the disassembly of the SNARE complex (Pan et al., 2005) is upregulated. At the synaptic active zone vesicle exocytosis is also regulated by RIMS1 (RAB3, upregulated) (Lonart, 2002) and VAPA (upregulated) (Lindhout et al., 2019) while EPN1 (downregulated) is involved with endocytosis (Jakobsson et al., 2008). Syntaxin 7 (STX7) is involved with the replenishment of readily releasable synaptic vesicles in the hippocampus, which allows for sustained neurotransmitter release (Mori et al., 2021).The exocyst complex is a multiple protein complex essential for targeting exocytic vesicles to specific docking sites on the plasma membrane. For example, in *Drosophila* SEC8 (EXOC4) is involved in the regulation of synaptic microtubule formation, regulation of synaptic growth and glutamate receptor trafficking (Liebl et al., 2005).

Wider Transport of Cargos Important in Neurological Function

Sorting Nexins (SNX) are important for correct intracellular transport including APP and AP-cleaving enzymes, dysregulation of which causes neurodegenerative disease (Zhang et al., 2018).

NudE Neurodevelopment Protein 1 Like 1 (NDEL, downregulated) is concentrated at the axon initial segment where it regulates dynein and the trafficking of transport cargos specifically bound for the axon (Kuijpers et al., 2016). GRIP1 (glutamate receptor-interacting protein), upregulated at 6 and 24 h, regulates the homeostatic shuttling of AMPARs between cytoplasmic and synaptic pools (Tan et al., 2015). A related protein GRIPAP1 (GRIP1-associated protein 1, also known as GRASP1) is upregulated at 24 h and is involved with endosomal recycling of AMPA receptors (Chiu et al., 2017). Members of the solute carrier family (SCL) are differentially expressed both in the transcriptome and proteome and are responsible for the transport of molecules across the cell membrane (Hu et al., 2020). Members of the Na^+ /K^+ ATPase family (ATP1 and ATP2) controlling extracellular K^+ and suggested to work in concert with the glutamate transporter are also differentially expressed both in the transcriptome and proteome data (Larsen et al., 2016).

Comparison With Other Molecular Studies Investigating the Effects of Secreted Amyloid Precursor Protein Alpha

Secreted amyloid precursor protein alpha promotes the expression of the IEG encoding the plasticity protein, ARC, in primary hippocampal neurons and that in turn regulates AMPA receptor synthesis and trafficking (Livingstone et al., 2019, 2021). Many attempts to identify the sAPPα receptor have finally provided evidence of two receptors that likely are the first points of contact for sAPPα functions. Its contact through an N terminal domain with $GABA_\beta R1a$ regulates the function of the receptor to modulate synaptic transmission and plasticity (Rice et al., 2019). The C terminal 16 amino acids that differentiate sAPPα from sAPPβ act to potentiate the nicotine acetyl choline receptor, a7-nAChR, that functions in facilitating LTP (Richter et al., 2018).

Two key studies with sAPPα and global gene expression have been carried out to date. Stein et al. (2004) showed that sAPPα increased the expression of several neuroprotective genes and protected organotypic hippocampal cultures from amyloid beta–induced tau phosphorylation and neuronal death. Transthyretin was highly expressed and necessary for sAPPα protection. (Ryan et al., 2013) measured time dependent changes in the expression of transcripts in organotypic rat hippocampus slice cultures in response to sAPPα as measured by an Affymetrix rat gene array. They showed chronological changes from 15 min to 2 h to 24 h with many unique changes at each time point and small numbers of overlaps. Most of the expression was upregulation at 15 min but downregulation predominated at the other two time points. Consistent with our study, IEGs/transcription factors were prominent in the upregulated genes (for example, FOS and EGR-1), as well as NFk-B and CREB regulated genes, whereas at 2 h, inflammatory response regulation was the most significant biological function of the highest scoring network. A recent mouse proteomic study comparing an AD model and healthy controls identified protein members for similar family group as this study (splicing factors, ribosomal proteins, proteasome, chaperones, syntaxins, and solute carrier proteins) (Elder et al., 2021). A genome wide association study (GWAS) identifying AD risk genes highlighted 11 causal genes, 4 of which were found in this study [sortin, nexin, syntaxin, and pleckstin homology domain proteins (Wingo et al., 2021)]. Our findings and those from Ryan et al. (2013) are consistent with a broader study of amyloid precursor protein family members in the adult cortex (Aydin et al., 2011).

Limitations of the Study

The transcriptome and proteome outputs are samplings of very large datasets, and the setting of relatively high stringency will inevitably lead to some relevant data being removed from the analysis as false negatives. Proteome analysis relies on the analysis of the intensity of peaks that are affirmed in technical replicates within statistical boundaries. This means proteins present at low levels tend to show lower reproducibility and often fail statistical significance. In this case ∼3,200 proteins passed

our stringent filters were analysed for differential regulation between the time points. Nevertheless, the advantages of the analytical tools facilitate a grouping of the individual protein data through known functional interactions, and functional annotation through the three main GO aspects of Biological Process, Molecular Function and Cellular Component giving an integrated picture of what features of the neuron are being affected. While validation of the many individual changes seen in both transcripts and proteins throughout their time courses would be desirable by independent methods such as quantitative PCR for the transcripts, and immunocytochemistry and Western analysis for the proteins, these methods are applicable in reality to a very small proportion of the differentially expressed molecules of the data set. Indeed Aebersold et al. (2013) have argued that targeted proteomic methods provide a better method of validation than Western blotting. Here, the study aimed to establish a chronological global profile of a gene expression changes and to determine from the collective data whether dynamic physiological changes could be derived.

Future Directions

This study has established small and large molecular hubs that are activated in responses to sAPPα and these will be rich sources for elucidating the detailed molecular pathways of the sAPPα mediated effects on phenotype of the neuronal cells like memory enhancement (Meziane et al., 1998), neuroprotection (Turner et al., 2007), neurogenesis (Caille et al., 2004; Baratchi et al., 2012), and neurotrophy (Chasseigneaux et al., 2011). Recombinant sAPPα also enhances LTP (Mockett et al., 2019) and spatial learning (Ishida et al., 1997; Taylor et al., 2008). sAPPα is protective against memory impairments (Fol et al., 2016; Tan et al., 2018) but the details of how that occurs through the myriad of signalling pathways is still to be elucidated. Understanding these detailed mechanisms of how sAPPα mediates it global functions is important if the molecule is to be exploited for its therapeutic potential.

This study of the way in which sAPPα influences the gene expression profile specifically of the human neuron to fulfil its protective and growth roles has shown there is a comprehensive response in the proteins that are related to the functions of neurological significance. From the initial direct interaction of sAPPα with cellular components there is a large ripple effect that spreads to affect broadly the wider function of the neuron and to change its character.

DATA AVAILABILITY STATEMENT

The original contributions presented in the study are publicly available. This data can be found here: GEO submission GSE197725 and the ProteomeXchange Consortium *via* the PRIDE repository PXD031704 (Perez-Riverol et al., 2022).

AUTHOR CONTRIBUTIONS

KP helped plan the research, carried out the experimental work, and co-wrote the manuscript. WT supervised the project and co-wrote the manuscript. SH co-supervised the project and assisted with the writing of the manuscript. TK managed the proteome aspect of the study and its analysis and assisted with the writing of the manuscript. OJ provided the electrophysiology experimental expertise to validate the human neurons used for the study. All authors contributed to the article and approved the submitted version.

FUNDING

We acknowledge the Health Research Council of New Zealand for a programme grant #16/597 that supported this work and KP.

ACKNOWLEDGMENTS

We also acknowledge Monika Zavodna for preparing the libraries and completing the RNA-seq and Elizabeth Permina for preparing the RNA-seq files for analysis.

SUPPLEMENTARY MATERIAL

The Supplementary Material for this article can be found online at: https://www.frontiersin.org/articles/10.3389/fnins.2022.858524/full#supplementary-material

Supplementary Figure 1 | Differentially regulated proteins at 6 h. STRING functional network analysis illustrating that >80% of the differentially expressed proteins [log2 (FC) ± 0.58, $p \leq 0.01$] in the 6 h SWATH-MS data set fit into one or more enriched Gene Ontology (GO) group. Diagram shows proteins and their relationship to others when searched against the human protein database. Proteins (nodes) are coloured to represent enriched GO terms. Biological processes GO terms: red, cytoskeletal organisation; purple, membrane organisation; light green, intracellular transport; yellow, protein localisation; pink, immune response activating cell signalling pathways; dark green, gene expression. Cellular Component GO terms: teal, vesicle; orange, mitochondria; mauve, synapse; brown, axon.

Supplementary Figure 2 | Differentially regulated proteins at 24 h. STRING functional network analysis illustrating that >80% of the differentially expressed proteins [log2 (FC) ± 0.58, $p \leq 0.01$] in the 24 h SWATH-MS data set fit into one or more enriched Gene Ontology (GO) groups. Diagram shows proteins and their relationship to others when searched against the human protein database. Proteins (nodes) are coloured to represent enriched GO terms. Biological processes GO terms: red, cytoskeletal organisation; purple, membrane organisation; light green, intracellular transport; yellow, protein localisation; pink, immune response activating cell signalling pathways; dark green, gene expression. Cellular Component GO terms: teal, vesicle; orange, mitochondria; mauve, synapse; brown, axon.

Supplementary Table 1 | RNA sequencing data of differentially expressed transcripts at 30 min and 2 h.

Supplementary Table 2 | SWATH-MS data of differentially regulated proteins at 2 h, 6 h, and 24 h.

Supplementary Table 3 | SWATH-MS 6 h STRING enrichment: molecular function and biological process GO Terms.

Supplementary Table 4 | SWATH-MS 24 h STRING enrichment: cellular component, molecular function and biological process GO Terms.

Supplementary Table 5 | SWATH-MS identification of proteins with neuronal functions.

Supplementary Table 6 | Neuronal function proteins differentially regulated at 6 h and 24 h.

REFERENCES

Abraham, W. C., Dragunow, M., and Tate, W. P. (1991). The role of immediate early genes in the stabilization of long-term potentiation. *Mol. Neurobiol.* 5, 297–314. doi: 10.1007/BF02935553

Aebersold, R., Burlingame, A. L., and Bradshaw, R. A. (2013). Western blots versus selected reaction monitoring assays: time to turn the tables? *Mol. Cell Proteomics* 12, 2381–2382. doi: 10.1074/mcp.E113.031658

Albrecht, J., and Zielińska, M. (2019). Exchange-mode glutamine transport across CNS cell membranes. *Neuropharmacology* 161:107560. doi: 10.1016/j.neuropharm.2019.03.003

Allinson, T. M., Parkin, E. T., Turner, A. J., and Hooper, N. M. (2003). ADAMs family members as amyloid precursor protein alpha-secretases. *J. Neurosci. Res.* 74, 342–352. doi: 10.1002/jnr.10737

Antonucci, F., Corradini, I., Fossati, G., Tomasoni, R., Menna, E., and Matteoli, M. (2016). SNAP-25, a known presynaptic protein with emerging postsynaptic functions. *Front. Synapt. Neurosci.* 8:7. doi: 10.3389/fnsyn.2016.00007

Asai, M., Hattori, C., Szabó, B., Sasagawa, N., Maruyama, K., Tanuma, S.-I., et al. (2003). Putative function of ADAM9, ADAM10, and ADAM17 as APP α-secretase. *Biochem. Biophys. Res. Commun.* 301, 231–235. doi: 10.1016/s0006-291x(02)02999-6

Atkin, G., Hunt, J., Minakawa, E., Sharkey, L., Tipper, N., Tennant, W., et al. (2014). F-box only protein 2 (Fbxo2) regulates amyloid precursor protein levels and processing. *J. Biol. Chem.* 289, 7038–7048. doi: 10.1074/jbc.M113.515056

Aydin, D., Filippov, M. A., Tschäpe, J. A., Gretz, N., Prinz, M., Eils, R., et al. (2011). Comparative transcriptome profiling of amyloid precursor protein family members in the adult cortex. *BMC Genomics* 12:160. doi: 10.1186/1471-2164-12-160

Ayka, A., and Şehirli, A. Ö (2020). The role of the SLC transporters protein in the neurodegenerative disorders. *Clin. Psychopharmacol. Neurosci.* 18, 174–187. doi: 10.9758/cpn.2020.18.2.174

Babic, M., and Zinsmaier, K. E. (2011). Memory, synapse stability, and β-adducin. *Neuron* 69, 1039–1041. doi: 10.1016/j.neuron.2011.03.004

Baratchi, S., Evans, J., Tate, W. P., Abraham, W. C., and Connor, B. (2012). Secreted amyloid precursor proteins promote proliferation and glial differentiation of adult hippocampal neural progenitor cells. *Hippocampus* 22, 1517–1527. doi: 10.1002/hipo.20988

Basak, I., Hansen, R. A., Ward, M. E., and Hughes, S. M. (2021). Deficiency of the lysosomal protein CLN5 alters lysosomal function and movement. *Biomolecules* 11:1412. doi: 10.3390/biom11101412

Blom, H., Rönnlund, D., Scott, L., Westin, L., Widengren, J., Aperia, A., et al. (2013). Spatial distribution of DARPP-32 in dendritic spines. *PLoS One* 8:e75155. doi: 10.1371/journal.pone.0075155

Bodakuntla, S., Jijumon, A. S., Villablanca, C., Gonzalez-Billault, C., and Janke, C. (2019). Microtubule-associated proteins: structuring the cytoskeleton. *Trends Cell Biol.* 29, 804–819. doi: 10.1016/j.tcb.2019.07.004

Bolger, A. M., Lohse, M., and Usadel, B. (2014). Trimmomatic: a flexible trimmer for illumina sequence data. *Bioinformatics* 30, 2114–2120. doi: 10.1093/bioinformatics/btu170

Brohée, S., and van Helden, J. (2006) Evaluation of clustering algorithms for protein-protein interaction networks. *BMC Bioinformatics* 7:488. 10.1186/1471-2105-7-488

Budnik, V., and Salinas, P. C. (2011). Wnt signaling during synaptic development and plasticity. *Curr. Opin. Neurobiol.* 21, 151–159. doi: 10.1016/j.conb.2010.12.002

Caille, I., Allinquant, B., Dupont, E., Bouillot, C., Langer, A., Muller, U., et al. (2004). Soluble form of amyloid precursor protein regulates proliferation of progenitors in the adult subventricular zone. *Development* 131, 2173–2181. doi: 10.1242/dev.01103

Chan, K. T., Creed, S. J., and Bear, J. E. (2011). Unraveling the enigma: progress towards understanding the coronin family of actin regulators. *Trends Cell Biol.* 21, 481–488. doi: 10.1016/j.tcb.2011.04.004

Chasseigneaux, S., Dinc, L., Rose, C., Chabret, C., Coulpier, F., Topilko, P., et al. (2011). Secreted amyloid precursor protein beta and secreted amyloid precursor protein alpha induce axon outgrowth *in vitro* through Egr1 signaling pathway. *PLoS One* 6:e16301. doi: 10.1371/journal.pone.0016301

Chen, C. C., and Lau, L. F. (2009). Functions and mechanisms of action of CCN matricellular proteins. *Int. J. Biochem. Cell Biol.* 41, 771–783. doi: 10.1016/j.biocel.2008.07.025

Chen, L., Xiao, D., Tang, F., Gao, H., and Li, X. (2020a). CAPN6 in disease: an emerging therapeutic target (Review). *Int. J. Mol. Med.* 46, 1644–1652. doi: 10.3892/ijmm.2020.4734

Chen, Y., Xu, J., Zhang, Y., Ma, S., Yi, W., Liu, S., et al. (2020b). Coronin 2B regulates dendrite outgrowth by modulating actin dynamics. *FEBS Lett.* 594, 2975–2987. doi: 10.1002/1873-3468.13886

Chen, Y., Zheng, J., Li, X., Zhu, L., Shao, Z., Yan, X., et al. (2020c). Wdr47 controls neuronal polarization through the camsap family microtubule minus-end-binding proteins. *Cell Rep.* 31:107526. doi: 10.1016/j.celrep.2020.107526

Chen, T. T., Klassen, T. L., Goldman, A. M., Marini, C., Guerrini, R., and Noebels, J. L. (2013). Novel brain expression of ClC-1 chloride channels and enrichment of CLCN1 variants in epilepsy. *Neurology* 80, 1078–1085. doi: 10.1212/WNL.0b013e31828868e7

Chiu, S. L., Diering, G. H., Ye, B., Takamiya, K., Chen, C. M., Jiang, Y., et al. (2017). GRASP1 regulates synaptic plasticity and learning through endosomal recycling of AMPA receptors. *Neuron* 93, 1405.e8–1419.e8. doi: 10.1016/j.neuron.2017.02.031

Chu, Y., and Corey, D. R. (2012). RNA sequencing: platform selection, experimental design, and data interpretation. *Nucleic Acid Ther.* 22, 271–274. doi: 10.1089/nat.2012.0367

Claasen, A. M., Guevremont, D., Mason-Parker, S. E., Bourne, K., Tate, W. P., Abraham, W. C., et al. (2009). Secreted amyloid precursor protein-alpha upregulates synaptic protein synthesis by a protein kinase G-dependent mechanism. *Neurosci. Lett.* 460, 92–96. doi: 10.1016/j.neulet.2009.05.040

Coley, A. A., and Gao, W.-J. (2018). PSD95: a synaptic protein implicated in schizophrenia or autism? *Prog. Neuro Psychopharmacol. Biol. Psychiatry* 82, 187–194. doi: 10.1016/j.pnpbp.2017.11.016

Collins, B. C., Gillet, L. C., Rosenberger, G., Rost, H. L., Vichalkovski, A., Gstaiger, M., et al. (2013). Quantifying protein interaction dynamics by SWATH mass spectrometry: application to the 14-3-3 system. *Nat. Methods* 10, 1246–1253. doi: 10.1038/nmeth.2703

Covington, K. R., and Fuqua, S. A. W. (2014). Role of MTA2 in human cancer. *Cancer Metastasis Rev.* 33, 921–928. doi: 10.1007/s10555-014-9518-0

de Curtis, I. (2019). The Rac3 GTPase in neuronal development, neurodevelopmental disorders, and cancer. *Cells* 8:1063. doi: 10.3390/cells8091063

de Hoop, M. J., Huber, L. A., Stenmark, H., Williamson, E., Zerial, M., Parton, R. G., et al. (1994). The involvement of the small GTP-binding protein Rab5a in neuronal endocytosis. *Neuron* 13, 11–22. doi: 10.1016/0896-6273(94)90456-1

De Rossi, P., Nomura, T., Andrew, R. J., Masse, N. Y., Sampathkumar, V., Musial, T. F., et al. (2020). Neuronal BIN1 regulates presynaptic neurotransmitter release and memory consolidation. *Cell Rep.* 30, 3520.e7–3535.e7. doi: 10.1016/j.celrep.2020.02.026

Demmer, J., Dragunow, M., Lawlor, P. A., Mason, S. E., Leah, J. D., Abraham, W. C., et al. (1993). Differential expression of immediate early genes after hippocampal long-term potentiation in awake rats. *Brain Res. Mol. Brain Res.* 17, 279–286. doi: 10.1016/0169-328x(93)90012-e

Derivery, E., Sousa, C., Gautier, J. J., Lombard, B., Loew, D., and Gautreau, A. (2009). The Arp2/3 activator WASH controls the fission of endosomes through a large multiprotein complex. *Dev. Cell.* 17, 712–723. doi: 10.1016/j.devcel.2009.09.010

Dobin, A., Davis, C. A., Schlesinger, F., Drenkow, J., Zaleski, C., Jha, S., et al. (2013). STAR: ultrafast universal RNA-seq aligner. *Bioinformatics* 29, 15–21. doi: 10.1093/bioinformatics/bts635

Duclot, F., and Kabbaj, M. (2017). The role of early growth response 1 (EGR1) in brain plasticity and neuropsychiatric disorders. *Front. Behav. Neurosci.* 11:35. doi: 10.3389/fnbeh.2017.00035

Elder, M. K., Erdjument-Bromage, H., Oliveira, M. M., Mamcarz, M., Neubert, T. A., and Klann, E. (2021). Age-dependent shift in the de novo proteome accompanies pathogenesis in an Alzheimers disease mouse model. *Commun. Biol.* 4:823. doi: 10.1038/s42003-021-02324-6

Fenster, C. P., Chisnell, H. K., Fry, C. R., and Fenster, S. D. (2010). The role of CD4-dependent signaling in interleukin-16 induced c-Fos expression and facilitation of neurite outgrowth in cerebellar granule neurons. *Neurosci. Lett.* 485, 212–216. doi: 10.1016/j.neulet.2010.09.014

Fernandopulle, M. S., Prestil, R., Grunseich, C., Wang, C., Gan, L., and Ward, M. E. (2018). Transcription factor-mediated differentiation of human iPSCs into neurons. *Curr. Protoc. Cell Biol.* 79:e51. doi: 10.1002/cpcb.51

Fol, R., Braudeau, J., Ludewig, S., Abel, T., Weyer, S. W., Roederer, J. P., et al. (2016). Viral gene transfer of APPsalpha rescues synaptic failure in an Alzheimers disease mouse model. *Acta Neuropathol.* 131, 247–266. doi: 10.1007/s00401-015-1498-9

Foot, N., Henshall, T., and Kumar, S. (2017). Ubiquitination and the regulation of membrane proteins. *Physiol. Rev.* 97, 253–281. doi: 10.1152/physrev.00012.2016

Freeman, C., Seaman, M. N., and Reid, E. (2013). The hereditary spastic paraplegia protein strumpellin: characterisation in neurons and of the effect of disease mutations on WASH complex assembly and function. *Biochim. Biophys. Acta* 1832, 160–173. doi: 10.1016/j.bbadis.2012.10.011

Fu, C. A., Shen, M., Huang, B. C., Lasaga, J., Payan, D. G., and Luo, Y. (1999). TNIK, a novel member of the germinal center kinase family that activates the c-Jun N-terminal kinase pathway and regulates the cytoskeleton. *J. Biol. Chem.* 274, 30729–30737. doi: 10.1074/jbc.274.43.30729

Galloni, C., Carra, D., Abella, J. V. G., Kjær, S., Singaravelu, P., Barry, D. J., et al. (2021). MICAL2 enhances branched actin network disassembly by oxidizing Arp3B-containing Arp2/3 complexes. *J. Cell Biol.* 220:e202102043. doi: 10.1083/jcb.202102043

Gandolfi, D., Cerri, S., Mapelli, J., Polimeni, M., Tritto, S., Fuzzati-Armentero, M. T., et al. (2017). Activation of the CREB/c-Fos pathway during long-term synaptic plasticity in the cerebellum granular layer. *Front. Cell Neurosci.* 11:184. doi: 10.3389/fncel.2017.00184

Genovese, I., Giamogante, F., Barazzuol, L., Battista, T., Fiorillo, A., Vicario, M., et al. (2020). Sorcin is an early marker of neurodegeneration, Ca2+ dysregulation and endoplasmic reticulum stress associated to neurodegenerative diseases. *Cell Death Dis.* 11:861. doi: 10.1038/s41419-020-03063-y

Gillet, L. C., Navarro, P., Tate, S., Rost, H., Selevsek, N., Reiter, L., et al. (2012). Targeted data extraction of the MS/MS spectra generated by data-independent acquisition: a new concept for consistent and accurate proteome analysis. *Mol Cell Proteomics* 11:O111.016717. doi: 10.1074/mcp.O111.016717

Gottschall, P. E., and Howell, M. D. (2015). ADAMTS expression and function in central nervous system injury and disorders. *Matrix Biol.* 44, 70–76. doi: 10.1016/j.matbio.2015.01.014

Gu, Y., Deng, Z., Paredez, A. R., DeBolt, S., Wang, Z.-Y., and Somerville, C. (2008). Prefoldin 6 is required for normal microtubule dynamics and organization in *Arabidopsis*. *Proc. Natl. Acad. Sci. U.S.A.* 105, 18064–18069. doi: 10.1073/pnas.0808652105

Guardia, C. M., De Pace, R., Mattera, R., and Bonifacino, J. S. (2018). Neuronal functions of adaptor complexes involved in protein sorting. *Curr. Opin. Neurobiol.* 51, 103–110. doi: 10.1016/j.conb.2018.02.021

Guetg, C., Lienemann, P., Sirri, V., Grummt, I., Hernandez-Verdun, D., Hottiger, M. O., et al. (2010). The NoRC complex mediates the heterochromatin formation and stability of silent rRNA genes and centromeric repeats. *EMBO J.* 29, 2135–2146. doi: 10.1038/emboj.2010.17

Gulbranson, D. R., Davis, E. M., Demmitt, B. A., Ouyang, Y., Ye, Y., Yu, H., et al. (2017). RABIF/MSS4 is a Rab-stabilizing holdase chaperone required for GLUT4 exocytosis. *Proc. Natl. Acad. Sci. U.S.A.* 114, E8224–E8233. doi: 10.1073/pnas.1712176114

Guo, C., Cho, K. S., Li, Y., Tchedre, K., Antolik, C., Ma, J., et al. (2018). IGFBPL1 regulates axon growth through IGF-1-mediated signaling cascades. *Sci. Rep.* 8:2054. doi: 10.1038/s41598-018-20463-5

Guo, W., Polich, E. D., Su, J., Gao, Y., Christopher, D. M., Allan, A. M., et al. (2015). Fragile X proteins FMRP and FXR2P control synaptic GluA1 expression and neuronal maturation *via* distinct mechanisms. *Cell Rep.* 11, 1651–1666. doi: 10.1016/j.celrep.2015.05.013

Haditsch, U., Leone, D. P., Farinelli, M., Chrostek-Grashoff, A., Brakebusch, C. I, Mansuy, M., et al. (2009). A central role for the small GTPase Rac1 in hippocampal plasticity and spatial learning and memory. *Mol. Cell Neurosci.* 41, 409–419. doi: 10.1016/j.mcn.2009.04.005

Hempel, M., Cremer, K., Ockeloen, C. W., Lichtenbelt, K. D., Herkert, J. C., Denecke, J., et al. (2015). De novo mutations in CHAMP1 cause intellectual disability with severe speech impairment. *Am. J. Hum. Genet.* 97, 493–500. doi: 10.1016/j.ajhg.2015.08.003

Heo, S., Diering, G. H., Na, C. H., Nirujogi, R. S., Bachman, J. L., Pandey, A., et al. (2018). Identification of long-lived synaptic proteins by proteomic analysis of synaptosome protein turnover. *Proc. Natl. Acad. Sci. U.S.A.* 115:E3827. doi: 10.1073/pnas.1720956115

Hiltunen, M., Lu, A., Thomas, A. V., Romano, D. M., Kim, M., Jones, P. B., et al. (2006). Ubiquilin 1 modulates amyloid precursor protein trafficking and Abeta secretion. *J. Biol. Chem.* 281, 32240–32253. doi: 10.1074/jbc.M603106200

Hirokawa, N., Niwa, S., and Tanaka, Y. (2010). Molecular motors in neurons: transport mechanisms and roles in brain function, development, and disease. *Neuron* 68, 610–638. doi: 10.1016/j.neuron.2010.09.039

Ho, G. J. I, Smirnova, V., Akaaboune, M., Hantaï, D., and Festoff, B. W. (1994). Serine proteases and their serpin inhibitors in Alzheimers disease. *Biomed. Pharmacother.* 48, 296–304. doi: 10.1016/0753-3322(94)90175-9

Honda, T., Sakisaka, T., Yamada, T., Kumazawa, N., Hoshino, T., Kajita, M., et al. (2006). Involvement of nectins in the formation of puncta adherentia junctions and the mossy fiber trajectory in the mouse hippocampus. *Mol. Cell Neurosci.* 31, 315–325. doi: 10.1016/j.mcn.2005.10.002

Hong, J. H., Kaustov, L., Coyaud, E., Srikumar, T., Wan, J., Arrowsmith, C., et al. (2015). KCMF1 (potassium channel modulatory factor 1) Links RAD6 to UBR4 (ubiquitin N-recognin domain-containing E3 ligase 4) and lysosome-mediated degradation. *Mol. Cell Proteomics* 14, 674–685. doi: 10.1074/mcp.M114.042168

Hu, C., Tao, L., Cao, X., and Chen, L. (2020). The solute carrier transporters and the brain: physiological and pharmacological implications. *Asian J. Pharm. Sci.* 15, 131–144. doi: 10.1016/j.ajps.2019.09.002

Hwang, J., Estick, C. M., Ikonne, U. S., Butler, D., Pait, M. C., Elliott, L. H., et al. (2019). The role of lysosomes in a broad disease-modifying approach evaluated across transgenic mouse models of alzheimers disease and parkinsons disease and models of mild cognitive impairment. *Int. J. Mol. Sci.* 20:4432. doi: 10.3390/ijms20184432

Hyun, J. H., Eom, K., Lee, K.-H., Bae, J. Y., Bae, Y. C., Kim, M.-H., et al. (2015). Kv1.2 mediates heterosynaptic modulation of direct cortical synaptic inputs in CA3 pyramidal cells. *J. Physiol.* 593, 3617–3643. doi: 10.1113/JP270372

Impagnatiello, M. A., Weitzer, S., Gannon, G., Compagni, A., Cotten, M., and Christofori, G. (2001). Mammalian sprouty-1 and -2 are membrane-anchored phosphoprotein inhibitors of growth factor signaling in endothelial cells. *J. Cell Biol.* 152, 1087–1098. doi: 10.1083/jcb.152.5.1087

Inaki, M., Yoshikawa, S., Thomas, J. B., Aburatani, H., and Nose, A. (2007). Wnt4 is a local repulsive cue that determines synaptic target specificity. *Curr. Biol.* 17, 1574–1579. doi: 10.1016/j.cub.2007.08.013

Ishida, A., Furukawa, K., Keller, J. N., and Mattson, M. P. (1997). Secreted form of beta-amyloid precursor protein shifts the frequency dependency for induction of LTD, and enhances LTP in hippocampal slices. *Neuroreport* 8, 2133–2137. doi: 10.1097/00001756-199707070-00009

Jakobsson, J., Gad, H., Andersson, F., Löw, P., Shupliakov, O., and Brodin, L. (2008). Role of epsin 1 in synaptic vesicle endocytosis. *Proc. Natl. Acad. Sci. U.S.A.* 105, 6445–6450. doi: 10.1073/pnas.0710267105

Jarrar, W., Dias, J. M., Ericson, J., Arnold, H.-H., and Holz, A. (2015). Nkx2.2 and Nkx2.9 are the key regulators to determine cell fate of branchial and visceral motor neurons in caudal hindbrain. *PLoS One* 10:e0124408. doi: 10.1371/journal.pone.0124408

Jayachandran, R., Liu, X., Bosedasgupta, S., Müller, P., Zhang, C. L., Moshous, D., et al. (2014). Coronin 1 regulates cognition and behavior through modulation of cAMP/protein kinase a signaling. *PLoS Biol.* 12:e1001820. doi: 10.1371/journal.pbio.1001820

Jin, Y.-R., and Yoon, J. K. (2012). The R-spondin family of proteins: emerging regulators of WNT signaling. *Int. J. Biochem. Cell Biol.* 44, 2278–2287. doi: 10.1016/j.biocel.2012.09.006

Johnson, G. V., and Jope, R. S. (1992). The role of microtubule-associated protein 2 (MAP-2) in neuronal growth, plasticity, and degeneration. *J. Neurosci. Res.* 33, 505–512. doi: 10.1002/jnr.490330402

Katzman, A., and Alberini, C. M. (2018). NLGN1 and NLGN2 in the prefrontal cortex: their role in memory consolidation and strengthening. *Curr. Opin. Neurobiol.* 48, 122–130. doi: 10.1016/j.conb.2017.12.003

Kuijpers, M., van de Willige, D., Freal, A., Chazeau, A., Franker, M. A., Hofenk, J., et al. (2016). Dynein regulator NDEL1 controls polarized cargo transport at the axon initial segment. *Neuron* 89, 461–471. doi: 10.1016/j.neuron.2016.01.022

Kurshan, P. T., Phan, A. Q., Wang, G. J., Crane, M. M., Lu, H., and Shen, K. (2014). Regulation of synaptic extracellular matrix composition is critical for proper synapse morphology. *J. Neurosci.* 34, 12678–12689. doi: 10.1523/JNEUROSCI.1183-14.2014

Larrayoz, I. M., Ferrero, H., Martisova, E., Gil-Bea, F. J., Ramírez, M. J., and Martínez, A. (2017). Adrenomedullin contributes to age-related memory loss in mice and is elevated in aging human brains. *Front. Mol. Neurosci.* 10:384.

Larráyoz, I. M., and Martínez, A. (2012). Proadrenomedullin N-terminal 20 peptide increases kinesins velocity both *in vitro* and *in vivo*. *Endocrinology* 153, 1734–1742. doi: 10.1210/en.2011-1685

Larsen, B. R., Stoica, A., and MacAulay, N. (2016). Managing brain extracellular K+ during neuronal activity: the physiological role of the Na+/K+-ATPase subunit isoforms. *Front. Physiol.* 7:141. doi: 10.3389/fphys.2016.00141

Lefterov, I. M., Koldamova, R. P., and Lazo, J. S. (2000). Human bleomycin hydrolase regulates the secretion of amyloid precursor protein. *FASEB J.* 14, 1837–1847. doi: 10.1096/fj.99-0938com

Lehrman, E. K., Wilton, D. K., Litvina, E. Y., Welsh, C. A., Chang, S. T., Frouin, A., et al. (2018). CD47 protects synapses from excess microglia-mediated pruning during development. *Neuron* 100, 120.e–134.e. doi: 10.1016/j.neuron.2018.09.017

Lenoir, M., Kufareva, I., Abagyan, R., and Overduin, M. (2015). Membrane and protein interactions of the pleckstrin homology domain superfamily. *Membranes* 5, 646–663. doi: 10.3390/membranes5040646

Li, G., Han, L., Chou, T. C., Fujita, Y., Arunachalam, L., Xu, A., et al. (2007). RalA and RalB function as the critical GTP sensors for GTP-dependent exocytosis. *J. Neurosci.* 27, 190–202. doi: 10.1523/JNEUROSCI.2537-06.2007

Li, P., Merrill, S. A., Jorgensen, E. M., and Shen, K. (2016). Two clathrin adaptor protein complexes instruct axon-dendrite polarity. *Neuron* 90, 564–580. doi: 10.1016/j.neuron.2016.04.020

Li, X., and Buxbaum, J. N. (2011). Transthyretin and the brain re-visited: is neuronal synthesis of transthyretin protective in Alzheimers disease? *Mol. Neurodegener.* 6:79. doi: 10.1186/1750-1326-6-79

Liang, J., Xia, L., Oyang, L., Lin, J., Tan, S., Yi, P., et al. (2020). The functions and mechanisms of prefoldin complex and prefoldin-subunits. *Cell Biosci.* 10:87. doi: 10.1186/s13578-020-00446-8

Liebl, F. L. W., Chen, K., Karr, J., Sheng, Q., and Featherstone, D. E. (2005). Increased synaptic microtubules and altered synapse development in *Drosophila* sec8 mutants. *BMC Biol.* 3:27. doi: 10.1186/1741-7007-3-27

Lim, R., Sugino, T., Nolte, H., Andrade, J., Zimmermann, B., Shi, C., et al. (2019). Deubiquitinase USP10 regulates Notch signaling in the endothelium. *Science* 364, 188–193. doi: 10.1126/science.aat0778

Lin, T. B., Lai, C. Y., Hsieh, M. C., Wang, H. H., Cheng, J. K., Chau, Y. P., et al. (2015). VPS26A-SNX27 interaction-dependent mGluR5 recycling in dorsal horn neurons mediates neuropathic pain in rats. *J. Neurosci.* 35, 14943–14955. doi: 10.1523/JNEUROSCI.2587-15.2015

Lindhout, F. W., Cao, Y., Kevenaar, J. T., Bodzêta, A., Stucchi, R., Boumpoutsari, M. M., et al. (2019). VAP-SCRN1 interaction regulates dynamic endoplasmic reticulum remodeling and presynaptic function. *EMBO J.* 38:e101345. doi: 10.15252/embj.2018101345

Liu, T., Zhang, T., Nicolas, M., Boussicault, L., Rice, H., Soldano, A., et al. (2021). The amyloid precursor protein is a conserved Wnt receptor. *eLife* 10:e69199. doi: 10.7554/eLife.69199

Livingstone, R. W., Elder, M. K., Barrett, M. C., Westlake, C. M., Peppercorn, K., Tate, W. P., et al. (2019). Secreted amyloid precursor protein-alpha promotes arc protein synthesis in hippocampal neurons. *Front. Mol. Neurosci.* 12:198. doi: 10.3389/fnmol.2019.00198

Livingstone, R. W., Elder, M. K., Singh, A., Westlake, C. M., Tate, W. P., Abraham, W. C., et al. (2021). Secreted amyloid precursor protein-alpha enhances LTP through the synthesis and trafficking of Ca(2+)-permeable AMPA receptors. *Front. Mol. Neurosci.* 14:660208. doi: 10.3389/fnmol.2021.660208

Lonart, G. (2002). RIM1: an edge for presynaptic plasticity. *Trends Neurosci.* 25, 329–332. doi: 10.1016/s0166-2236(02)02193-8

Machnicka, B., Czogalla, A., Hryniewicz-Jankowska, A., Bogusławska, D. M., Grochowalska, R., Heger, E., et al. (2014). Spectrins: a structural platform for stabilization and activation of membrane channels, receptors and transporters. *Biochim. Biophys. Acta Biomembr.* 1838, 620–634. doi: 10.1016/j.bbamem.2013.05.002

Maftei, D., Ratano, P., Fusco, I., Marconi, V., Squillace, S., Negri, L., et al. (2019). The prokineticin receptor antagonist PC1 rescues memory impairment induced by β amyloid administration through the modulation of prokineticin system. *Neuropharmacology* 158:107739. doi: 10.1016/j.neuropharm.2019.107739

Malek, M., Guillaumot, P., Huber, A. L., Lebeau, J., Pétrilli, V., Kfoury, A., et al. (2012). LAMTOR1 depletion induces p53-dependent apoptosis *via* aberrant lysosomal activation. *Cell Death Dis.* 3, e300–e300. doi: 10.1038/cddis.2012.39

Mandela, P., and Ma, X.-M. (2012). Kalirin, a key player in synapse formation, is implicated in human diseases. *Neural Plast.* 2012:728161. doi: 10.1155/2012/728161

Marshall, T. W., Aloor, H. L., and Bear, J. E. (2009). Coronin 2A regulates a subset of focal-adhesion-turnover events through the cofilin pathway. *J. Cell Sci.* 122, 3061–3069. doi: 10.1242/jcs.051482

Mata, A. M., and Sepulveda, M. R. (2010). Plasma membrane Ca-ATPases in the nervous system during development and ageing. *World J. Biol. Chem.* 1, 229–234. doi: 10.4331/wjbc.v1.i7.229

McCrossan, Z. A., Lewis, A., Panaghie, G., Jordan, P. N., Christini, D. J., Lerner, D. J., et al. (2003). MinK-related peptide 2 modulates Kv2.1 and Kv3.1 potassium channels in mammalian brain. *J. Neurosci.* 23, 8077–8091. doi: 10.1523/JNEUROSCI.23-22-08077.2003

Meziane, H., Dodart, J. C., Mathis, C., Little, S., Clemens, J., Paul, S. M., et al. (1998). Memory-enhancing effects of secreted forms of the beta-amyloid precursor protein in normal and amnestic mice. *Proc. Natl. Acad. Sci. U.S.A.* 95, 12683–12688. doi: 10.1073/pnas.95.21.12683

Mignogna, M. L., and D'Adamo, P. (2018). Critical importance of RAB proteins for synaptic function. *Small GTPases* 9, 145–157. doi: 10.1080/21541248.2016.1277001

Milstein, A. D., and Nicoll, R. A. (2008). Regulation of AMPA receptor gating and pharmacology by TARP auxiliary subunits. *Trends Pharmacol. Sci.* 29, 333–339. doi: 10.1016/j.tips.2008.04.004

Mizoguchi, A., Nakanishi, H., Kimura, K., Matsubara, K., Ozaki-Kuroda, K., Katata, T., et al. (2002). Nectin: an adhesion molecule involved in formation of synapses. *J. Cell Biol.* 156, 555–565. doi: 10.1083/jcb.200103113

Mockett, B. G., Guévremont, D., Elder, M. K., Parfitt, K. D., Peppercorn, K., Morrissey, J., et al. (2019). Glutamate receptor trafficking and protein synthesis mediate the facilitation of LTP by secreted amyloid precursor protein-alpha. *J. Neurosci.* 39:3188. doi: 10.1523/JNEUROSCI.1826-18.2019

Mockett, B. G., Richter, M., Abraham, W. C., and Muller, U. C. (2017). Therapeutic potential of secreted amyloid precursor protein APPsalpha. *Front. Mol. Neurosci.* 10:30. doi: 10.3389/fnmol.2017.00030

Moore, E. E., Presnell, S., Garrigues, U., Guilbot, A., LeGuern, E., Smith, D., et al. (2002). Expression of IL-17B in neurons and evaluation of its possible role in the chromosome 5q-linked form of charcot-marie-tooth disease. *Neuromuscul. Disord.* 12, 141–150. doi: 10.1016/s0960-8966(01)00250-4

Morgan, J. R., Di Paolo, G., Werner, H., Shchedrina, V. A., Pypaert, M., Pieribone, V. A., et al. (2004). A role for talin in presynaptic function. *J. Cell Biol.* 167, 43–50. doi: 10.1083/jcb.200406020

Mori, Y., Takenaka, K.-I., Fukazawa, Y., and Takamori, S. (2021). The endosomal Q-SNARE, Syntaxin 7, defines a rapidly replenishing synaptic vesicle recycling pool in hippocampal neurons. *Commun. Biol.* 4, 981–981. doi: 10.1038/s42003-021-02512-4

Morris, G. (2011). *Secreted Amyloid Precursor Protein Alpha Mediates Neuroprotection and Gene Expression*. Dunedin: University of Otago.

Muñoz-Lasso, D. C., Romá-Mateo, C., Pallardó, F. V., and Cabo, P. G. (2020). Much more than a scaffold: cytoskeletal proteins in neurological disorders. *Cells* 9:358. doi: 10.3390/cells9020358

O'Neill, A. C., Kyrousi, C., Klaus, J., Leventer, R. J., Kirk, E. P., Fry, A., et al. (2018). A primate-specific isoform of LEKHG6 regulates neurogenesis and neuronal migration. *Cell Rep.* 25, 2729.e6–2741.e6. doi: 10.1016/j.celrep.2018.11.029

Pan, P. Y., Cai, Q., Lin, L., Lu, P. H., Duan, S., and Sheng, Z. H. (2005). SNAP-29-mediated modulation of synaptic transmission in cultured hippocampal neurons. *J. Biol. Chem.* 280, 25769–25779. doi: 10.1074/jbc.M502356200

Paul, V., and Ekambaram, P. (2011). Involvement of nitric oxide in learning & memory processes. *Indian J. Med. Res.* 133, 471–478.

Perez-Riverol, Y., Bai, J., Bandla, C., García-Seisdedos, D., Hewapathirana, S., Kamatchinathan, S., et al. (2022). The PRIDE database resources in 2022: a hub for mass spectrometry-based proteomics evidences. *Nucleic Acids Res.* 50, D543–D552. doi: 10.1093/nar/gkab1038

Poirier, R., Cheval, H., Mailhes, C., Charnay, P., Davis, S., and Laroche, S. (2007). Paradoxical role of an Egr transcription factor family member, Egr2/Krox20, in learning and memory. *Front. Behav. Neurosci.* 1:6. doi: 10.3389/neuro.08.006

Pourhoseini, S., Goswami-Sewell, D., and Zuniga-Sanchez, E. (2021). Neurofascin is a novel component of rod photoreceptor synapses in the outer retina. *Front. Neural Circ.* 15:635849. doi: 10.3389/fncir.2021.635849

Pribyl, M., Hodny, Z., and Kubikova, I. (2021). Suprabasin-a review. *Genes* 12:108. doi: 10.3390/genes12010108

Rajgor, D., Sanderson, T. M., Amici, M., Collingridge, G. L., and Hanley, J. G. (2018). NMDAR-dependent Argonaute 2 phosphorylation regulates miRNA activity and dendritic spine plasticity. *EMBO J.* 37:e97943. doi: 10.15252/embj.201797943

Redlingshöfer, L., McLeod, F., Chen, Y., Camus, M. D., Burden, J. J., Palomer, E., et al. (2020). Clathrin light chain diversity regulates membrane deformation *in vitro* and synaptic vesicle formation *in vivo*. *Proc. Natl. Acad. Sci. U.S.A.* 117:23527. doi: 10.1073/pnas.2003662117

Renaud, L., Picher-Martel, V., Codron, P., and Julien, J.-P. (2019). Key role of UBQLN2 in pathogenesis of amyotrophic lateral sclerosis and frontotemporal dementia. *Acta Neuropathol. Commun.* 7:103. doi: 10.1186/s40478-019-0758-7

Rice, H. C., de Malmazet, D., Schreurs, A., Frere, S., Van Molle, I., Volkov, A. N., et al. (2019). Secreted amyloid-β precursor protein functions as a GABA(B)R1a ligand to modulate synaptic transmission. *Science* 363:eaao4827.

Richter, M. C., Ludewig, S., Winschel, A., Abel, T., Bold, C., Salzburger, L. R., et al. (2018). Distinct *in vivo* roles of secreted APP ectodomain variants APPsα and APPsβ in regulation of spine density, synaptic plasticity, and cognition. *EMBO J.* 37:e98335. doi: 10.15252/embj.201798335

Ritchie, M. E., Phipson, B., Wu, D., Hu, Y., Law, C. W., Shi, W., et al. (2015). limma powers differential expression analyses for RNA-sequencing and microarray studies. *Nucleic Acids Res.* 43:e47. doi: 10.1093/nar/gkv007

Ritter, B., Modregger, J., Paulsson, M., and Plomann, M. (1999). PACSIN 2, a novel member of the PACSIN family of cytoplasmic adapter proteins. *FEBS Lett.* 454, 356–362. doi: 10.1016/s0014-5793(99)00830-3

Rosenthal, S. L., Wang, X., Demirci, F. Y., Barmada, M. M., Ganguli, M., Lopez, O. L., et al. (2012). Beta-amyloid toxicity modifier genes and the risk of Alzheimers disease. *Am. J. Neurodegener. Dis.* 1, 191–198.

Russo, M. W., Sevetson, B. R., and Milbrandt, J. (1995). Identification of NAB1, a repressor of NGFI-A- and Krox20-mediated transcription. *Proc. Natl. Acad. Sci. U.S.A.* 92, 6873–6877. doi: 10.1073/pnas.92.15.6873

Ryan, M., Tan, V. T. Y., Thompson, N., Guévremont, D., Mockett, B. G., Tate, W. P., et al. (2021). Lentivirus-mediated expression of human secreted amyloid precursor protein-alpha promotes long-term induction of neuroprotective genes and pathways in a mouse model of alzheimers disease. *J. Alzheimers Dis.* 79, 1075–1090. doi: 10.3233/JAD-200757

Ryan, M. M., Morris, G. P., Mockett, B. G., Bourne, K., Abraham, W. C., Tate, W. P., et al. (2013). Time-dependent changes in gene expression induced by secreted amyloid precursor protein-alpha in the rat hippocampus. *BMC Genom.* 14:376. doi: 10.1186/1471-2164-14-376

Sanrattana, W., Maas, C., and de Maat, S. (2019). SERPINs-from trap to treatment. *Front. Med.* 6:25. doi: 10.3389/fmed.2019.00025

Sasaki, J., Kofuji, S., Itoh, R., Momiyama, T., Takayama, K., Murakami, H., et al. (2010). The PtdIns(3,4)P(2) phosphatase INPP4A is a suppressor of excitotoxic neuronal death. *Nature* 465, 497–501. doi: 10.1038/nature09023

Sase, S., Almad, A. A., Boecker, C. A., Guedes-Dias, P., Li, J. J., Takanohashi, A., et al. (2020). TUBB4A mutations result in both glial and neuronal degeneration in an H-ABC leukodystrophy mouse model. *eLife* 9:e52986. doi: 10.7554/eLife.52986

Saunders, A. M., Strittmatter, W. J., Schmechel, D., St. George-Hyslop, P. H., Pericak-Vance, M. A., Joo, S. H., et al. (1993). Association of apolipoprotein E allele ∈4 with late-onset familial and sporadic Alzheimers disease. *Neurology* 43:1467. doi: 10.1212/wnl.43.8.1467

Schurch, N. J., Schofield, P., Gierliński, M., Cole, C., Sherstnev, A., Singh, V., et al. (2016). How many biological replicates are needed in an RNA-seq experiment and which differential expression tool should you use? *RNA* 22, 839–851. doi: 10.1261/rna.053959.115

Seddik, R., Jungblut, S. P., Silander, O. K., Rajalu, M., Fritzius, T., Besseyrias, V., et al. (2012). Opposite effects of KCTD subunit domains on GABA(B) receptor-mediated desensitization. *J. Biol. Chem.* 287, 39869–39877. doi: 10.1074/jbc.M112.412767

Shimojo, M., Madara, J., Pankow, S., Liu, X., Yates, J. III, Südhof, T. C., et al. (2019). Synaptotagmin-11 mediates a vesicle trafficking pathway that is essential for development and synaptic plasticity. *Genes Dev.* 33, 365–376. doi: 10.1101/gad.320077.118

Sosa, L. J., Caceres, A., Dupraz, S., Oksdath, M., Quiroga, S., and Lorenzo, A. (2017). The physiological role of the amyloid precursor protein as an adhesion molecule in the developing nervous system. *J. Neurochem.* 143, 11–29. doi: 10.1111/jnc.14122

Spence, E. F., Kanak, D. J., Carlson, B. R., and Soderling, S. H. (2016). The Arp2/3 complex is essential for distinct stages of spine synapse maturation, including synapse unsilencing. *J. Neurosci.* 36, 9696–9709. doi: 10.1523/JNEUROSCI.0876-16.2016

Stahl, R., Schilling, S., Soba, P., Rupp, C., Hartmann, T., Wagner, K., et al. (2014). Shedding of APP limits its synaptogenic activity and cell adhesion properties. *Front. Cell Neurosci.* 8:410. doi: 10.3389/fncel.2014.00410

Stein, T. D., Anders, N. J., DeCarli, C., Chan, S. L., Mattson, M. P., and Johnson, J. A. (2004). Neutralization of transthyretin reverses the neuroprotective effects of secreted amyloid precursor protein (APP) in APPSW mice resulting in tau phosphorylation and loss of hippocampal neurons: support for the amyloid hypothesis. *J. Neurosci.* 24, 7707–7717. doi: 10.1523/JNEUROSCI.2211-04.2004

Subramaniam, M., Hawse, J. R., Rajamannan, N. M., Ingle, J. N., and Spelsberg, T. C. (2010). Functional role of KLF10 in multiple disease processes. *BioFactors* 36, 8–18. doi: 10.1002/biof.67

Sun, X., Bernstein, M. J., Meng, M., Rao, S., Sørensen, A. T., Yao, L., et al. (2020). Functionally distinct neuronal ensembles within the memory engram. *Cell* 181, 410.e17–423.e17. doi: 10.1016/j.cell.2020.02.055

Svenningsson, P., Nishi, A., Fisone, G., Girault, J. A., Nairn, A. C., and Greengard, P. (2004). DARPP-32: an integrator of neurotransmission. *Annu. Rev. Pharmacol. Toxicol.* 44, 269–296. doi: 10.1146/annurev.pharmtox.44.101802.121415

Sweetman, E., Kleffmann, T., Edgar, C., de Lange, M., Vallings, R., and Tate, W. (2020). A SWATH-MS analysis of myalgic encephalomyelitis/chronic fatigue syndrome peripheral blood mononuclear cell proteomes reveals mitochondrial dysfunction. *J. Transl. Med.* 18:365. doi: 10.1186/s12967-020-02533-3

Takago, H., Oshima-Takago, T., and Moser, T. (2018). Disruption of otoferlin alters the mode of exocytosis at the mouse inner hair cell ribbon synapse. *Front. Mol. Neurosci.* 11:492. doi: 10.3389/fnmol.2018.00492

Takahashi, K., Asano, N., Imatani, A., Kondo, Y., Saito, M., Takeuchi, A., et al. (2020). Sox2 induces tumorigenesis and angiogenesis of early-stage esophageal squamous cell carcinoma through secretion of Suprabasin. *Carcinogenesis* 41, 1543–1552. doi: 10.1093/carcin/bgaa014

Tan, H. L., Queenan, B. N., and Huganir, R. L. (2015). GRIP1 is required for homeostatic regulation of AMPAR trafficking. *Proc. Natl. Acad. Sci. U.S.A.* 112:10026. doi: 10.1073/pnas.1512786112

Tan, V. T. Y., Mockett, B. G., Ohline, S. M., Parfitt, K. D., Wicky, H. E., Peppercorn, K., et al. (2018). Lentivirus-mediated expression of human secreted amyloid precursor protein-alpha prevents development of memory and plasticity deficits in a mouse model of Alzheimers disease. *Mol. Brain* 11:7. doi: 10.1186/s13041-018-0348-9

Tanabe, Y., Fujita, E., Hayashi, Y. K., Zhu, X., Lubbert, H., Mezaki, Y., et al. (2013). Synaptic adhesion molecules in Cadm family at the neuromuscular junction. *Cell Biol. Int.* 37, 731–736. doi: 10.1002/cbin.10092

Taylor, C. J., Ireland, D. R., Ballagh, I., Bourne, K., Marechal, N. M., Turner, P. R., et al. (2008). Endogenous secreted amyloid precursor protein-alpha regulates hippocampal NMDA receptor function, long-term potentiation and spatial memory. *Neurobiol. Dis.* 31, 250–260. doi: 10.1016/j.nbd.2008.04.011

Telias, M. (2019). Molecular mechanisms of synaptic dysregulation in fragile X syndrome and autism spectrum disorders. *Front. Mol. Neurosci.* 12:51. doi: 10.3389/fnmol.2019.00051

Terunuma, M., Revilla-Sanchez, R., Quadros, I. M., Deng, Q., Deeb, T. Z., Lumb, M., et al. (2014). Postsynaptic GABAB receptor activity regulates excitatory neuronal architecture and spatial memory. *J. Neurosci.* 34, 804–816. doi: 10.1523/JNEUROSCI.3320-13.2013

Tikiyani, V., and Babu, K. (2019). Claudins in the brain: unconventional functions in neurons. *Traffic* 20, 807–814. doi: 10.1111/tra.12685

Trejo, J., Massamiri, T., Deng, T., Dewji, N. N., Bayney, R. M., and Brown, J. H. (1994). A direct role for protein kinase C and the transcription factor Jun/AP-1 in the regulation of the Alzheimers beta-amyloid precursor protein gene. *J. Biol. Chem.* 269, 21682–21690. doi: 10.1016/s0021-9258(17)31860-4

Turner, P. R., Bourne, K., Garama, D., Carne, A., Abraham, W. C., and Tate, W. P. (2007). Production, purification and functional validation of human secreted amyloid precursor proteins for use as neuropharmacological reagents. *J. Neurosci. Methods* 164, 68–74. doi: 10.1016/j.jneumeth.2007.04.001

Uchida, S., and Shumyatsky, G. P. (2015). Deceivingly dynamic: learning-dependent changes in stathmin and microtubules. *Neurobiol. Learn. Mem.* 124, 52–61. doi: 10.1016/j.nlm.2015.07.011

Varnum, M. M., Kiyota, T., Ingraham, K. L., Ikezu, S., and Ikezu, T. (2015). The anti-inflammatory glycoprotein, CD200, restores neurogenesis and enhances amyloid phagocytosis in a mouse model of Alzheimers disease. *Neurobiol. Aging* 36, 2995–3007. doi: 10.1016/j.neurobiolaging.2015.07.027

Vatsa, N., and Jana, N. R. (2018). UBE3A and its link with autism. *Front. Mol. Neurosci.* 11:448. doi: 10.3389/fnmol.2018.00448

Walker, C. S., Brockie, P. J., Madsen, D. M., Francis, M. M., Zheng, Y., Koduri, S., et al. (2006). Reconstitution of invertebrate glutamate receptor function depends on stargazin-like proteins. *Proc. Natl. Acad. Sci. U.S.A.* 103, 10781–10786. doi: 10.1073/pnas.0604482103

Wang, C., Ward, M. E., Chen, R., Liu, K., Tracy, T. E., Chen, X., et al. (2017). Scalable production of iPSC-derived human neurons to identify tau-lowering compounds by high-content screening. *Stem Cell Rep.* 9, 1221–1233. doi: 10.1016/j.stemcr.2017.08.019

Wang, H., Dey, D., Carrera, I., Minond, D., Bianchi, E., Xu, S., et al. (2013). COPS5 (Jab1) protein increases β site processing of amyloid precursor protein and amyloid β peptide generation by stabilizing RanBP9 protein levels. *J. Biol. Chem.* 288, 26668–26677. doi: 10.1074/jbc.M113.476689

Wang, R., Walker, C. S., Brockie, P. J., Francis, M. M., Mellem, J. E., Madsen, D. M., et al. (2008). Evolutionary conserved role for TARPs in the gating of glutamate receptors and tuning of synaptic function. *Neuron* 59, 997–1008. doi: 10.1016/j.neuron.2008.07.023

Weijts, B. G., Bakker, W. J., Cornelissen, P. W., Liang, K. H., Schaftenaar, F. H., Westendorp, B., et al. (2012). E2F7 and E2F8 promote angiogenesis through transcriptional activation of VEGFA in cooperation with HIF1. *EMBO J.* 31, 3871–3884. doi: 10.1038/emboj.2012.231

Weiner, J. A., Wang, X., Tapia, J. C., and Sanes, J. R. (2005). Gamma protocadherins are required for synaptic development in the spinal cord. *Proc. Natl. Acad. Sci. U.S.A.* 102, 8–14. doi: 10.1073/pnas.0407931101

Wingo, A. P., Liu, Y., Gerasimov, E. S., Gockley, J., Logsdon, B. A., Duong, D. M., et al. (2021). Integrating human brain proteomes with genome-wide association data implicates new proteins in Alzheimers disease pathogenesis. *Nat. Genet.* 53, 143–146. doi: 10.1038/s41588-020-00773-z

Wiśniewski, J. R. (2017). Filter-aided sample preparation: the versatile and efficient method for proteomic analysis. *Methods Enzymol.* 585, 15–27. doi: 10.1016/bs.mie.2016.09.013

Wood, W. E., Lovell, P. V., Mello, C. V., and Perkel, D. J. (2011). Serotonin, *via* HTR2 receptors, excites neurons in a cortical-like premotor nucleus necessary for song learning and production. *J. Neurosci.* 31, 13808–13815. doi: 10.1523/JNEUROSCI.2281-11.2011

Xia, J. H., Liu, C. Y., Tang, B. S., Pan, Q., Huang, L., Dai, H. P., et al. (1998). Mutations in the gene encoding gap junction protein beta-3 associated with autosomal dominant hearing impairment. *Nat. Genet.* 20, 370–373. doi: 10.1038/3845

Xu, H., Cao, H., and Xiao, G. (2016). Signaling *via* PINCH: functions, binding partners and implications in human diseases. *Gene* 594, 10–15. doi: 10.1016/j.gene.2016.08.039

Yamada, S., Uchimura, E., Ueda, T., Nomura, T., Fujita, S., Matsumoto, K., et al. (2007). Identification of twinfilin-2 as a factor involved in neurite outgrowth by RNAi-based screen. *Biochem. Biophys. Res. Commun.* 363, 926–930. doi: 10.1016/j.bbrc.2007.09.069

Young, M.-J., Hsu, K.-C., Lin, T. E., Chang, W.-C., and Hung, J.-J. (2019). The role of ubiquitin-specific peptidases in cancer progression. *J. Biomed. Sci.* 26:42. doi: 10.1186/s12929-019-0522-0

Yu, Y., Shintani, T., Takeuchi, Y., Shirasawa, T., and Noda, M. (2018). Protein tyrosine phosphatase receptor type J (PTPRJ) regulates retinal axonal projections by inhibiting Eph and Abl kinases in mice. *J. Neurosci.* 38, 8345–8363. doi: 10.1523/JNEUROSCI.0128-18.2018

Yuzaki, M. (2011). Cbln1 and its family proteins in synapse formation and maintenance. *Curr. Opin. Neurobiol.* 21, 215–220. doi: 10.1016/j.conb.2011.01.010

Zhang, H., Huang, T., Hong, Y., Yang, W., Zhang, X., Luo, H., et al. (2018). The retromer complex and sorting nexins in neurodegenerative diseases. *Front. Aging Neurosci.* 10:79. doi: 10.3389/fnagi.2018.00079

Zhang, L., Zhu, T., Miao, H., and Liang, B. (2021). The calcium binding protein S100A11 and its roles in diseases. *Front. Cell Dev. Biol.* 9:693262. doi: 10.3389/fcell.2021.693262

Zhang, X. F., Zhao, Y. F., Zhu, S. W., Huang, W. J., Luo, Y., Chen, Q. Y., et al. (2015). CXCL1 triggers caspase-3 dependent Tau cleavage in long-term neuronal cultures and in the hippocampus of aged mice: implications in Alzheimers disease. *J. Alzheimers Dis.* 48, 89–104. doi: 10.3233/JAD-150041

Zhang, Z. Y., Bai, H. H., Guo, Z., Li, H. L., Diao, X. T., Zhang, T. Y., et al. (2020). Ubiquitination and functional modification of GluN2B subunit-containing NMDA receptors by Cbl-b in the spinal cord dorsal horn. *Sci. Signal.* 13:eaaw1519. doi: 10.1126/scisignal.aaw1519

Zhao, Z., Sagare, A. P., Ma, Q., Halliday, M. R., Kong, P., Kisler, K., et al. (2015). Central role for PICALM in amyloid-β blood-brain barrier transcytosis and clearance. *Nat. Neurosci.* 18, 978–987. doi: 10.1038/nn.4025

Zhou, J. H., Wang, X. T., Zhou, L., Zhou, L., Xu, F. X., Su, L. D., et al. (2017). Ablation of TFR1 in purkinje cells inhibits mGlu1 trafficking and impairs motor coordination, but not autistic-like behaviors. *J. Neurosci.* 37, 11335–11352. doi: 10.1523/JNEUROSCI.1223-17.2017

Zorumski, C. F., and Izumi, Y. (1998). Modulation of LTP induction by NMDA receptor activation and nitric oxide release. *Prog. Brain Res.* 118, 173–182. doi: 10.1016/s0079-6123(08)63207-0

Conflict of Interest: The authors declare that the research was conducted in the absence of any commercial or financial relationships that could be construed as a potential conflict of interest.

Publisher's Note: All claims expressed in this article are solely those of the authors and do not necessarily represent those of their affiliated organizations, or those of the publisher, the editors and the reviewers. Any product that may be evaluated in this article, or claim that may be made by its manufacturer, is not guaranteed or endorsed by the publisher.

frontiers | Frontiers in Neuroscience

SYSTEMATIC REVIEW
published: 10 June 2022
doi: 10.3389/fnins.2022.859651

Magnetic Resonance Imaging and Its Clinical Correlation in Spinocerebellar Ataxia Type 3: A Systematic Review

Kah Hui Yap[1], *Hanani Abdul Manan*[2,3]*, *Noorazrul Yahya*[4], *Shahrul Azmin*[1], *Shahizon Azura Mohamed Mukari*[2] and *Norlinah Mohamed Ibrahim*[1]

[1] Department of Medicine, Universiti Kebangsaan Malaysia (UKM) Medical Centre, Kuala Lumpur, Malaysia, [2] Makmal Pemprosesan Imej Kefungsian, Department of Radiology, Universiti Kebangsaan Malaysia (UKM) Medical Centre, Kuala Lumpur, Malaysia, [3] Department of Radiology and Intervency, Hospital Pakar Kanan-Kanak, Children Specialist Hospital, Universiti Kebangsaan Malaysia (UKM), Kuala Lumpur, Malaysia, [4] School of Diagnostic and Applied Health Sciences, Faculty of Health Sciences, National University of Malaysia, Kuala Lumpur, Malaysia

Background: Spinocerebellar ataxia type 3 (SCA3) is a complex cerebrocerebellar disease primarily characterized by ataxia symptoms alongside motor and cognitive impairments. The heterogeneous clinical presentation of SCA3 necessitates correlations between magnetic resonance imaging (MRI) and clinical findings in reflecting progressive disease changes. At present, an attempt to systematically examine the brain-behavior relationship in SCA3, specifically, the correlation between MRI and clinical findings, is lacking.

Objective: We investigated the association strength between MRI abnormality and each clinical symptom to understand the brain-behavior relationship in SCA3.

Methods: We conducted a systematic review on Medline and Scopus to review studies evaluating the brain MRI profile of SCA3 using structural MRI (volumetric, voxel-based morphometry, surface analysis), magnetic resonance spectroscopy, and diffusion tensor imaging, including their correlations with clinical outcomes.

Results: Of 1,767 articles identified, 29 articles met the eligibility criteria. According to the National Institutes of Health quality assessment tool for case-control studies, all articles were of excellent quality. This systematic review found that SCA3 neuropathology contributes to widespread brain degeneration, affecting the cerebellum and brainstem. The disease gradually impedes the cerebral cortex and basal ganglia in the late stages of SCA3. Most findings reported moderate correlations (r = 0.30–0.49) between MRI features in several regions and clinical findings. Regardless of the MRI techniques, most studies focused on the brainstem and cerebellum.

Conclusions: Clinical findings suggest that rather than individual brain regions, the connectivity between different brain regions in distributed networks (i.e., cerebellar-cerebral network) may be responsible for motor and neurocognitive function in SCA3. This review highlights the importance of evaluating the progressive changes of the cerebellar-cerebral networks in SCA3 patients, specifically the functional connectivity. Given the relative lack of knowledge about functional connectivity on SCA3, future studies should investigate possible functional connectivity abnormalities in SCA3 using fMRI.

Keywords: spinocerebellar ataxia type 3, magnetic resonance imaging, motor, neurocognition, cerebellar-cerebral network, functional compensation

OPEN ACCESS

Edited by:
Sean Austin O. Lim,
DePaul University, United States

Reviewed by:
Paola Feraco,
University of Bologna, Italy
Francesca Tona,
Sapienza University, Italy

***Correspondence:**
Hanani Abdul Manan
hanani@ukm.edu.my

Specialty section:
This article was submitted to Neurodegeneration, a section of the journal Frontiers in Neuroscience

Received: *21 January 2022*
Accepted: *10 May 2022*
Published: *10 June 2022*

Citation:
Yap KH, Abdul Manan H, Yahya N, Azmin S, Mohamed Mukari SA and Mohamed Ibrahim N (2022) Magnetic Resonance Imaging and Its Clinical Correlation in Spinocerebellar Ataxia Type 3: A Systematic Review. Front. Neurosci. 16:859651. doi: 10.3389/fnins.2022.859651

INTRODUCTION

Spinocerebellar ataxia type 3 (SCA3) is the most common dominantly inherited ataxia worldwide (Paulson, 2012). SCA3 neuropathology involves mutation of cytosine-adenine-guanine (CAG) repeat in the *ATXN3* gene that codes for the *ataxin-3* protein. This elongated polyglutamine tract formed protein aggregates primarily deposited and resulted in cerebellar cell deaths (Pedroso et al., 2013). As a result, SCA3 is primarily characterized by progressive cerebellar degeneration, resulting in increasingly worsening ataxia symptoms, including gait abnormalities, dysarthria, and abnormal eye movements (Bodranghien et al., 2016). Ataxia severity is commonly measured using the Scale for the Assessment and Rating of Ataxia (SARA; 0–40) and the International Cooperative Ataxia Rating Scale (ICARS; 0–100) (Zhou et al., 2011). Apart from the cerebellum, individual differences in the extracerebellar involvement further contribute to the varying degree of ataxia, non-ataxia, and cognitive impairment in SCA3 (Lindsay and Storey, 2017). In addition, the severity of ataxia may exacerbate the cognitive impairment on pen-and-paper tests (Yap et al., 2022b). Therefore, clinical measures alone might not reflect progressive disease changes, requiring correlations with objective measures such as magnetic resonance imaging (MRI) (Döhlinger et al., 2008).

Magnetic resonance imaging has many advantages, including high spatial resolution, and is capable of morphological and functional imaging. Advanced MRI techniques are able to assess structural and volumetric changes, metabolic alterations (magnetic resonance spectroscopy; MRS), white matter integrity (diffusion-tensor imaging; DTI), and functional abnormalities (task-based and resting-state functional MRI; fMRI) (Currie et al., 2013). These neuroimages may provide biologically-relevant measures that may be valuable biomarkers for spinocerebellar ataxia (SCA) (Adanyeguh et al., 2018).

MRI structural abnormalities have been widely reported in SCA3 and correlations with clinical findings have been explored (Wan et al., 2020). However, functional connectivity abnormalities have been poorly assessed and there is a relative lack of knowledge about fMRI application on SCA3. A recent review has discussed the relationship between MRI structural abnormalities, disease severity, CAG repeats, and disease duration qualitatively (Wan et al., 2020). However, an attempt to systematically examine the association between brain regions and clinical scales is lacking (Wan et al., 2020). Therefore, understanding the association strength between MRI abnormality and each clinical symptom will help understand the brain-behavior relationship in SCA3. We systematically reviewed published articles that have evaluated the brain MRI profile of SCA3, including studies that reported correlations with clinical outcomes. We aimed to identify brain regions responsible for motor and cognitive decline in SCA3, respectively.

METHODS

Search Strategy

We performed a literature search using two electronic databases: Medline (Ovid) and Scopus. The search identified articles providing information on the brain MRI profile of SCA3 with or without comparisons against healthy comparisons (HC). We included only original articles written in English and reported human studies. To avoid selection bias, we excluded articles with fewer than 12 participants in each group (i.e., SCA3 vs. HC) (Szucs and Ioannidis, 2020). We also excluded studies that used MRI with $<$ 1.5 Tesla field (T) to minimize the risk of Type II error. We considered 1.5 and 3.0 T MRI as equal there was little difference in the diagnostic accuracy (Wardlaw et al., 2012). We searched the articles on March 23, 2021, using Medical Subject Headings (MeSH) terms such as "SCA3" and "Machado-Joseph disease," coupled with terms related to MRI, such as "volumetric," "morphometric," "functional," "resting-state," "magnetic resonance," "spectroscopy" "diffusion tensor imaging," "tractography," "MRI," "DTI," "white matter," and "gray matter."

Data Extraction and Analysis

The first author performed an initial eligibility screening by going through the titles and abstracts of 1,767 initially identified articles, then cross-checked by another author. As illustrated in **Figure 1**, we adhered to the Preferred Reporting Items for Systematic Review and Meta-Analyses (PRISMA) reporting guidelines (Page et al., 2021). Finally, we included a total of 29 articles in this review. Twenty papers examined structural MRI [volumetric: $n = 12$ (Bürk et al., 1996; Etchebehere et al., 2001; Yoshizawa et al., 2003; Liang et al., 2009; Schulz et al., 2010; Camargos et al., 2011; D'Abreu et al., 2011; Ogawa et al., 2012; De Rezende et al., 2015; Nunes et al., 2015; Rezende et al., 2018; Jao et al., 2019b), voxel-based morphometry (VBM): $n = 8$ (Schulz et al., 2010; D'Abreu et al., 2012; Guimarães et al., 2013; Lopes et al., 2013; Kang et al., 2014; Hernandez-Castillo et al., 2017; Peng et al., 2019; Guo et al., 2020), and surface analysis: $n = 4$ (De Rezende et al., 2015; Nunes et al., 2015; Rezende et al., 2018; Arruda et al., 2020)], seven papers examined MRS (Lei et al., 2011; Lirng et al., 2012; Wang et al., 2012; Lopes et al., 2013; Chen et al., 2014; Adanyeguh et al., 2015; Peng et al., 2019), and ten papers examined DTI (Guimarães et al., 2013; Lopes et al., 2013; Kang et al., 2014; Nunes et al., 2015; Wu et al., 2017; Rezende et al., 2018; Jao et al., 2019a; Peng et al., 2019; Meira et al., 2020; Inada et al., 2021). We summarized findings in **Supplementary Table 3** and outlined the details in **Supplementary Table 2**. Subsequently, we synthesized the findings into two parts: (1) Difference in MRI-related findings between SCA3 and HC, and (2) MRI-related findings and their correlation with clinical scales in SCA3, specifically, ataxia, non-ataxia, and cognitive function. Due to the lack of findings, that is, three or fewer articles, we only discussed these findings concerning avenues for future studies, if applicable: 3D fractal dimension (3D-FD) analysis: $n = 3$ (Huang et al., 2017; Jao et al., 2019b; Wang et al., 2020), texture analysis: $n = 1$ (De Oliveira et al., 2010), relaxometry: $n = 1$ (Guimarães et al., 2013), and neuromelanin contrast: $n = 1$ (Nakata et al., 2020), and task-based fMRI (Duarte et al., 2016).

As per the National Health Medical Research Council guidelines (National Health Medical Research Council, 2009), we classified all 29 studies as Level III-2 evidence. We adapted the

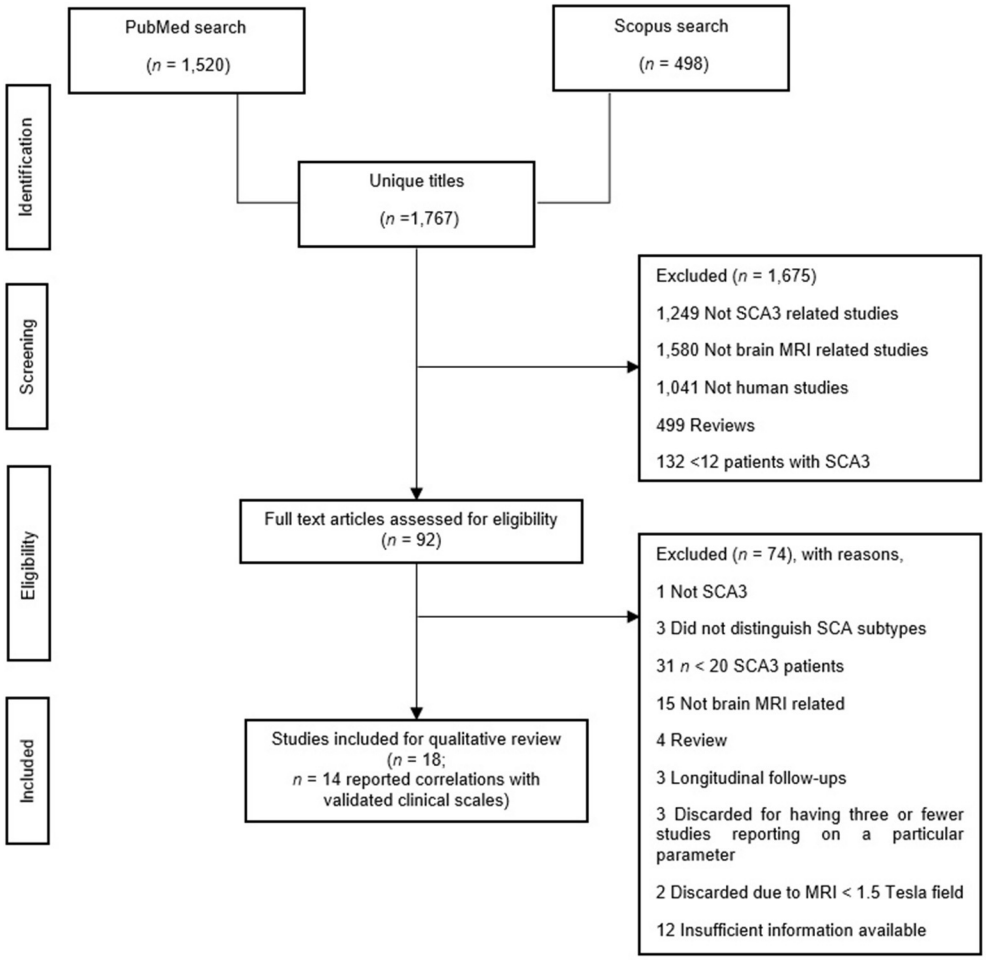

FIGURE 1 | Study search in accordance with the PRISMA guideline (Page et al., 2021).

National Institutes of Health quality assessment tool for case-control studies (National Institutes of Health, 2019). The results, displayed in **Supplementary Table 1**, showed that all studies were of excellent quality due to the consistent use of standardized diagnostic criteria in screening SCA3 patients and HC.

In the present review, we were interested in the outcomes of validated clinical scales, including the SARA and ICARS for ataxia severity and well-established neuropsychological tests for cognitive impairment. We did not consider outcomes derived from subscales from SARA and ICARS. In addition, screening tests usually lack validation and may be vulnerable to ceiling effects, making them relatively insensitive when used in isolation. Such screening tests included Mini-Mental State Examination (Franco-Marina et al., 2010) and the Montreal Cognitive Assessment (Smith et al., 2007).

The correlation coefficient, *r*, was recorded as the correlation between the clinical and MRI outcomes in SCA3. The *r* values of 0.10, 0.30, and 0.50 indicate small, moderate, and strong correlations, respectively (Cohen, 2013). In this review, a larger *r* indicated a stronger correlation between clinical and MRI outcomes in SCA3 (Cohen, 2013). Given the nature of the tests (e.g., higher scores in SARA indicate greater severity, whereas higher scores in ICARS indicate a lower severity), we only considered the absolute values. We did not consider studies that reported correlation without providing the *r* values.

RESULTS

SCA3 vs. Healthy Comparisons

Structural MRI

Cerebrum (Cortical)

Two studies analyzed the volumetric changes in the cortical regions of SCA3 patients (Schulz et al., 2010; Jao et al., 2019b). Both studies reported atrophy in the temporal lobe. While the first study reported atrophy in the frontal, parietal, and occipital lobes (Jao et al., 2019b), the second study reported non-significant increased volume in these regions (Schulz et al., 2010).

Six studies analyzed the VBM changes in the cortical regions' gray matter volume (GMV) (Schulz et al., 2010; D'Abreu et al.,

2012; Lopes et al., 2013; Hernandez-Castillo et al., 2017; Peng et al., 2019; Guo et al., 2020). While a study reported no change in the overall GMV in the cerebral hemisphere (Schulz et al., 2010), reduced GMV were reported separately in cerebral lobes, including frontal (precentral gyrus, and superior, medial, and inferior frontal gyri), parietal (postcentral gyrus, superior, and inferior parietal lobes, and association cortex), temporal (insula, fusiform gyrus, and middle, and superior temporal gyri), and occipital (lingual gyrus, cuneus, and occipital gyri) lobes. Lack of change in the GMV of the overall cerebral hemispheres may suggest that individual difference in the SCA3 neuropathology differentially affects the cortical regions, which may explain heterogeneous clinical manifestation across SCA3 patients (Pedroso et al., 2013). Alternatively, using a small sample size (nSCA3 = 24 vs. nHC = 31) and four different scanners may contribute to the methodological limitation that may explain the null finding (Schulz et al., 2010).

Four studies analyzed the surface of the cortical regions (De Rezende et al., 2015; Nunes et al., 2015; Rezende et al., 2018; Arruda et al., 2020). These studies reported reduced cortical thickness in the frontal (precentral and superior frontal gyri), temporal (superior temporal gyrus), and occipital lobes. While surface analysis selectively investigates cortical thickness, VBM provides a composite measure of GMV, including cortical surface area or cortical folding, as well as cortical thickness (Hutton et al., 2009). This difference between VBM and surface analysis may explain the inconsistent findings regarding the GMV of the parietal lobe; that is, reduced cortical folding and surface area contributes to the GMV loss in the parietal lobe. Conversely, a relatively preserved cortical thickness in the parietal lobe may only be affected later in the SCA3 pathology.

Cerebrum (Subcortical)

Five studies analyzed the volumetric changes in the subcortical regions of SCA3 patients (D'Abreu et al., 2011; De Rezende et al., 2015; Nunes et al., 2015; Rezende et al., 2018; Jao et al., 2019b). These studies reported atrophy in the diencephalon (ventral diencephalon and thalamus), limbic system (limbic lobe and hippocampus), basal ganglia (globus pallidus, putamen, caudate, and substantia nigra), and lenticular fasciculus.

Six studies analyzed the VBM changes in the GMV of subcortical regions (Schulz et al., 2010; D'Abreu et al., 2012; Guimarães et al., 2013; Lopes et al., 2013; Kang et al., 2014; Guo et al., 2020). All studies consistently reported reduced GMV in the limbic system (limbic lobe and posterior cingulate), and claustrum. Three studies reported reduced GMV in the basal ganglia (lentiform nucleus, caudate, and putamen), absent in the remaining study characterized by a smaller sample size and the use of four different scanners (Schulz et al., 2010).

Only one study analyzed and reported reduced cortical thickness of the limbic system (posterior cingulate) (Rezende et al., 2018). This scarcity in research is likely because while theory and convention informed the classification of the limbic system under the subcortical region (Berkowitz, 2016), the limbic system involves cortical structures (Rolls, 2015). This classification may explain the scarcity of surface analysis on the limbic system.

Brainstem

Nine studies analyzed the volumetric changes in the brainstem of SCA3 patients (Bürk et al., 1996; Yoshizawa et al., 2003; Liang et al., 2009; Schulz et al., 2010; Camargos et al., 2011; Ogawa et al., 2012; De Rezende et al., 2015; Nunes et al., 2015; Rezende et al., 2018). These studies reported widespread atrophy in the overall brainstem, including pons, midbrain, and medulla. Two studies reported atrophy in the midbrain, while one study did not show any changes in the aforementioned brain regions (Liang et al., 2009). While the sample size may not explain the discrepancy in findings, the difference in the brain structure across ethnicity may be contributory (i.e., East Asian vs. Western) (Tang et al., 2018).

Six studies analyzed the VBM changes in the GMV of the brainstem (Schulz et al., 2010; D'Abreu et al., 2012; Guimarães et al., 2013; Kang et al., 2014; Hernandez-Castillo et al., 2017; Peng et al., 2019). These studies consistently reported reduced GMV in the overall brainstem, including medulla, midbrain, and pyramids. Conversely, three studies reported reduced GMV in the pons, while one did not. A smaller sample size may explain the absence of reduced GMV in the pons (Schulz et al., 2010). Similar to the GMV in the brainstem, the overall brainstem also showed reduced WBV, including medulla, pyramids, pons, and midbrain.

Cerebellum

Ten studies analyzed the volumetric changes in the cerebellum of SCA3 patients (Bürk et al., 1996; Etchebehere et al., 2001; Liang et al., 2009; Schulz et al., 2010; Camargos et al., 2011; Ogawa et al., 2012; De Rezende et al., 2015; Nunes et al., 2015; Rezende et al., 2018; Jao et al., 2019b). These studies consistently reported atrophy in the overall cerebellum, including cerebellar hemispheres and vermis.

Eight studies analyzed the VBM changes in the GMV of the cerebellum (Schulz et al., 2010; D'Abreu et al., 2012; Guimarães et al., 2013; Lopes et al., 2013; Kang et al., 2014; Hernandez-Castillo et al., 2017; Peng et al., 2019; Guo et al., 2020). These studies consistently reported reduced GMV in the cerebellum, including cerebellar hemispheres (cerebellar hemispheres, tonsil, and inferior semilunar lobule) and vermis (overall, culmen, declive, uvula, fastigium, and tuber). On the other hand, two studies analyzed the white matter volume (WMV) (Schulz et al., 2010; Guimarães et al., 2013). These studies reported reduced WMV in the overall cerebellum, including left cerebellar hemisphere, vermis (tonsil, dentate, uvula, fastigium, and tuber, sparing the nodule), and cerebellar peduncles.

Summary

SCA3 neuropathology involves widespread atrophy across the brain, including cortical and subcortical cerebral regions, brainstem, and cerebellum. The present findings suggest that the volumetric loss in the cerebrum involved both GMV loss and cortical thinning. On the other hand, findings on the brainstem and cerebellum implicated that the volumetric loss in these regions is not restricted to GMV loss; WMV loss is similarly

prominent in these regions (Schulz et al., 2010; Guimarães et al., 2013). Future studies may investigate the difference between GMV and WMV loss in the cerebrum, contributing to the heterogeneous clinical profile in SCA3 patients.

MRS

The levels of N-acetyl aspartate (NAA), glutamate (Glu), Choline (Cho), myo-Inositol (myo-Ins), and Creatinine (Cr) are the primary metabolites being studied. NAA and Glu concentration reflects the neuronal viability and integrity, in which reduced concentrations indicate neuronal and axonal injury or loss (Moffett et al., 2007). Cho is a precursor of acetylcholine and is essential for cell membrane and neurotransmitter metabolism. Myo-Ins is a biomarker for glial activation in response to neuronal injury and degeneration (Duarte et al., 2012). Cr reflects brain energy metabolism and is relatively stable under normal conditions, serving as a reference for comparison (Lirng et al., 2012).

Cerebrum (Subcortical)

Only one study analyzed and reported reduced NAA/Cr and NAA/Cho in the diencephalon (thalamus) of SCA3 patients (Peng et al., 2019). The same study reported no change of NAA/Cr in the basal ganglia (putamen) (Peng et al., 2019).

Brainstem

Only one study reported reduced NAA and glutamate (Glu) and increased Cr and myo-Ins in the brainstem (pons) (Adanyeguh et al., 2015). The finding suggests that changes in NAA/Cr ratio in the pons may represent a better early biomarker for SCA3 neuropathology (Adanyeguh et al., 2015; Peng et al., 2019). Consistently, changes in the pons, alongside the cerebellum, are promising biomarkers for the disease progression in SCA3 (Adanyeguh et al., 2018).

Cerebellum

Six studies analyzed the metabolic changes in the cerebellum of SCA3 patients (Lei et al., 2011; Lirng et al., 2012; Wang et al., 2012; Chen et al., 2014; Adanyeguh et al., 2015; Peng et al., 2019). One study reported reduced NAA and Glu and increased Cr and myo-Ins in the vermis (Adanyeguh et al., 2015). The remaining studies consistently reported reduced NAA/Cr in the cerebellar hemispheres, vermis (overall and dentate), and middle cerebellar peduncles. Four studies reported reduced NAA/Cho in the cerebellar hemispheres, vermis (overall and dentate), and middle cerebellar peduncles.

Conversely, while four studies reported no change in the Cho/Cr in the overall cerebellum (Lei et al., 2011; Lirng et al., 2012; Wang et al., 2012; Chen et al., 2014), a study reported reduced Cho/Cr in the vermis (Peng et al., 2019). This finding suggests that the SCA3 neuropathology may affect the vermis in the early stage of the disease. The vermis is typically more affected than the cerebellar hemispheres in genetic disorders (Aldinger and Doherty, 2016), although this finding has not been replicated in the SCA3 population.

A study reported that the following metabolites were reduced in the cerebellum: NAA/Total Cr (Cr+PCr) ratio, NAA+N-acetyl-aspartyl-glutamate (NAA+NAAG)/Cr+PCr ratio, and glutamine (Glx)/Cr+PCr ratio (Lopes et al., 2013). The same study also reported that the following metabolites did not change in the cerebellum: Glu/Cr+PCr ratio, phosphorylcholine (PCh)/Cr+PCr ratio, and myo-Ins/Cr+PCr ratio (Lopes et al., 2013).

Summary

While far from being a sensitive biomarker, MRS findings may explain the metabolic changes and neuronal dysfunction before the neuronal loss and clinical manifestation of SCA3 (Chen et al., 2014). Reduced NAA and Glu primarily present in the pons and vermis of SCA3 patients imply reduced metabolism and neuronal loss in these regions (Adanyeguh et al., 2015). Conversely, increased myo-Ins is likely a response to the degenerative nature of SCA3, while increased Cr may be a compensatory response to maintain the energy supply of brain tissue (Brewer and Wallimann, 2000). The lack of studies on the absolute concentration of individual metabolites compared to metabolite ratios is likely because the latter offers a more robust approach in accounting for a small sample size (Hoch et al., 2017).

Overall, reduced metabolism primarily involves the brainstem (pons) and cerebellum (vermis). These findings may represent an early biomarker of the SCA3 neuropathology that precedes structural loss. Compared to its structural counterpart, MRS studies using individual metabolites on the cerebrum of SCA3 are lacking. Likewise, several metabolite ratios were preliminary and deserved further study (Lopes et al., 2013).

DTI

We only considered fractional anisotropy (FA) to represent a reliable marker for DTI changes (Bennett et al., 2010). Fractional anisotropy (FA) is sensitive to microstructural changes, reflecting white matter fiber density, axonal diameter, and myelination. A higher FA indicates greater white matter integrity and vice versa (Dong et al., 2012).

Cerebrum (Cortical)

Four studies reported reduced FA in the frontal (precentral and middle frontal gyri), parietal (postcentral gyrus temporal), and occipital lobes (Kang et al., 2014; Rezende et al., 2018; Jao et al., 2019a; Inada et al., 2021).

Cerebrum (Subcortical)

Five studies reported reduced FA in the corona radiata, internal and external capsules, thalamic radiation, forceps, cingulate fasciculus, parietal-temporal superior and inferior longitudinal fasciculus, and corpus callosum (Kang et al., 2014; Rezende et al., 2018; Jao et al., 2019a; Meira et al., 2020; Inada et al., 2021).

Brainstem

Eight studies analyzed the FA changes in the brainstem (Guimarães et al., 2013; Lopes et al., 2013; Kang et al., 2014; Wu et al., 2017; Rezende et al., 2018; Jao et al., 2019a; Meira et al., 2020; Inada et al., 2021). These studies reported reduced FA in the brainstem (overall and pons). Regarding the tracts, studies reported reduced FA in the cortical-spinal tract, lemniscus, and pons crossing tract.

Cerebellum

Seven studies analyzed the FA changes in the cerebellum (Guimarães et al., 2013; Kang et al., 2014; Wu et al., 2017; Rezende et al., 2018; Jao et al., 2019a; Peng et al., 2019; Inada et al., 2021). A study reported reduced FA in the cerebellar hemispheres and vermis (nodule, culmen, dentate, fastigium, and lingual) (Guimarães et al., 2013). Regarding the tracts, studies reported reduced FA in the cerebellar peduncles (overall, superior, middle, and inferior cerebellar peduncles).

Summary

DTI studies reported a widespread decrease in FA in the white matter across the whole brain, with relatively more studies in the cerebellum and the brainstem. These studies also reported white matter abnormalities in several fiber pathways. These fibers typically involved cerebellar connecting tracts, including cerebellar peduncles, thalamic radiations, and cortical-spinal tract. These findings suggest that apart from individual brain regions that are impaired, disrupted connectivity between cerebellum from other brain regions is equally contributory to the clinical manifestations in SCA3.

MRI vs. Clinical Correlations in SCA3

Motor (Ataxia)

Structural MRI

Cerebrum (Cortical). A study reported that ataxia severity using SARA moderately correlates with GMV of frontal (precentral gyrus: $r = -0.30$, middle frontal cortex: $r = -0.33$, paracentral lobule: $r = -0.31$), and temporal (transverse temporal gyrus: $r = -0.30$, superior temporal sulcus: $r = -0.35$, transverse temporal cortex: $r = -0.35$) lobes (De Rezende et al., 2015). Another study showed that ataxia severity using ICARS moderately correlates with the GMV of occipital ($r = 0.44$) lobes, and strongly correlates with the GMV of the frontal ($r = 0.62$), parietal ($r = 0.57$), temporal ($r = 0.72$) lobes (D'Abreu et al., 2012). The findings showed that the correlations were more consistent using SARA; the r ranged between −0.35 and −0.30. Before attributing the findings to the differences in clinical scales, it is important to rule out potential confounding factors. Specifically, one study correlates SARA scores with specific regions (e.g., gyrus) (De Rezende et al., 2015), whereas another study correlates ICARS with the entire lobe (D'Abreu et al., 2012).

Cerebrum (Subcortical). Two studies reported correlations between changes in the subcortical regions and ataxia severity using SARA (Schulz et al., 2010; De Rezende et al., 2015). A study reported that ataxia severity moderately correlates with the volumetric changes in the dorsal striatum ($r = -0.36$); the correlation was marginally stronger when only the caudate nucleus was taken into account ($r = -0.46$) (Schulz et al., 2010). Another study reported strong correlations between SARA and the volumetric changes in the diencephalon (right: $r = 0.58$, left: $r = 0.64$, thalamus: $r = 0.62$) (De Rezende et al., 2015). Consistent with the findings, the caudate nucleus and thalamus are among the subcortical regions most affected in SCA3 (Meira et al., 2020). Degeneration in the thalamus may contribute to the severity of ataxia (Rüb et al., 2003). On the other hand, striatal degeneration may result in parkinsonism in SCA3 (Nunes et al., 2015), confounding the SARA scores.

Brainstem. Ataxia severity using SARA moderately correlates with the volumetric changes in the midbrain ($r = -0.47$) and medulla ($r = -0.48$), and strongly correlates with the volumetric changes in the total brainstem ($r = -0.58 \sim -0.68$) (Schulz et al., 2010; De Rezende et al., 2015), and pons ($r = -0.56$) (Schulz et al., 2010). Similarly, ICARS strongly correlates with volumetric changes in the total brainstem ($r = -0.62$), midbrain ($r = -0.53$) and pons ($r = -0.57 \sim -0.68$) (Liang et al., 2009; Camargos et al., 2011).

Cerebellum. Ataxia severity using SARA moderately correlates with the volumetric changes in the total cerebellum ($r = -0.42 \sim -0.45$) (Liang et al., 2009; Schulz et al., 2010) and cerebellar hemispheres ($r = -0.46$) (Schulz et al., 2010). Similarly, ataxia severity using ICARS moderately correlates with the volumetric changes in the right hemisphere ($r = -0.49$), while strongly correlates with the volumetric changes in the total cerebellum ($r = -0.60$), left hemisphere ($r = -0.63$), and vermis ($r = -0.52$) (Camargos et al., 2011). Likewise, ataxia severity using ICARS strongly correlates with the GMV of the total cerebellum ($r = 0.73$) (D'Abreu et al., 2012). Lastly, a study showed that the SARA moderately correlates with the WMV of the cerebellum ($r = -0.46$) (Arruda et al., 2020). The discrepancy in the r suggests that GMV of the total cerebellum may represent a more sensitive biomarker than volumetric changes and WMV for ataxia severity in SCA3.

Summary. Overall, the findings are consistent with a previous finding that both SARA and ICARS are similarly reliable and effective in assessing ataxia severity in SCA3 (Zhou et al., 2011). More studies, exploring correlations between SARA and ICARS and MRI abnormalities, are needed to confirm the findings. Nevertheless, the results are consistent with the body of evidence that structural loss in the cerebellum and brainstem, especially the GMV, contribute toward ataxia severity in SCA3 (Eichler et al., 2011). Thalamus atrophy may exacerbate ataxia severity in SCA3 (Rüb et al., 2003). Interestingly, ataxia severity in SCA3 was also associated with cortical atrophy, to which further investigations are needed to examine its role in ataxia.

MRS

Brainstem. Ataxia severity using SARA strongly correlates with NAA ($r = -0.82$), Cr ($r = 0.64$), and myo-Ins ($r = 0.69$) in the brainstem (Adanyeguh et al., 2015).

Cerebellum. Ataxia severity using SARA showed no correlation between SARA and NAA/Cr ratio in the total cerebellum (Wang et al., 2012; Adanyeguh et al., 2015). However, when examining specific cerebellar regions, SARA moderately correlates with the NAA/Cr ratio in the dentate nucleus ($r = 0.45$) and strongly correlates with the middle cerebellar peduncle ($r = 0.95$) (Lei et al., 2011). Ataxia severity using ICARS moderately correlates with NAA/Cr in the middle cerebellar peduncle ($r = -0.45$) and strongly correlates with the dentate nucleus ($r = -0.50$) (Peng et al., 2019). The discrepancy in findings using different clinical

measures provides an avenue for future study on the reliability of SARA and ICARS in correlating with the NAA/Cr ratio.

Ataxia severity using SARA showed no correlation between SARA and Cho/Cr ratio in the total cerebellum (Wang et al., 2012; Adanyeguh et al., 2015). Regarding specific cerebellar regions, SARA moderately correlates with Cho/Cr ratio in the cerebellar hemispheres ($r = -0.39$) and dentate nucleus ($r = 0.36$), and strongly correlates with the vermis ($r = 0.93$) (Lei et al., 2011). Also, ataxia severity using ICARS moderately correlates with Cho/Cr ratio in the dentate nucleus ($r = -0.37$) (Peng et al., 2019). The correlation between Cho/Cr ratio in the dentate nucleus and ataxia severity measured by SARA and ICARS is similar. The finding suggests that the difference in the predictive value between SARA and ICARS for Cho/Cr ratio was minimal. Therefore, a strong correlation between Cho/Cr ratio in the vermis and ataxia severity is unlikely attributed to the type of scale, thereby representing a reliable biomarker.

Lastly, a study reported that ataxia severity using SARA moderately correlates with the NAA/Cho ratio cerebellar hemispheres ($r = 0.46$) and vermis ($r = 0.37$) (Lei et al., 2011).

Summary. Correlation between ataxia severity and MRS changes was scarcely studied in SCA3 patients. Specifically, only a single study established the correlation between ataxia severity and individual metabolite change in the brainstem of SCA3 patients (Adanyeguh et al., 2015). At present, changes in the metabolite ratios are not uniform across the cerebellum. Specifically, reduced Cho/Cr in the vermis may represent a more accurate MRS biomarker for ataxia severity in SCA3 patients due to its strong correlation with SARA scores.

DTI

Cerebrum (Subcortical). A study reported that ataxia severity using ICARS moderately correlates with FA of the posterior thalamic radiation ($r = 0.44$) (Wu et al., 2017).

Brainstem. A study reported that ataxia severity using SARA moderately correlates with FA of the left cortical-spinal tract ($r = -0.47$), and strongly correlates with FA of the right cortical-spinal tract ($r = -0.51$) (Meira et al., 2020). Another study reported that ataxia severity using ICARS strongly correlates with the FA of the medial lemniscus ($r = -0.52$) (Wu et al., 2017).

Cerebellum. A study reported no correlation between ataxia severity using SARA and FA in the total cerebellum (Guimarães et al., 2013). Ataxia severity using ICARS moderately to strongly correlates with FA in the superior ($r = -0.43 \sim -0.64$) (Wu et al., 2017; Peng et al., 2019), middle ($r = -0.42$), and inferior ($r = -0.60$) cerebellar peduncles (Peng et al., 2019).

Summary. There is no established correlation between SARA and FA in the total cerebellum, whereas ataxia severity using ICARS correlated with FA in several white matter tracts. These findings suggest that FA in white matter tracts indicates ataxia severity than FA of other brain regions, including the total cerebellum. These findings remain preliminary, and each tract's contribution deserves further exploration.

Motor (Non-ataxia)

There was no association between Burke–Marsden–Fahn's Dystonia Rating Scale (BMFDRS) and MRI techniques, including structural MRI and DTI. Similar to ataxia scales, one possible explanation for the lack of correlation is that the BMFDRS is susceptible to other movement difficulties (Kuiper et al., 2016). Nevertheless, the study reported the presence of precentral and paracentral cortices atrophy and more severe thalamus atrophy in SCA3 patients with dystonia compared to their non-dystonic counterparts (Nunes et al., 2015). In addition, midbrain atrophy may also contribute to dystonia in SCA3 (Vidailhet et al., 1999). Further studies are needed to identify brain regions that contribute to dystonia in SCA3 patients.

Neurocognition

We conducted an a-priori categorization of neuropsychological tests into three neurocognitive domains informed by theory and convention (Strauss et al., 2006; Lezak et al., 2012). These domains were (1) general intelligence, (2) working memory (WM), and (3) executive aspect of language. All of which were related to the executive function (EF) (Miyake et al., 2000; Van Aken et al., 2016; Tamura et al., 2018).

General Intelligence

General intelligence is a construct that represents a person's verbal and non-verbal reasoning abilities (Kamphaus, 2005).

Structural MRI

Cerebrum (Cortical). One study reported that verbal reasoning using the Similarities subtest strongly correlates with the cortical thickness of the left precentral gyrus ($r = 0.82$) and right superior occipital gyrus ($r = 0.84$) (De Rezende et al., 2015). On the other hand, non-verbal reasoning using Raven's Progressive Matrices (RPM) strongly correlates with the cortical thickness of the left middle occipital gyrus ($r = 0.90$) (De Rezende et al., 2015). Contradictorily, these measures of general intelligence are commonly associated with frontal and parietal cortices but not precentral and occipital gyri (Gläscher et al., 2009). Therefore, rather than playing a direct role in general intelligence, cortical thickness in the precentral and occipital gyri may share a parallel neurodegenerative process in the SCA3 neuropathology that impedes general intelligence.

MRS

Cerebellum. One study reported that the RPM moderately correlates with Glu ($r = -0.42$) and Glx ($r = -0.41$) in the cerebellum (Lopes et al., 2013). The correlation between the cerebellar metabolites and RPM may be attributed to the extensive reciprocal connections between the cerebellum and areas of the cerebrum (Bostan et al., 2013), which disrupts cognitive function (Stoodley and Schmahmann, 2010). Negative correlations between metabolites and RPM are likely related to the processing techniques such as global signal regression than actual anti-correlated activity (Murphy et al., 2009).

Working Memory

MRS

Cerebellum. One study reported that auditory WM using Digit Span (DS) moderately correlates with the NAA ($r = 0.42$) and NAA + NAAG ($r = 0.43$) in the cerebellum (Lopes et al., 2013), consistent with the finding that the cerebellum plays a role in the processing of auditory WM (Tomlinson et al., 2014).

DTI

Brainstem. One study reported that auditory WM using DS moderately correlates with the FA of the brainstem ($r = 0.49$) (Lopes et al., 2013). The relationship between the brainstem and WM is shown when WM plays an essential role in the early precortical sensory processing, in this case, auditory-evoked brainstem response (Sörqvist et al., 2012). The finding suggests that brainstem degeneration is associated with the WM impairment in SCA3.

Language

MRS

Cerebellum. One study reported that semantic verbal fluency strongly correlates with the PCh ($r = 0.66$) and GPC + PCh ($r = 0.69$) in the cerebellum (Lopes et al., 2013). This finding highlights the cerebellum's role in motor and sequential speech processing (Leggio et al., 2000). Specifically, an impaired cerebellar cortex-ventral dentate nucleus-thalamus-prefrontal cortex circuit in SCA3 is heavily implicated in strategic word retrieval (Tamura et al., 2018).

Summary

Existing findings on the correlations between neurocognition and neurodegenerative process in SCA3 are restricted to EF. The correlations between neurocognition the cerebellum in SCA3 were at least moderate. This finding is consistent with the cerebellum's role in EF processing due to its extensive reciprocal connections with areas of the cerebrum, including the prefrontal and posterior parietal cortex and the basal ganglia (Stoodley and Schmahmann, 2010; Bostan et al., 2013). Contradictorily, no correlation was found with the prefrontal-striatal circuit, which is impaired in SCA3 and plays a crucial role in higher-order cognitive functions (Alexander et al., 1986; Yap et al., 2022b). Instead, strong correlations were found between general intelligence and precentral gyrus and superior occipital gyrus (De Rezende et al., 2015). This finding determines whether these regions are simultaneously affected alongside the distributed network involved in the EF processing in SCA3.

DISCUSSION

In this review, we demonstrated widespread brain degeneration with moderate correlations between MRI features in several regions and clinical findings in SCA3 patients. Regardless of the MRI techniques, most studies focused on the brainstem and cerebellum. This trend aligns with the body of evidence that suggests that these regions are affected earlier than the cerebrum (Rezende et al., 2018). These early degenerations are consistent with ataxia being the key symptom observed in SCA3 (Bodranghien et al., 2016). Interestingly, the structural loss of the cerebellum in SCA3 was less affected than other SCA subtypes (Schulz et al., 2010). Instead, studies reported degenerative atrophy of various cerebral structures in SCA3, including cortical and sub-cortical regions (Schulz et al., 2010; D'Abreu et al., 2012; De Rezende et al., 2015). As the disease progresses, the SCA3 neuropathology gradually affects the cerebrum, in which extensive atrophy is observed in the cerebral cortex and basal ganglia in the late stages of SCA3 (Rezende et al., 2018). This process results in widespread brain degeneration, contributing to and exacerbating non-ataxia and cognitive impairment in SCA3 (Lindsay and Storey, 2017).

We also examined the MRI abnormalities that may explain the clinical manifestations in SCA3 based on correlation studies. SARA and ICARS represent the most frequently used ataxia scales for SCA3 patients. Regardless of the MRI techniques, the correlation findings were similar between SARA and ICARS (Rüb et al., 2003; Eichler et al., 2011; Bodranghien et al., 2016). Consistently, SARA and ICARS are equally reliable in measuring ataxia severity in SCA3. However, a relatively higher inter-rater reliability, functional relevance, and timesaving nature confer advantages to the SARA (Zhou et al., 2011).

In contrast to the ataxia symptoms, the MRI correlates to the cognitive impairment in SCA3 have not been comprehensively evaluated. Specifically, existing findings focused only on the EF of SCA3 patients. Interestingly, some MRI abnormalities showed associations between EF and the left precentral gyrus and right superior occipital gyrus (De Rezende et al., 2015), rather than the frontal and parietal cortices (Gläscher et al., 2009). We postulate that these regions shared a parallel neurodegenerative process with the cognitive decline in SCA3. Alternatively, these regions may play a pivotal role in the distributed networks serving these neurocognitive domains.

At present, the correlations between the structural MRI, MRS, and DTI changes in several regions and ataxia and cognitive impairment were mainly in the moderate range ($r = 0.30$–0.49) (Cohen, 2013). In support, a study that used 3D-FD analysis showed a similar correlation between the cerebellar cortex and SARA scores ($r = -0.33$) (Wang et al., 2020). In addition, there was no correlation between dystonia using BMFDRS and MRI techniques in SCA3 patients. The presence of clinical syndrome may compound each other; that is, ataxia and dystonia may exacerbate each other when measured with their respective clinical scales. Likewise, motor impairment is often a confounding factor for clinical scales from truly reflecting cognitive impairment (Yap et al., 2022b). This issue is often exacerbated as few tests assess only a single domain (i.e., true process-pure tests), thereby affecting the test utility in the cerebellar patient population. Nevertheless, these symptoms are part of the clinical syndrome of SCA3 and are nearly impossible to disentangle from studying one another.

In addition, the involvement of multiple brain regions in SCA3 may also complicate the correlational findings. For example, several different brain regions may contribute to ataxia severity, including the thalamus, pons, and cerebellum (Rüb et al., 2003; Eichler et al., 2011; Bodranghien et al., 2016). This finding may explain moderate correlations between each

brain region and the corresponding clinical findings. More importantly, it may represent the difference between isolated cerebellar (e.g., cerebellar stroke) and complex cerebrocerebellar diseases (e.g., SCA3), to which the latter involves both cerebellar and cerebral degeneration.

We postulate that in a complex cerebrocerebellar disease like SCA3, degeneration in any part of the brain region and its connections in the same distributed network may result in the same clinical symptom (Benowitz and Carmichael, 2010), despite each playing a different role in the process. For example, severe ataxia is not only observed when the cerebellum is impaired (Bodranghien et al., 2016); the disruption in the connection between the cerebellum and motor cortex in SCA3 also results in the same symptom (Maas et al., 2021). Specifically, the cerebellum projects to the contralateral premotor and primary motor cortices with sensory and motor information necessary to adapt movements in response to feedback, termed the motor network (Spampinato et al., 2020). Likewise, disruption in the cerebellar-cerebral network and prefrontal-striatal circuit were involved in the cognitive impairment in SCA3 (Lindsay and Storey, 2017). In this case, the cerebellum serves as a hub in the network that prepares for neural processing to optimize the action sequencing on the EF task (Beuriat et al., 2020). Cerebellar degeneration compounds the EF impairment due to the frontal lobe atrophy in SCA3 patients (Klinke et al., 2010).

IMPLICATIONS

This review highlights two research gaps in the literature. First, the brain-behavior relationship in SCA3 has not been comprehensively evaluated using MRI-based brain networks. We postulate that a distributed network, rather than an individual brain region such as the cerebellum, is responsible for the clinical syndrome in SCA3 (Beuriat et al., 2020; Spampinato et al., 2020). In support, the 3D-FD analysis showed that SCA3 neuropathology involves dissociation in the cerebellar-cerebral network (Huang et al., 2017; Jao et al., 2019b). Second, most studies mainly aimed at investigating the structural loss in SCA3 patients, including attempts to increase the sensitivity of the scan, such as texture analysis (De Oliveira et al., 2010) and neuromelanin contrast (Nakata et al., 2020), whereas functional activation has been scarcely studied. Functional activation allows the inference of brain regions and networks involved in a particular motor or cognitive process (Berman et al., 2006). At present, a relaxometry study showed decreased T2-relaxation values in the white matter of the right cerebellar hemisphere alongside structural loss (Guimarães et al., 2013), and a task-based fMRI study showed that a paced motor task elicited increased activations in the motor network SCA3 patients irrespective of gray matter loss (Duarte et al., 2016). These findings are similar to other neurodegenerative diseases such as Alzheimer's disease, which increases activation in early disease stage (Yap et al., 2017). Together with the presence of brain structural and metabolic changes before the clinical manifestation (Wu et al., 2017; Joers et al., 2018; Rezende et al., 2018), the findings imply functional reorganization of the brain and that compensatory activation is in play (Duarte et al., 2016), which gradually decline as the disease progresses (Yap et al., 2017). Notably, the compensatory activation may also obscure the correlations between brain structural and metabolic changes and clinical findings, which may also explain the moderate association strengths. Therefore, we need more findings on the fMRI for SCA3 patients, especially the resting-state networks.

The importance of these findings points to the pivotal role of adaptive or maladaptive compensatory activation. A maladaptive compensatory activation is shown when dysfunction in the brain region results in its inability to downregulate other brain regions in the same distributed network. Therefore, the increased activation disrupts clinical performance (Franzen et al., 2013; Jones et al., 2016). Conversely, adaptive compensatory activation may imply that neuroplasticity is present in SCA3 patients, providing support for early physical and cognitive rehabilitation. While restorative neurorehabilitation has been widely studied in the SCA3 population, findings for non-pharmacological approaches for SCA, such as cognitive rehabilitation and psychotherapy on other aspects of psychological symptoms, are lacking (Yap et al., 2022a).

LIMITATIONS

This review has several limitations. Firstly, different MRI techniques have not been consistently studied across different brain regions in the SCA3 population, specifically the cerebrum. Likewise, correlations between clinical impairment and brain regions were not consistently reported. Therefore, we could not conclude whether the absence of correlations was due to non-significant findings or was not assessed. Secondly, SCA3 patients are commonly characterized by peripheral nerve involvement, which further exacerbating test performances through non-ataxia symptoms such as muscle weakness and sensory disturbances (Van De Warrenburg et al., 2004). It is essential to rule out these factors before correlating the brain MRI abnormalities and clinical syndrome. Thirdly, a potential problem with MRI studies involved multiple comparisons, which increases the likelihood of false positives (Lindquist and Mejia, 2015). This problem applies to comparing brain regions between SCA3 and HC and the number of correlations conducted. Therefore, Bonferroni correction may help address the problem (Lindquist and Mejia, 2015). However, it is also possible that none of the true positives would survive multiple comparison corrections. Lastly, there is a lack of knowledge on the brain degenerative patterns between SCA3 patients from Western and East Asian countries. The difference in the brain structure may affect the degenerative pattern, although this has not been studied (Tang et al., 2018). In addition, factors such as test norms, age, gender, culture, education level, and functional level may further affect the degenerative pattern and correlations between MRI and clinical findings.

CONCLUSION

SCA3 neuropathology contributes to widespread brain degeneration. We speculate that the connectivity between different brain regions in distributed networks is responsible

for motor and neurocognitive function in SCA3. However, this topic remains scarcely studied in SCA3. Therefore, future studies should investigate possible functional connectivity abnormalities in SCA3 using fMRI.

DATA AVAILABILITY STATEMENT

The original contributions presented in the study are included in the article/**Supplementary Material**, further inquiries can be directed to the corresponding author/s.

AUTHOR CONTRIBUTIONS

Funding acquisition was performed by NM. Literature search was performed by KY and HA. The first draft of this review was written by KY. All authors critically revised the work, contributed to the study conception and design, and read and approved the final version of the review.

FUNDING

This work was supported by the Dana Impak Perdana Grant (DIP-2019-007) received by NM from Universiti Kebangsaan Malaysia.

SUPPLEMENTARY MATERIAL

The Supplementary Material for this article can be found online at: https://www.frontiersin.org/articles/10.3389/fnins.2022.859651/full#supplementary-material

REFERENCES

Adanyeguh, I. M., Henry, P., Nguyen, T. M., Rinaldi, D., Jauffret, C., Valabregue, R., et al. (2015). *In vivo* neurometabolic profiling in patients with spinocerebellar ataxia types 1, 2, 3, and 7. *Mov. Disord.* 30, 662–670. doi: 10.1002/mds.26181

Adanyeguh, I. M., Perlbarg, V., Henry, P.-G., Rinaldi, D., Petit, E., Valabregue, R., et al. (2018). Autosomal dominant cerebellar ataxias: imaging biomarkers with high effect sizes. *NeuroImage: Clinical* 19, 858–867. doi: 10.1016/j.nicl.2018.06.011

Aldinger, K. A., and Doherty, D. (2016). "The genetics of cerebellar malformations," in *Seminars in Fetal and Neonatal Medicine* (Elsevier), 21, 321–332. doi: 10.1016/j.siny.2016.04.008

Alexander, G. E., Delong, M. R., and Strick, P. L. (1986). Parallel organization of functionally segregated circuits linking basal ganglia and cortex. *Annu. Rev. Neurosci.* 9, 357–381. doi: 10.1146/annurev.ne.09.030186.002041

Arruda, W. O., Meira, A. T., Ono, S. E., De Carvalho Neto, A., Betting, L. E. G. G., Raskin, S., et al. (2020). Volumetric MRI changes in spinocerebellar ataxia (SCA3 and SCA10) patients. *Cerebellum* 19, 536–543. doi: 10.1007/s12311-020-01137-3

Bennett, I. J., Madden, D. J., Vaidya, C. J., Howard, D. V., and Howard, J. H. Jr. (2010). Age-related differences in multiple measures of white matter integrity: a diffusion tensor imaging study of healthy aging. *Hum. Brain Mapp.* 31, 378–390. doi: 10.1002/hbm.20872

Benowitz, L. I., and Carmichael, S. T. (2010). Promoting axonal rewiring to improve outcome after stroke. *Neurobiol. Dis.* 37, 259–266. doi: 10.1016/j.nbd.2009.11.009

Berkowitz, A. (2016). *Lange Clinical Neurology and Neuroanatomy: A Localization-Based Approach*. New York, NY: McGraw-Hill Education.

Berman, M. G., Jonides, J., and Nee, D. E. (2006). Studying mind and brain with fMRI. *Soc. Cogn. Affect. Neurosci.* 1, 158–161. doi: 10.1093/scan/nsl019

Beuriat, P.-A., Cohen-Zimerman, S., Smith, G. N., Krueger, F., Gordon, B., and Grafman, J. (2020). A new insight on the role of the cerebellum for executive functions and emotion processing in adults. *Front. Neurol.* 11, 1668. doi: 10.3389/fneur.2020.593490

Bodranghien, F., Bastian, A., Casali, C., Hallett, M., Louis, E. D., Manto, M., et al. (2016). Consensus paper: revisiting the symptoms and signs of cerebellar syndrome. *Cerebellum* 15, 369–391. doi: 10.1007/s12311-015-0687-3

Bostan, A. C., Dum, R. P., and Strick, P. L. (2013). Cerebellar networks with the cerebral cortex and basal ganglia. *Trends Cogn. Sci.* 17, 241–254. doi: 10.1016/j.tics.2013.03.003

Brewer, G. J., and Wallimann, T. W. (2000). Protective effect of the energy precursor creatine against toxicity of glutamate and β-amyloid in rat hippocampal neurons. *J. Neurochem.* 74, 1968–1978. doi: 10.1046/j.1471-4159.2000.0741968.x

Bürk, K., Abele, M., Fetter, M., Dichgans, J., Skalej, M., Laccone, F., et al. (1996). Autosomal dominant cerebellar ataxia type I clinical features and MRI in families with SCA1, SCA2 and SCA3. *Brain* 119, 1497–1505. doi: 10.1093/brain/119.5.1497

Camargos, S. T., Marques, W. Jr., and Santos, A. C. D. (2011). Brain stem and cerebellum volumetric analysis of Machado Joseph disease patients. *Arq. Neuropsiquiatr.* 69, 292–296. doi: 10.1590/S0004-282X2011000300005

Chen, H.-C., Lirng, J.-F., Soong, B.-W., Guo, W. Y., Wu, H.-M., Chen, C. C.-C., et al. (2014). The merit of proton magnetic resonance spectroscopy in the longitudinal assessment of spinocerebellar ataxias and multiple system atrophy-cerebellar type. *Cereb. Ataxias* 1, 1–10. doi: 10.1186/s40673-014-0017-4

Cohen, J. (2013). *Statistical Power Analysis for the Behavioral Sciences*. Hoboken: Academic Press. doi: 10.4324/9780203771587

Currie, S., Hadjivassiliou, M., Craven, I. J., Wilkinson, I. D., Griffiths, P. D., and Hoggard, N. (2013). Magnetic resonance imaging biomarkers in patients with progressive ataxia: current status and future direction. *Cerebellum* 12, 245–266. doi: 10.1007/s12311-012-0405-3

D'Abreu, A., França, M. C. Jr., Yasuda, C. L., Campos, B. A., Lopes-Cendes, I., and Cendes, F. (2012). Neocortical atrophy in Machado-Joseph disease: a longitudinal neuroimaging study. *J. Neuroimaging* 22, 285–291. doi: 10.1111/j.1552-6569.2011.00614.x

D'Abreu, A., França, M. C. Jr., Yasuda, C. L., Souza, M. S., Lopes-Cendes, Í., and Cendes, F. (2011). Thalamic volume and dystonia in Machado–Joseph disease. *J. Neuroimaging* 21, e91–e93. doi: 10.1111/j.1552-6569.2010.00464.x

De Oliveira, M. S., D'abreu, A., França, M. C. Jr., Lopes-Cendes, I., Cendes, F., and Castellano, G. (2010). MRI-texture analysis of corpus callosum, thalamus, putamen, and caudate in Machado-Joseph disease. *J. Neuroimaging* 22, 46–52. doi: 10.1111/j.1552-6569.2010.00553.x

De Rezende, T., D'abreu, A., Guimarães, R., Lopes, T., Lopes-Cendes, I., Cendes, F., et al. (2015). Cerebral cortex involvement in Machado– Joseph disease. *Eur. J. Neurol.* 22, 277–e224. doi: 10.1111/ene.12559

Döhlinger, S., Hauser, T.-K., Borkert, J., Luft, A. R., and Schulz, J. B. (2008). Magnetic resonance imaging in spinocerebellar ataxias. *Cerebellum* 7, 204. doi: 10.1007/s12311-008-0025-0

Dong, G., Devito, E., Huang, J., and Du, X. (2012). Diffusion tensor imaging reveals thalamus and posterior cingulate cortex abnormalities in internet gaming addicts. *J. Psychiatr. Res.* 46, 1212–1216. doi: 10.1016/j.jpsychires.2012.05.015

Duarte, J. M., Lei, H., Mlynárik, V., and Gruetter, R. (2012). The neurochemical profile quantified by *in vivo* 1H NMR spectroscopy. *Neuroimage* 61, 342–362. doi: 10.1016/j.neuroimage.2011.12.038

Duarte, J. V., Faustino, R., Lobo, M., Cunha, G., Nunes, C., Ferreira, C., et al. (2016). Parametric fMRI of paced motor responses uncovers novel whole-brain imaging biomarkers in spinocerebellar ataxia type 3. *Hum. Brain Mapp.* 37, 3656–3668. doi: 10.1002/hbm.23266

Eichler, L., Bellenberg, B., Hahn, H., Köster, O., Schöls, L., and Lukas, C. (2011). Quantitative assessment of brain stem and cerebellar atrophy in spinocerebellar

ataxia types 3 and 6: impact on clinical status. *Am. J. Neuroradiol.* 32, 890–897. doi: 10.3174/ajnr.A2387

Etchebehere, E. C., Cendes, F., Lopes-Cendes, I., Pereira, J. A., Lima, M. C., Sansana, C. R., et al. (2001). Brain single-photon emission computed tomography and magnetic resonance imaging in Machado-Joseph disease. *Arch. Neurol.* 58, 1257–1263. doi: 10.1001/archneur.58.8.1257

Franco-Marina, F., García-González, J. J., Wagner-Echeagaray, F., Gallo, J., Ugalde, O., Sánchez-García, S., et al. (2010). The Mini-mental State Examination revisited: ceiling and floor effects after score adjustment for educational level in an aging Mexican population. *Int. Psychogeriatr.* 22, 72–81. doi: 10.1017/S1041610209990822

Franzen, J. D., Heinrichs-Graham, E., White, M. L., Wetzel, M. W., Knott, N. L., and Wilson, T. W. (2013). Atypical coupling between posterior regions of the default mode network in attention-deficit/hyperactivity disorder: a pharmaco-magnetoencephalography study. *J. Psychiatry Neurosci.* 38, 333. doi: 10.1503/jpn.120054

Gläscher, J., Tranel, D., Paul, L. K., Rudrauf, D., Rorden, C., Hornaday, A., et al. (2009). Lesion mapping of cognitive abilities linked to intelligence. *Neuron* 61, 681–691. doi: 10.1016/j.neuron.2009.01.026

Guimarães, R. P., D'abreu, A., Yasuda, C. L., França, M. C. Jr., Silva, B. H., Cappabianco, F. A., et al. (2013). A multimodal evaluation of microstructural white matter damage in spinocerebellar ataxia type 3. *Mov. Disord.* 28, 1125–1132. doi: 10.1002/mds.25451

Guo, J., Chen, H., Biswal, B. B., Guo, X., Zhang, H., Dai, L., et al. (2020). Gray matter atrophy patterns within the cerebellum-neostriatum-cortical network in SCA3. *Neurology* 95, e3036–e3044. doi: 10.1212/WNL.0000000000010986

Hernandez-Castillo, C. R., Diaz, R., Campos-Romo, A., and Fernandez-Ruiz, J. (2017). Neural correlates of ataxia severity in spinocerebellar ataxia type 3/Machado-Joseph disease. *Cereb. Ataxias* 4, 1–4. doi: 10.1186/s40673-017-0065-7

Hoch, S. E., Kirov, I. I., and Tal, A. (2017). When are metabolic ratios superior to absolute quantification? A statistical analysis. *NMR Biomed.* 30, e3710. doi: 10.1002/nbm.3710

Huang, S.-R., Wu, Y.-T., Jao, C.-W., Soong, B.-W., Lirng, J.-F., Wu, H.-M., et al. (2017). CAG repeat length does not associate with the rate of cerebellar degeneration in spinocerebellar ataxia type 3. *Neuroimage Clin.* 13, 97–105. doi: 10.1016/j.nicl.2016.11.007

Hutton, C., Draganski, B., Ashburner, J., and Weiskopf, N. (2009). A comparison between voxel-based cortical thickness and voxel-based morphometry in normal aging. *Neuroimage* 48, 371–380. doi: 10.1016/j.neuroimage.2009.06.043

Inada, B. S. Y., Rezende, T. J. R., Pereira, F. V., Garcia, L. Á. L., Da Rocha, A. J., Neto, P. B., et al. (2021). Corticospinal tract involvement in spinocerebellar ataxia type 3: a diffusion tensor imaging study. *Neuroradiology* 63, 217–224. doi: 10.1007/s00234-020-02528-3

Jao, C.-W., Soong, B.-W., Huang, C.-W., Duan, C.-A., Wu, C.-C., Wu, Y.-T., et al. (2019a). Diffusion tensor magnetic resonance imaging for differentiating multiple system atrophy cerebellar type and spinocerebellar ataxia type 3. *Brain Sci.* 9, 354. doi: 10.3390/brainsci9120354

Jao, C.-W., Soong, B.-W., Wang, T.-Y., Wu, H.-M., Lu, C.-F., Wang, P.-S., et al. (2019b). Intra-and inter-modular connectivity alterations in the brain structural network of spinocerebellar ataxia type 3. *Entropy.* 21, 317. doi: 10.3390/e21030317

Joers, J. M., Deelchand, D. K., Lyu, T., Emir, U. E., Hutter, D., Gomez, C. M., et al. (2018). Neurochemical abnormalities in premanifest and early spinocerebellar ataxias. *Ann. Neurol.* 83, 816–829. doi: 10.1002/ana.25212

Jones, D. T., Knopman, D. S., Gunter, J. L., Graff-Radford, J., Vemuri, P., Boeve, B. F., et al. (2016). Cascading network failure across the Alzheimer's disease spectrum. *Brain* 139, 547–562. doi: 10.1093/brain/awv338

Kamphaus, R. W. (2005). "Assessment of adolescent and adult intelligence," in *Clinical Assessment of Child and Adolescent Intelligence* (New York, NY: Springer), 291–331. doi: 10.1007/978-0-387-29149-9_11

Kang, J.-S., Klein, J., Baudrexel, S., Deichmann, R., Nolte, D., and Hilker, R. (2014). White matter damage is related to ataxia severity in SCA3. *J. Neurol.* 261, 291–299. doi: 10.1007/s00415-013-7186-6

Klinke, I., Minnerop, M., Schmitz-Hübsch, T., Hendriks, M., Klockgether, T., Wüllner, U., et al. (2010). Neuropsychological features of patients with spinocerebellar ataxia (SCA) types 1, 2, 3, and 6. *Cerebellum* 9, 433–442. doi: 10.1007/s12311-010-0183-8

Kuiper, M. J., Vrijenhoek, L., Brandsma, R., Lunsing, R. J., Burger, H., Eggink, H., et al. (2016). The Burke-Fahn-Marsden dystonia rating scale is age-dependent in healthy children. *Mov. Disord. Clin. Pract.* 3, 580–586. doi: 10.1002/mdc3.12339

Leggio, M. G., Silveri, M. C., Petrosini, L., and Molinari, M. (2000). Phonological grouping is specifically affected in cerebellar patients: a verbal fluency study. *J. Neurol. Neurosurg. Psychiatry* 69, 102–106. doi: 10.1136/jnnp.69.1.102

Lei, L., Liao, Y., Liao, W., Zhou, J., Yuan, Y., Wang, J., et al. (2011). Magnetic resonance spectroscopy of the cerebellum in patients with spinocerebellar ataxia type 3/Machado-Joseph disease. *Zhong Nan da Xue Xue Bao Yi Xue Ban* 36, 511–519. doi: 10.3969/j.issn.1672-7347.2011.06.007

Lezak, M., Howieson, D., Bigler, E., and Tranel, D. (2012). *Neuropsychological Assessment.* OXford: Oxford University Press.

Liang, X., Jiang, H., Chen, C., Zhou, G., Wang, J., Zhang, S., et al. (2009). The correlation between magnetic resonance imaging features of the brainstem and cerebellum and clinical features of spinocerebellar ataxia 3/Machado-Joseph disease. *Neurol. India* 57, 578. doi: 10.4103/0028-3886.57803

Lindquist, M. A., and Mejia, A. (2015). Zen and the art of multiple comparisons. *Psychosom. Med.* 77, 114. doi: 10.1097/PSY.0000000000000148

Lindsay, E., and Storey, E. (2017). Cognitive changes in the spinocerebellar ataxias due to expanded polyglutamine tracts: a survey of the literature. *Brain Sci.* 7, 83–102. doi: 10.3390/brainsci7070083

Lirng, J.-F., Wang, P.-S., Chen, H.-C., Soong, B.-W., Guo, W. Y., Wu, H.-M., et al. (2012). Differences between spinocerebellar ataxias and multiple system atrophy-cerebellar type on proton magnetic resonance spectroscopy. *PLoS ONE* 7, e47925. doi: 10.1371/journal.pone.0047925

Lopes, T. M., Anelyssa, D., Junior, M. C. F., Yasuda, C. L., Betting, L. E., Samara, A. B., et al. (2013). Widespread neuronal damage and cognitive dysfunction in spinocerebellar ataxia type 3. *J. Neurol.* 260, 2370–2379. doi: 10.1007/s00415-013-6998-8

Maas, R. P., Van De Warrenburg, B. P., and Schutter, D. J. (2021). Inverse associations between cerebellar inhibition and motor impairment in spinocerebellar ataxia type 3. *Brain Stimul.* 14, 351–357. doi: 10.1016/j.brs.2021.01.020

Meira, A. T., Arruda, W. O., Ono, S. E., Franklin, G. L., De Carvalho Neto, A., Raskin, S., et al. (2020). Analysis of diffusion tensor parameters in spinocerebellar ataxia type 3 and type 10 patients. *Parkinson. Relat. Disord.* 78, 73–78. doi: 10.1016/j.parkreldis.2020.06.460

Miyake, A., Friedman, N. P., Emerson, M. J., Witzki, A. H., Howerter, A., and Wager, T. D. (2000). The unity and diversity of executive functions and their contributions to complex "frontal lobe" tasks: a latent variable analysis. *Cogn. Psychol.* 41, 49–100. doi: 10.1006/cogp.1999.0734

Moffett, J. R., Ross, B., Arun, P., Madhavarao, C. N., and Namboodiri, A. M. (2007). N-Acetylaspartate in the CNS: from neurodiagnostics to neurobiology. *Progress Neurobiol.* 81, 89–131. doi: 10.1016/j.pneurobio.2006.12.003

Murphy, K., Birn, R. M., Handwerker, D. A., Jones, T. B., and Bandettini, P. A. (2009). The impact of global signal regression on resting state correlations: are anti-correlated networks introduced? *Neuroimage* 44, 893–905. doi: 10.1016/j.neuroimage.2008.09.036

Nakata, Y., Sakamoto, A., and Kawata, A. (2020). Neuromelanin imaging analyses of the substantia nigra in patients with Machado-Joseph disease. *Neuroradiology* 62, 1433–1439. doi: 10.1007/s00234-020-02479-9

National Health Medical Research Council. (2009). *NHMRC additional levels of evidence and grades for recommendations for developers of guidelines.*

National Institutes of Health. (2019). *Study Quality Assessment Tools.* Available online at: https://www.nhlbi.nih.gov/health-topics/study-quality-assessment-tools (accessed April 20, 2021).

Nunes, M. B., Martinez, A. R. M., Rezende, T. J. R., Friedman, J. H., Lopes-Cendes, I., D'abreu, A., et al. (2015). Dystonia in Machado–Joseph disease: clinical profile, therapy and anatomical basis. *Parkinson. Relat. Disord.* 21, 1441–1447. doi: 10.1016/j.parkreldis.2015.10.016

Ogawa, Y., Ito, S., Makino, T., Kanai, K., Arai, K., and Kuwabara, S. (2012). Flattened facial colliculus on magnetic resonance imaging in Machado–Joseph disease. *Mov. Disord.* 27, 1041–1046. doi: 10.1002/mds.25060

Page, M., Mckenzie, J. B., Pm, Boutron, I., Hoffmann, T., Mulrow, C. S., L, Tetzlaff, J., et al. (2021). The PRISMA 2020 statement: an updated guideline for reporting systematic reviews. *BMJ* 372, n71. doi: 10.1136/bmj.n71

Paulson, H. (2012). Machado–Joseph disease/spinocerebellar ataxia type 3. *Handb. Clin. Neurol.* 103, 437–449. doi: 10.1016/B978-0-444-51892-7.00027-9

Pedroso, J. L., Franca, M. C. Jr., Braga-Neto, P., D'abreu, A., Saraiva-Pereira, M. L., Saute, J. A., et al. (2013). Nonmotor and extracerebellar features in Machado-Joseph disease: a review. *Mov. Disord.* 28, 1200–1208. doi: 10.1002/mds.25513

Peng, H., Liang, X., Long, Z., Chen, Z., Shi, Y., Xia, K., et al. (2019). Gene-related cerebellar neurodegeneration in SCA3/MJD: a case-controlled imaging-genetic study. *Front. Neurol.* 10, 1025. doi: 10.3389/fneur.2019.01025

Rezende, T. J. R., De Paiva, J. L. R., Martinez, A. R. M., Lopes-Cendes, I., Pedroso, J. L., Barsottini, O. G. P., et al. (2018). Structural signature of SCA3: from presymptomatic to late disease stages. *Ann. Neurol.* 84, 401–408. doi: 10.1002/ana.25297

Rolls, E. T. (2015). Limbic systems for emotion and for memory, but no single limbic system. *Cortex* 62, 119–157. doi: 10.1016/j.cortex.2013.12.005

Rüb, U., Del Turco, D., Del Tredici, K., De Vos, R., Brunt, E., Reifenberger, G., et al. (2003). Thalamic involvement in a spinocerebellar ataxia type 2 (SCA2) and a spinocerebellar ataxia type 3 (SCA3) patient, and its clinical relevance. *Brain* 126, 2257–2272. doi: 10.1093/brain/awg234

Schulz, J. B., Borkert, J., Wolf, S., Schmitz-Hübsch, T., Rakowicz, M., Mariotti, C., et al. (2010). Visualization, quantification and correlation of brain atrophy with clinical symptoms in spinocerebellar ataxia types 1, 3 and 6. *Neuroimage* 49, 158–168. doi: 10.1016/j.neuroimage.2009.07.027

Smith, T., Gildeh, N., and Holmes, C. (2007). The montreal cognitive assessment: validity and utility in a memory clinic setting. *Can. J. Psychiatry* 52, 329–332. doi: 10.1177/070674370705200508

Sörqvist, P., Stenfelt, S., and Rönnberg, J. (2012). Working memory capacity and visual–verbal cognitive load modulate auditory–sensory gating in the brainstem: toward a unified view of attention. *J. Cogn. Neurosci.* 24, 2147–2154. doi: 10.1162/jocn_a_00275

Spampinato, D. A., Celnik, P. A., and Rothwell, J. C. (2020). Cerebellar–motor cortex connectivity: one or two different networks? *J. Neurosci.* 40, 4230–4239. doi: 10.1523/JNEUROSCI.2397-19.2020

Stoodley, C. J., and Schmahmann, J. D. (2010). Evidence for topographic organization in the cerebellum of motor control versus cognitive and affective processing. *Cortex* 46, 831–844. doi: 10.1016/j.cortex.2009.11.008

Strauss, E., Sherman, E. M., and Spreen, O. (2006). *A Compendium of Neuropsychological Tests: Administration, Norms, and Commentary*. Oxford: Oxford University Press.

Szucs, D., and Ioannidis, J. P. (2020). Sample size evolution in neuroimaging research: an evaluation of highly-cited studies (1990–2012) and of latest practices (2017–2018) in high-impact journals. *Neuroimage* 221, 117164. doi: 10.1016/j.neuroimage.2020.117164

Tamura, I., Takei, A., Hamada, S., Soma, H., Nonaka, M., Homma, S., et al. (2018). Executive dysfunction in patients with spinocerebellar ataxia type 3. *J. Neurol.* 265, 1563–1572. doi: 10.1007/s00415-018-8883-y

Tang, Y., Zhao, L., Lou, Y., Shi, Y., Fang, R., Lin, X., et al. (2018). Brain structure differences between Chinese and Caucasian cohorts: a comprehensive morphometry study. *Hum. Brain Mapp.* 39, 2147–2155. doi: 10.1002/hbm.23994

Tomlinson, S. P., Davis, N. J., Morgan, H. M., and Bracewell, R. M. (2014). Cerebellar contributions to verbal working memory. *Cerebellum* 13, 354–361. doi: 10.1007/s12311-013-0542-3

Van Aken, L., Kessels, R. P., Wingbermühle, E., Van Der Veld, W. M., and Egger, J. I. (2016). Fluid intelligence and executive functioning more alike than different? *Acta Neuropsychiatr.* 28, 31–37. doi: 10.1017/neu.2015.46

Van De Warrenburg, B. P., Notermans, N. C., Schelhaas, H. J., Van Alfen, N., Sinke, R. J., Knoers, N. V., et al. (2004). Peripheral nerve involvement in spinocerebellar ataxias. *Arch. Neurol.* 61, 257–261. doi: 10.1001/archneur.61.2.257

Vidailhet, M., Dupel, C., Lehéricy, S., Remy, P., Dormont, D., Serdaru, M., et al. (1999). Dopaminergic dysfunction in midbrain dystonia: anatomoclinical study using 3-dimensional magnetic resonance imaging and fluorodopa F 18 positron emission tomography. *Arch. Neurol.* 56, 982–989. doi: 10.1001/archneur.56.8.982

Wan, N., Chen, Z., Wan, L., Tang, B., and Jiang, H. (2020). MR imaging of SCA3/MJD. *Front. Neurosci.* 14, 749. doi: 10.3389/fnins.2020.00749

Wang, P.-S., Chen, H.-C., Wu, H.-M., Lirng, J.-F., Wu, Y.-T., and Soong, B.-W. (2012). Association between proton magnetic resonance spectroscopy measurements and CAG repeat number in patients with spinocerebellar ataxias 2, 3, or 6. *PLoS ONE* 7, e47479. doi: 10.1371/journal.pone.0047479

Wang, P.-S., Wu, Y.-T., Wang, T.-Y., Wu, H.-M., Soong, B.-W., and Jao, C.-W. (2020). Supratentorial and infratentorial lesions in spinocerebellar Ataxia Type 3. *Front. Neurol.* 11, 124. doi: 10.3389/fneur.2020.00124

Wardlaw, J. M., Brindle, W., Casado, A. M., Shuler, K., Henderson, M., Thomas, B., et al. (2012). A systematic review of the utility of 1.5 versus 3 Tesla magnetic resonance brain imaging in clinical practice and research. *Eur. Radiol.* 22, 2295–2303. doi: 10.1007/s00330-012-2500-8

Wu, X., Liao, X., Zhan, Y., Cheng, C., Shen, W., Huang, M., et al. (2017). Microstructural alterations in asymptomatic and symptomatic Patients with spinocerebellar ataxia Type 3: a tract-based spatial statistics study. *Front. Neurol.* 8, 714–722. doi: 10.3389/fneur.2017.00714

Yap, K. H., Azmin, S., Che Hamzah, J., Ahmad, N., Van De Warrenburg, B., and Mohamed Ibrahim, N. (2022a). Pharmacological and non-pharmacological management of spinocerebellar ataxia: a systematic review. *J. Neurol.* 269, 2315–2337. doi: 10.1007/s00415-021-10874-2

Yap, K. H., Kessels, R. P. C., Azmin, S., Van De Warrenburg, B., and Mohamed Ibrahim, N. (2022b). Neurocognitive changes in spinocerebellar ataxia type 3: a systematic review with a narrative design. *Cerebellum* 21, 314–327. doi: 10.1007/s12311-021-01282-3

Yap, K. H., Ung, W. C., Ebenezer, E. G. M., Nordin, N., Chin, P. S., Sugathan, S., et al. (2017). Visualizing hyperactivation in neurodegeneration based on prefrontal oxygenation: a comparative study of mild Alzheimer's disease, mild cognitive impairment, and healthy controls. *Front. Aging Neurosci.* 9, 287. doi: 10.3389/fnagi.2017.00287

Yoshizawa, T., Watanabe, M., Frusho, K., and Shoji, S. (2003). Magnetic resonance imaging demonstrates differential atrophy of pontine base and tegmentum in Machado–Joseph disease. *J. Neurol. Sci.* 215, 45–50. doi: 10.1016/S0022-510X(03)00185-0

Zhou, J., Lei, L., Liao, X., Wang, J., Jiang, H., Tang, B., et al. (2011). Related factors of ICARS and SARA scores on spinocerebellar ataxia type 3/Machado-Joseph disease. *J. Central South Univ. Med. Sci.* 36, 498–503. doi: 10.3969/j.issn.1672-7347.2011.06.005

Conflict of Interest: The authors declare that the research was conducted in the absence of any commercial or financial relationships that could be construed as a potential conflict of interest.

frontiers | Frontiers in Neuroscience

TYPE Original Research
PUBLISHED 22 July 2022
DOI 10.3389/fnins.2022.905709

OPEN ACCESS

EDITED BY
Sean Austin O. Lim,
DePaul University, United States

REVIEWED BY
Xinglong Yang,
The First Affiliated Hospital of Kunming Medical University, China
Panpan Hu,
Anhui Medical University, China

*CORRESPONDENCE
Jian Jun Ma
majj1124@163.com

SPECIALTY SECTION
This article was submitted to Neurodegeneration, a section of the journal Frontiers in Neuroscience

RECEIVED 27 March 2022
ACCEPTED 04 July 2022
PUBLISHED 22 July 2022

CITATION
Zheng JH, Sun WH, Ma JJ, Wang ZD, Chang QQ, Dong LR, Shi XX, Li MJ, Gu Q, Chen SY and Li DS (2022) Differences in neuroanatomy and functional connectivity between motor subtypes of Parkinson's disease. *Front. Neurosci.* 16:905709. doi: 10.3389/fnins.2022.905709

Differences in neuroanatomy and functional connectivity between motor subtypes of Parkinson's disease

Jin Hua Zheng[1,2,3], Wen Hua Sun[1,2], Jian Jun Ma[1,2,3]*, Zhi Dong Wang[1,2], Qing Qing Chang[1,2], Lin Rui Dong[1,2], Xiao Xue Shi[1,2], Ming Jian Li[1,3], Qi Gu[1,2,3], Si Yuan Chen[1,2,3] and Dong Sheng Li[1,2,3]

[1]Department of Neurology, Henan Provincial People's Hospital, Zhengzhou, China, [2]Department of Neurology, People's Hospital of Zhengzhou University, Zhengzhou, China, [3]Department of Neurology, People's Hospital of Henan University, Zhengzhou, China

Background: The "postural instability/gait difficulty" (PIGD) and "tremor-dominant" (TD) motor subtypes of Parkinson's disease (PD) differ in their clinical manifestations. The neurological basis of these differences is unclear.

Methods: We performed voxel-based morphometric analysis and measured amplitudes of low-frequency fluctuation (ALFF) on 87 PIGD patients and 51 TD patients. We complemented this neuroanatomical comparison with seed-to-voxel analysis to explore differences in functional connectivity.

Results: The PIGD group showed significantly smaller gray matter volume in the medial frontal gyrus (mainly on the right side) than the TD group. Across all patients, gray matter volume in the medial frontal gyrus correlated negatively with severity of PIGD symptoms after controlling for age ($r = -0.250$, $p = 0.003$), but this correlation was not observed in separate analyses of only PIGD or TD patients. The PIGD group showed greater functional connectivity of the right superior frontal gyrus with the left lingual gyrus, right lateral occipital cortex, and right lingual gyrus. ALFF did not differ significantly between the two groups.

Conclusion: Postural instability/gait difficulty may be associated with smaller gray matter volume in medial frontal gyrus than TD, as well as with greater functional connectivity between the right superior frontal gyrus and occipital cortex. These results may help explain the clinical differences between the two motor subtypes of PD.

KEYWORDS

Parkinson's disease, MRI, voxel-based morphometry, tremor-dominant, postural instability

Introduction

Parkinson's disease (PD) is a progressive neurodegenerative disorder whose main clinical manifestations include bradykinesia, tremor, rigidity, and gait/postural disturbance. PD can be further divided into various motor subtypes: tremor-dominant (TD), postural instability/gait difficulty (PIGD), and mixed subtypes (Jankovic et al., 1990). The different subtypes show different clinical course and prognosis (Marras et al., 2002; Rajput et al., 2009). PIGD patients, for example, suffer more rapid motor progression than TD patients, they are at higher risk of dementia and they tend to respond less to medication (Jankovic et al., 1990; Rajput et al., 2009). Exploring the differences between PIGD and TD subtypes may help clarify their neural mechanisms and guide the development of future treatments.

Studies based on voxel-based morphometry (VBM), a classic automated technique in magnetic resonance imaging (MRI) (Ashburner and Friston, 2000), have provided the first clues to neuroanatomical differences between PIGD and TD patients, yet the results have been inconsistent. For example, some researchers have reported smaller gray matter volume (GMV) in all major brain lobes and subcortical areas in PIGD than in TD (Rosenberg-Katz et al., 2013), while others found smaller GMV only in the frontal cortex, and even this lost statistical significance after correcting for covariates (Al-Bachari et al., 2017). Another study found no significant volume differences in any brain region between patients with the akinetic/rigidity subtype of PD and patients with the TD subtype (Karunanayaka et al., 2016). This conflicting literature highlights the need for further neuroanatomical comparisons between PIGD and TD, especially involving groups larger than the 15–30 patients per arm in the abovementioned studies.

Analysis of the amplitudes of low-frequency fluctuations (ALFF) can complement the neuroanatomical information from VBM to provide data on neural activity (Zuo et al., 2010). ALFF studies have suggested differences between PIGD and TD, yet with inconsistent results. For example, one study linked TD to higher ALFF in the bilateral putamen and cerebellar posterior lobe, but lower ALFF in the bilateral temporal gyrus and left superior parietal lobule (Chen et al., 2015), while another study linked TD to higher activity in temporal lobes, but lower activity in frontal lobes (Hou et al., 2015). Again, this conflicting literature based primarily on small samples highlights the need for larger studies to elucidate potential differences in spontaneous neural activity between PIGD and TD subtypes.

Therefore, we used VBM and ALFF analysis to compare neuroanatomy and local neural activity between reasonably large samples of PIGD and TD patients. We also complemented this neuroanatomical comparison with seed-to-voxel analysis to explore differences in functional connectivity.

Methods

Subjects

This prospective study was approved by the Ethics Committee of Henan Provincial People's Hospital, and written informed consent was obtained from all participants at the Department of Neurology of Henan Provincial People's Hospital (Zhengzhou, China) between February 2019 and January 2020. The inclusion criteria were as follows: (1) clinically established PD, based on the Movement Disorder Society Clinical Diagnostic Criteria for PD (Postuma et al., 2015), (2) no family history of PD in first-degree relatives, (3) no MRI evidence of structural lesions related to other neurological disorders, (4) no head movement artifacts during the MRI session, (5) no serious cognitive impairment that might affect questionnaire responses, (6) no history of nervous system surgery, and (7) no severe psychosis or psychological diseases.

Clinical assessment

Patients underwent clinical assessments and MRI examinations while on medication. Clinical data were collected on name, age, sex, disease duration, and medication status. All patients were assessed using the Unified Parkinson's Disease Rating Scale (UPDRS) (Jankovic et al., 1990) and the Movement Disorder Society's Unified Parkinson's Disease Rating Scale (MDS-UPDRS) (Goetz et al., 2008).

Medications taken by the patients at the time of the study were calculated as the levodopa equivalent daily dose (LEDD) (Tomlinson et al., 2010). Disease severity was assessed in terms of Hoehn and Yahr (H-Y) stage (Hoehn and Yahr, 1967) and Part III of the MDS-UPDRS (Goetz et al., 2008). Cognitive function was assessed using the Mini-Mental State Examination (MMSE) after adjusting for age and education level (Crum et al., 1993). Anxiety and depression were assessed using the Hamilton anxiety scale (HAMA) (Hamilton, 1959) and Hamilton depression scale (HAMD) (Hamilton, 1960).

Assignment to postural instability/gait difficulty or tremor-dominant subtypes

The UPDRS items for TD and PIGD subtypes were used to calculate mean TD and PIGD scores (Jankovic et al., 1990). TD patients were defined to be those whose ratio of the mean UPDRS tremor score (8 items) to mean UPDRS PIGD score (5 items) was $\geq$ 1.5. PIGD patients were defined as those whose ratio $\leq$ 1. Patients whose ratios fell outside these ranges were classified as "indeterminate." In addition, patients who had a positive mean value in the numerator but a zero in the denominator were classified as TD, while patients with a zero

in the numerator and a positive mean in the denominator were classified as PIGD. Patients with zeros in both the numerator and denominator were classified as indeterminate.

MRI

Structural MRI

Images were acquired using a 3-T Siemens MAGNETOM Prisma MRI scanner with a 64-channel head coil. The parameters for T1-weighted sequences were as follows: 3-dimensional magnetization-prepared rapid gradient-echo (3D-MPRAGE) sequence, echo time (TE) = 3.43 ms, repetition time (TR) = 5,000 ms, inversion time (TI) = 755 ms, flip angle = 4°, slice thickness = 1.00 mm, number of slices = 208, bandwidth = 240 Hz/pixel, matrix = 256 × 256, field of view (FOV) = 256 × 256 mm^2, and voxel size = 1.0 × 1.0 × 1.0 mm^3.

MRI scans were visually checked to exclude those with severe vascular lesions, space-occupying lesions, or motion artifacts. Statistical Parametric Mapping version 12b (SPM12b)[1] was used to preprocess images and analyze VBM data. First, unified segmentation was applied to the structural T1-weighted images, then the resulting probability maps for gray matter and white matter were spatially normalized to the Montreal Neurological Institute (MNI) template using a high-level non-linear warping algorithm involving diffeomorphic anatomical registration through exponentiated Lie algebra (DARTEL) (Ashburner, 2007). The modulated volumes were smoothed using a Gaussian kernel featuring a full width at half-maximum of 8 mm.

Resting-state fMRI

Participants were asked to lie still, relax, and keep their eyes open throughout the scanning session. Functional images were obtained using axial echo-planar imaging with the following parameters: *TR* = 2,000 ms, *TE* = 35 ms, flip angle = 80°, FOV = 240 × 240 mm^2, matrix size = 94 × 94, voxel dimensions 2.20 × 2.20 × 2.20 mm^3, slice thickness = 2.2 mm, number of slices = 75, and number of time points = 180.

SPM12b and the CONN functional connectivity toolbox version 18_b (Whitfield-Gabrieli and Nieto-Castanon, 2012)[2] were used to preprocess images and analyze resting-state fMRI data. Preprocessing of data from all functional sequences involved the following steps: (1) functional slice-timing correction, (2) functional realignment and unwarping (subject motion estimation and correction), (3) functional outlier detection using on-line tools at www.nitrc.org/projects/artifact_detect, (4) structural centering to (0, 0, 0) via translation, (5) functional direct normalization to MNI space, and (6) functional smoothing via spatial convolution with a Gaussian kernel. Subjects were excluded if their head motion exceeded 2 mm in displacement or 2° in rotation. Functional images were resliced at a resolution of 2 × 2 × 2 mm^3 and smoothed using a Gaussian kernel featuring a full width at half-maximum of 8 mm. Next, regression was used to minimize effects due to head motion or to the presence of white matter or cerebrospinal fluid. Effects due to low-frequency drift or high-frequency physiological noise were minimized using bandpass filtering, such that only frequencies higher than 0.01 and smaller than 0.08 Hz were retained. Systematic shifts were minimized using detrending.

Statistical analysis

Analyses of clinicodemographic characteristics

Statistical analyses of clinicodemographic characteristics were performed using the Statistical Package for Social Sciences (SPSS) for Windows (version 22.0; SPSS, Chicago, IL, United States). Differences associated with $p < 0.05$ were considered significant. Continuous data were reported as mean and standard deviation (SD), while categorical data were reported as frequency and percentage. Differences were assessed for significance using the *t*-test and χ^2 test as appropriate.

Analyses of voxel-based morphometry and amplitudes of low-frequency fluctuation

We performed first-level analysis in the CONN pipeline to generate ALFF maps. To standardize data across subjects, the ALFF of each voxel was divided by the global mean ALFF value using the DPABI toolbox (version 4.0) (Yan et al., 2016).

Smoothed GMV images or standardized ALFF maps were compared between PIGD and TD patients using SPM12 and a significance threshold of uncorrected $p = 0.001$ at the initial voxel level and a false discovery rate-adjusted $p = 0.05$ at the cluster level. Spearson's correlation analysis and partial correlation analysis were performed to explore potential relationships between neuroimaging findings and clinical characteristics.

Functional connectivity analysis

We used first-level analysis of the CONN pipeline to generate functional connectivity maps between the seed and every other voxel in the brain. Correlations were calculated using a general linear model and bivariate correlation weighted by the hemodynamic response function. Differences in seed-to-voxel connectivity between PIGD and TD groups were assessed for significance using a two-samples *t*-test in second-level analysis of the CONN pipeline. The significance threshold was defined as a significance threshold of uncorrected $p = 0.001$ at the initial voxel level and a false discovery rate-adjusted $p = 0.05$ at the cluster level.

1 www.fil.ion.ucl.ac.uk/spm

2 http://www.nitrc.org/projects/conn

Results

Clinicodemographic features

Of the 176 patients considered for enrollment, 38 patients were excluded because they were indeterminate. The remaining patients were assigned to PIGD ($n = 87$) or TD ($n = 51$). The two groups did not differ significantly in age, sex, or disease duration (all $p > 0.05$; Table 1). The PIGD group showed significantly higher H-Y stage, LEDDs and scores on the MDS-UPDRS Parts I-III, HAMD and HAMA (all $p < 0.05$). Conversely, the PIGD group showed lower MMSE score, although the difference did not achieve significance ($p = 0.071$).

Comparison of gray matter volume by brain region

In GMV comparisons, age, sex, and disease duration were not treated as covariates because they did not differ significantly between the TD and PIGD groups. The PIGD group showed significantly smaller GMV in the medial frontal gyrus than the TD group, mainly on the right side [MNI coordinates (1.5 43.5 25.5); cluster size, 967 voxels; peak t-value, 4.5408, $p < 0.001$ at the voxel level and a false discovery rate-adjusted $p < 0.05$ at the cluster level; Figure 1A). Among all patients in the study, GMV in the medial frontal gyrus did not correlate significantly with age, disease duration, MDS-UPDRS Part III score, falling score, or freezing score (all $p > 0.05$; Table 2). In contrast, it did correlate negatively with walking score, gait score, postural stability score, and PIGD score, even after controlling for age (all $p < 0.05$; Table 2 and Figure 1B).

In contrast to the results obtained with all patients, GMV in the medial frontal gyrus did not correlate significantly with PIGD score after controlling for age in separate analyses involving only TD patients ($r = 0.184$, $p = 0.202$) or PIGD patients ($r = -0.157$, $p = 0.150$).

Comparison of spontaneous brain activity by region

No significant ALFF differences were identified between the PIGD and TD groups in any brain region ($p < 0.001$ at the voxel level and a false discovery rate-adjusted $p < 0.05$ at the cluster level).

Comparison of functional connectivity

VBM detected neuroanatomical differences between the two groups in the medial frontal gyrus, which was located within the superior frontal gyrus, so we selected the left and right superior frontal gyri as seeds. Seed-to-voxel analysis revealed greater functional connectivity of the right superior frontal gyrus with the left lingual gyrus, right lateral occipital cortex, and right lingual gyrus in the PIGD group ($p < 0.001$ at the voxel level and a false discovery rate-adjusted $p < 0.05$ at the cluster level; Table 3 and Figure 2). Among all patients in the study, PIGD score did not correlate significantly with how strongly the right superior frontal gyrus showed functional connectivity with the left lingual gyrus ($r = -0.010$, $p = 0.931$), right lingual gyrus ($r = -0.035$, $p = 0.747$), or right lateral occipital cortex ($r = -0.003$, $p = 0.978$) after controlling for age. The same analysis revealed no significant differences between PIGD and TD patients in connectivity between the left superior

TABLE 1 Clinicodemographic characteristics of Parkinson's disease patients.

Characteristic	TD group ($n = 51$)	PIGD group ($n = 87$)	t/χ^2 value	p-value
Male	31(60.8)	54(62.1)	0.022	0.881
Age at MRI scan, year	61.7 ± 7.5	62.4 ± 6.6	−0.628	0.531
PD duration, year	6.1 ± 3.8	7.1 ± 4.7	−1.308	0.193
H-Y stage	2.2 ± 0.6	2.7 ± 0.9	−4.051	0.001
MDS-UPDRS scores				
Part I	9.2 ± 5.2	12.7 ± 6.3	−3.332	0.001
Part II	13.7 ± 6.0	20.3 ± 8.7	−4.783	0.001
Part III	34.7 ± 13.9	42.7 ± 18.9	−2.657	0.009
MMSE score	26.3 ± 3.4	25.1 ± 3.9	1.822	0.071
HAMD score	9.6 ± 4.8	12.3 ± 6.1	−2.958	0.004
HAMA score	9.9 ± 5.8	12.1 ± 6.9	−1.997	0.048
LEDD (mg)	349.0 ± 259.5	527.7 ± 348.4	−3.430	0.001

Values are n (%) or mean ± SD, unless otherwise indicated.
BPV, brain parenchyma volume; GMV, gray matter volume; HAMA, Hamilton Anxiety Scale; HAMD, Hamilton Depression Scale; H-Y, Hoehn and Yahr; LEDD, levodopa equivalent daily dose; MDS-UPDRS, Movement Disorder Society Unified Parkinson's Disease Rating Scale; PD, Parkinson's disease; PIGD, postural instability/gait difficulty; TD, tremor-dominant.

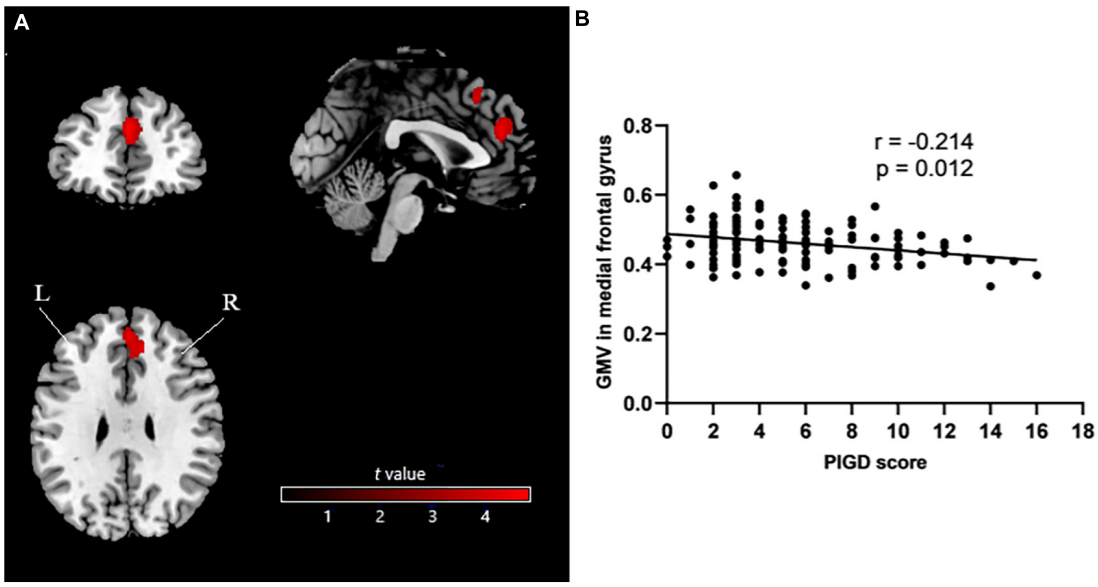

FIGURE 1
(A) Voxel-based morphometry showing smaller GMV in medial frontal gyrus (mainly on the right side) in PIGD patients than in TD patients. **(B)** Analysis of potential correlation between GMV in medial frontal gyrus and PIGD score. GMV, gray matter volume; PIGD, postural instability/gait difficulty; TD, tremor-dominant; L, left; R, right.

frontal gyrus and any other voxel in the brain ($p < 0.001$ at the voxel level and a false discovery rate-adjusted $p < 0.05$ at the cluster level).

Discussion

Our study suggests for the first time that patients with the PIGD subtype of PD have significantly smaller GMV in the medial frontal gyrus than patients with the TD subtype. In fact, GMV in the medial frontal gyrus negatively correlated with severity of PIGD symptoms across our entire sample, even after controlling for age. We further found that PIGD patients had greater functional connectivity of the right superior frontal gyrus with the left lingual gyrus, right lateral occipital cortex, and right lingual gyrus than TD patients. Nevertheless, the two groups did not differ significantly in ALFF. Our results identify some neuroanatomical and connectivity differences that may help to explain the differences in presentation, course and prognosis between PIGD and TD subtypes of PD.

TABLE 2 Analysis of correlations between gray matter volume in medial frontal gyrus and clinical characteristics of patients with Parkinson's disease.

Characteristic	Uncorrected		Corrected for age	
	r	p	r	p
Age	−0.147	0.085	–	–
Disease duration	−0.049	0.566	−0.071	0.407
MDS-UPDRS Part III score	−0.128	0.136	−0.137	0.111
Falling score	0.127	0.138	−0.159	0.064
Freezing score	−0.093	0.276	−0.153	0.074
Walking score	−0.243	0.004	−0.228	0.007
Gait score	−0.284	0.001	−0.258	0.002
Postural stability score	−0.284	0.001	−0.195	0.023
PIGD score	−0.214	0.012	−0.250	0.003

MDS-UPDRS, Movement Disorder Society Unified Parkinson's Disease Rating Scale; PIGD, postural instability/gait difficulty.

Our finding of smaller GMV in the medial frontal gyrus in PIGD is consistent with previous work suggesting greater Lewy body formation and amyloid plaque load in the cortex of patients with PIGD (Selikhova et al., 2009). This greater cortical pathology may, in fact, help explain the more severe clinical characteristics of PIGD compared to TD (Selikhova et al., 2009; Rosenberg-Katz et al., 2013), including extensive atrophy of frontal lobe, parietal, occipital, temporal, and subcortical areas (Rosenberg-Katz et al., 2013). Indeed, our PIGD patients showed higher H-Y stage, LEDDs and scores on MDS-UPDRS Parts I-III, HAMD, and HAMA than TD patients. Numerous studies have documented that PIGD is associated with more severe motor and non-motor symptoms, faster disease progression, and worse daily life experience than TD (Jankovic et al., 1990; Rajput et al., 2009; Ren et al., 2020a,b).

We found that among all patients in our sample, GMV in the medial frontal gyrus correlated negatively with severity of PIGD symptoms, strengthening support for the link between

TABLE 3 Seed-to-voxel analysis showing greater functional connectivity in PIGD patients than in TD patients.

Region	R/L	Cluster size	MNI coordinates (x, y, z)			T score	p-FDR
Lingual gyrus	L	336	−12	−56	−2	0.003	0.003
Lateral occipital cortex	R	256	+30	−76	+12	0.007	0.007
Lingual gyrus	R	169	+26	−48	+2	0.029	0.029

The seed was the right superior frontal gyrus.
PIGD, postural instability/gait difficulty; TD, tremor-dominant; MNI, Montreal Neurological Institute; FDR, false discovery rate; L, left; R, right.

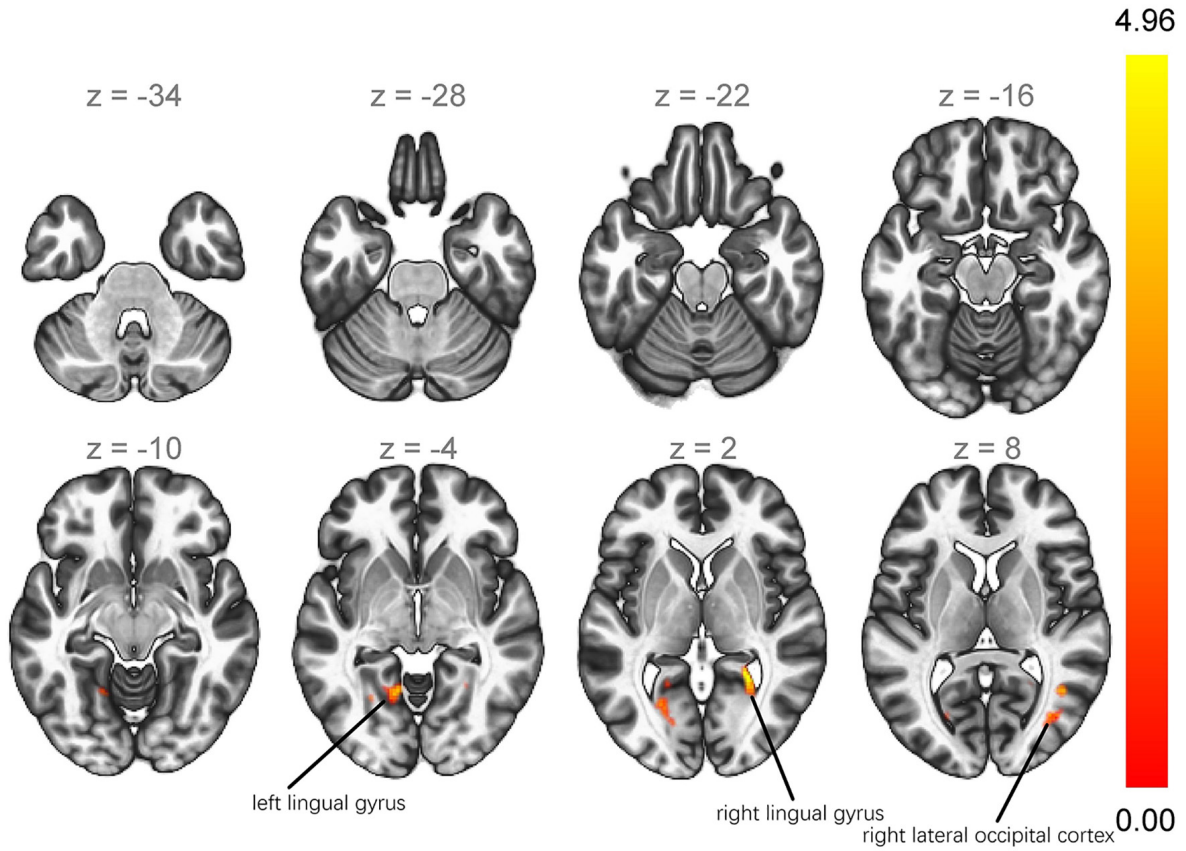

FIGURE 2
Seed-to-voxel analysis showing greater functional connectivity of the right superior frontal gyrus with the left lingual gyrus, right lateral occipital cortex, and right lingual gyrus in PIGD patients than in TD patients. PIGD, postural instability/gait difficulty; TD, tremor-dominant.

atrophy in the medial frontal gyrus and the PIGD subtype of PD. However, we failed to detect such a correlation in separate analyses of only PIGD or TD patients, which may reflect the small samples. Our results contrast with two VBM studies that failed to detect differences in brain volume between the PIGD and TD groups (Karunanayaka et al., 2016; Al-Bachari et al., 2017). Nevertheless, our results are likely to be reliable because of the reasonably large sample and our strict correction for multiple comparisons.

Consistent with our analysis, studies have linked abnormal function of the medial frontal gyrus to gait problems in PD. The medial frontal gyrus forms part of the medial prefrontal cortex, which is important for maintaining a flexible, effective walking pattern (Hinton et al., 2019). Impaired activation of the medial frontal area may account for patients' difficulties in initiating movements (Playford et al., 1992), and the PD-associated gait disturbance known as "freezing of gait" (Gilat et al., 2018) has been linked to a bilateral decrease in perfusion of Brodmann area 11 (Matsui et al., 2005) and to abnormal cerebral blood flow (Imamura et al., 2012). High-frequency repetitive transcranial magnetic stimulation of the medial prefrontal cortex can reduce gait freezing and variability as well as improve UPDRS scores (Dagan et al., 2017). In this way, our results and the literature strongly argue that atrophy

of the medial frontal gyrus is related to the PIGD subtype in PD. We failed to find a correlation between gray matter volume of the medial frontal gyrus and freezing score, which may reflect that we analyzed all our patients while they were on medication.

At the same time, we found no ALFF differences between PIGD and TD patients. This suggests that there was no difference in spontaneous brain activity between them during the on-medication phase. Our results contrast with previous work that reported higher or lower activity in certain brain regions of PIGD patients (Chen et al., 2015; Hou et al., 2015). This discrepancy may reflect differences in when MRI was performed: we performed MRI only during the on-medication phase, when symptoms may have been milder than during the off-medication phase. Further studies should examine whether ALFF differs between patients of different subtypes during the off-medication phase.

Our finding that most neuroanatomical differences between PIGD and TD lay in the superior frontal gyrus is consistent with a study that found that improvement of motor symptoms after deep brain stimulation of the subthalamic nucleus was associated with an increase in cortical thickness in the superior frontal region (Muthuraman et al., 2017). We found greater functional connectivity of the right superior frontal gyrus with the left lingual gyrus, right lateral occipital cortex, and right lingual gyrus in the PIGD group than in the TD group. It makes sense that dysfunction in the lingual gyrus, particularly on the right side, may trigger walking or balance problems. The lingual gyrus, located in the occipital cortex (also known as visual association cortex), participates in spatial orientation (Schiltz et al., 1999) and visuospatial information processing (Renier et al., 2010; Collignon et al., 2011). The right hemisphere is much more involved than the left one in processing visual information (de Jong et al., 1999; Woolley et al., 2010), so the right hemisphere influences balance (Suarez et al., 2009) and turning (Davidsdottir et al., 2008). However, PIGD score in our sample was not associated with how strongly the right superior frontal gyrus was functionally connected to the left lingual gyrus, right lingual gyrus or right lateral occipital cortex. We hypothesize that the PIGD score reflects the severity of postural instability/gait difficulty, but not the severity of neural network abnormalities.

The extrastriate body area, located in the lateral occipital cortex, integrates visual, spatial attention, and sensory-motor signals in order to represent the observer's body (Astafiev et al., 2004). The right extrastriate body area may even increase its activity in this respect in order to compensate for loss of function by the dorsal premotor cortex (van Nuenen et al., 2012). This leads us to hypothesize that the enhanced functional connectivity in PIGD brain may compensate for frontal atrophy in order to mitigate postural instability and gait difficulties.

Our results should be interpreted with caution in light of several limitations. First, a patient's PD subtype can change as the disease progresses; for example, the subtype of some patients shifts from TD to PIGD after approximately six years (von Coelln et al., 2021). This is less likely to affect our results, however, since the average disease duration in our TD group was 6.1 years. Second, we performed clinical evaluations and MRI during the on-medication phase, when symptoms may be milder. This may help explain why we observed no significant ALFF differences between PIGD and TD patients. Future studies should clarify whether spontaneous brain activity differs between the two subtypes during the off-medication phase. Our study lacked a healthy control group, which should be included in future work. Nevertheless, this did not prevent us from identifying differences between Parkinson's subtypes, which was the focus of our study. One study reported significantly smaller medial frontal GMV in PD patients without cognitive impairment than in healthy controls (Nishio et al., 2010), so whether this holds true for different PD subtypes remains to be seen.

Conclusion

Our study provides the first evidence that the PIGD subtype of PD is associated with smaller GMV in the medial frontal gyrus and greater functional connectivity of the right superior frontal gyrus with the left lingual gyrus, right lateral occipital cortex, and right lingual gyrus than the TD subtype. Our results may guide further research into the differences underlying the motor subtypes of PD, which in turn may lead to personalized therapies.

Data availability statement

The raw data supporting the conclusions of this article will be made available by the authors, without undue reservation.

Ethics statement

The studies involving human participants were reviewed and approved by the Ethics Committee of Henan Provincial People's Hospital. The patients/participants provided their written informed consent to participate in this study.

Author contributions

JZ: conceptualization, data curation, formal analysis, investigation, methodology, visualization, writing—original

draft, and writing—review and editing. WS: conceptualization, data curation, formal analysis, methodology, visualization, and writing—review and editing. JM: conceptualization, project administration, supervision, writing—review and editing, and funding acquisition. ZW, ML, and SC: data curation and formal analysis. QC, XS, and QG: data curation and investigation. LD: data curation, formal analysis, and resources. DL: project administration and validation. All authors contributed to the article and approved the submitted version.

Funding

This work was supported by the Henan Province Medical Science and Technology Research Program (SBGJ2021 02035).

Conflict of interest

The authors declare that the research was conducted in the absence of any commercial or financial relationships that could be construed as a potential conflict of interest.

Publisher's note

References

Al-Bachari, S., Vidyasagar, R., Emsley, H. C., and Parkes, L. M. (2017). Structural and physiological neurovascular changes in idiopathic Parkinson's disease and its clinical phenotypes. *J. Cereb. Blood Flow Metab.* 37, 3409–3421. doi: 10.1177/0271678X16688919

Ashburner, J. (2007). A fast diffeomorphic image registration algorithm. *Neuroimage* 38, 95–113. doi: 10.1016/j.neuroimage.2007.07.007

Ashburner, J., and Friston, K. J. (2000). Voxel-based morphometry–the methods. *Neuroimage* 11(6 Pt. 1), 805–821. doi: 10.1006/nimg.2000.0582

Astafiev, S. V., Stanley, C. M., Shulman, G. L., and Corbetta, M. (2004). Extrastriate body area in human occipital cortex responds to the performance of motor actions. *Nat. Neurosci.* 7, 542–548. doi: 10.1038/nn1241

Chen, H. M., Wang, Z. J., Fang, J. P., Gao, L. Y., Ma, L. Y., Wu, T., et al. (2015). Different patterns of spontaneous brain activity between tremor-dominant and postural instability/gait difficulty subtypes of Parkinson's disease: a resting-state fMRI study. *CNS Neurosci. Ther.* 21, 855–866. doi: 10.1111/cns.12464

Collignon, O., Vandewalle, G., Voss, P., Albouy, G., Charbonneau, G., Lassonde, M., et al. (2011). Functional specialization for auditory-spatial processing in the occipital cortex of congenitally blind humans. *Proc. Natl. Acad. Sci. U.S.A.* 108, 4435–4440. doi: 10.1073/pnas.1013928108

Crum, R. M., Anthony, J. C., Bassett, S. S., and Folstein, M. F. (1993). Population-based norms for the mini-mental state examination by age and educational level. *JAMA* 269, 2386–2391. doi: 10.1001/jama.1993.03500180078038

Dagan, M., Herman, T., Mirelman, A., Giladi, N., and Hausdorff, J. M. (2017). The role of the prefrontal cortex in freezing of gait in Parkinson's disease: insights from a deep repetitive transcranial magnetic stimulation exploratory study. *Exp. Brain Res.* 235, 2463–2472. doi: 10.1007/s00221-017-4981-9

Davidsdottir, S., Wagenaar, R., Young, D., and Cronin-Golomb, A. (2008). Impact of optic flow perception and egocentric coordinates on veering in Parkinson's disease. *Brain* 131(Pt. 11), 2882–2893. doi: 10.1093/brain/awn237

de Jong, B. M., Frackowiak, R. S., Willemsen, A. T., and Paans, A. M. (1999). The distribution of cerebral activity related to visuomotor coordination indicating perceptual and executional specialization. *Brain Res. Cogn. Brain Res.* 8, 45–59. doi: 10.1016/s0926-6410(99)00005-1

Gilat, M., Lígia Silva de Lima, A., Bloem, B. R., Shine, J. M., Nonnekes, J., Lewis, S. J. G., et al. (2018). Freezing of gait: promising avenues for future treatment. *Parkinsonism Relat. Disord.* 52, 7–16. doi: 10.1016/j.parkreldis.2018.03.009

Goetz, C. G., Tilley, B. C., Shaftman, S. R., Stebbins, G. T., Fahn, S., Martinez-Martin, P., et al. (2008). Movement disorder society-sponsored revision of the unified Parkinson's disease rating scale (MDS-UPDRS): scale presentation and clinimetric testing results. *Mov. Disord.* 23, 2129–2170.

Hamilton, M. (1959). The assessment of anxiety states by rating. *Br. J. Med. Psychol.* 32, 50–55. doi: 10.1111/j.2044-8341.1959.tb00467.x

Hamilton, M. (1960). A rating scale for depression. *J. Neurol. Neurosurg. Psychiatry* 23, 56–62. doi: 10.1136/jnnp.23.1.56

Hinton, D. C., Thiel, A., Soucy, J. P., Bouyer, L., and Paquette, C. (2019). Adjusting gait step-by-step: brain activation during split-belt treadmill walking. *Neuroimage* 202:116095. doi: 10.1016/j.neuroimage.2019.116095

Hoehn, M. M., and Yahr, M. D. (1967). Parkinsonism: onset, progression and mortality. *Neurology* 17, 427–442. doi: 10.1212/WNL.17.5.427

Hou, Y., Zhang, J., Chen, B., and Wu, T. (2015). [Local brain activity in different motor subtypes of Parkinson's disease with fMRI]. *Zhonghua Yi Xue Za Zhi* 95, 483–488.

Imamura, K., Okayasu, N., and Nagatsu, T. (2012). Cerebral blood flow and freezing of gait in Parkinson's disease. *Acta Neurol. Scand.* 126, 210–218. doi: 10.1111/j.1600-0404.2012.01652.x

Jankovic, J., McDermott, M., Carter, J., Gauthier, S., Goetz, C., Golbe, L., et al. (1990). Variable expression of Parkinson's disease: a base-line analysis of the DATATOP cohort. The parkinson study group. *Neurology* 40, 1529–1534. doi: 10.1212/wnl.40.10.1529

Karunanayaka, P. R., Lee, E. Y., Lewis, M. M., Sen, S., Eslinger, P. J., Yang, Q. X., et al. (2016). Default mode network differences between rigidity- and tremor-predominant Parkinson's disease. *Cortex* 81, 239–250. doi: 10.1016/j.cortex.2016.04.021

Marras, C., Rochon, P., and Lang, A. E. (2002). Predicting motor decline and disability in Parkinson disease: a systematic review. *Arch. Neurol.* 59, 1724–1728. doi: 10.1001/archneur.59.11.1724

Matsui, H., Udaka, F., Miyoshi, T., Hara, N., Tamaura, A., Oda, M., et al. (2005). Three-dimensional stereotactic surface projection study of freezing of gait and brain perfusion image in Parkinson's disease. *Mov. Disord.* 20, 1272–1277. doi: 10.1002/mds.20520

Muthuraman, M., Deuschl, G., Koirala, N., Riedel, C., Volkmann, J., Groppa, S., et al. (2017). Effects of DBS in parkinsonian patients depend on the structural integrity of frontal cortex. *Sci. Rep.* 7:43571. doi: 10.1038/srep43571

Nishio, Y., Hirayama, K., Takeda, A., Hosokai, Y., Ishioka, T., Suzuki, K., et al. (2010). Corticolimbic gray matter loss in Parkinson's disease without dementia. *Eur. J. Neurol.* 17, 1090–1097. doi: 10.1111/j.1468-1331.2010.02980.x

Playford, E. D., Jenkins, I. H., Passingham, R. E., Nutt, J., Frackowiak, R. S., Brooks, D. J., et al. (1992). Impaired mesial frontal and putamen activation in Parkinson's disease: a positron emission tomography study. *Ann. Neurol.* 32, 151–161. doi: 10.1002/ana.410320206

Postuma, R. B., Berg, D., Stern, M., Poewe, W., Olanow, C. W., Oertel, W., et al. (2015). MDS clinical diagnostic criteria for Parkinson's disease. *Mov. Disord.* 30, 1591–1601. doi: 10.1002/mds.26424

Rajput, A. H., Voll, A., Rajput, M. L., Robinson, C. A., and Rajput, A. (2009). Course in Parkinson disease subtypes: a 39-year clinicopathologic study. *Neurology* 73, 206–212. doi: 10.1212/WNL.0b013e3181ae7af1

Ren, J., Hua, P., Li, Y., Pan, C., Yan, L., Yu, C., et al. (2020a). Comparison of three motor subtype classifications in de novo Parkinson's disease patients. *Front. Neurol.* 11:601225. doi: 10.3389/fneur.2020.601225

Ren, J., Hua, P., Pan, C., Li, Y., Zhang, L., Zhang, W., et al. (2020b). Non-motor symptoms of the postural instability and gait difficulty subtype in de novo Parkinson's disease patients: a cross-sectional study in a single center. *Neuropsychiatr. Dis. Treat.* 16, 2605–2612. doi: 10.2147/NDT.S280960

Renier, L. A., Anurova, I., De Volder, A. G., Carlson, S., VanMeter, J., Rauschecker, J. P., et al. (2010). Preserved functional specialization for spatial processing in the middle occipital gyrus of the early blind. *Neuron* 68, 138–148. doi: 10.1016/j.neuron.2010.09.021

Rosenberg-Katz, K., Herman, T., Jacob, Y., Giladi, N., Hendler, T., Hausdorff, J. M., et al. (2013). Gray matter atrophy distinguishes between Parkinson disease motor subtypes. *Neurology* 80, 1476–1484. doi: 10.1212/WNL.0b013e31828cfaa4

Schiltz, C., Bodart, J. M., Dubois, S., Dejardin, S., Michel, C., Roucoux, A., et al. (1999). Neuronal mechanisms of perceptual learning: changes in human brain activity with training in orientation discrimination. *Neuroimage* 9, 46–62. doi: 10.1006/nimg.1998.0394

Selikhova, M., Williams, D. R., Kempster, P. A., Holton, J. L., Revesz, T., Lees, A. J., et al. (2009). A clinico-pathological study of subtypes in Parkinson's disease. *Brain* 132(Pt. 11), 2947–2957. doi: 10.1093/brain/awp234

Suarez, H., Geisinger, D., Suarez, A., Carrera, X., Buzo, R., Amorin, I., et al. (2009). Postural control and sensory perception in patients with Parkinson's disease. *Acta Otolaryngol.* 129, 354–360. doi: 10.1080/00016480802495446

Tomlinson, C. L., Stowe, R., Patel, S., Rick, C., Gray, R., Clarke, C. E., et al. (2010). Systematic review of levodopa dose equivalency reporting in Parkinson's disease. *Mov. Disord.* 25, 2649–2653. doi: 10.1002/mds.23429

van Nuenen, B. F., Helmich, R. C., Buenen, N., van de Warrenburg, B. P., Bloem, B. R., Toni, I., et al. (2012). Compensatory activity in the extrastriate body area of Parkinson's disease patients. *J. Neurosci.* 32, 9546–9553. doi: 10.1523/JNEUROSCI.0335-12.2012

von Coelln, R., Gruber-Baldini, A. L., Reich, S. G., Armstrong, M. J., Savitt, J. M., Shulman, L. M., et al. (2021). The inconsistency and instability of Parkinson's disease motor subtypes. *Parkinsonism Relat. Disord.* 88, 13–18. doi: 10.1016/j.parkreldis.2021.05.016

Whitfield-Gabrieli, S., and Nieto-Castanon, A. (2012). Conn: a functional connectivity toolbox for correlated and anticorrelated brain networks. *Brain Connect.* 2, 125–141. doi: 10.1089/brain.2012.0073

Woolley, D. G., Wenderoth, N., Heuninckx, S., Zhang, X., Callaert, D., Swinnen, S. P., et al. (2010). Visual guidance modulates hemispheric asymmetries during an interlimb coordination task. *Neuroimage* 50, 1566–1577. doi: 10.1016/j.neuroimage.2010.01.012

Yan, C. G., Wang, X. D., Zuo, X. N., and Zang, Y. F. (2016). Data processing & analysis for (resting-state) brain imaging. *Neuroinformatics* 14, 339–351. doi: 10.1007/s12021-016-9299-4

Zuo, X. N., Di Martino, A., Kelly, C., Shehzad, Z. E., Gee, D. G., Klein, D. F., et al. (2010). The oscillating brain: complex and reliable. *Neuroimage* 49, 1432–1445. doi: 10.1016/j.neuroimage.2009.09.037

frontiers | Frontiers in Neuroscience

TYPE Systematic Review
PUBLISHED 10 August 2022
DOI 10.3389/fnins.2022.952096

OPEN ACCESS

EDITED BY
Yang Zhang,
Chongqing University, China

REVIEWED BY
Sinead M. O'Donovan,
University of Toledo, United States
Kejing Lao,
Xi'an Medical University, China

*CORRESPONDENCE
Andrea Kwakowsky
andrea.kwakowsky@nuigalway.ie

†These authors have contributed equally to this work

SPECIALTY SECTION
This article was submitted to Neurodegeneration, a section of the journal Frontiers in Neuroscience

RECEIVED 24 May 2022
ACCEPTED 14 July 2022
PUBLISHED 10 August 2022

CITATION
Wood OWG, Yeung JHY, Faull RLM and Kwakowsky A (2022) EAAT2 as a therapeutic research target in Alzheimer's disease: A systematic review. *Front. Neurosci.* 16:952096. doi: 10.3389/fnins.2022.952096

EAAT2 as a therapeutic research target in Alzheimer's disease: A systematic review

Oliver W. G. Wood[1†], Jason H. Y. Yeung[1†], Richard L. M. Faull[1] and Andrea Kwakowsky[1,2*]

[1]Department of Anatomy and Medical Imaging, Faculty of Medical and Health Sciences, Centre for Brain Research, University of Auckland, Auckland, New Zealand, [2]Pharmacology and Therapeutics, Galway Neuroscience Centre, School of Medicine, Ollscoil na Gaillimhe – University of Galway, Galway, Ireland

Glutamate is the main excitatory neurotransmitter in the human central nervous system, responsible for a wide variety of normal physiological processes. Glutamatergic metabolism and its sequestration are tightly regulated in the normal human brain, and it has been demonstrated that dysregulation of the glutamatergic system can have wide-ranging effects both in acute brain injury and neurodegenerative diseases. The excitatory amino acid transporter 2 (EAAT2) is the dominant glutamatergic transporter in the human brain, responsible for efficient removal of glutamate from the synaptic cleft for recycling within glial cells. As such, it has a key role in maintaining excitatory-inhibitory homeostasis. Animal studies have demonstrated dysregulation or alterations of EAAT2 expression can have implications in neurodegenerative disorders. Despite extensive research into glutamatergic alterations in AD mouse models, there is a lack of studies examining the expression of EAAT2 within the AD human brain. In this systematic review, 29 articles were identified that either analyzed EAAT2 expression in the AD human brain or used a human-derived cell culture. Studies were inconclusive as to whether EAAT2 was upregulated or downregulated in AD. However, changes in localization and correlation between EAAT2 expression and symptomatology was noted. These findings implicate EAAT2 alterations as a key process in AD progression and highlight the need for further research into the characterization of EAAT2 processes in normal physiology and disease in human tissue and to identify compounds that can act as EAAT2 neuromodulators.

KEYWORDS

glutamate transporter, EAAT2, hippocampus, Alzheimer's disease, human brain

Introduction

Alzheimer's disease (AD) is a progressive neurodegenerative condition that is the most common form of dementia, causing impairments in memory and cognitive function (Revi, 2020). Due to an aging population worldwide, the incidence of AD is predicted to increase rapidly in the coming years (Brookmeyer et al., 2007). As such, there is now an increasing need to develop a disease-modifying treatment or preventative

approach for AD due to the social and economic burden associated with rising incidence. Many promising scientific interventions based on animal models have failed to translate into effective therapies in humans, raising doubts about the current leading theories behind AD's etiology (Tolar et al., 2019). Analyzing postmortem human brain tissue to determine cellular alterations to disease-relevant proteins is, therefore, a very valuable method to identify potential human-specific therapeutic targets for AD.

The main pathological hallmarks of AD are the aggregation of extracellular amyloid-beta (Aβ) plaques and intracellular tangles of the microtubule-associated protein tau (Bloom, 2014). These pathologies severely affect the hippocampal regions and the entorhinal cortex, causing neuronal cell loss and memory impairment (Braak and Braak, 1991). Neuronal death eventually spreads throughout the temporal cortex and to other brain regions in late disease (Braak and Braak, 1991). Other notable pathological features of AD include vascular deficits, mitochondrial damage, inflammation, and damage to neurotransmitter systems, which are contributing factors to extensive neuronal death (Šerý et al., 2013; Wang and Reddy, 2017; Hampel et al., 2018).

Glutamate is the primary excitatory neurotransmitter of the central nervous system (CNS), involved in a variety of vital functions, including neuronal communication and regulation of neuronal activity (Danbolt, 2001). Glutamate concentrations in the extracellular space are usually tightly regulated, and dysregulation can lead to overexcitation of postsynaptic neurons, potentially causing glutamate excitotoxicity. A growing body of evidence suggests glutamate dysfunction as a core component in the pathogenesis of neurodegenerative diseases, including AD (Hynd et al., 2004). Glutamate reuptake from the extracellular space is regulated by a class of transporters known as the excitatory amino acid transporters (EAATs).

There are five isoforms of the EAATs, with their expression being cell type and brain region specific (Malik and Willnow, 2019). The isoforms EAAT1 and EAAT2 are primarily expressed on astrocytes, with high expression in the cerebellum and throughout the entire brain, respectively (Kim et al., 2011; Pajarillo et al., 2019). EAAT3 is expressed throughout the brain, while EAAT4 expression is predominantly found in the cerebellum (Malik and Willnow, 2019). EAAT5 expression is mainly restricted to photoreceptors and bipolar cells in the retina (Arriza et al., 1997). EAAT2, encoded by the *SLC1A2* gene and also referred to by its rodent nomenclature, glutamate transporter 1 (GLT-1), is responsible for 90% of glutamate uptake in the mature brain (Kim et al., 2011; Pajarillo et al., 2019). Its expression is hence critical for controlling extracellular glutamate concentrations.

Several past animal studies have suggested that EAAT2 alteration occurs in AD. EAAT2 translocation has also been demonstrated in AD models and may play a role in EAAT2 dysfunction. EAAT2 haploinsufficiency has been shown to hasten cognitive decline in an AD mouse model, indicating that EAAT2 expression may play a critical factor in dictating AD progression (Mookherjee et al., 2011). Cross-linking of EAAT2 both *in vitro* and *ex vivo* in mouse hippocampal brain was found to alter astrocytic currents and neuronal EPSCs, although transporter function was preserved (Murphy-Royal et al., 2015). These findings support the notion that astrocytes are actively involved in shaping excitatory neurotransmission and highlight the importance of normal surface diffusion of glutamate transporters at the synapse in maintaining homeostasis and cellular signaling processes. In mouse hippocampal slices, $A\beta_{1-42}$ induces rapid EAAT2 mislocalization and internalization in astrocytes, which leads to reduced cell surface expression and a marked reduction in glutamate reuptake from the extracellular space (Scimemi et al., 2013). Despite significant evidence pointing to glutamatergic dysfunction in AD, the majority of current literature has used mouse or other animal tissue studies to assess EAAT2 alterations and test therapeutic strategies for AD. However, only a limited amount of literature has used human tissue or cells to understand what may be happening to EAAT2 in AD.

Overall, this review aims to discuss the current evidence of EAAT2 expression and functional alteration in AD, a critical knowledge gap given that AD is ultimately a human disease. In addition, whether the existing literature warrants further research to investigate this glutamate transporter as a therapeutic target for the treatment or intervention of AD will be discussed.

Methodology

We performed a comprehensive literature search of PubMed, Web of Science and Scopus databases from 1991 through to 2022. Specific search terms used were Title, Abstract, Keywords/MeSH terms ("Excitatory Amino Acid Transporter 2" [Mesh] OR "SLC1A2 protein, human" [Supplementary Concept]) OR "Glt-1" OR "Glutamate transporter 1" OR "solute carrier family 1 member 2") AND Title, Abstract, Keywords/MeSH terms: (Alzheimer Disease). Five hundred and six relevant articles were identified and collated in EndNote X8 (Clarivate Analytics, Philadelphia, PA, USA). Duplicates were removed using the Rayyan systematic review software (Rayyan QCRI, RRID:SCR_017584), and then sorted for inclusion or exclusion. Each abstract was screened independently by the first two authors to identify the articles that met our inclusion criteria of human-based studies with an EAAT2 focus. All authors discussed any conflicts to determine whether to include or exclude articles from this review. The inclusion criteria for this review were any EAAT2 study relevant to AD, including human-derived cultured cells, even those where EAAT2 may not have necessarily been the main focus of the study. Hence, animal-based studies or studies with no relevance to EAAT2 or AD

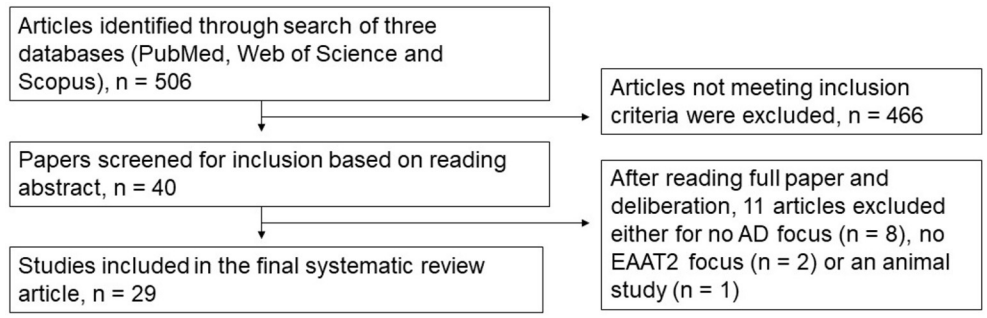

FIGURE 1
Flow diagram detailing the article selection process.

were excluded. Twenty-nine articles were selected based on this criterion, and all authors agreed on this selection. The article selection process is shown in Figure 1, and the included studies are shown in Table 1 (postmortem studies) and Table 2 (cell cultures and other studies).

Summary of findings

Only a small group of studies in current literature have investigated the expression of EAAT2 in human postmortem tissue, and this is reflected by the relatively small number of papers that met the inclusion criteria for this review. These articles have yielded contradictory findings regarding EAAT2 expression in AD, even for some studies investigating the same brain regions. In addition, a handful of studies have utilized human-derived cultured cells to investigate EAAT2 dysfunction in AD. Overall, despite a small sample size, it would appear these results broadly support findings from animal work and suggest a role for Aβ induced dysfunction of EAAT2 in AD.

Postmortem human tissue

Temporal cortex and hippocampus

Some research has concluded EAAT2 protein expression is reduced in AD postmortem hippocampal (Abdul et al., 2009) and temporal gyrus tissue (Hoshi et al., 2018). However, a recently published study by our laboratory group revealed no quantitative EAAT2 alterations in the hippocampus, subiculum, entorhinal cortex, or superior temporal gyrus (Yeung et al., 2021). Despite this, changes to the expression pattern of EAAT2 were evident, with higher immunoreactivity noticeable in the neuropil (Yeung et al., 2021). The notion that EAAT2 expression level may not be altered in AD is further supported by earlier evidence from Beckstrøm et al. (1999), who found varying EAAT2 levels in the inferior temporal gyrus for both control and AD cases, but no clear association with AD. However, Jacob et al. (2007) and Scott et al. (2011) provided evidence for a decrease in EAAT2 mRNA expression in the AD temporal cortex, complicating current literature. Further results include those from Simpson et al. (2010), who reported variability in EAAT2 staining patterns between AD cases and a significant inverse relationship between GFAP and EAAT2 expression. Rothstein et al. (1992) reported no change to high-affinity glutamate transport. In addition, Woltjer et al. (2010) found an increase in detergent-insoluble EAAT2 in both the AD hippocampus and frontal cortex.

Interestingly, one study reported that cognitively intact patients with AD-related pathology in the entorhinal cortex showed greater GLT-1 immunoreactivity and greater mRNA expression than those with symptoms of dementia (Kobayashi et al., 2018). This is a fascinating result as no other study in postmortem tissue has revealed that different levels of EAAT2 expression might be correlated to clinical symptoms in the presence of AD pathology.

Frontal cortex

Similar to the temporal cortex, there is conflicting information in the frontal cortex regarding potential changes to the expression of EAAT2 in AD. Several studies have suggested no changes to EAAT2 expression in AD and dementia (Kirvell et al., 2010; Garcia-Esparcia et al., 2018; Poirel et al., 2018). Others have reported a decreased mRNA (Jacob et al., 2007; Tian et al., 2010; Scott et al., 2011) and protein (Li et al., 1997) EAAT2 expression. Tian et al. (2010) also found evidence for a decreased association of EAAT2 with lipid rafts in AD cases, potentially indicating a reduction in membrane expression.

Other anatomical areas

Compared to the temporal and frontal cortices, the expression of EAAT2 in other brain areas has not been as extensively studied. Jacob et al. (2007) found no evidence of EAAT2 alteration in AD postmortem cerebellar tissue. In the

TABLE 1 Summary of human postmortem EAAT2 studies included in this systematic review.

Study number	References	Aim/description	Main methodology/s	Subject/culture characteristics	Brain region examined	Main study findings (specific to EAAT2/AD)
1	Abdul et al. (2009)	Investigate whether nuclear factor of activated T-cells (NFAT) nuclear translocation is evident in AD -Examine EAAT2 expression in postmortem brain and determine whether activation of the NFAT pathway could be responsible for potential decreases in EAAT2	Western blot	12 control, 10 MCI, and 18 AD postmortem cases	Hippocampal sections—membrane fraction homogenate	EAAT2 protein expression significantly decreased in both MCI and AD cases relative to control
2	Beckstrøm et al. (1999)	To determine whether reduced glutamate uptake may be relevant in AD by measuring levels of EAAT1 and EAAT2 in control and AD postmortem tissue	Western blot	10 control and 10 AD cases	Inferior temporal gyrus	Case variability in EAAT2 levels between both AD and control cases but no significant correlation seen between EAAT2 levels and AD diagnosis
3	Flowers et al. (2001)	To examine whether EAAT2 splice variants retaining intron 7 or skipping exon 9 can be identified in the postmortem amyotrophic lateral sclerosis (ALS) motor cortex (with the inclusion of several AD cases)	TaqMan qPCR assay for quantification of EAAT2 mRNA transcripts in postmortem tissue	17 ALS cases, 7 AD cases, 19 control cases	Motor cortex, spinal cortex, anterior frontal gyrus, occipital cortex	The variant EAAT2 mRNA transcripts were detected in all cases across all brain regions. No significant difference in ratio of "variant" to "normal" transcripts in ALS or AD cases
4	Garcia-Esparcia et al. (2018)	Examine GLT1/EAAT2 mRNA and protein expression in control, AD and dementia with Lewy body (DLB) cases	RT-Q-PCR and Western blot	39 middle aged control, 20 AD and 9 DLB cases	Frontal cortex, Brodmann area 8	Neither GLT-1/EAAT2 mRNA nor protein expression were significantly altered in AD cases compared to controls
5	Hoshi et al. (2018)	To investigate the correlation between GLT-1 and aquaporin-4 (AQP4) expression in the human AD brain	Immunohistochemistry	5 control and 8 AD cases	Inferior, middle and superior temporal lobe	Significantly reduced GLT-1 expression in AD Two different patterns of GLT-1 and AQP4 in AD (i) uneven GLT-1 expression in neuropil but intense AQP4 expression (ii) co-expression of GLT-1 and AQP4 in plaque like structures
6	Jacob et al. (2007)	Examine EAAT1/2 gene and protein expression in postmortem human brain	Q-RT-PCR and gene chip array	22 AD cases, 10 control cases	Gyrus frontalis medialis, hippocampus, and cerebellum	Gene chip array: SLC1A2 (EAAT2 gene) downregulated in AD cases (gyrus frontalis medialis), but no change in hippocampus or cerebellum mRNA (Q-RT-PCR): EAAT2 mRNA expression decreased in hippocampus. No change in gyrus frontalis medialis or cerebellum

(Continued)

10.3389/fnins.2022.952096

TABLE 1 Continued

Study number	References	Aim/description	Main methodology/s	Subject/culture characteristics	Brain region examined	Main study findings (specific to EAAT2/AD)
7	Kirvell et al. (2010)	To determine protein expression of glutamatergic components in vascular dementia postmortem tissue	Western blot	8 Control, 8 Vascular Dementia (VaD), 15 Mixed VaD/AD, 7 AD and 8 stroke no dementia (SND) cases.	Frontal cortex (Brodmann areas 9 and 20)	EAAT2 protein expression not significantly altered for any case group relative to control
8	Kobayashi et al. (2018)	Examine potential neuroprotective role of astrocytes in AD—looking at GLT-1/EAAT2 expression	Immunohistochemistry	19 control cases (no dementia/AD pathology (N-N), 10 cases with AD pathology but no dementia (AD-N), and 18 with AD pathology and dementia (AD-D)	Entorhinal cortex (EC)	Significantly higher GLT-1 positive area in AD-N cases compared to those in the AD-D group for both layers I/II and III-VI of the EC Significantly lower GLT-1 positive area in AD-D cases compared to N-N cases in layer II/III of EC but not layers III–VI
9	Lauderback et al. (2001)	Investigate the mechanisms behind decreased glutamate uptake in AD—exploring a connection between lipid peroxidation product 4-hydroxy-2-non-enal (HNE) and GLT-1	Immunoprecipitation and Western blot	7 Control and 4 AD cases	Inferior parietal lobule	Western blot analysis of HNE-modified proteins results in an increased GLT-1 immunoreactivity suggesting their co-expression in AD
10	Li et al. (1997)	To determine which glutamate transporter subtype is most affected by AD and determine any correlations to abnormal amyloid precursor protein expression.	Western blot and RNase protection assay and Immunohistochemistry	4 Control and 12 AD cases	Frontal cortex	No significant change to EAAT2 mRNA levels in AD cases, but EAAT2 protein levels are significantly decreased.
11	Poirel et al. (2018)	To investigate the expression of synaptic markers in dementia	Western blot	171 cases—(includes both control and AD cases). Cases grouped into clinical dementia ratings (CDR) 0 (38 cases), 0.5 (21), 1 (18), 2 (14), 3 (38), 4 (21), and 5 (21)	Frontal cortex (Brodmann area 9)	No expressional alterations to EAAT2 protein in AD cases and no correlation between the CDR and EAAT2 protein expression
12	Pow and Cook (2009)	To analyze the expression of exon skipping variants of EAAT1-3 in AD postmortem tissue	Immunohistochemistry	3 control and 3 AD cases	Temporal cortex	Exon-9 skipping variant is evident in the AD temporal cortex. Glial cells and occasional neurons are labeled

(Continued)

10.3389/fnins.2022.952096

TABLE 1 Continued

Study number	References	Aim/description	Main methodology/s	Subject/culture characteristics	Brain region examined	Main study findings (specific to EAAT2/AD)
13	Rothstein et al. (1992)	To investigate whether glutamate transport is responsible for a suggested abnormal metabolism of glutamate in amyotrophic lateral sclerosis (ALS) and other neurodegenerative diseases	Quantification of sodium dependent glutamate uptake from homogenized postmortem tissue using radioactive hydrogen isotope	17 control cases (no neurological disease), 13 amyotrophic lateral sclerosis (ALS) cases, 12 Huntington's disease cases and 15 AD cases	Spinal cord, motor cortex, somatosensory cortex, striatum, and hippocampus	Mean V_{max} (indicative of relative density of EAAT2) and K_t (affinity) values for high affinity glutamate transport were not changed in AD tissue compared to control for any region, suggesting no change to EAAT2 expression in AD. (somatosensory cortex not examined for AD cases).
14	Sasaki et al. (2009)	To examine the relationship between phosphorylated tau and EAAT2 in AD and other tauopathies	Western blot Immunoprecipitation Immunohistochemistry	3 Control, 4 AD, 2 progressive supranuclear palsy (PSP) and 2 corticobasal degeneration (CBD) cases	Temporal cortex	EAAT2 co-precipitated with p-tau in disease cases but not control EAAT2 partially co-localizes with tau in AD tissue Detergent insoluble EAAT2 evident in AD cases
15	Scott et al. (2011)	To examine EAAT2 expression in the AD postmortem brain, including alternatively spliced variants	RT-PCR	15 Control, 12 AD and 10 AD/Lewy body disease cases	Inferior frontal, Inferior temporal, primary motor, and occipital cortices	Decreased mRNA expression of wild-type EAAT2 in all analyzed areas in AD. Increased wild-type EAAT2 mRNA copy number with increasing pathological severity in AD (irrespective of brain region) Splice variant EAAT2b mRNA levels slightly decreased in AD tissue Both exon 7 and 9 skipping variants of EAAT2 show an increase in mRNA copy number with increasing pathological severity in AD
16	Simpson et al. (2010)	To investigate astrocyte pathology and relationship to AD related changes	Immunohistochemistry	42 AD cases (8 definite, 14 probable, 20 possible based on CERAD criteria)	Lateral temporal cortex	Variability in staining pattern of EAAT2 and GFAP visible in AD—grouped into three categories, minimal, moderate or extensive immunoreactivity Significant inverse relationship between EAAT2 and GFAP staining
17	Thai (2002)	Investigate whether EAAT2 may be involved in AD related neuronal changes	Immunohistochemistry	21 brains from autopsy cases—split into three groups—cognitively normal, AD-related pathology but cognitively normal and AD	Various brain regions (cerebellum/brainstem, medial temporal lobe, and frontal cortices/basal ganglia)	EAAT2 immunoreactive neurons found in AD, but not control cases

(Continued)

10.3389/fnins.2022.952096

TABLE 1 Continued

Study number	References	Aim/description	Main methodology/s	Subject/culture characteristics	Brain region examined	Main study findings (specific to EAAT2/AD)
18	Thal et al. (2010)	To investigate whether neuropathological features and perivascular protein expression differ between cases with cerebral amyloid angiopathy (CAA) and AD	Immunohistochemistry	71 AD cases 309 Control cases. CAA cases determined from analysis of vascular deposition of amyloid-beta	Occipital cortex −20 cortical vessels in layers II and III studied for association with EAAT2 positive astrocytic processes	Expression of perivascular EAAT2—decreased in astrocytes of AD cases with capillary CAA but not in AD cases lacking capillary CAA and control cases
19	Tian et al. (2010)	To investigate whether EAAT2's association with lipid rafts is disrupted in AD cases *via* Western blotting	Lipid raft preparation Western blot	6 AD and 11 AD cases	Frontal cortex (Brodmann areas 9 and 10)	EAAT2 protein levels significantly decreased in AD frontal cortex Significantly decreased association of EAAT2 with lipid rafts in AD cases over control
20	Woltjer et al. (2010)	To investigate whether accumulation of detergent-soluble EAAT2 is related to the CDR in AD cases	ELISA and Immunohistochemistry	Hippocampus −22 AD, 14 CDR 0.5 cases, 13 control, and 4 PD Frontal cortex 55 AD, 23 CDR 0.5 cases, 20 control and 4 PD	Hippocampus and frontal cortex	Detergent insoluble EAAT2 significantly increased in the hippocampus and frontal cortex of AD patients relative to control
21	Yeung et al. (2021)	Investigation of EAAT2 protein expression in the AD postmortem medial temporal lobe	Quantitative fluorescent Immunohistochemistry	7 control and 6 AD cases	Hippocampus, subiculum, entorhinal cortex, and superior temporal gyrus	No significant quantitative changes in EAAT2 expression in AD in any region investigated Higher EAAT2 staining was evident in the neuropil of AD cases

10.3389/fnins.2022.952096

TABLE 2 Summary of cell culture, gene expression and other human EAAT2 studies included in this systematic review.

Study number	References	Aim/description	Main methodology	Subject/culture characteristics	Brain region examined	Main study findings (specific to EAAT2/AD)
22	Batarseh et al. (2017)	To examine whether oleocanthal (in extra virgin olive oil) can rescue GLT-1 deficits in protein expression related to oligomeric Aβ exposure in astrocytes	Western blot	CCF-STTG1 human astrocytoma cell line	Cultured cells	Aβo exposure significantly reduced GLT-1 expression, which was rescued with oleocanthal co-treatment
23	Han et al. (2016)	Examine whether EAAT2 mRNA and protein expression is disturbed by Aβ exposure in human astrocytes and whether insulin could offer protection	RT-PCR and Western Blot	Human astrocyte cell line (HA-1800)	Cultured cells	EAAT2 mRNA levels not altered after Aβ exposure, but protein expression is significantly decreased. Insulin co-treatment rescues EAAT2 deficit
24	Liang et al. (2002)	To explore whether estrogen treatment can restore deficient glutamate transporter activity in cultured human astrocytes (while also investigating GLT-1 and GLAST expression)	Western blot	Primary human astrocytes—prepared from 8 control and 8 AD donors	Cultured cells	AD astrocytes express less GLT-1 protein than control astrocytes
25	Meng and Mei (2019)	To determine whether certain genes are differentially expressed in AD	Bioinformatics study	RNA-seq expression data from human brain samples from four separate studies from the AMP-AD programme. 1. ROSMAP study (640 samples) 2. MSBB study (938 samples) 3. MayoPilot study (93 samples) 4. MayoBB study (556 samples) Cases grouped as control and AD samples based on clinical annotation from the four different projects. After quality control evaluations, 1,045 AD and 622 control RNA-seq samples were used to calculate the Spearman correlation between AD and normal gene pairs	ROSMAP—Sequence data is from dorsolateral prefrontal cortex, posterior cingulate cortex and head of caudate nucleus. MSBB study—four different brain regions with separate sequence data, parahippocampal gyrus, inferior frontal gyrus, superior temporal gyrus and frontal pole Mayo studies—sequence data is from temporal cortex and cerebellum	SLC1A2 (EAAT2 gene) is not differentially expressed in AD (not significantly different between AD and control)

(Continued)

10.3389/fnins.2022.952096

TABLE 2 Continued

Study number	References	Aim/description	Main methodology	Subject/culture characteristics	Brain region examined	Main study findings (specific to EAAT2/AD)
26	Meng et al. (2020)	Explore the correlation between EAAT2 and ADORA2A serum levels in AD—use as a biomarker?	EAAT2 ELISA detection kit	60 healthy controls, 68 AD cases	Serum expression of EAAT2 and ADORA2A analyzed *via* ELISA	The AD group showed significantly lower EAAT2 serum levels compared to control. Severity of AD showed a significant negative correlation to serum EAAT2 level
27	Sharma et al. (2019)	To investigate the differential roles that astrocytic and neuronal EAAT2 deficiencies might play in AD primarily using mice models. Also compare gene expression profiles of mice to the human condition	Data mining of GSE48350 from the Gene Expression Omnibus repository. Generated lists of differentially expressed genes in human AD and aging. Extent of overlap between astrocytic and neuronal deficient EAAT2 mice and humans determined using rank-rank hypergeometric overlap (RRHO)	N/A	N/A	Astrocytic EAAT2 deficient, but not neuronal EAAT2 deficient mice show overlap with the gene expression profiles in human AD and aging
28	Zoia et al. (2004)	Examine whether platelet expression of glutamate transporters is altered in AD	Western blotting and RT-PCR	60 control and 10 AD patients (blood samples taken)	Platelets prepared from patient blood	No change in EAAT2 protein or mRNA expression in platelets in AD
29	Zoia et al. (2011)	To explore glutamate uptake and transporter expression in human fibroblasts after exposure to non-fibrillar $A\beta_{1-42}$	Semi quantitative RT-PCR and Western blotting	Human fibroblasts prepared from skin biopsies of 15 healthy controls and 6 AD patients	Cultured cells	No changes to protein or mRNA EAAT2 expression after exposure to non-fibrillar $A\beta_{1-42}$

10.3389/fnins.2022.952096

parietal cortex, there is evidence that a lipid peroxidation product 4-hydroxy-2-nonenal (HNE) is co-expressed with EAAT2, potentially indicating oxidative damage and loss of transporter function (Lauderback et al., 2001). However, the significance of this finding and whether it is true for other brain regions needs further investigation.

Alternatively-spliced variants and neuronal expression of EAAT2 in Alzheimer's disease

Several studies have researched whether alternatively spliced variants of the EAAT2 protein have altered expression and subsequently play a role in the pathophysiology of AD. Scott et al. (2011) found that both the exon seven and exon nine skipping variants have an increased mRNA copy number with increasing pathological severity in AD cases. Neuronal expression of the exon nine skipping EAAT2 variant has been reported in AD postmortem tissue *via* immunohistochemistry (Pow and Cook, 2009). However, Flowers et al. (2001) found no change in the expression of intron seven retaining and exon nine skipping transcripts in AD, although this was a small sample of AD cases. Thai (2002) also provided evidence for EAAT2 accumulation in neurons in AD but not in control postmortem brains, but it is uncertain if this is the full length or a splice variant of EAAT2.

Human cell culture studies

Several studies utilizing human-derived cultured cells have also been used to investigate potential alterations to EAAT2 expression in AD. Batarseh et al. (2017) found reduced GLT-1 protein expression in a human astrocyte cell line after Aβ exposure. Another study confirmed this result but revealed that while EAAT2 protein levels are decreased after Aβ exposure, there was no change to EAAT2 mRNA transcript levels (Han et al., 2016). This discrepancy between mRNA and protein EAAT2 levels has also been documented in AD postmortem tissue (Li et al., 1997; Kobayashi et al., 2018). Thus, it is postulated that modifications to EAAT2 protein expression in AD result from posttranslational disturbances.

Zoia et al. (2011) found no change to both EAAT2 mRNA and protein in fibroblasts derived from AD patients after Aβ exposure, but this is perhaps unrelated to what is happening to astrocytic expression of EAAT2 in AD. Liang et al. (2002) also found a decrease in GLT-1 protein expression in astrocytes cultured from AD patients. Therefore, these studies suggest that exposure to Aβ may induce a loss of the EAAT2 protein in astrocytes, while mRNA levels are not affected. However, the functional consequences for glutamate uptake are still unknown and the exact reason behind the mRNA-protein discrepancy needs more clarification.

Other relevant studies

One study found that serum levels of EAAT2 were lower in AD patients than in control, and this decrease was inversely correlated to the clinical symptoms of AD (Meng et al., 2020). This finding indicates that ELISA analysis of EAAT2 levels in patient serum may be a potential diagnostic tool for AD, although more work is needed to establish whether this change is specific to AD alone.

Only one paper from the reviewed studies used a bioinformatic approach to investigate EAAT2 gene expression in AD. Meng and Mei (2019) found that by analyzing RNA-seq datasets from four different projects, *SLC1A2* was not a differentially expressed gene in AD. Multiple brain regions were represented in the mRNAseq data including the dorsolateral prefrontal cortex, parahippocampal gyrus, inferior frontal gyrus, temporal cortex, and cerebellum (see Table 2, study 25 for full details).

Discussion

There are several possible explanations for the differing results regarding the expression of both EAAT2 mRNA and protein in AD postmortem tissue from the studies included in this review. These results could simply indicate that there is high patient variability of EAAT2 mRNA or protein expression in AD. Additionally, low sample sizes often seen in human studies, mainly due to tissue availability, can produce potentially variable and confounding results. For example, some studies included in this review only used three AD and three control cases (Pow and Cook, 2009). This sample size does not give confidence that these results are replicable across the population. Other factors to consider when looking at the results of postmortem studies are the heterogeneity of AD, stage of disease, age and sex differences, postmortem delay, and medication effects. At this stage, it is unclear how these factors may influence the EAAT2 mRNA and protein expression as well as preservation in the postmortem human brain, an important fact to consider when interpreting variable results between studies. A final point is that different EAAT2/GLT-1 antibodies between studies, likely targeting different regions of the protein, may also be playing a role in conflicting results.

EAAT2 protein expression

Based on early previous evidence from radiolabeling, an ∼30% reduction in [^{3}H] aspartate binding was revealed in

the postmortem AD brain, signaling a significant dysfunction in glutamate uptake (Masliah et al., 1996). This is likely to play a role in AD progression, with implications such as glutamate excitotoxicity, a well-documented concept in the literature (Conway, 2020; Manisha et al., 2020). However, how this might relate to EAAT2 expression in the human AD brain is still unclear. Animal studies have suggested that Aβ may be responsible for decreases in EAAT2 expression (Takahashi et al., 2015; Huang et al., 2018). In addition, amyloid-beta administration has been shown to result in the mislocalization of EAAT2 (Manisha et al., 2020). However, it is uncertain if this is the reason behind EAAT2 alterations (both expressional and qualitative) previously documented in AD postmortem tissue (Li et al., 1997; Abdul et al., 2009; Hoshi et al., 2018; Yeung et al., 2021). After Aβ treatment, HNE and GLT-1 conjugation and impairments in glutamate uptake were reported in rat cortical synaptosomes (Keller et al., 1997). This result potentially indicates that the same changes seen with HNE and GLT-1 co-precipitation in the human brain by Lauderback et al. (2001) are related to Aβ exposure. More work is needed to establish the exact cellular mechanisms behind Aβ induced dysfunction of EAAT2. Interestingly, certain studies within the same brain region have shown contradictory results regarding EAAT2 protein expression (Abdul et al., 2009; Yeung et al., 2021). A possible explanation could be the methodology used. Abdul et al. (2009) reported a significant decrease in EAAT2 protein expression in the AD hippocampus *via* analysis of the membrane fraction in a Western blot. This result possibly indicates that EAAT2 expression on astrocytic membranes is reduced in AD, which seems to be in agreement with Tian et al.'s (2010) finding of a significantly decreased association between lipid rafts and EAAT2 in AD. However, our previous study reported no significant quantitative differences in EAAT2 staining in hippocampal regions. Despite this, we did note higher EAAT2 staining in the neuropil that appeared to show less co-localization with GFAP stained astrocytic main branches, also perhaps indicative of EAAT2 astrocytic loss (Yeung et al., 2021). Interestingly, this EAAT2 expression pattern in AD cases (higher staining in the neuropil) appears similar to immunohistochemical images from the hippocampus published by Li et al. (1997). However, no quantitative data was provided in this study for hippocampal areas, raising validity concerns about this comparison. Further analysis is needed to determine if this expression pattern seen in the AD hippocampus represents a loss of EAAT2 on astrocytic membranes or whether this is simply EAAT2 staining on fine astrocytic processes that were not stained with GFAP. Animal work also supports that the underlying pathophysiology is related more to a displacement of transporters than reduced transporter expression, as total EAAT2 expression from the same whole-cell protein lysates was not changed by $A\beta_{1-42}$ in mouse hippocampal slices (Scimemi et al., 2013). More research is needed to validate this theory of EAAT2 astrocytic displacement, investigating if EAAT2 cell surface trafficking pathways are altered in AD, as this can have functional implications on glutamate uptake and thus play a key role in neurodegeneration.

EAAT2 mRNA expression

Both cell culture models and human postmortem studies have reported a loss of EAAT2 protein expression in AD, despite no disturbances to EAAT2 mRNA expression (Li et al., 1997; Han et al., 2016). It suggests that any modification to EAAT2 protein expression by Aβ may be posttranslational, but how this may occur is uncertain. However, two studies included in this review reported decreased EAAT2 mRNA in AD tissue (Jacob et al., 2007; Scott et al., 2011), highlighting the contradictory nature of these results, and the inability to rely on the current literature available to accurately determine the processes impacting on EAAT2 mRNA and protein expression in AD. It is also possible that both protein and mRNA expression are differentially affected by AD in distinct brain regions. However, the theory that EAAT2 mRNA expression may be preserved in AD, is supported by findings that *SLC1A2* gene expression is not altered in AD (Meng and Mei, 2019). Although the RNAseq data used was from multiple brain regions, it cannot be ruled out that there might be subtle anatomical and layer-specific variations to *SLC1A2* expression in response to AD. Further work is needed to confirm EAAT2 mRNA and protein expression in AD, given the contradictory results reported in the above discussed studies.

EAAT2 solubility and aggregation

A decrease in EAAT2 astrocytic protein expression was noted in an AD model by Scimemi et al. (2013), who found $A\beta_{1-42}$ can cause rapid mislocalization of EAAT2 cell surface expression on astrocytes. Additionally, Woltjer et al. (2010) revealed that detergent-insoluble EAAT2 in the hippocampus and frontal cortex of AD patients was higher than control cases, indicating possible aggregation of EAAT2 in AD. Further analysis, though, revealed no evidence of an association between EAAT2 and amyloid plaques (Woltjer et al., 2010). Perhaps EAAT2 expression is lost from astrocytic membranes in AD and forms insoluble structures, independent of Aβ plaques which could explain these results. The increased EAAT2 in the neuropil seen in our earlier study (Yeung et al., 2021) could also be indicative of aggregation. Sasaki et al. (2009) noted that high molecular weight EAAT2 was detected in the detergent-insoluble fraction of their analyses, again potentially suggesting aggregation of EAAT2 in AD. However, it is uncertain if this is insoluble EAAT2 alone or its co-association with tau or amyloid aggregates. This study did indicate EAAT2 co-precipitates with p-tau (Sasaki et al., 2009), so EAAT2 and tau co-aggregates

may occur in AD. Additionally, Hoshi et al. (2018) reported plaque-like staining of EAAT2 in AD, which was co-expressed with aquaporin-4. These results seem to suggest EAAT2 protein expression may be lost from astrocytic membranes in AD and form aggregates. However, it is not clear where EAAT2 expression might be translocated to, or what consequences this may have for progression of disease or neurodegeneration.

EAAT2 as a neuroprotective factor

There is evidence that the preservation of EAAT2 expression on astrocytes may be neuroprotective in the presence of AD pathology (Kobayashi et al., 2018). Lower immunoreactivity of GLT-1 was seen in entorhinal layers I/II and III–VI of cases with dementia (AD-D) compared to control, but those with AD pathology but no dementia (AD-N) showed no change to GLT-1 positive area over control (Kobayashi et al., 2018). This result implies that the maintenance of EAAT2 expression in the presence of AD pathology is neuroprotective and may even be a key factor in determining AD symptomatology, more so than other established pathological AD changes. This study is the only postmortem human evidence supporting the maintenance of or increased EAAT2 expression as a therapeutic target in AD. A study investigating potential differences in serum expression of EAAT2 between control and AD patients found significantly lower expression of EAAT2 in their AD group (Meng et al., 2020). Interestingly, when AD subjects were grouped into "mild," "moderate," and "severe" based on the severity of the disease, severe subjects had significantly lower serum expression of EAAT2, and a significant negative correlation between severity and EAAT2 serum expression was noted (Meng et al., 2020). Although it cannot be certain that serum levels of EAAT2 reflect the expression of the protein in the brain, these results broadly seem to support the Kobayashi study. Numerous research from animal studies further supports that higher EAAT2 transporter activity in the presence of AD pathology may be neuroprotective and these results are discussed in the subsequent therapeutics chapter.

EAAT2 splice variants

Alternatively-spliced variants of the EAAT2 protein (intron seven retaining and exon nine skipping) have been documented in both control and AD postmortem tissue, although there was no alteration to their mRNA expression noted in neurological disease (Flowers et al., 2001). However, conflicting evidence suggests an increased mRNA expression of exon 7 and 9 skipping splice variants in AD cases, which was found to correlate with increased pathological severity (Scott et al., 2011). Gebhardt et al. (2010) found evidence for the formation of heteromeric wild-type EAAT2 and variant protein complexes in HEK293 cells. In addition, it was found that cells co-transfected with wild-type and variant EAAT2 showed a reduction in glutamate-dependent activity measured by EC_{50} and Hill coefficients (Gebhardt et al., 2010). It remains to be determined if this reduction is relevant in the human brain. Due to the small number of studies in current literature, more investigation is needed into the splice variants of EAAT2 and their relationship to AD.

Neuronal expression of EAAT2

Neuronal expression of EAAT2 is still a highly debated area of research. Historically, EAAT2 expression and thus glutamate uptake was thought to be localized exclusively to astrocytes (Milton et al., 1997; Rimmele and Rosenberg, 2016). More recent work though has indicated a small amount of EAAT2 immunoreactivity is likely to be localized to neurons (Roberts et al., 2014). In one immunohistochemistry study, in both the white and gray matter, ∼80% of identifiable immunoreactivity for EAAT2 was deemed attributable to astrocytic processes. The remaining immunoreactivity was seen in axon terminals, dendrites or was unidentifiable (Melone et al., 2011). However, the exact differences in physiological function between neuronal and astrocytic EAAT2 are still not well-understood, although EAAT2 expressed on astrocytic processes perform the vast majority of glutamate reuptake and is also responsible for protection against glutamate excitotoxicity (Petr et al., 2015; Danbolt et al., 2016). The study from Sharma et al. (2019) found that an astrocytic deficiency of EAAT2 in mice, rather than neuronal, is more correlated with gene expression profiles seen in aging and AD, indicating that it is likely astrocytic EAAT2 that is affected in AD. Without further study though, it cannot be conclusively ruled out that changes to neuronal EAAT2 may have a role to play in AD.

It has been suggested that neuronal accumulation of EAAT2 may be relevant to neuron degeneration in AD (Pow and Cook, 2009). Some studies have found EAAT2 immunoreactive neurons throughout many brain regions in AD (Thai, 2002). Others have suggested that splice variants of EAAT2 may become translated in stressed neurons and have provided evidence for their accumulation in AD (Pow and Cook, 2009). However, it is inconclusive whether these results reflect true neuronal staining, as neither of these studies included a neuronal marker. Therefore, these immunoreactive "neurons" described in AD tissue may be astrocytic labeling wrapping around neurons or staining of other neuronal-like structures. Future research needs to establish whether EAAT2 accumulation in neurons is relevant in AD and whether this could contribute to AD pathophysiology.

EAAT2 transporter activity in Alzheimer's disease

There are several previous studies in the literature that have investigated the functionality of the EAAT2 transporter in postmortem brains by assessing glutamate uptake. Some of these studies have shown a reduction in glutamate uptake in postmortem AD tissue (Hardy et al., 1987; Procter et al., 1988), while others have found no change (Beckstrøm et al., 1999). An article from Petr et al. (2015), suggests that these discrepancies may be due to the methodology used. From using both astrocytic and neuronal specific knockouts of GLT-1 in mice, they noted that interestingly, neuronal but not astrocytic GLT-1/EAAT2 made a significant contribution to glutamate uptake measured in synaptosomes (Petr et al., 2015). This is paradoxical, as neuronal or axon terminal EAAT2 only accounts for ∼20% of its total labeling (Melone et al., 2011), so the astrocytic contribution to uptake would be expected to be much greater. The authors postulate that tissue homogenization may differentially affect astrocytic and neuronal EAAT2 function, with the former being suggested to be localized to leaky compartments and thus is unable to play a role in glutamate uptake. An alternative explanation is that the astrocytic EAAT2 (or a large proportion) may not be functional, perhaps due to environmental context (Petr et al., 2015). Reconstituting synaptosomes in liposomes removed this bias in their study, a step which they suggest may have caused discrepancies in earlier studies, as without reconstitution, astrocytic EAAT2 activity may be completely removed in a fashion unrelated to AD (i.e., unable to contribute to glutamate uptake or not functional; Petr et al., 2015). It is also entirely plausible that the differing results reported in literature may just reflect low sample sizes and variability associated with human tissue use. Moreover, the Petr et al. (2015) study is ultimately an animal study, so we cannot be sure this effect also occurs in human tissue. Nevertheless, these findings highlight the need to carefully consider methodology when comparing results between studies measuring glutamate uptake in AD, as well as the complicated nature of assessing glutamate uptake from both astrocytes and neurons in postmortem tissue.

Evidence for EAAT2 modulation as a valid therapeutic target for the treatment of AD

Modulation of EAATs may have positive therapeutic effects, with their ability to alter glutamate levels providing a logical link in managing glutamate excitotoxicity in the AD brain. Upregulation of EAAT2 has been shown to reduce excitotoxic damage seen in a variety of acute and chronic neurological diseases, and over-expression of EAAT3 appears to protect against toxicity by decreasing the levels of extracellular glutamate (Lewerenz et al., 2006; Sheldon and Robinson, 2007). Furthermore, beneficial effects of memantine, an NMDAR antagonist approved by the FDA for the symptomatic management of AD, indicate that a reduction in circulating glutamate may provide another avenue toward reducing overexcitation of glutamatergic neurons (Plosker and Lyseng-Williamson, 2005).

There has been a focus on identifying and testing novel compounds with EAAT2-enhancing properties to identify their effect on AD models. Synthetic compound LDN/OSU-0212320 improved cognitive functions in the $APP_{Sw,Ind}$ mouse model by increasing EAAT2 expression through translational activation (Takahashi et al., 2015). Other methods of EAAT2 modulation have also been explored. A recent medical hypothesis published by Manisha et al. (2020) described increasing EAAT2 activity by promoting glutamate ligand binding through allosteric modulator GT949. Enhancement of glutamate ligand binding is effective in promoting EAAT2 activity independent of substrate pharmacokinetics (Kortagere et al., 2018). Improving EAAT2 activity through increased allosteric binding might be an effective mechanism through which AD-associated EAAT2 dysfunction can be ameliorated.

The antibiotic ceftriaxone is a known activator of EAAT2 transcription, and several studies have investigated whether treatment with this compound may be beneficial in animal models of AD (Zumkehr et al., 2015; Fan et al., 2018; Hamidi et al., 2019). These results suggest that the upregulation of EAAT2 has beneficial effects on cognition and neuronal activity in animal models of AD and is a promising therapeutic target. Human research shows that increased EAAT2 expression is associated with cognitively intact subjects with AD pathology (Kobayashi et al., 2018), potentially validating enhancement of EAAT2 activity as a good therapeutic approach for AD. However, as an antibiotic compound, there are likely to be numerous off-target effects and problems with delivering this drug across the blood-brain barrier. Human research from Lee et al. (2008) has indicated that the NF-kB pathway is responsible for the ceftriaxone dependent upregulation of EAAT2. Perhaps this information could be used to design or search for treatment options that can act similarly to ceftriaxone to induce EAAT2 upregulation. However, more clarification and research is needed before upregulating EAAT2 can be considered a valid strategy to treat the human condition.

Additional novel and well-established compounds have also been examined for their potential affinity and synergistic properties in modulating the EAAT2 transporter. For example, the vitamin E derivative trolox is effective in ameliorating mislocalization of astrocytic EAAT2 in mice exposed to Aβ (Scimemi et al., 2013). Medications used for non-neurodegenerative conditions, such as minocycline, dexamethasone, and histamine, have been shown to have neuroprotective effects through the upregulation of EAAT2 (Fontana, 2015). Examination of current therapeutics used

TABLE 3 A summary of possible avenues to restore EAAT2 function and treat Alzheimer's disease.

EAAT2 modulation strategies to increase glutamate clearance and treat AD	References
Translational activation of EAAT2	Kong et al., 2014; Takahashi et al., 2015; Zumkehr et al., 2015; Fan et al., 2018; Hamidi et al., 2019; Manisha et al., 2020
Allosteric modulation to promote glutamate binding	Manisha et al., 2020
Restore aberrant mislocalization of EAAT2	Scimemi et al., 2013

for other neurodegenerative disorders might also be useful as potential drugs for AD. Riluzole, currently approved for the management of amyotrophic lateral sclerosis, has been shown to promote activation of EAAT2 translation and reducing excitotoxic cellular injury in cultured neurons (Kong et al., 2014). Overall, EAAT2 modulation does appear to have neuroprotective effects in AD models, although further studies will be required to explore the applicability of these compounds and their suitability as disease-modifying therapies for AD. A short summary of EAAT2 modulation strategies in the current literature are outlined in Table 3.

Future implications and conclusion

Overall, in this review, we highlight the contradictory nature of existing literature and indicate a potential for maintained EAAT2 astrocytic expression as a potential therapeutic option in AD. First and foremost, though, more research is needed to truly establish what happens to EAAT2 expression on astrocytic membranes in AD, how this may be related to Aβ and tau pathologies, and what effect this may have on excitotoxic glutamate disturbances. In addition, the potential contribution of these changes to AD's clinical symptoms and progression has to be explored. EAAT2 modulation may still be a valid therapeutic strategy for AD treatment or prevention, but these unknowns need answering before compounds aiming to restore EAAT2 function or expression are trialed extensively in clinics to treat AD.

Data availability statement

The original contributions presented in the study are included in the article/Supplementary material, further inquiries can be directed to the corresponding author/s.

Author contributions

OW, JY, and AK: conceptualization, methodology, and writing—original draft preparation. OW, JY, AK, and RF: writing—review and editing. AK and RF: supervision and funding acquisition. AK: project administration. All authors have read and agreed to the published version of the manuscript.

Funding

This work was supported by Alzheimer's New Zealand Charitable Trust (AK; 370836), Alzheimer's New Zealand (AK; 3718869), Freemasons New Zealand (AK; 3719321), Aotearoa Foundation, Centre for Brain Research and University of Auckland (AK; 3705579), and Health Research Council of New Zealand (RLF; 3627373).

Conflict of interest

The authors declare that the research was conducted in the absence of any commercial or financial relationships that could be construed as a potential conflict of interest.

Publisher's note

All claims expressed in this article are solely those of the authors and do not necessarily represent those of their affiliated organizations, or those of the publisher, the editors and the reviewers. Any product that may be evaluated in this article, or claim that may be made by its manufacturer, is not guaranteed or endorsed by the publisher.

References

Abdul, H. M., Sama, M. A., Furman, J. L., Mathis, D. M., Beckett, T. L., Weidner, A. M., et al. (2009). Cognitive decline in Alzheimer's disease is associated with selective changes in calcineurin/NFAT signaling. *J. Neurosci.* 29, 12957–12969. doi: 10.1523/JNEUROSCI.1064-09.2009

Arriza, J. L., Eliasof, S., Kavanaugh, M. P., and Amara, S. G. (1997). Excitatory amino acid transporter 5, a retinal glutamate transporter coupled to a chloride conductance. *Proc. Natl. Acad. Sci. U.S.A.* 94, 4155–4160. doi: 10.1073/pnas.94.8.4155

Batarseh, Y. S., Mohamed, L. A., Al Rihani, S. B., Mousa, Y. M., Siddique, A. B., El Sayed, K. A., et al. (2017). Oleocanthal ameliorates amyloid-β oligomers' toxicity on astrocytes and neuronal cells: *in vitro* studies. *Neuroscience* 352, 204–215. doi: 10.1016/j.neuroscience.2017.03.059

Beckstrøm, H., Julsrud, L., Haugeto, O., Dewar, D., Graham, D. I., Lehre, K. P., et al. (1999). Interindividual differences in the levels of the glutamate transporters GLAST and GLT, but no clear correlation with Alzheimer's disease. *J. Neurosci. Res.* 55, 218–229. doi: 10.1002/(SICI)1097-4547(19990115)55:2<218::AID-JNR9>3.0.CO;2-L

Bloom, G. S. (2014). Amyloid-β and tau: the trigger and bullet in Alzheimer disease pathogenesis. *JAMA Neurol.* 71, 505–508. doi: 10.1001/jamaneurol.2013.5847

Braak, H., and Braak, E. (1991). Neuropathological stageing of Alzheimer-related changes. *Acta Neuropathol.* 82, 239–259. doi: 10.1007/BF00308809

Brookmeyer, R., Johnson, E., Ziegler-Graham, K., and Arrighi, H. M. (2007). Forecasting the global burden of Alzheimer's disease. *Alzheimers Dement.* 3, 186–191. doi: 10.1016/j.jalz.2007.04.381

Conway, M. E. (2020). Alzheimer's disease: targeting the glutamatergic system. *Biogerontology* 21, 257–274. doi: 10.1007/s10522-020-09860-4

Danbolt, N. C. (2001). Glutamate uptake. *Prog. Neurobiol.* 65, 1–105. doi: 10.1016/S0301-0082(00)00067-8

Danbolt, N. C., Furness, D. N., and Zhou, Y. (2016). Neuronal vs. glial glutamate uptake: Resolving the conundrum. *Neurochem. Int.* 98, 29–45. doi: 10.1016/j.neuint.2016.05.009

Fan, S., Xian, X., Li, L., Yao, X., Hu, Y., Zhang, M., et al. (2018). Ceftriaxone improves cognitive function and upregulates GLT-1-related glutamate-glutamine cycle in APP/PS1 mice. *J. Alzheimers. Dis.* 66, 1731–1743. doi: 10.3233/JAD-180708

Flowers, J. M., Powell, J. F., Leigh, P. N., Andersen, P., and Shaw, C. E. (2001). Intron 7 retention and exon 9 skipping EAAT2 mRNA variants are not associated with amyotrophic lateral sclerosis. *Ann. Neurol.* 49, 643–649. doi: 10.1002/ana.1029

Fontana, A. C. (2015). Current approaches to enhance glutamate transporter function and expression. *J. Neurochem.* 134, 982–1007. doi: 10.1111/jnc.13200

Garcia-Esparcia, P., Diaz-Lucena, D., Ainciburu, M., Torrejón-Escribano, B., Carmona, M., Llorens, F., et al. (2018). Glutamate transporter GLT1 expression in Alzheimer disease and dementia with lewy bodies. *Front. Aging Neurosci.* 10, 122. doi: 10.3389/fnagi.2018.00122

Gebhardt, F. M., Mitrovic, A. D., Gilbert, D. F., Vandenberg, R. J., Lynch, J. W., and Dodd, P. R. (2010). Exon-skipping splice variants of excitatory amino acid transporter-2 (EAAT2) form heteromeric complexes with full-length EAAT2. *J. Biol. Chem.* 285, 31313–31324. doi: 10.1074/jbc.M110.153494

Hamidi, N., Nozad, A., Sheikhkanloui Milan, H., Salari, A. A., and Amani, M. (2019). Effect of ceftriaxone on paired-pulse response and long-term potentiation of hippocampal dentate gyrus neurons in rats with Alzheimer-like disease. *Life Sci.* 238, 116969. doi: 10.1016/j.lfs.2019.116969

Hampel, H., Mesulam, M. M., Cuello, A. C., Farlow, M. R., Giacobini, E., Grossberg, G. T., et al. (2018). The cholinergic system in the pathophysiology and treatment of Alzheimer's disease. *Brain* 141, 1917–1933. doi: 10.1093/brain/awy132

Han, X., Yang, L., Du, H., Sun, Q., Wang, X., Cong, L., et al. (2016). Insulin attenuates beta-amyloid-associated Insulin/AKT/EAAT signaling perturbations in human astrocytes. *Cell. Mol. Neurobiol.* 36, 851–864. doi: 10.1007/s10571-015-0268-5

Hardy, J., Cowburn, R., Barton, A., Reynolds, G., Lofdahl, E., O'carroll, A.-M., et al. (1987). Region-specific loss of glutamate innervation in Alzheimer's disease. *Neurosci. Lett.* 73, 77–80. doi: 10.1016/0304-3940(87)90034-6

Hoshi, A., Tsunoda, A., Yamamoto, T., Tada, M., Kakita, A., and Ugawa, Y. (2018). Altered expression of glutamate transporter-1 and water channel protein aquaporin-4 in human temporal cortex with Alzheimer's disease. *Neuropathol. Appl. Neurobiol.* 44, 628–638. doi: 10.1111/nan.12475

Huang, S., Tong, H., Lei, M., Zhou, M., Guo, W., Li, G., et al. (2018). Astrocytic glutamatergic transporters are involved in Aβ-induced synaptic dysfunction. *Brain Res.* 1678, 129–137. doi: 10.1016/j.brainres.2017.10.011

Hynd, M. R., Scott, H. L., and Dodd, P. R. (2004). Glutamate-mediated excitotoxicity and neurodegeneration in Alzheimer's disease. *Neurochem. Int.* 45, 583–595. doi: 10.1016/j.neuint.2004.03.007

Jacob, C. P., Koutsilieri, E., Bartl, J., Neuen-Jacob, E., Arzberger, T., Zander, N., et al. (2007). Alterations in expression of glutamatergic transporters and receptors in sporadic Alzheimer's disease. *J. Alzheimers Dis.* 11, 97–116. doi: 10.3233/JAD-2007-11113

Keller, J. N., Mark, R. J., Bruce, A. J., Blanc, E., Rothstein, J. D., Uchida, K., et al. (1997). 4-Hydroxynonenal, an aldehydic product of membrane lipid peroxidation, impairs glutamate transport and mitochondrial function in synaptosomes. *Neuroscience* 80, 685–696. doi: 10.1016/S0306-4522(97)00065-1

Kim, K., Lee, S. G., Kegelman, T. P., Su, Z. Z., Das, S. K., Dash, R., et al. (2011). Role of excitatory amino acid transporter-2 (EAAT2) and glutamate in neurodegeneration: opportunities for developing novel therapeutics. *J. Cell. Physiol.* 226, 2484–2493. doi: 10.1002/jcp.22609

Kirvell, S. L., Elliott, M. S., Kalaria, R. N., Hortobágyi, T., Ballard, C. G., and Francis, P. T. (2010). Vesicular glutamate transporter and cognition in stroke: a case-control autopsy study. *Neurology* 75, 1803–1809. doi: 10.1212/WNL.0b013e3181fd6328

Kobayashi, E., Nakano, M., Kubota, K., Himuro, N., Mizoguchi, S., Chikenji, T., et al. (2018). Activated forms of astrocytes with higher GLT-1 expression are associated with cognitive normal subjects with Alzheimer pathology in human brain. *Sci. Rep.* 8, 1712. doi: 10.1038/s41598-018-19442-7

Kong, Q., Chang, L. C., Takahashi, K., Liu, Q., Schulte, D. A., Lai, L., et al. (2014). Small-molecule activator of glutamate transporter EAAT2 translation provides neuroprotection. *J. Clin. Invest.* 124, 1255–1267. doi: 10.1172/JCI66163

Kortagere, S., Mortensen, O. V., Xia, J., Lester, W., Fang, Y., Srikanth, Y., et al. (2018). Identification of novel allosteric modulators of glutamate transporter EAAT2. *ACS Chem. Neurosci.* 9, 522–534. doi: 10.1021/acschemneuro.7b00308

Lauderback, C. M., Hackett, J. M., Huang, F. F., Keller, J. N., Szweda, L. I., Markesbery, W. R., et al. (2001). The glial glutamate transporter, GLT-1, is oxidatively modified by 4-hydroxy-2-nonenal in the Alzheimer's disease brain: the role of Abeta1-42. *J. Neurochem.* 78, 413–416. doi: 10.1046/j.1471-4159.2001.00451.x

Lee, S. G., Su, Z. Z., Emdad, L., Gupta, P., Sarkar, D., Borjabad, A., et al. (2008). Mechanism of ceftriaxone induction of excitatory amino acid transporter-2 expression and glutamate uptake in primary human astrocytes. *J. Biol. Chem.* 283, 13116–13123. doi: 10.1074/jbc.M707697200

Lewerenz, J., Klein, M., and Methner, A. (2006). Cooperative action of glutamate transporters and cystine/glutamate antiporter system Xc- protects from oxidative glutamate toxicity. *J. Neurochem.* 98, 916–925. doi: 10.1111/j.1471-4159.2006.03921.x

Li, S., Mallory, M., Alford, M., Tanaka, S., and Masliah, E. (1997). Glutamate transporter alterations in Alzheimer disease are possibly associated with abnormal APP expression. *J. Neuropathol. Exp. Neurol.* 56, 901–911. doi: 10.1097/00005072-199708000-00008

Liang, Z., Valla, J., Sefidvash-Hockley, S., Rogers, J., and Li, R. (2002). Effects of estrogen treatment on glutamate uptake in cultured human astrocytes derived from cortex of Alzheimer's disease patients. *J. Neurochem.* 80, 807–814. doi: 10.1046/j.0022-3042.2002.00779.x

Malik, A. R., and Willnow, T. E. (2019). Excitatory amino acid transporters in physiology and disorders of the central nervous system. *Int. J. Mol. Sci.* 20, 5671. doi: 10.3390/ijms20225671

Manisha, C., Selvaraj, A., Jubie, S., Moola Joghee Nanjan, C., Moola Joghee, N., Clement, J. P., et al. (2020). Positive allosteric activation of glial EAAT-2 transporter protein: a novel strategy for Alzheimer's disease. *Med Hypothes.* 142, 109794. doi: 10.1016/j.mehy.2020.109794

Masliah, E., Hansen, L., Alford, M., Deteresa, R., and Mallory, M. (1996). Deficient glutamate tranport is associated with neurodegeneration in Alzheimer's disease. *Ann. Neurol.* 40, 759–766. doi: 10.1002/ana.410400512

Melone, M., Bellesi, M., Ducati, A., Iacoangeli, M., and Conti, F. (2011). Cellular and synaptic localization of EAAT2a in human cerebral cortex. *Front. Neuroanat.* 4, 151. doi: 10.3389/fnana.2010.00151

Meng, G., and Mei, H. (2019). Transcriptional dysregulation study reveals a core network involving the progression of Alzheimer's disease. *Front. Aging Neurosci.* 11, 101. doi: 10.3389/fnagi.2019.00101

Meng, S. X., Wang, B., and Li, W. T. (2020). Serum expression of EAAT2 and ADORA2A in patients with different degrees of Alzheimer's disease. *Eur. Rev. Med. Pharmacol. Sci.* 24, 11783–11792. doi: 10.26355/eurrev_202011_23833

Milton, I. D., Banner, S. J., Ince, P. G., Piggott, N. H., Fray, A. E., Thatcher, N., et al. (1997). Expression of the glial glutamate transporter EAAT2 in the human CNS: an immunohistochemical study. *Mol. Brain Res.* 52, 17–31. doi: 10.1016/S0169-328X(97)00233-7

Mookherjee, P., Green, P. S., Watson, G. S., Marques, M. A., Tanaka, K., Meeker, K. D., et al. (2011). GLT-1 loss accelerates cognitive deficit onset in an Alzheimer's disease animal model. *J. Alzheimers. Dis.* 26, 447–455. doi: 10.3233/JAD-2011-110503

Murphy-Royal, C., Dupuis, J. P., Varela, J. A., Panatier, A., Pinson, B., Baufreton, J., et al. (2015). Surface diffusion of astrocytic glutamate transporters shapes synaptic transmission. *Nat. Neurosci.* 18, 219–226. doi: 10.1038/nn.3901

Pajarillo, E., Rizor, A., Lee, J., Aschner, M., and Lee, E. (2019). The role of astrocytic glutamate transporters GLT-1 and GLAST in neurological disorders: potential targets for neurotherapeutics. *Neuropharmacology* 161, 107559. doi: 10.1016/j.neuropharm.2019.03.002

Petr, G. T., Sun, Y., Frederick, N. M., Zhou, Y., Dhamne, S. C., Hameed, M. Q., et al. (2015). Conditional deletion of the glutamate transporter GLT-1 reveals that astrocytic GLT-1 protects against fatal epilepsy while neuronal GLT-1 contributes significantly to glutamate uptake into synaptosomes. *J. Neurosci.* 35, 5187–5201. doi: 10.1523/JNEUROSCI.4255-14.2015

Plosker, G. L., and Lyseng-Williamson, K. A. (2005). Memantine: a pharmacoeconomic review of its use in moderate-to-severe Alzheimer's disease. *Pharmacoeconomics* 23, 193–206. doi: 10.2165/00019053-200523020-00010

Poirel, O., Mella, S., Videau, C., Ramet, L., Davoli, M. A., Herzog, E., et al. (2018). Moderate decline in select synaptic markers in the prefrontal cortex (BA9) of patients with Alzheimer's disease at various cognitive stages. *Sci. Rep.* 8, 938. doi: 10.1038/s41598-018-19154-y

Pow, D. V., and Cook, D. G. (2009). Neuronal expression of splice variants of "glial" glutamate transporters in brains afflicted by Alzheimer's disease: unmasking an intrinsic neuronal property. *Neurochem. Res.* 34, 1748–1757. doi: 10.1007/s11064-009-9957-0

Procter, A. W., Palmer, A. M., Francis, P. T., Lowe, S. L., Neary, D., Murphy, E., et al. (1988). Evidence of glutamatergic denervation and possible abnormal metabolism in Alzheimer's disease. *J. Neurochem.* 50, 790–802. doi: 10.1111/j.1471-4159.1988.tb02983.x

Revi, M. (2020). Alzheimer's disease therapeutic approaches. *Adv. Exp. Med. Biol.* 1195, 105–116. doi: 10.1007/978-3-030-32633-3_15

Rimmele, T. S., and Rosenberg, P. A. (2016). GLT-1: the elusive presynaptic glutamate transporter. *Neurochem. Int.* 98, 19–28. doi: 10.1016/j.neuint.2016.04.010

Roberts, R. C., Roche, J. K., and Mccullumsmith, R. E. (2014). Localization of excitatory amino acid transporters EAAT1 and EAAT2 in human postmortem cortex: a light and electron microscopic study. *Neuroscience* 277, 522–540. doi: 10.1016/j.neuroscience.2014.07.019

Rothstein, J. D., Martin, L. J., and Kuncl, R. W. (1992). Decreased glutamate transport by the brain and spinal cord in amyotrophic lateral sclerosis. *N. Engl. J. Med.* 326, 1464–1468. doi: 10.1056/NEJM199205283262204

Sasaki, K., Shimura, H., Itaya, M., Tanaka, R., Mori, H., Mizuno, Y., et al. (2009). Excitatory amino acid transporter 2 associates with phosphorylated tau and is localized in neurofibrillary tangles of tauopathic brains. *FEBS Lett.* 583, 2194–2200. doi: 10.1016/j.febslet.2009.06.015

Scimemi, A., Meabon, J. S., Woltjer, R. L., Sullivan, J. M., Diamond, J. S., and Cook, D. G. (2013). Amyloid-beta1-42 slows clearance of synaptically released glutamate by mislocalizing astrocytic GLT-1. *J. Neurosci.* 33, 5312–5318. doi: 10.1523/JNEUROSCI.5274-12.2013

Scott, H. A., Gebhardt, F. M., Mitrovic, A. D., Vandenberg, R. J., and Dodd, P. R. (2011). Glutamate transporter variants reduce glutamate uptake in Alzheimer's disease. *Neurobiol. Aging* 32, 553.e1–553.e11. doi: 10.1016/j.neurobiolaging.2010.03.008

Šerý, O., Povová, J., Míšek, I., Pešák, L., and Janout, V. (2013). Review paperMolecular mechanisms of neuropathological changes in Alzheimer's disease: a review. *Folia Neuropathol.* 51, 1–9. doi: 10.5114/fn.2013.34190

Sharma, A., Kazim, S. F., Larson, C. S., Ramakrishnan, A., Gray, J. D., McEwen, B. S., et al. (2019). Divergent roles of astrocytic versus neuronal EAAT2 deficiency on cognition and overlap with aging and Alzheimer's molecular signatures. *Proc. Natl. Acad. Sci. U.S.A.* 116, 21800–21811. doi: 10.1073/pnas.1903566116

Sheldon, A. L., and Robinson, M. B. (2007). The role of glutamate transporters in neurodegenerative diseases and potential opportunities for intervention. *Neurochem. Int.* 51, 333–355. doi: 10.1016/j.neuint.2007.03.012

Simpson, J. E., Ince, P. G., Lace, G., Forster, G., Shaw, P. J., Matthews, F., et al. (2010). Astrocyte phenotype in relation to Alzheimer-type pathology in the ageing brain. *Neurobiol. Aging* 31, 578–590. doi: 10.1016/j.neurobiolaging.2008.05.015

Takahashi, K., Kong, Q., Lin, Y., Stouffer, N., Schulte, D. A., Lai, L., et al. (2015). Restored glial glutamate transporter EAAT2 function as a potential therapeutic approach for Alzheimer's disease. *J. Exp. Med.* 212, 319–332. doi: 10.1084/jem.20140413

Thai, D. R. (2002). Excitatory amino acid transporter EAAT-2 in tangle-bearing neurons in Alzheimer's disease. *Brain Pathol.* 12, 405–411. doi: 10.1111/j.1750-3639.2002.tb00457.x

Thal, D. R., Papassotiropoulos, A., Saido, T. C., Griffin, W. S., Mrak, R. E., Kölsch, H., et al. (2010). Capillary cerebral amyloid angiopathy identifies a distinct APOE epsilon4-associated subtype of sporadic Alzheimer's disease. *Acta Neuropathol.* 120, 169–183. doi: 10.1007/s00401-010-0707-9

Tian, G., Kong, Q., Lai, L., Ray-Chaudhury, A., and Lin, C. L. (2010). Increased expression of cholesterol 24S-hydroxylase results in disruption of glial glutamate transporter EAAT2 association with lipid rafts: a potential role in Alzheimer's disease. *J. Neurochem.* 113, 978–989. doi: 10.1111/j.1471-4159.2010.06661.x

Tolar, M., Abushakra, S., and Sabbagh, M. (2019). The path forward in Alzheimer's disease therapeutics: reevaluating the amyloid cascade hypothesis. *Alzheimer's Dement.* 16, 1553–1560. doi: 10.1016/j.jalz.2019.09.075

Wang, R., and Reddy, P. H. (2017). Role of glutamate and NMDA receptors in Alzheimer's disease. *J. Alzheimers. Dis.* 57, 1041–1048. doi: 10.3233/JAD-160763

Woltjer, R. L., Duerson, K., Fullmer, J. M., Mookherjee, P., Ryan, A. M., Montine, T. J., et al. (2010). Aberrant detergent-insoluble excitatory amino acid transporter 2 accumulates in Alzheimer disease. *J. Neuropathol. Exp. Neurol.* 69, 667–676. doi: 10.1097/NEN.0b013e3181e24adb

Yeung, J. H. Y., Palpagama, T. H., Wood, O. W. G., Turner, C., Waldvogel, H. J., Faull, R. L. M., et al. (2021). EAAT2 expression in the hippocampus, subiculum, entorhinal cortex and superior temporal gyrus in Alzheimer's disease. *Front. Cell. Neurosci.* 15, 702824. doi: 10.3389/fncel.2021.702824

Zoia, C., Cogliati, T., Tagliabue, E., Cavaletti, G., Sala, G., Galimberti, G., et al. (2004). Glutamate transporters in platelets: EAAT1 decrease in aging and in Alzheimer's disease. *Neurobiol. Aging* 25, 149–157. doi: 10.1016/S0197-4580(03)00085-X

Zoia, C. P., Riva, C., Isella, V., Proserpio, P., Terruzzi, A., Arban, S., et al. (2011). Nonfibrillar Abeta 1–42 inhibits glutamate uptake and phosphorylates p38 in human fibroblasts. *Alzheimer Dis. Assoc. Disord.* 25, 1641172. doi: 10.1097/WAD.0b013e3181f9860f

Zumkehr, J., Rodriguez-Ortiz, C. J., Cheng, D., Kieu, Z., Wai, T., Hawkins, C., et al. (2015). Ceftriaxone ameliorates tau pathology and cognitive decline *via* restoration of glial glutamate transporter in a mouse model of Alzheimer's disease. *Neurobiol. Aging* 36, 2260–2271. doi: 10.1016/j.neurobiolaging.2015.04.005

frontiers | Frontiers in Neuroscience

TYPE Original Research
PUBLISHED 16 August 2022
DOI 10.3389/fnins.2022.954332

OPEN ACCESS

EDITED BY
Fernando Peña-Ortega,
National Autonomous University of Mexico, Mexico

REVIEWED BY
Antonio Suppa,
Sapienza University of Rome, Italy
Pavel Ernesto Rueda-Orozco,
National Autonomous University of Mexico, Mexico

*CORRESPONDENCE
Jun Chen
whuchenjun@163.com

†These authors have contributed equally to this work and share first authorship

SPECIALTY SECTION
This article was submitted to Neurodegeneration, a section of the journal Frontiers in Neuroscience

RECEIVED 27 May 2022
ACCEPTED 22 July 2022
PUBLISHED 16 August 2022

CITATION
Cheng Y, Yang H, Liu WV, Wen Z and Chen J (2022) Alterations of brain activity in multiple system atrophy patients with freezing of gait: A resting-state fMRI study. *Front. Neurosci.* 16:954332. doi: 10.3389/fnins.2022.954332

Alterations of brain activity in multiple system atrophy patients with freezing of gait: A resting-state fMRI study

Yilin Cheng[1†], Huaguang Yang[1†], Weiyin Vivian Liu[2], Zhi Wen[1] and Jun Chen[1*]

[1]Department of Radiology, Renmin Hospital of Wuhan University, Wuhan, China, [2]MR Research, GE Healthcare, Beijing, China

Background: Freezing of gait (FOG) in multiple system atrophy (MSA) is characterized by a higher risk of falls and a reduced quality of life; however, the mechanisms underlying these effects have yet to be identified by neuroimaging. The aim of this study was to investigate the differences in functional network when compared between MSA patients with and without freezing.

Methods: Degree centrality (DC) based on the resting-state functional magnetic resonance imaging was computed in 65 patients with MSA and 36 healthy controls. Brain regions with statistically different DC values between groups were selected as seed points for a second seed-based functional connectivity (FC) analysis. The relationships between brain activity (DC and FC alterations) and the severity of freezing symptoms were then investigated in the two groups of patients with MSA.

Results: Compared to MSA patients without FOG symptoms (MSA-nFOG), patients with MSA-FOG showed an increased DC in the left middle temporal gyrus but a reduced DC in the right superior pole temporal gyrus, left anterior cingulum cortex, left thalamus, and right middle frontal gyrus. Furthermore, in patients with MSA-FOG, the DC in the left thalamus was negatively correlated with FOG scores. Using the left thalamus as a seed, secondary seed-based functional connectivity analysis revealed that patients with MSA-FOG commonly showed the left thalamus-based FC abnormalities in regions related to cognition and emotion. In contrast to the patients with MSA-nFOG, patients with MSA-FOG showed an increased FC between the left thalamus and the left middle temporal gyrus (MTG), right inferior parietal lobule (IPL), bilateral cerebellum_8, and left precuneus.

Conclusion: Freezing of gait is associated with centrality of the impaired thalamus network. Abnormal FC between the thalamus and left MTG, right IPL, bilateral cerebellum_8, and left precuneus was involved in FOG. These results provide new insight into the pathophysiological mechanism of FOG in MSA.

KEYWORDS

multiple system atrophy, freezing of gait, degree centrality, functional connectivity, fMRI

Introduction

Multiple system atrophy (MSA) is a sporadic and progressive neurodegenerative disease that is manifested by prominent autonomic nerve function symptoms such as urinary retention and orthostatic hypotension (Fanciulli et al., 2019). Freezing of gait (FOG) is a debilitating symptom defined as a brief, episodic absence or marked reduction in forward progression of the feet despite the intention to walk (Nutt et al., 2011). Epidemiological studies have shown that approximately 76% of patients with MSA experience a frozen gait, thus leading to an increased risk of fall and a reduced quality of life (Gurevich and Giladi, 2003). Although the incidence of MSA with frozen symptoms gradually increases with disease progression, not all patients with MSA develop FOG (Factor, 2008). Therefore, identifying FOG-driven alterations in the associated pathophysiological mechanism may help to provide a better understanding of this disabling symptom and help clinicians to provide appropriate interventions.

Functional magnetic resonance imaging (fMRI) techniques appear to be ideally suited to investigate the neuropathology of FOG. It was previously found that regional homogeneity values in the left supplementary motor area and the left superior frontal region were significantly reduced in patients with Parkinson's disease (PD) and FOG when compared to PD patients without FOG (Zhou et al., 2018). Patients with PD-FOG showed wider alterations in the resting-state network than patients with non-FOG; furthermore, freezing severity was modulated by the left superior temporal gyrus in patients with PD (Liu et al., 2019). Patients with PD-FOG also showed more significant reductions in the volume of the cortical gray matter in the parietal lobe and subcortical caudate areas (Kostic et al., 2012; Herman et al., 2014) and increased damage in the white matter of the corticopontine-cerebellar pathways (Wang et al., 2016) than PD patients without FOG. Taken together, these data indicate that structural integrity and the potential functional disconnection of cortical regions and the subcortical nucleus are related to FOG in PD. However, FOG symptoms are more common in patients with MSA than in patients with PD (Factor, 2008). To date, such investigations have not been conducted in patients with MSA.

To explore the impairments in the functional network of MSA patients with FOG symptoms, we first used data-driven research methods to analyze DC to detect the hub alteration in the FOG-associated network in patients with MSA. The advantage of this strategy is to avoid bias caused by seed point selection. In the second step, we used a secondary seed-based functional connection method to select altered DC brain areas as seeds to investigate the cortical hub-based circuit in the regulation of FOG in patients with MSA from point to surface. We hypothesized that patients with MSA-FOG would have impairments in cortical and subcortical structure and function and that these impairments would reflect the severity of FOG in patients with MSA. By selecting these brain regions as seed points, we further hypothesized that these specific brain regions would be used mainly to cooperate or antagonize the abnormalities of other brain networks participating in the regulation of FOG symptoms in patients with MSA.

Materials and methods

Subjects

In total, 65 patients with MSA and 36 healthy controls (HCs) were recruited from the Department of Neurology at Renmin Hospital of Wuhan University. All participants were Han Chinese and right-handed. The inclusion criteria were patients who were diagnosed with probable or possible MSA (H-Y stage score $\leq$ 4, Mini-Mental State Examination, MMSE score $\geq$ 25) by a movement disorder specialist according to the 2008 Second Edition MSA Diagnostic Criteria (Gilman et al., 2008). Patients were excluded if they had a history of other neurological diseases or any predominant physical diseases. This study, involving human participants, was reviewed and approved by the Renmin Hospital of Wuhan University Ethics Committee. The patients provided their written informed consent to participate in this study.

All patients experienced a 12-h drug washout before examination (clinical motor and non-motor scale evaluation and MRI scans). MSA disease severity and stage was scored using the Unified Multiple System Atrophy Rating Scale III (UMSARS III) and the Hoehn and Yahr (H-Y) stage, respectively. Global cognitive function and mood of the patients with MSA were assessed by the Mini-Mental State Examination (MMSE), and the 24-item Hamilton Depression Rating Scale (HAMD-24), respectively.

Freezing episodes were observed by experienced neurologists during hospital visits, self-reported by patients, or described by their caregivers. Patients were diagnosed as the so-called freezers who had a positive FOG according to items 1 and 3 on the FOG questionnaire (FOG-Q) (Giladi et al., 2009). If the patients, or their family members, could not understand the definition of FOG, a description or a possible FOG subtype was determined by neurologists during hospital visits. According to the FOG-Q scale, there were 36 patients with MSA-FOG and 29 MSA patients without FOG (MSA-nFOG). Patients with MSA were follow-up patients who were taking levodopa drugs and were classified as the "OFF-FOG" group.

MRI acquisition

All subjects underwent an MRI examination with a 3T MRI scanner (GE Discovery MR750W; GE Healthcare, United States) using a 16-channel head coil. Participants completed a high-resolution, three-dimensional, sagittal magnetization gradient echo imaging sequence (3D-T1) with the following acquisition parameters: repetition time/echo time = 8.5/3.3, matrix = 256 × 256, flip angle = 12°, voxel size = 1.0 mm × 1.0 mm × 1.0 mm, slice thickness = 1 mm without slice gap, FOV = 256 mm^2 × 256 mm^2, and slice number = 180. The participants also received a blood oxygen level-dependent (BOLD) sequence scan using the following parameters: repetition time = 2,000 ms, echo time = 25 ms, flip angle = 90°, slice number = 40, slice thickness = 3 mm without slice gap, FOV = 240 mm × 240 mm, matrix size = 64 × 64, and voxel size = 3 mm × 3 mm × 3 mm.

Degree centrality and functional connectivity analysis

Degree centrality analysis

Resting-state functional MRI data processing and analysis were performed using DPABI software (Data Processing and Analysis for Brain Imaging, version 6.0[1]). The first 10 time points were discarded due to non-homogeneity of magnetic resonance field strength and a noise adaptation period for subjects. The remaining images were slice timed and realigned; subjects with head movement greater than 0 mm or 2.5° in any direction were excluded from subsequent analysis. The remaining data were then normalized into a Montreal Neurological Institute template standard space of 3 mm^3 × 3 mm^3 × 3 mm^3 (DARTEL technique) (Ashburner, 2007). For the regression of nuisance covariates, we applied Friston-24 parameters and removed signals from the white matter and cerebrospinal fluid. Subsequently, linear trends were removed and band-pass filtered (0.01–0.08 Hz). Any volume with a frame-wise displacement value exceeding 0.5 images was excluded to remove nuisance covariate effects.

DPABI software was used to analyze the non-smoothened and preprocessed fMRI data, so that we could calculate density correlations. Pearson's correlation method was utilized to correlate the time series of each voxel and those of all other voxels to create a whole brain DC map and obtain the connection matrix of correlation coefficients for the whole brain. $R > 0.25$ was selected as the threshold value to eliminate low time correlations caused by signal noise (Wang et al., 2018; Yang et al., 2020). Then, 6 mm × 6 mm × 6 mm full width at half maximum Gaussian kernels were used to spatially smoothen all individual zDC maps. Only positively weighted Pearson's correlation coefficients were considered as the number of functional connections at the individual level because of the uncertainty arising when interpreting negative values.

Secondary seed-based functional connectivity analysis

For seed-based FC calculation, the preprocessed image was further smoothened with a 6 mm^3 Gaussian kernel. We selected significant DC alterations associated with the FOG-Q scale as hubs between the MSA-FOG and patients with MSA-nFOG. Specifically, we extracted the reference time series from the DC results by averaging the time series of every voxel in seed regions and conducted further correlation analyses between the time courses and time series of voxels inside and outside of the seed regions in the entire brain. The correlation coefficients were then converted into *Z*-values using Fisher's r-to-z transformation. In addition, we further analyzed the FC map of the spherical region within a 3-mm radius that covered the peak group difference between DC values to eliminate seed selection-related influences (refer to **supplementary material 1**).

Statistical analysis

Statistical Package for the Social Sciences (SPSS) version 22.0 software (SPSS Inc., Chicago, IL, United States) was

1 www.restfmri.net

used to compare demographic and clinical variables between groups. Demographic data were presented as mean ± standard deviation (SD) for continuous variables. The independent sample *t*-test and Kruskal–Wallis test, or analysis of variance (ANOVA) followed by Tukey's test for normally distributed data or the Bonferroni test for non-normally distributed data, were used for cross-group comparisons of quantitative variables. The chi-squared test was used to compare categorical variables. We set the threshold at $p < 0.05$ for the level of significance.

The SPM statistical analysis module was used for neuroimaging data. One-way ANOVA was used to identify DC differences among the MSA-FOG, MSA-nFOG, and HC groups by controlling confounding factors including age, gender, MMSE, Unified Multiple System Atrophy Rating Scale (UMSARS), and HAMD score covariates; then, significant different brain areas were extracted as a mask. Next, *post hoc* and multiple comparison corrections (FDR correction, $p < 0.05$) were performed to identify the differences between groups within the masks and in the whole brain.

To identify the relationship between brain activity and the severity of FOG, Pearson's correlation was computed between the DC values and FOGQ scores. Brain regions with significantly different FOG-related DC values were selected as seeds for a secondary seed-based FC analysis.

Results

Clinical and neuropsychological characteristics

The demographic and clinical characteristics of the MSA-FOG, MSA-nFOG, and HC groups are shown in Table 1. There were no significant differences between the three groups in terms of age, gender, education, and MMSE scores. Furthermore, there were no significant differences between the MSA-FOG and MSA-nFOG groups with regard to clinical subtypes, H-Y grade, and the UMSARS score.

Degree centrality analysis

Compared to the HC group, the MSA-FOG group showed an increased DC in the left inferior, middle and superior temporal gyrus, the left middle occipital gyrus, and the left hippocampus but a reduced DC in the right inferior orbit frontal gyrus, right superior temporal gyrus, right anterior cingulum cortex, and right medial frontal gyrus. The patients with MSA-nFOG had an increased DC in the cerebellum vermis IV/V and left middle temporal gyrus but a reduced DC in the right inferior orbit frontal gyrus and bilateral middle orbit frontal gyrus. Compared to the MSA-nFOG group, the MSA-FOG group showed an increased DC in the left middle temporal gyrus but a decreased DC in the right superior pole temporal gyrus, left anterior cingulum cortex, left thalamus, and right middle frontal gyrus (Figure 1 and Table 2).

Seed-based functional connectivity analysis

Compared to the HC group, the MSA-FOG group showed a decreased thalamus-based FC in the bilateral MTG, right hippocampus, right insula, right inferior frontal cortex, and right calcarine. In contrast, the MSA-nFOG group showed a decreased thalamus-based FC in the inferior and middle temporal gyrus. Direct comparison of the MSA-FOG and MSA-nFOG groups revealed thalamus-based FC in the left middle temporal gyrus, right inferior parietal lobule, bilateral cerebellum_8, and the left precuneus (Figures 2, 3 and Table 3).

TABLE 1 Demographic and clinical characteristics.

Characteristics (mean ± SD)	Control ($n = 36$)	MSA-FOG ($n = 36$)	MSA-nFOG ($n = 29$)	F/χ^2	*P*-value
Age (years)	63.25 ± 3.34	64.50 ± 7.31	62.83 ± 8.32	0.59	0.56
Gender (male, female)	22:14	16:20	15:14	1.20	0.28
Education	11.72 ± 2.74	10.14 ± 3.08	10.48 ± 3.78	2.43	0.09
Disease duration	N	4.17 ± 1.96	2.67 ± 1.32	2.32	0.13
UMSARS score	N	37.51 ± 14.10	29.67 ± 15.91	0.67	0.42
Hoehn and Yahr	N	2.94 ± 0.98	2.40 ± 0.76	0.80	0.38
LEED (mg/day)	N	548.60 ± 308.14	403.02 ± 230.45	2.43	0.12
Clinical phenotype (P/C)	N	16:20	16:13	2.04	0.36
MMSE score	28.67 ± 1.07	28.31 ± 0.92	28.52 ± 1.09	1.13	0.328
HAMD-24 score	1.69 ± 2.35	2.50 ± 1.82	2.21 ± 1.50	1.57	0.214

SD, standard deviation; MSA, multiple system atrophy; MSA-FOG, multiple system atrophy with freezing of gait symptoms; MSA-nFOG, multiple system atrophy without freezing of gait symptoms; HCs, healthy controls; UMSARS, Unified Multiple System Atrophy Rating Scale; LEED, levodopa equivalent dose; P/C, Parkinson's type/cerebellar type; MMSE, Mini-Mental State Examination; HAMD-24, 24 items Hamilton Depression Scale; $p < 0.05$ was considered statistically significant.

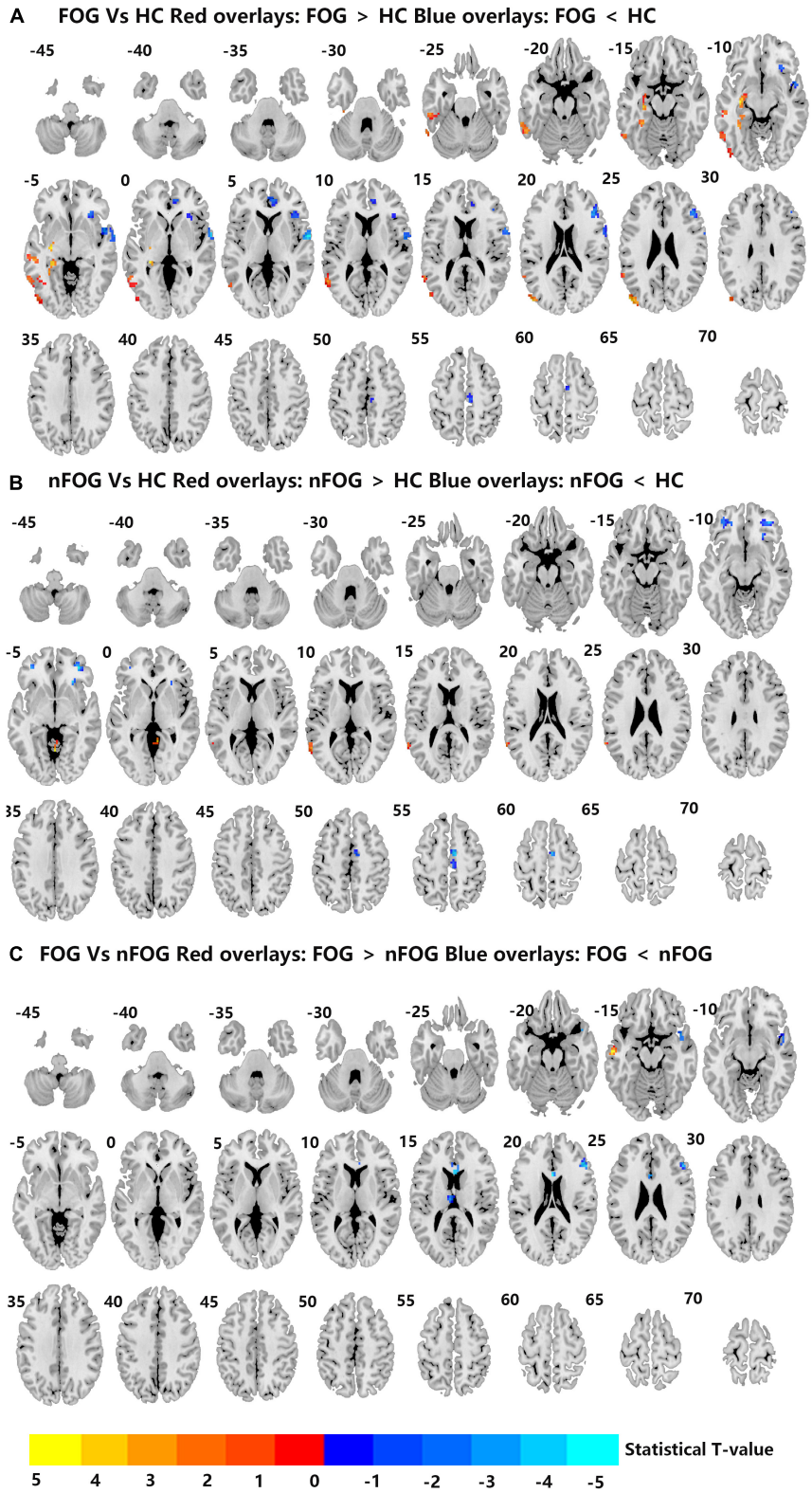

FIGURE 1
(A–C) Differences in degree centrality among the MSA-FOG, MSA-nFOG, and HC groups. The threshold value was set as an FDR-corrected $p < 0.05$. MSA-FOG, multiple system atrophy with freezing of gait; MSA-nFOG, multiple system atrophy without freezing of gait symptoms; HCs, healthy controls.

Correlation between degree centrality and seed-based functional connectivity changes with depression scores in the multiple system atrophy group

Cerebral areas of the zDC results between the MSA-FOG group and MSA-nFOG group were used to conduct correlation analysis; only the left thalamus zDC was shown to be related to the clinical FOGQ score (**Figure 2**). Then, using the left thalamus as a seed, we identified brain regions showing FC alterations between the MSA-FOG group and the MSA-nFOG group; none of the resulting areas (left middle temporary gyrus, right inferior parietal lobe, bilateral cerebellum_8, and left precuneus) were significantly correlated with FOGQ scores (**Figure 2**).

Discussion

Freezing of gait is a common and disabling symptom in patients with MSA (Gurevich and Giladi, 2003). As the first step in our study, DC values were used to identify the differences of hubs in resting-state fMRI among patients with MSA-FOG, patients with MSA-nFOG, and HCs. Then, in the second stage, differences in ROI-based FC in patients with MSA with FOG were used to detect DC alterations. DC values were found to vary more widely in patients with MSA-FOG than patients with MSA-nFOG; significantly reduced DC values were detected in the thalamus of patients with MSA-FOG when compared to the MSA-nFOG and HC groups. Furthermore, the mean zDC values for the thalamus were negatively correlated with FOGQ scores. In addition, thalamus-dominated FC analyses indicated that increased thalamus-based FC, including the bilateral cerebellum_8, the right IPL, and the left MTG could provide new insight into the thalamus-dominated pathophysiological mechanism underlying FOG in MSA.

Of the areas showing alterations in DC, only the left thalamus was identified to be positively correlated with the severity of FOG; other DCs showing intergroup differences between the MSA-FOG and MSA-nFOG groups were not correlated with FOGQ scores. These results suggested that the disruption of DC in the thalamus was involved in the pathophysiological mechanism underlying FOG and may serve as a potential neuroimaging marker. In fact, by connecting with

TABLE 2 Brain area differences in degree centrality between patients with MSA and HC.

Brain regions	Hem	Cluster	BA	Peak MNI co-ordinate			*T*-value
				X	*y*	*Z*	
MSA-FOG vs. HC							
Inferior temporal gyrus	L	39	20	−54	−27	−30	4.10
Middle temporal gyrus	L	179	21	−63	−54	12	3.89
Hippocampus	L	47	37	−30	−33	−3	4.55
Superior temporal gyrus	L	20	NA	51	9	−6	−4.27
Inferior orbit frontal gyrus	R	37	47	27	27	−6	−4.14
Superior temporal gyrus	R	93	48	63	0	3	−5.74
Anterior cingulum cortex	R	36	10	9	45	3	−4.10
Middle occipital gyrus	L	46	NA	−48	−81	24	4.21
Medial frontal gyrus	R	23	6	6	−9	60	−3.45
MSA-nFOG vs. HC							
Inferior orbit frontal gyrus	R	22	47	27	27	−6	−4.04
Middle orbit frontal gyrus	L	25	47	−36	45	−6	−3.74
Middle orbit frontal gyrus	R	28	47	36	45	−6	−4.47
Cerebellum Vermis IV and V	NA	21	NA	0	−60	6	3.62
Middle temporal gyrus	L	28	37	−60	−57	9	3.19
MSA-FOG vs. MSA-n FOG							
Superior pole temporal gyrus	R	25	48	48	6	−12	−3.59
Middle temporal gyrus	L	19	21	−60	−12	−15	3.87
Anterior cingulum cortex	L	35	NA	0	18	18	−3.87
Thalamus	L	20	NA	−6	−15	15	−3.31
Middle frontal gyrus	R	25	45	48	27	21	−3.66

A negative *T*-value represents decreased degree in MSA group. MSA-FOG, MSA-nFOG, multiple system atrophy patients with and without freezing of gait symptoms. BA, Brodmann area. L, R, left and right.

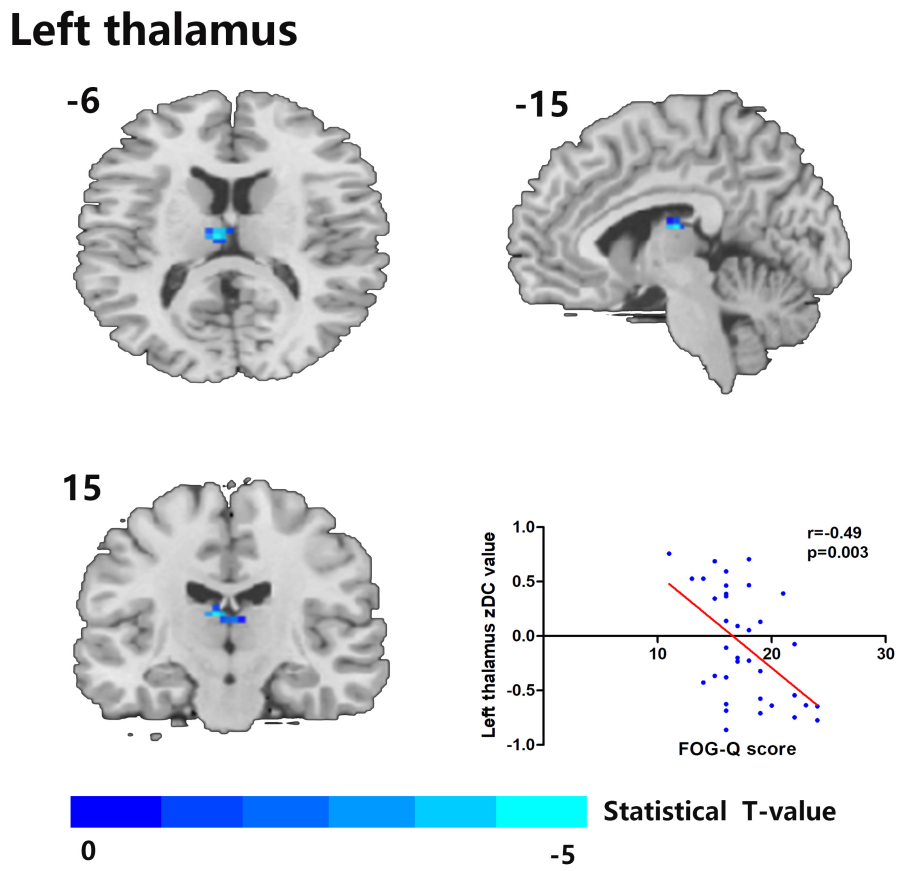

FIGURE 2
The left thalamus was the only degree centrality (DC)-altered brain area in correlation with FOG-Q scores between MSA-FOG and MSA-nFOG groups. Scatter plot showed a negative correlation between FOG-Q scores and the left thalamus zDC values in patients with MSA-FOG.

the basal ganglia, the cerebellum, and the cortex, the thalamus participates in feedback and feed-forward mechanisms and plays a modulatory role in the integration of information across the parallel motor, cognitive and limbic circuits (Alexander et al., 1986; Haber and McFarland, 2001; Borra et al., 2015; Quartarone et al., 2020). Our results further highlight the importance of the thalamus in MSA patients with FOG symptoms. From the perspective of transmitter disorder, this is easy to explain; on the one hand, normal postural function depends in part on the ability of the postural control system to integrate visual, proprioceptive, and vestibular sensory information. The degeneration of cholinergic neurons in the brainstem pedunculopontine nucleus complex and their thalamic efferent terminals can directly cause postural control deficits (which will induce FOG or fall symptoms) in both PD and MSA diseases (Gilman et al., 2010; Bohnen et al., 2019; Wilson et al., 2021). On the other hand, supported by findings that dopamine therapy is a protective factor in patients with MSA (Yang et al., 2022), we hypothesize that a reduction in dopamine availability or effectiveness in patients with both PD and MSA results in reduced inhibitory action in the thalamic nuclei that trigger thalamo-striatal feedback or thalamo-cortical feed-forward mechanisms during the augmentation of motor output and the indirect induction of FOG symptoms (Nanda et al., 2009), which can be proved by the fact that striatal dopaminergic denervation is critical in the pathophysiology of FOG in MSA, given that it occurs most frequently when patients are in the OFF state and all patients recruited in this study belong to dopamine-responsive FOG variations. Of course, the present fMRI study only indicated that thalamic DC alterations were involved in the regulation of FOG symptoms in patients with MSA. Whether this process involves a disorder in the cholinergic neurons or dopamine transmitter function needs further PET-specific transport receptor research.

It is worth noting that patients with MSA-P and MSA-C subtypes (MSA Parkinsonian and the cerebellar variant) were included in this study. The incidence of FOG was almost equal in the MSA-P and MSA-C subtypes in our study; this finding is inconsistent with previous studies, which found that thalamic injury was more significant in patients with MSA-P (Minnerop et al., 2007; Campabadal et al., 2022; Yang et al., 2022). Furthermore, we found no significant difference between the

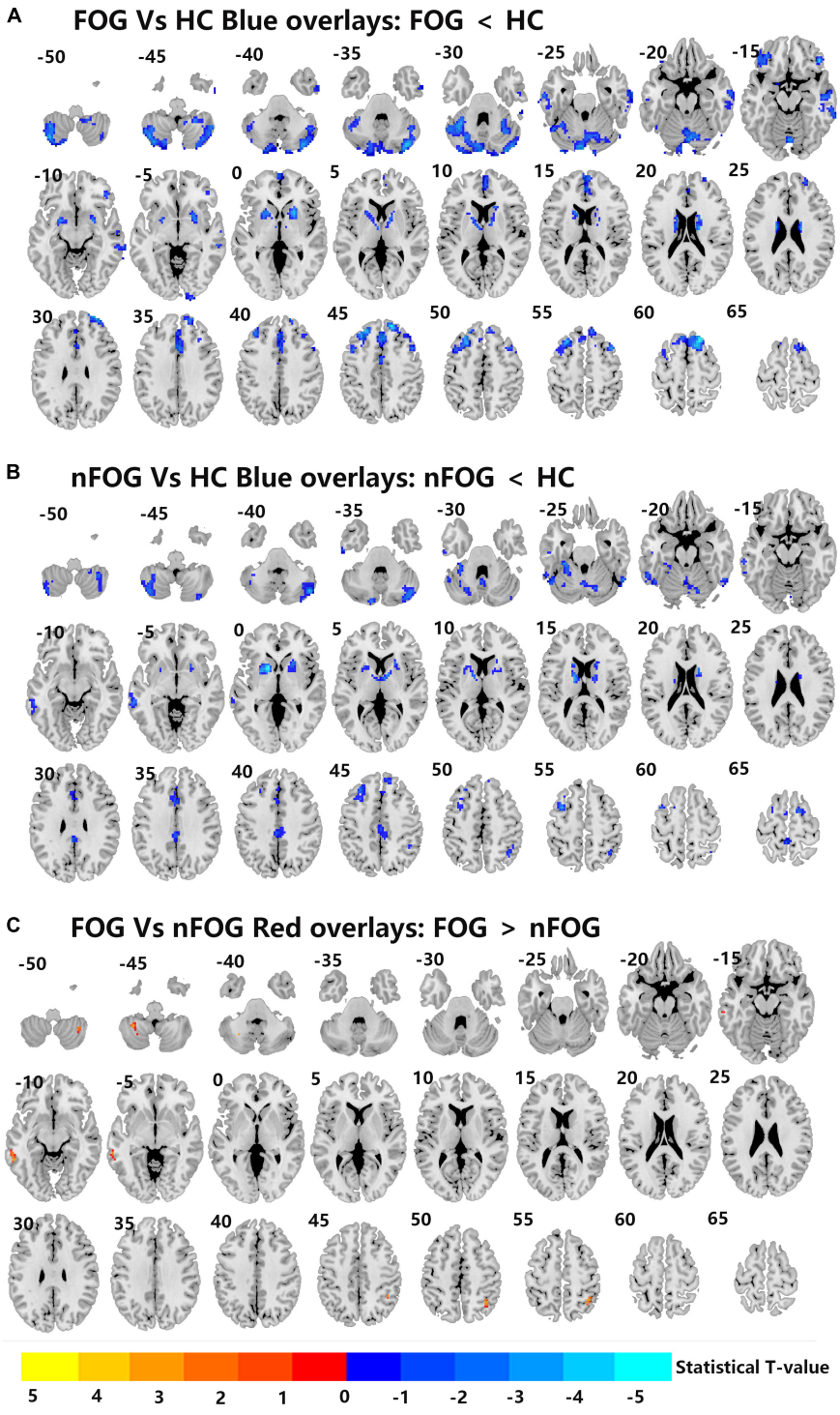

FIGURE 3
(A–C) Differences in left thalamus dominated FC among MSA-FOG, MSA-nFOG, and HCs using *post hoc* correction for two-sample *t*-test (FDR-corrected $p = 0.05$).

two subtypes in terms of non-motor symptoms and autonomic nervous function symptoms or when compared between the presence and absence of FOG symptoms. Although MSA-P and MSA-C subtypes were characterized by impairments in the supratentorial basal ganglia and infratentorial cerebellum, respectively, both MSA variants showed dysfunction in the

thalamus and cerebellum (Minnerop et al., 2007; Dash et al., 2019); therefore, any dysfunction in the cerebellar-thalamo-cortical (CTC) or striatal-thalamo-cortical (STC) circuits in patients with MSA would be expected to lead to the onset of FOG; this possibility requires further investigation.

Compared to the patients with MSA-nFOG, the patients with MSA-FOG showed a decreased FC between the thalamus and the bilateral cerebellum. Abnormal cerebellar processing is expected to reflect FOG symptoms in patients with MSA. The cerebellar processing of proprioceptive information is important in the regulation of ongoing movements and the maintenance of a stable gait (Takakusaki, 2008). The most consistent finding arising from studies of MSA is damage to the cerebellar structure. Previous studies found that cerebellar injury is a clear risk factor for FOG symptoms in patients with MSA (Gurevich and Giladi, 2003) and that the cerebellar locomotor region is responsible for FOG-like symptoms (Fasano et al., 2017). In this study, we first revealed FOG symptoms in patients with MSA by the application of neuroimaging techniques despite indirect focus on the cerebellum; our findings were consistent with previous studies, thus suggesting that the cerebellum could play an important role in the neural mechanisms underlying FOG symptoms in patients with MSA. In addition, increased FC between the thalamus and cerebellum may imply a compensatory role through the CTC circuits in patients with MSA-FOG. Unfortunately, our correlation

TABLE 3 Brain area differences in right thalamus dominated FC network between patients with MSA and HC.

Brain regions	Hem	Cluster	BA	Peak MNI co-ordinate			*T*-value
				x	*y*	*Z*	
MSA-FOG vs. HC							
Cerebellum crus2	L	1536	NA	42	−78	−33	−5.56
Cerebellum_8	R	60	NA	9	−48	−48	−4.66
Inferior temporal gyrus	R	39	NA	57	−3	−42	−4.13
Inferior temporal gyrus	L	33	20	−60	−12	−24	−4.03
Middle temporal gyrus	R	189	20	63	−33	−12	−4.67
Inferior frontal gyrus	L	63	11	−30	42	−15	−4.65
Putamen	L	152	48	−24	3	−9	−5.01
Medial frontal gyrus	R	116	NA	0	63	18	−4.85
Putamen	R	159	11	21	12	−3	−5.41
Superior frontal gyrus	R	643	8	18	27	60	−5.94
MSA-nFOG vs. HC							
Cerebellum_Crus2	L	121	NA	−39	−72	−48	−4.92
Cerebellum_8	R	69	NA	33	−48	−54	−5.93
Cerebellum_Crus2	R	126	NA	45	−69	−39	−5.83
Inferior temporal gyrus	L	23	20	−57	−15	−33	−4.58
Cerebellum_6	L	95	NA	−30	−33	−24	−5.29
Cerebellum_6	R	65	NA	15	−66	−24	−4.80
Inferior temporal gyrus	R	30	37	57	−54	−24	−4.89
Middle temporal gyrus	L	72	21	−63	−36	−6	−4.80
Putamen	L	291	NA	−15	9	0	−6.75
Middle cingulum cortex	L	110	23	−3	−30	36	−4.57
Middle frontal gyrus	L	61	9	−30	30	45	−5.06
Inferior parietal lobule	R	30	40	39	−54	51	−4.63
Precuneus	L	28	5	−3	−39	66	−4.69
Superior frontal gyrus	R	30	6	18	−3	69	−4.80
MSA-FOG vs. MSA-nFOG							
Middle temporal gyrus	L	40	20	−57	−45	−9	3.50
Inferior parietal lobule	R	29	40	39	−54	51	3.54
Cerebellum_8	R	19	NA	39	−48	−57	4.00
Cerebellum_8	L	21	NA	−33	−48	−45	3.48
Precuneus	L	19	5	−6	−42	60	3.28

A negative *T*-value represents decreased right thalamus dominated FC in MSA group. MSA-FOG, MSA-nFOG, multiple system atrophy patients with and without freezing of gait symptoms; BA, Brodmann area; L, R, left and right.

analysis did not detect a reduction in the cerebellar ZFC value in relation to FOG score. Future studies should involve a larger number of patients and directly compare the changes in cerebellar structure and function between FOG and patients with nFOG; such analysis should identify specific neuroimaging mechanisms in the cerebellum of patients with MSA.

In addition to the thalamus and cerebellum, when compared to patients with MSA-nFOG, the patients with MSA-FOG also showed DC abnormalities in the right superior pole temporal gyrus, left middle temporal gyrus, left anterior cingulum cortex right, inferior orbit frontal gyrus, and the right middle frontal gyrus, as well as thalamus-based FC dysfunction in the left middle temporal gyrus, right inferior parietal lobule, and left precuneus. Both the inferior orbit frontal gyrus and the superior/middle temporal gyrus are known to be more engaged in non-motor (memory and emotional) processing, whereas the middle frontal gyrus, the cingulum cortex, and the inferior parietal lobule belong to the node of default-mode network (DMN). Our current findings add to the body of the literature that supports the fact that the regulation of FOG in patients with MSA depends on non-motor circuits. It is worth noting that patients with MSA-FOG showed reduced DC in the thalamus but an increase in the FC between the thalamus and non-motor cortex, although no specific correlation was detected between the non-motor cortex and clinical FOGQ scores. We hypothesize that the purpose of the increased thalamus-nonmotor circuit FC was to overcome the reduced level of processing in the depleted sensorimotor circuits. Over time, it is likely that altered processing in these compensatory circuits predisposes them for gait breakdown and the onset of FOG.

There were limitations in our study that need to be considered. First, despite a 12 h washout before the scan, the influence of the medication used cannot be fully excluded; the specific effect of levodopa on MSA and the effects of residual dopamine on FOG remain unknown (Nonnekes et al., 2020). Second, as described in the previous studies (Wang et al., 2018; Yang et al., 2020), we only used $r > 0.25$ as a threshold in our study when calculating DC. In the future studies, we aim to include other thresholds for comparison; this may help us to eliminate the influence of methodological choice on experimental results. Third, the clinical symptoms of patients with MSA and patients with spinocerebellar ataxia partially overlap; therefore, to avoid the impact of misdiagnosis on our experimental results, we conducted a series of spinocerebellar ataxia 1, 2, 3, 6, and 7 gene tests (the most common subtypes in the Chinese population) (Wang et al., 2010), and the lack of detection for other genetic subtypes has had an inevitable effect on FOG research in patients with MSA. Comprehensive genetic testing is recommended in the future studies to rule out confounding diseases, such as hereditary and subacute diseases combined with degeneration of the spinal cord. Fourth, the thalamus of each hemisphere can be subdivided into 15 subregions. Each thalamic subregion participates in different functional processes, either individually or collaboratively. Thus, considering the overall functional changes may not reveal panoramic information relating to specific thalamic nuclei; this is a notable limitation of this study. Multicenter prospective cohort studies and longer follow-ups of FOG symptoms might overcome these limitations.

Conclusion

In this RS-fMRI study, we showed that the thalamus is the hub region for DC alterations in FOG-associated MSA. Behavioral associations and thalamocortical connectivity suggested that the non-motor circuit played a compensatory role in MSA. These findings provide neuroimaging evidence for a better clinical understanding of non-pure depression and may help us to develop new therapeutic strategies.

Data availability statement

The raw dataset is not publicly available due to the inherently identifiable nature of the data. Requests to access the datasets should be directed to YC, Elim2501436@163.com.

Ethics statement

The studies involving human participants were reviewed and approved by the Renmin Hospital of Wuhan University Ethics Committee. The patients/participants provided their written informed consent to participate in this study.

Author contributions

YC, HY, and JC conceived the study. YC, HY, and ZW collected and analyzed the data. WVL contributed to the writing – review and language polishment. JC revised the article and finally approved the version to be submitted. All authors read and approved the final manuscript.

Acknowledgments

We thank all the participants and their families.

Conflict of interest

WVL is an employee of GE Healthcare, Beijing.

The remaining authors declare that the research was conducted in the absence of any commercial or financial relationships that could be construed as a potential conflict of interest.

Publisher's note

All claims expressed in this article are solely those of the authors and do not necessarily represent those of their affiliated organizations, or those of the publisher, the editors and the reviewers. Any product that may be evaluated in this article, or claim that may be made by its manufacturer, is not guaranteed or endorsed by the publisher.

Supplementary material

The Supplementary Material for this article can be found online at: https://www.frontiersin.org/articles/10.3389/fnins.2022.954332/full#supplementary-material

References

Alexander, G. E., DeLong, M. R., and Strick, P. L. (1986). Parallel organization of functionally segregated circuits linking basal ganglia and cortex. *Ann. Rev. Neurosci.* 9, 357–381. doi: 10.1146/annurev.ne.09.030186.002041

Ashburner, J. (2007). A fast diffeomorphic image registration algorithm. *Neuroimage* 38, 95–113. doi: 10.1016/j.neuroimage.2007.07.007

Bohnen, N. I., Kanel, P., Zhou, Z., Koeppe, R. A., Frey, K. A., Dauer, W. T., et al. (2019). Cholinergic system changes of falls and freezing of gait in Parkinson's disease. *Ann. Neurol.* 85, 538–549. doi: 10.1002/ana.25430

Borra, E., Gerbella, M., Rozzi, S., and Luppino, G. (2015). Projections from caudal ventrolateral prefrontal areas to brainstem preoculomotor structures and to basal ganglia and cerebellar oculomotor loops in the macaque. *Cereb Cortex* 25, 748–764. doi: 10.1093/cercor/bht265

Campabadal, A., Abos, A., Segura, B., Monte-Rubio, G., Perez-Soriano, A., Giraldo, D. M., et al. (2022). Differentiation of multiple system atrophy subtypes by gray matter atrophy. *J. Neuro.* 32, 80–89. doi: 10.1111/jon.12927

Dash, S. K., Stezin, A., Takalkar, T., George, L., Kamble, N. L., Netravathi, M., et al. (2019). Abnormalities of white and grey matter in early multiple system atrophy: Comparison of parkinsonian and cerebellar variants. *Eur. Radiol.* 29, 716–724. doi: 10.1007/s00330-018-5594-9

Factor, S. A. (2008). The clinical spectrum of freezing of gait in atypical parkinsonism. *Mov. Dis.* 23, S431–S438. doi: 10.1002/mds.21849

Fanciulli, A., Stankovic, I., Krismer, F., Seppi, K., Levin, J., and Wenning, G. K. (2019). Multiple system atrophy. *Int. Rev. Neurobiol.* 149, 137–192. doi: 10.1016/bs.irn.2019.10.004

Fasano, A., Laganiere, S. E., Lam, S., and Fox, M. D. (2017). Lesions causing freezing of gait localize to a cerebellar functional network. *Ann. Neurol.* 81, 129–141. doi: 10.1002/ana.24845

Giladi, N., Tal, J., Azulay, T., Rascol, O., Brooks, D. J., Melamed, E., et al. (2009). Validation of the freezing of gait questionnaire in patients with Parkinson's disease. *Mov. Dis.* 24, 655–661. doi: 10.1002/mds.21745

Gilman, S., Koeppe, R. A., Nan, B., Wang, C. N., Wang, X., Junck, L., et al. (2010). Cerebral cortical and subcortical cholinergic deficits in parkinsonian syndromes. *Neurology* 74, 1416–1423. doi: 10.1212/WNL.0b013e3181dc1a55

Gilman, S., Wenning, G. K., Low, P. A., Brooks, D. J., Mathias, C. J., Trojanowski, J. Q., et al. (2008). Second consensus statement on the diagnosis of multiple system atrophy. *Neurology* 71, 670–676. doi: 10.1212/01.wnl.0000324625.00404.15

Gurevich, T., and Giladi, N. (2003). Freezing of gait in multiple system atrophy (MSA). *Parkinsonism Relat. Dis.* 9, 169–174. doi: 10.1016/s1353-8020(02)00049-4

Haber, S., and McFarland, N. R. (2001). The place of the thalamus in frontal cortical-basal ganglia circuits. *Neuroscientist* 7, 315–324. doi: 10.1177/107385840100700408

Herman, T., Rosenberg-Katz, K., Jacob, Y., Giladi, N., and Hausdorff, J. M. (2014). Gray matter atrophy and freezing of gait in Parkinson's disease: Is the evidence black-on-white? *Mov. Dis.* 29, 134–139. doi: 10.1002/mds.25697

Kostic, V. S., Agosta, F., Pievani, M., Stefanova, E., Jecmenica-Lukic, M., Scarale, A., et al. (2012). Pattern of brain tissue loss associated with freezing of gait in Parkinson disease. *Neurology* 78, 409–416. doi: 10.1212/WNL.0b013e318245d23c

Liu, Y., Li, M., Chen, H., Wei, X., Hu, G., Yu, S., et al. (2019). Alterations of regional homogeneity in Parkinson's disease patients with freezing of gait: A resting-state fMRI study. *Front. Aging Neurosci.* 11:276. doi: 10.3389/fnagi.2019.00276

Minnerop, M., Specht, K., Ruhlmann, J., Schimke, N., Abele, M., Weyer, A., et al. (2007). Voxel-based morphometry and voxel-based relaxometry in multiple system atrophy-a comparison between clinical subtypes and correlations with clinical parameters. *Neuroimage* 36, 1086–1095. doi: 10.1016/j.neuroimage.2007.04.028

Nanda, B., Galvan, A., Smith, Y., and Wichmann, T. (2009). Effects of stimulation of the centromedian nucleus of the thalamus on the activity of striatal cells in awake rhesus monkeys. *Eur. J. Neurosci.* 29, 588–598. doi: 10.1111/j.1460-9568.2008.06598.x

Nonnekes, J., Bereau, M., and Bloem, B. R. (2020). Freezing of gait and its levodopa paradox. *JAMA Neurol.* 77, 287–288. doi: 10.1001/jamaneurol.2019.4006

Nutt, J. G., Bloem, B. R., Giladi, N., Hallett, M., Horak, F. B., and Nieuwboer, A. (2011). Freezing of gait: moving forward on a mysterious clinical phenomenon. *Lancet Neurol.* 10, 734–744. doi: 10.1016/S1474-4422(11)70143-0

Quartarone, A., Cacciola, A., Milardi, D., Ghilardi, M. F., Calamuneri, A., Chillemi, G., et al. (2020). New insights into cortico-basal-cerebellar connectome: clinical and physiological considerations. *Brain* 143, 396–406. doi: 10.1093/brain/awz310

Takakusaki, K. (2008). Forebrain control of locomotor behaviors. *Brain Res. Rev.* 57, 192–198. doi: 10.1016/j.brainresrev.2007.06.024

Wang, H., Chen, H., Wu, J., Tao, L., Pang, Y., Gu, M., et al. (2018). Altered resting-state voxel-level whole-brain functional connectivity in depressed Parkinson's disease. *Parkinsonism Relat. Dis.* 50, 74–80. doi: 10.1016/j.parkreldis.2018.02.019

Wang, J. L., Wu, Y. Q., Lei, L. F., Shen, L., Jiang, H., Zhou, Y. F., et al. (2010). [Polynucleotide repeat expansion of nine spinocerebellar ataxia subtypes and dentatorubral-pallidoluysian atrophy in healthy Chinese han population]. *Zhonghua Yi Xue Yi Chuan Xue Za Zhi* 27, 501–505. doi: 10.3760/cma.j.issn.1003-9406.2010.05.006

Wang, M., Jiang, S., Yuan, Y., Zhang, L., Ding, J., Wang, J., et al. (2016). Alterations of functional and structural connectivity of freezing of gait in Parkinson's disease. *J. Neurol.* 263, 1583–1592. doi: 10.1007/s00415-016-8174-4

Wilson, J., Yarnall, A. J., Craig, C. E., Galna, B., Lord, S., Morris, R., et al. (2021). Cholinergic basal forebrain volumes predict gait decline in Parkinson's disease. *Mov. Dis.* 36, 611–621. doi: 10.1002/mds.28453

Yang, H., Liu, W. V., Wang, S., Yang, W., Liu, C., Wen, Z., et al. (2022). Freezing of gait in multiple system atrophy. *Front. Aging Neurosci.* 14:287. doi: 10.3389/fnagi.2022.833287

Yang, H., Luo, X., Yu, H., Guo, M., Cao, C., Li, Y., et al. (2020). Altered resting-state voxel-level whole-brain functional connectivity in multiple system atrophy patients with cognitive impairment. *Clin. Neurophys.* 131, 54–62. doi: 10.1016/j.clinph.2019.09.026

Zhou, C., Zhong, X., Yang, Y., Yang, W., Wang, L., Zhang, Y., et al. (2018). Alterations of regional homogeneity in freezing of gait in Parkinson's disease. *J. Neurol. Sci.* 387, 54–59. doi: 10.1016/j.jns.2018.01.021

frontiers | Frontiers in Neuroscience

TYPE Original Research
PUBLISHED 14 September 2022
DOI 10.3389/fnins.2022.948523

OPEN ACCESS

EDITED BY
Nicola B. Mercuri,
University of Rome "Tor Vergata", Italy

REVIEWED BY
Giuseppe Sancesario,
University of Rome "Tor Vergata", Italy
Salvatore Galati,
Istituto di Neuroscienze Cliniche della Svizzera Italiana, Switzerland

*CORRESPONDENCE
Asheeta A. Prasad
asheeta.prasad@unsw.edu.au

†These authors share senior authorship

SPECIALTY SECTION
This article was submitted to Neurodegeneration, a section of the journal Frontiers in Neuroscience

RECEIVED 20 May 2022
ACCEPTED 01 August 2022
PUBLISHED 14 September 2022

CITATION
Mazumder S, Bahar AY, Shepherd CE and Prasad AA (2022) Post-mortem brain histological examination in the substantia nigra and subthalamic nucleus in Parkinson's disease following deep brain stimulation. *Front. Neurosci.* 16:948523. doi: 10.3389/fnins.2022.948523

Post-mortem brain histological examination in the substantia nigra and subthalamic nucleus in Parkinson's disease following deep brain stimulation

Srestha Mazumder[1], Anita Y. Bahar[2], Claire E. Shepherd[2,3†] and Asheeta A. Prasad[1,4*†]

[1]School of Psychology, University of New South Wales, Sydney, NSW, Australia, [2]Neuroscience Research Australia, Sydney, NSW, Australia, [3]School of Medicine, University of New South Wales, Sydney, NSW, Australia, [4]School of Medical Sciences, Faculty of Medicine and Health, University of Sydney, Sydney, NSW, Australia

Parkinson's disease (PD) is a progressive neurodegenerative disorder, pathologically hallmarked by the loss of dopamine neurons in the substantia nigra (SN) and alpha-synuclein aggregation. Deep brain stimulation (DBS) of the subthalamic nucleus (STN) is a common target to treat the motor symptoms in PD. However, we have less understanding of the cellular changes in the STN during PD, and the impact of DBS on the STN and SN is limited. We examined cellular changes in the SN and STN in PD patients with and without STN-DBS treatment. Post-mortem brain tissues from 6 PD non-STN-DBS patients, 5 PD STN-DBS patients, and 6 age-matched controls were stained with markers for neurodegeneration (tyrosine hydroxylase, alpha-synuclein, and neuronal loss) and astrogliosis (glial fibrillary acidic protein). Changes were assessed using quantitative and semi-quantitative microscopy techniques. As expected, significant neuronal cell loss, alpha-synuclein pathology, and variable astrogliosis were observed in the SN in PD. No neuronal cell loss or astrogliosis was observed in the STN, although alpha-synuclein deposition was present in the STN in all PD cases. DBS did not alter neuronal loss, astrogliosis, or alpha-synuclein pathology in either the SN or STN. This study reports selective pathology in the STN with deposits of alpha-synuclein in the absence of significant neuronal cell loss or inflammation in PD. Despite being effective for the treatment of PD, this small post-mortem study suggests that DBS of the STN does not appear to modulate histological changes in astrogliosis or neuronal survival, suggesting that the therapeutic effects of DBS mechanism may transiently affect STN neural activity.

KEYWORDS

Parkinson's disease, deep brain stimulation, subthalamic nucleus, substantia nigra, alpha-synuclein

Introduction

First described over 200 years ago, Parkinson's disease (PD) is a neurodegenerative disorder characterized by debilitating tremor, rigidity, and bradykinesia (DeMaagd and Philip, 2015). PD is pathologically characterized at post-mortem by the abnormal deposition of alpha-synuclein in the form of Lewy bodies and Lewy neurites (Braak et al., 1999) that deposit in a progressive pattern throughout the brainstem, limbic, and neocortical brain regions (Braak et al., 2003). Increased neuroinflammation and neuronal cell loss are also prominent, particularly in the substantia nigra (SN) (Fearnley and Lees, 1991; Hardman et al., 1996; Hirsch et al., 2003). Currently, there are no treatments to halt or slow disease progression but deep brain stimulation (DBS) of the subthalamic nucleus (STN-DBS) is highly effective at relieving motor symptoms in PD (Limousin et al., 1995; Tagliati et al., 2010; Limousin and Foltynie, 2019; Jakobs et al., 2019). The irregular burst of neuronal firing in the STN in PD patients is destabilized by DBS (Bergman et al., 1994; Remple et al., 2011) but less is known about the STN pathology in PD or how this is impacted by DBS treatment.

Limited preclinical studies in rodents and non-human primates suggest that DBS may alter disease progression through a combination of neuroinflammatory and neurodegenerative changes (Temel et al., 2006; Wallace et al., 2007). Specifically, animal models show that STN-DBS decreases neuroinflammation expressed through microglia and astrocytes in the SN and slows down the loss of dopamine neurons (Charles et al., 2008; Spieles-Engemann et al., 2010; Tawfik et al., 2010; Vedam-Mai et al., 2012). However, there are only two post-mortem comparative neuropathology studies of PD patients with and without STN-DBS. Pal et al. (2017) carried out a semi-quantitative assessment of SN depigmentation and alpha-synuclein pathology and reported that STN-DBS subjects have higher alpha-synuclein density scores, but do not display differences in SN depigmentation. The study did not examine the STN and did not investigate changes in inflammation. In contrast, Pienaar et al. (2015) investigated microvascular integrity in PD patients with and without STN-DBS and reported significant vascular changes and lowered microglial activation following STN-DBS. Our study provides a quantitative analysis of cell loss, alpha-synuclein pathology, and inflammation in the STN and SN in PD cases with and without STN-DBS compared with controls.

Materials and methods

Cases

Formalin-fixed, paraffin-embedded 10 μm serial sections were obtained from the Sydney Brain Bank (SBB). Tissue was taken from the SN at the level of the red nucleus and at the most posterior level of the STN from 6 PD patients without DBS, 5 PD patients with STN-DBS, and 6 age-matched controls. The STN was delineated on an H&E-stained section as previously described in Pienaar et al. (2015). Briefly, the STN was identified as a compact nucleus located medial to the internal capsule and superolateral to the SN on coronal slices.

The research was carried out under UNSW Human Research Ethics Committee (HREC) approval (project no. HC180835). All PD cases met neuropathological criteria for PD with no coexisting disease (Dickson et al., 2009). PD STN-DBS cases were chosen on the basis of having an implanted electrode in the STN during life. All control subjects were free from neuropathological and clinical neurodegenerative or neuropsychiatric diseases.

Immunohistochemistry

Immunohistochemistry to detect astrocytes [anti-glial fibrillary acidic protein (GFAP)] and dopamine neurons (anti-TH) was carried out using the Novolink polymer detection system (Leica Biosystems #RE7150-K). Briefly, serial sections were deparaffinized in xylene and then rehydrated in serial ethanol dilutions. Sodium citrate buffer (0.1 M, pH 6) was used for antigen retrieval. Antigen retrieval was performed by placing the sections in boiling sodium citrate buffer for 3 min. Sections were then left to cool for 30 min before washing the slides in deionized water. Endogenous peroxide was neutralized using Novolink peroxide block for 5 min before the slides were washed in 0.1 M Tris-buffered saline (TBS, pH 7.3). Sections were then incubated for a further 5 min with Novolink protein block followed by three TBS washes. Primary antibodies anti-tyrosine hydroxylase (AB112, Abcam, 1:750) and anti-GFAP (AB7260, Abcam, 1:2,000) were diluted in TBS and added individually to sections placed in a humid box and incubated at 4°C overnight. On day 2, sections were washed in TBS before being incubated for 30 min in Novolink Polymer (Anti-rabbit Poly-HRP-IgG (<25 μg/ml) containing 10% (v/v) animal serum in TBS/0.09% ProClinTM 950) followed by TBS washes. Peroxide activity was developed using 3,3′-diaminobenzidine (DAB) working solution on all sections for 5 min followed by a rinse with tap water. Slides were then counterstained with hematoxylin for 3 min before a 5 min wash under running tap water. Prior to cover slipping, all sections were dehydrated in ethanol (70%, 95%, and 100%) before being placed in xylene. Sections were cover slipped with Entellan (ProSciTech, Kirwin, QLD, Australia).

Immunohistochemistry for alpha-synuclein was performed on a Discovery XT (Ventana Medical Systems Inc, Tucson, Arizona) autostainer using OmniMap and ChromoMap multimer technology detection systems. Antigen retrieval was performed for 30 min using cell conditioning 1 pretreatment solution before adding purified mouse anti-alpha-synuclein (610787, BD Biosciences-US, 1:7000). Slides were incubated

for 1 h prior to counterstaining with hematoxylin and cover slipping with Entellan.

Neurons in the STN and SN were identified with H&E stain. Sections were deparaffinized in xylene two times for 3 min followed by rehydration in 100% alcohol two times for 3 min. Sections were then transferred to 95% alcohol for 3 min followed by 70% alcohol for another 3 min before being placed into distilled water for 3 min. Sections were incubated in hematoxylin for 3 min followed by a rinse under running tap water. Sections were then incubated with lithium carbonate for 3 min and then washed under tap water. Eosin was added to the tissue section for 3 min before the slides were placed in 100% alcohol wash for 3 min two times followed by xylene for 3 min two times. Slides were then cover slipped with Entellan.

Quantitation

Slides were visualized on the Olympus BX51 microscope and captured using Zeiss AxioLab light microscope and software at 200× magnification. All assessments were performed by an investigator blinded to case details. Ten representative images were taken from one section per case, and from these, three images were chosen at random for quantitation. Immunoreactive cells were quantified using ImageJ.

In both the SN and STN, neurons were clearly identified by the presence of a clear cytoplasm and nucleolus. Tyrosine hydroxylase (TH) immunoreactivity was observed in the cell soma and proximal axon of neurons in the SN (Kordower et al., 2013). The number of neurons in each 200× field was counted, and the average was calculated.

Astrocytes were clearly identified by GFAP immunoreactivity in the cellular processes surrounding a nucleus. The total number of astrocytes in each 200× field was counted using ImageJ, and the average of the 3 fields was calculated.

Alpha-synuclein deposits were identified in the form of alpha-synuclein-positive Lewy bodies, Lewy neurites, and glial inclusion (Pal et al., 2017). ImageJ software was used to identify alpha-synuclein immunolabeling, and the average areal fraction of the 3 fields was calculated.

Statistics

IBM SPSS Statistics software 27 was used to carry out all statistical analyses. A power analysis was carried out using PASS software to calculate the sample size required to detect various effect sizes with 80% power. With groups of 5 cases, there was at least an 80% chance of detecting large differences (where mean differences were between 18 and 24 and standard deviations of less than 11). Non-parametric Kruskal–Wallis test statistics was used to assess differences between the three groups. Significance values were adjusted by the Bonferroni correction for multiple tests.

Results

Cases

Details of all cases, including age, gender, and disease duration, are provided in Table 1. All cases were matched for age (p = 0.17) and post-mortem delay (p = 0.69). Braak Lewy body stage (p = 0.89) and disease duration (p = 0.22) were not significantly different between PD and STN-DBS cases. These variables were therefore not considered further.

Analysis of cell loss and astrogliosis in the substantia nigra

Means and SEM of cellular counts are presented in Table 2. Compared with controls, both PD groups showed a significant decrease in total (PD no DBS p = 0.018, PD STN-DBS p = 0.009) and TH-positive neurons (PD no DBS p = 0.015, PD STN-DBS p = 0.011) in the SN with *no difference* between PD groups (total neurons p = 1.000, TH-positive neurons p = 1.000). There was a significant increase in the number of astrocytes in the PD group compared with controls (p = 0.028) but no significant increase in GFAP-positive astrocytes in STN-DBS compared with controls (p = 0.127) and no difference between PD and DBS group (p = 1.000) (Figures 1A,B).

Analysis of cell loss and inflammation in the subthalamic nucleus

In contrast to the SN, there was no significant difference in neuronal density (p = 0.358) or astrocytes (p = 0.612) in the STN between any groups (Table 2 and Figures 2A,B).

Alpha-synuclein pathology

Consistent with diagnosis, significantly greater alpha-synuclein pathology was seen in the SN of PD cases compared with controls (PD no DBS p = 0.008, PD STN-DBS p = 0.007,

TABLE 1 Demographic and clinical characteristics of all cases included.

Parameters	Control (n = 6)	PD (n = 6)	PD STN-DBS (n = 5)
Sex ratio (M:F)	6:0	6:0	3:2
Age at death (years)	81.33 ± 3.13	76.833 ± 1.86	74.40 ± 2.20
Disease duration (years)	N/A	14.667 ± 2.56	21.400 ± 2.83
Post-mortem delay (hours)	20.833 ± 3.84	16.167 ± 2.71	21.200 ± 5.68
Duration of STN-DBS (years)	N/A	N/A	10.2 ± 1.69
Braak Lewy body stage	N/A	V (4) VI (2)	V (3) VI (2)

Results are shown as the mean ± SEM. N/A, not applicable.

TABLE 2 Means and SEM of cellular analysis in substantia nigra (SN) and subthalamic nucleus (STN).

Brain region	Positive cell type	Control ($n = 6$)	PD ($n = 6$)	PD STN-DBS ($n = 5$)
Substantia nigra	Dopamine neurons (TH)	23.33 ± 2.69	7.50 ± 0.95*	6.60 ± 1.20*
	Cells (H&E)	27.72 ± 3.43	9.06 ± 0.96*	7.67 ± 1.48*
	Astrocytes (GFAP)	22.67 ± 2.46	38.39 ± 4.8*	33.66 ± 3.54*
	Alpha-synuclein	0.00 ± 0.00	1.50 ± 0.22*	1.60 ± 0.24*
Subthalamic nucleus	Cells (H&E)	17.06 ± 3.96	11.50 ± 1.02	11.87 ± 2.45
	Astrocytes (GFAP)	32.86 ± 4.37	30.70 ± 1.10	29.60 ± 5.15
	Alpha-synuclein	0.00 ± 0.00	1.33 ± 0.21*	1.60 ± 0.24*

*$p < 0.05$ versus control.

Table 2) with no differences between PD groups ($p = 1.000$, Table 2 and Figures 3A,B). The majority of alpha-synuclein pathology was in the form of Lewy neurites with occasional Lewy bodies present in the SN (see Figure 3B). Alpha-synuclein was also significantly increased in the STN in PD cases compared with controls (PD no DBS $p = 0.013$, PD STN-DBS $p = 0.004$) with no difference between PD and DBS groups ($p = 1.000$). Alpha-synuclein was predominantly observed in the form of neurites and glial inclusions in the STN (Figure 3D), although occasional Lewy bodies and alpha-synuclein-positive neurons were also seen (Figure 3D inserts).

Discussion

This is the first study to carry out a quantitative assessment of cell loss, alpha-synuclein pathology, and inflammation in the SN and the STN of PD patients with and without STN-DBS. Consistent with diagnosis, our study confirms significant loss of total and TH-positive neurons (69% of dopamine and 70% of total cells lost) and an increase in alpha-synuclein in the SN in PD. In contrast, despite the presence of significant alpha-synuclein pathology, we did not observe any loss of neurons or astrogliosis in the STN of our PD cases. Importantly, no loss of total or dopaminergic neurons, or changes in astrogliosis or alpha-synuclein deposition were observed following DBS, suggesting that STN-DBS may not exert its therapeutic effect *via* changes in neuronal loss, astrogliosis, or alpha-synuclein.

Our findings do not support previous animal studies showing that DBS may alter disease progression through decreased neuroinflammation and reduced dopamine cell loss (Wallace et al., 2007; Charles et al., 2008; Spieles-Engemann et al., 2010; Tawfik et al., 2010). Rather, they are consistent with human imaging studies showing that striatal dopamine levels are not affected following STN-DBS (Hilker et al., 2003; Strafella et al., 2003; Thobois et al., 2003). Although there are limited human brain tissue studies examining cellular changes following STN-DBS, one study has demonstrated neurogenesis in the subventricular zone, suggesting that DBS may be capable of increasing cellular plasticity even at sites remote from the electrode location (Vedam-Mai et al., 2014). Neuroprotective molecules such as BDNF have also been shown to be upregulated in the rodent basal ganglia post-DBS (Fischer et al., 2017; Fischer and Sortwell, 2018). Although our studies suggest that this is unlikely to prevent neuronal cell death in the human SN, an elegant study using optogenetics to elucidate the target cell types underlying DBS suggests that the therapeutic effects can be accounted for by selective stimulation of afferent axons, indicating that disruption of circuit loops could represent a common pathway for treatment (Gradinaru et al., 2009). Indeed, clinical studies show a significant increase in motor dysfunction with overnight "off" STN-DBS conditions compared with "on" state (Kojovic et al., 2019). A single pulse of STN-DBS has been recorded between 1 and 400 ms after stimulation (Baker et al., 2002), indicating DBS is linked to short-term changes in electrophysiological activity. In PD patients, electrophysiological recording show signature enhanced neural firing in the STN (Hammond et al., 2007) which is reduced by DBS (Eusebio et al., 2011). These studies and the findings from our histological analysis indicate that the therapeutic effects of DBS are transient and most likely occur through "inhibition," "excitation," or "disruption" of the cortico-basal ganglia loop (Chiken and Nambu, 2016).

Although gliosis is a normal response to brain injury and is commonly observed in neurodegenerative disorders such as Alzheimer's disease, reports of astrogliosis in the SN of PD patients are conflicting (Urbanc et al., 2002). Indeed, some post-mortem studies have reported mild increases in GFAP-positive astrocytes in the SN in PD (Mirza et al., 2000; McGeer and McGeer, 2008), while others have reported that the number and morphology of astrocytes remain unchanged (Knott et al., 1999; Tong et al., 2015). While our study did identify an increase in astrogliosis in the SN of our non-DBS PD cases, no significant change was seen in the SN of the STN-DBS cases, and no astrogliosis was present in the STN of either PD group, despite significant alpha-synuclein deposition. This is interesting, as primate studies suggest that DBS reduces glutamate toxicity (Wallace et al., 2007) and/or astrocyte-mediated abolition of spontaneous spindle oscillations (Hardman et al., 1996, 1997; Temel et al., 2006; Wallace et al., 2007) and may lower neuroinflammation. Recent studies also suggest that there is a relationship between astrocytic dysfunction and alpha-synuclein accumulation in PD (Tong et al., 2015) but this was certainly not observed in the STN in our study. It is clear that the role of astrocytes in PD is likely highly complex, and changes in astrocyte function are not easily captured using generic markers such as GFAP. Indeed, A1 astrocytes have been shown to be neurotoxic in PD (Hendrickx et al., 2017) and are involved in an

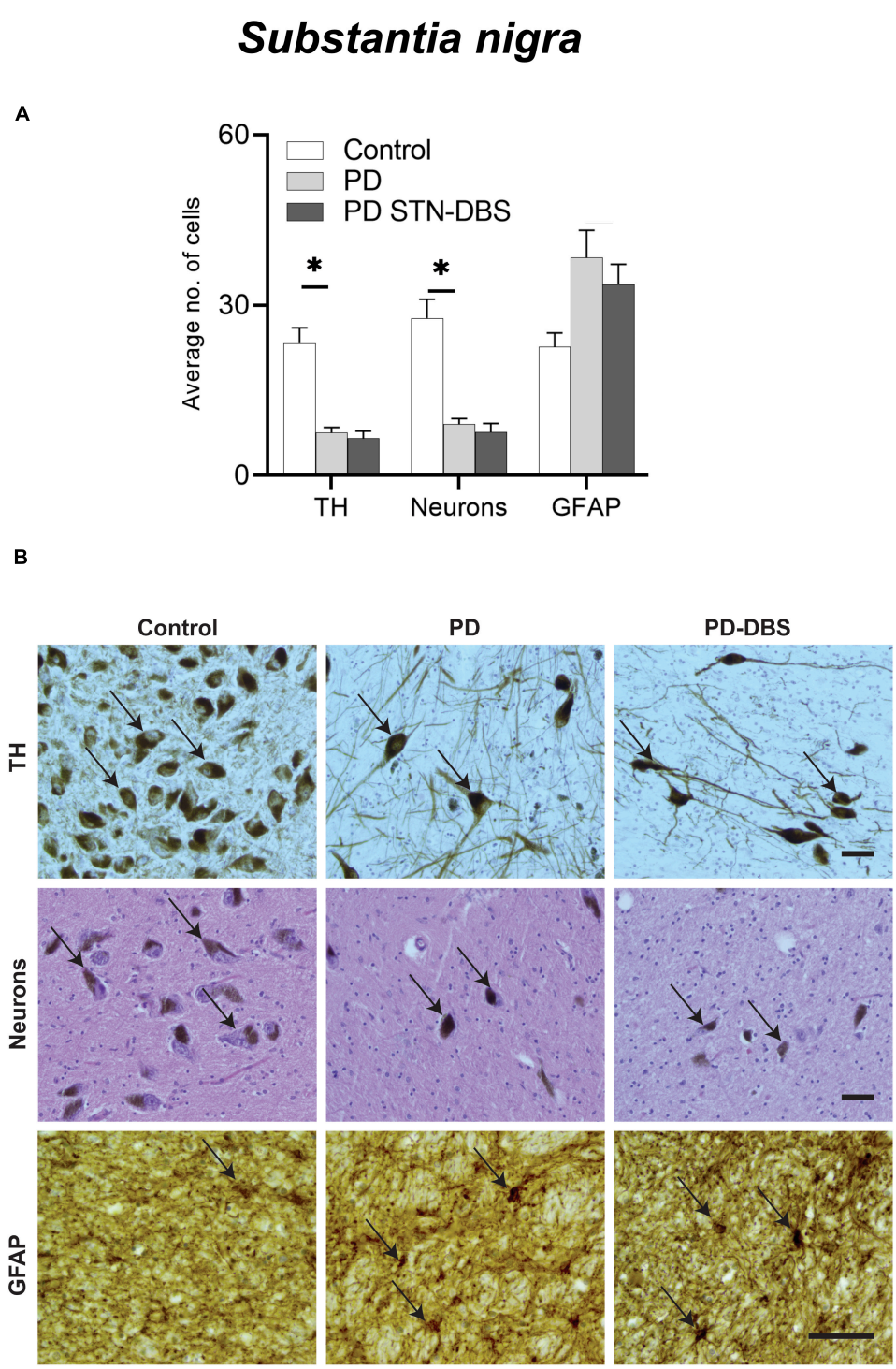

FIGURE 1
Quantitation of neuronal loss and astrogliosis in the substantia nigra (SN) of control, Parkinson's disease (PD) and PD STN-DBS cases. **(A)** Significant differences between control and PD cases were observed in neuronal loss ($p < 0.018$), TH neurons ($p < 0.015$), and astrogliosis (GFAP: $p = 0.028$). Comparison of PD patients with STN-DBS and PD patients without STN-DBS showed no differences in neuronal loss ($p = 1.000$), TH neurons ($p = 1.000$), or inflammatory marker (GFAP: $p = 1.000$). **(B)** Representative photomicrographs of TH (black arrows showing dopamine neurons), neuronal density identified by hematoxylin and eosin (black arrows showing H&E stained neurons), GFAP (black arrow showing astrocyte) in control, PD, and PD STN-DBS in the SN. All images were taken at 200× magnification. All values are expressed as mean ± SEM. * Indicates $p < 0.050$. Scale bar = 50 microns.

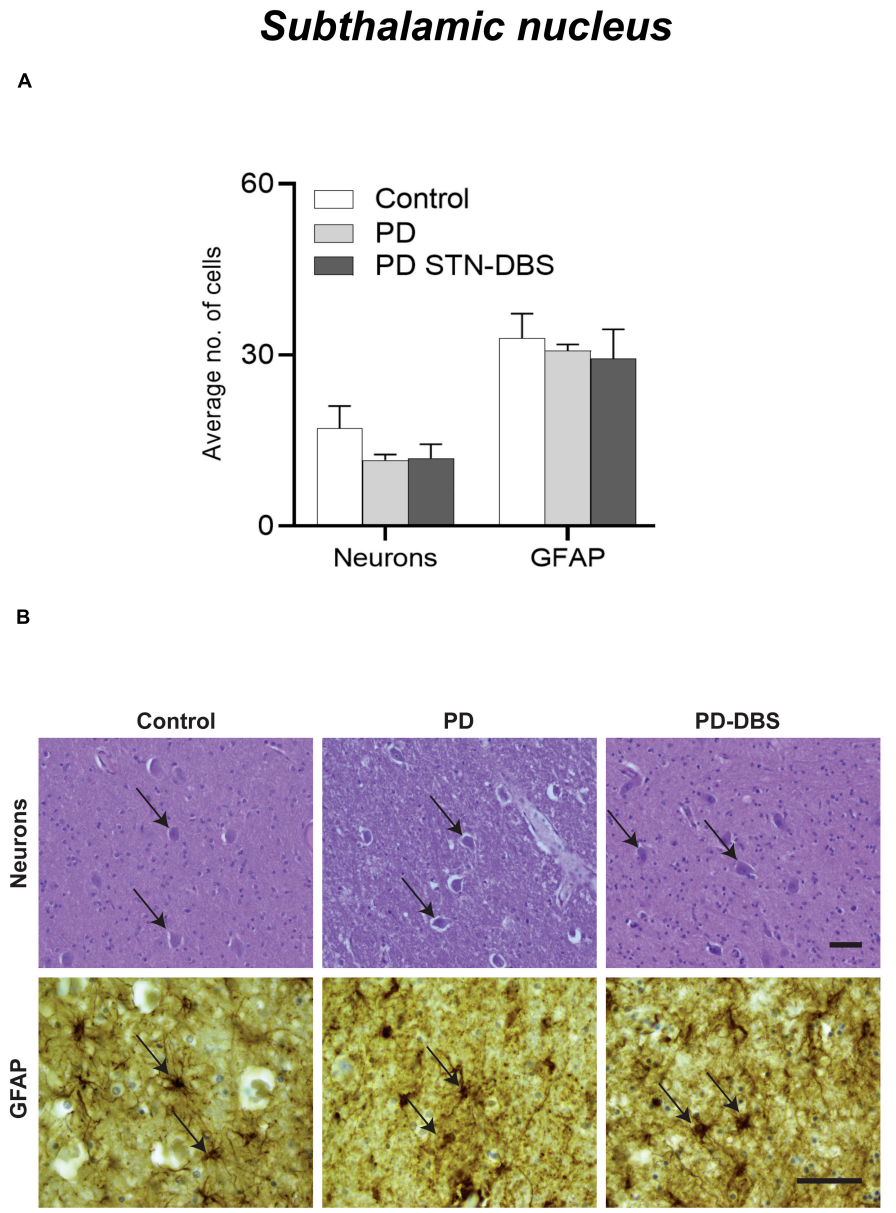

FIGURE 2
Quantitation of neuronal loss and astrogliosis in the subthalamic nucleus (STN) of control, Parkinson's disease (PD) and PD STN-DBS cases. **(A)** Between control and PD patients no significant difference was observed in neuronal (p = 0.358) or inflammatory marker (GFAP: p = 0.612). **(B)** Representative photomicrographs of neuronal density (black arrow showing H&E stained neuron), GFAP (black arrow showing astrocyte) in control, PD, and PD STN-DBS patients in the STN. All values are expressed as mean ± SEM. Scale bar = 50 microns.

intimate relationship with microglia to control the inflammatory response (Röhl and Sievers, 2005; Jo et al., 2017; Liddelow et al., 2017). To determine whether STN-DBS exerts a therapeutic effect *via* modulating neuroinflammation, future studies should utilize glial markers that recognize the morphologically and functionally diverse states of both astrocytes and microglia. Analysis of inflammatory cytokines and chemokines would also be informative. Although these studies would require access to frozen brain tissue, which is seldom available from DBS cases due to the need for whole brain fixation to delineate the electrode tract and termination point.

In contrast to Pal et al. (2017), we did not observe an increase in alpha-synuclein pathology in the SN following STN-DBS. Although differences in the methods of analysis and cohort size may explain the discrepancy between these studies, differences in the methods used for alpha-synuclein detection may also be relevant. Indeed, Pal et al. (2017) used Thioflavin S staining to identify Lewy bodies within the SN, whereas we carried out

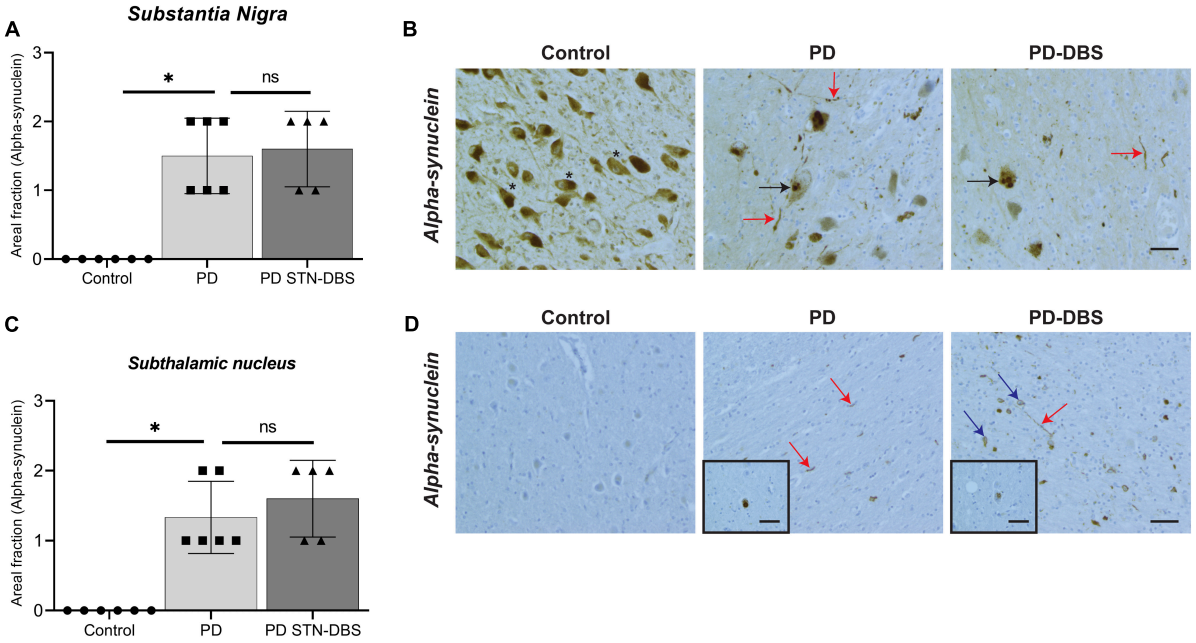

FIGURE 3
Quantitation of alpha-synuclein pathology in the substantia nigra (SN) and subthalamic nucleus (STN) of control, Parkinson's disease (PD) and PD STN-DBS cases. **(A)** No alpha-synuclein pathology was seen in the SN control cases. Alpha-synuclein pathology was significantly higher in PD (p = 0.008) and STN-DBS cases (p = 0.007). No changes in alpha-synuclein expression were seen in the SN in PD and STN-DBS patients (p = 1.000). **(B)** Asterisks indicate pigmented neurons in the SN. Both Lewy bodies (black arrows) and Lewy neurites (red arrows) were observed in the SN PD and Deep brain stimulation (DBS) cases. **(C)** In the control cases, no alpha-synuclein was present in the STN. Alpha-synuclein aggregates were significantly higher in PD (p = 0.013) and STN-DBS (p = 0.004) compared to controls with no differences between PD and STN-DBS cases (p = 1.000). **(D)** Lewy neurites (red arrows) and Lewy bodies (blue arrows) were observed in the STN in all PD cases (inserts in D). Occasional Lewy bodies and alpha-synuclein positive neurons were also seen (D inserts). All values are expressed as mean ± SEM. Scale bar = 50 microns.

alpha-synuclein immunohistochemistry on a Ventana stainer (see Section "Materials and methods"), which is considered the gold standard for Lewy body and Lewy neurite detection (Beach et al., 2008). Alpha-synuclein pathology in the STN has not been well investigated in PD with or without DBS. However, our findings are consistent with a previous case study that reported Lewy body formation in the STN in a PD case without DBS (Ohama and Ikuta, 1976). Most of the alpha-synuclein pathology we observed was in the form of Lewy neurites, although occasional Lewy bodies and neuronal cytoplasmic staining were seen (see **Figure 3**), which may also be attributable to the sensitive methods of immunohistochemical detection that were used in this study. Lewy neurites in axons appear prior to Lewy bodies and represent some of the earliest pathology seen in the PD brainstem (Braak et al., 1999, 2003). The predominance of Lewy neurites in PD cases both with and without DBS in the absence of significant neuronal loss suggests that the STN is affected later in the disease process as it may be more resistant to neurodegeneration in PD.

A significant limitation of this study is the number of cases that were available for analysis. However, access to well-characterized brain tissue from PD cases with DBS is limited, and we utilized all of the available cases in the SBB. While we could have increased the number of PD and control cases examined, we do not believe this would significantly impact our results as our observations in the PD without DBS and control cases were representative of findings from previous studies (Pienaar et al., 2015).

In conclusion, our findings demonstrate no significant effect of DBS on total or dopaminergic cell loss, alpha-synuclein pathology, or astrogliosis in the SN and STN. The absence of neuronal loss is consistent with other clinical and imaging studies indicating that STN-DBS may not be neuroprotective and most likely has a transient therapeutic effect (Lilleeng et al., 2014). While we did not observe a change in GFAP-positive astrogliosis in STN-DBS, it is widely acknowledged that PD-related neuroinflammation is a complex process, and we did not undertake a thorough analysis of glial subtypes or inflammatory modulators. Future studies should therefore address this limitation.

Data availability statement

The raw data supporting the conclusions of this article will be made available by the authors, without undue reservation.

Ethics statement

This research project was approved by the Human Research Ethics Committees of the University of New South Wales (HREC project no. HC180835). Brain tissues were obtained from the Sydney Brain Bank that holds ethical approval and informed consent from the participants for brain banking through UNSW HREC 200026.

Author contributions

SM contributed to writing – original draft, review, and editing, project administration, investigation, data curation, visualization, and formal analysis. AB was involved in the data curation, visualization, and formal analysis. CS and AP contributed to the conceptualization, methodology, software, validation, formal analysis, writing – review and editing, supervision, and project administration. All authors contributed to the article and approved the submitted version.

Funding

This work was supported by the National Health and Medical Research Council to AP (APP1160412) and by the UNSW Brain Sciences and Translational Neuroscience Seed Funding. Tissues were received from the Sydney Brain Bank which was supported by Neuroscience Research Australia and the University of New South Wales.

Acknowledgments

We thank Andrew Affleck for assistance with the preparation of the figures and Eve Slavich from UNSW Stats Central for conducting power analysis for this study.

Conflict of interest

The authors declare that the research was conducted in the absence of any commercial or financial relationships that could be construed as a potential conflict of interest.

Publisher's note

References

Baker, K. B., Montgomery, E. B., Rezai, A. R., Burgess, R., and Lüders, H. O. (2002). Subthalamic nucleus deep brain stimulus evoked potentials: Physiological and therapeutic implications. *Mov. Disord.* 17, 969–983. doi: 10.1002/mds.10206

Beach, T. G., White, C. L., Hamilton, R. L., Duda, J. E., Iwatsubo, T., Dickson, D. W., et al. (2008). Evaluation of alpha-synuclein immunohistochemical methods used by invited experts. *Acta Neuropathol.* 116, 277–288. doi: 10.1007/s00401-008-0409-8

Bergman, H., Wichmann, T., Karmon, B., and DeLong, M. (1994). The primate subthalamic nucleus. II. Neuronal activity in the MPTP model of parkinsonism. *J. Neurophysiol.* 72, 507–520. doi: 10.1152/jn.1994.72.2.507

Braak, H., Sandmann-Keil, D., Gai, W., and Braak, E. (1999). Extensive axonal Lewy neurites in Parkinson's disease: A novel pathological feature revealed by α-synuclein immunocytochemistry. *Neurosci. Lett.* 265, 67–69. doi: 10.1016/S0304-3940(99)00208-6

Braak, H., Tredici, K. D., Rüb, U., de Vos, R. A. I., Jansen Steur, E. N. H., and Braak, E. (2003). Staging of brain pathology related to sporadic Parkinson's disease. *Neurobiol. Aging* 24, 197–211. doi: 10.1016/S0197-4580(02)00065-9

Charles, P. D., Gill, C. E., Davis, T. L., Konrad, P. E., and Benabid, A. L. (2008). Is deep brain stimulation neuroprotective if applied early in the course of PD? *Nat. Clin. Pract. Neurol.* 4, 424–426. doi: 10.1038/ncpneuro0848

Chiken, S., and Nambu, A. (2016). Mechanism of deep brain stimulation: Inhibition, excitation, or disruption? *Neuroscientist* 22, 313–322. doi: 10.1177/1073858415581986

DeMaagd, G., and Philip, A. (2015). Parkinson's disease and its management: Part 1: Disease entity, risk factors, pathophysiology, clinical presentation, and diagnosis. *Pharm. Therap.* 40:504.

Dickson, D. W., Braak, H., Duda, J. E., Duyckaerts, C., Gasser, T., Halliday, G. M., et al. (2009). Neuropathological assessment of Parkinson's disease: Refining the diagnostic criteria. *Lancet Neurol.* 8, 1150–1157. doi: 10.1016/S1474-4422(09)70238-8

Eusebio, A., Thevathasan, W., Doyle Gaynor, L., Pogosyan, A., Bye, E., Foltynie, T., et al. (2011). Deep brain stimulation can suppress pathological synchronisation in parkinsonian patients. *J. Neurol. Neurosurg. Psychiatr.* 82, 569–573. doi: 10.1136/jnnp.2010.217489

Fearnley, J. M., and Lees, A. J. (1991). Ageing and Parkinson's disease: Substantia nigra regional selectivity. *Brain* 114(Pt 5), 2283–2301. doi: 10.1093/brain/114.5.2283

Fischer, D. L., and Sortwell, C. E. (2018). BDNF provides many routes toward STN DBS-mediated disease modification. *Mov. Disord.* 34, 22–34. doi: 10.1002/mds.27535

Fischer, D. L., Manfredsson, F. P., Kemp, C. J., Cole-Strauss, A., Lipton, J. W., Duffy, M. F., et al. (2017). Subthalamic nucleus deep brain stimulation does not modify the functional deficits or axonopathy induced by nigrostriatal α-synuclein overexpression. *Sci. Rep.* 7:16356. doi: 10.1038/s41598-017-16690-x

Gradinaru, V., Mogri, M., Thompson, K. R., Henderson, J. M., and Deisseroth, K. (2009). Optical deconstruction of parkinsonian neural circuitry. *Science* 324, 354–359. doi: 10.1126/science.1167093

Hammond, C., Bergman, H., and Brown, P. (2007). Pathological synchronization in Parkinson's disease: Networks, models and treatments. *Trends Neurosci.* 30, 357–364. doi: 10.1016/j.tins.2007.05.004

Hardman, C. D., Halliday, G. M., McRitchie, D. A., and Morris, J. G. (1997). The subthalamic nucleus in Parkinson's disease and progressive supranuclear palsy. *J. Neuropathol. Exp. Neurol.* 56, 132–142. doi: 10.1097/00005072-199702000-00003

Hardman, C., McRitchie, D., Halliday, G., Cartwright, H., and Morris, J. (1996). Substantia nigra pars reticulata neurons in Parkinson's disease. *Neurodegeneration* 5, 49–55. doi: 10.1006/neur.1996.0007

Hendrickx, D. A., van Eden, C. G., Schuurman, K. G., Hamann, J., and Huitinga, I. (2017). Staining of HLA-DR, Iba1 and CD68 in human microglia reveals partially overlapping expression depending on cellular morphology and pathology. *J. Neuroimmunol.* 309, 12–22. doi: 10.1016/j.jneuroim.2017.04.007

Hilker, R., Voges, J., Ghaemi, M., Lehrke, R., Rudolf, J., Koulousakis, A., et al. (2003). Deep brain stimulation of the subthalamic nucleus does not increase the striatal dopamine concentration in parkinsonian humans. *Mov. Disord* 18, 41–48. doi: 10.1002/mds.10297

Hirsch, E., Breidert, T., Rousselet, E., Hunot, S., Hartmann, A., and Michel, P. P. (2003). The role of glial reaction and inflammation in Parkinson's disease. *Ann. N. Y. Acad. Sci.* 991, 214–228. doi: 10.1111/j.1749-6632.2003.tb07478.x

Jakobs, M., Fomenko, A., Lozano, A. M., and Kiening, K. L. (2019). Cellular, molecular, and clinical mechanisms of action of deep brain stimulation-a systematic review on established indications and outlook on future developments. *EMBO Mol. Med.* 11:e9575. doi: 10.15252/emmm.201809575

Jo, M., Kim, J. H., Song, G. J., Seo, M., Hwang, E. M., and Suk, K. (2017). Astrocytic Orosomucoid-2 modulates microglial activation and neuroinflammation. *J. Neurosci.* 37, 2878–2894. doi: 10.1523/JNEUROSCI.2534-16.2017

Knott, C., Wilkin, G. P., and Stern, G. (1999). Astrocytes and microglia in the substantia nigra and caudate-putamen in Parkinson's disease. *Parkinsonism Relat. Disord.* 5, 115–122. doi: 10.1016/S1353-8020(99)00022-X

Kojovic, M., Higgins, A., Mir, P., and Jahanshahi, M. (2019). Enhanced motivational modulation of motor behaviour with subthalamic nucleus deep brain stimulation in Parkinson's disease. *Parkinsons Dis.* 2019:3604372. doi: 10.1155/2019/3604372

Kordower, J. H., Olanow, C. W., Dodiya, H. B., Chu, Y., Beach, T. G., Adler, C. H., et al. (2013). Disease duration and the integrity of the nigrostriatal system in Parkinson's disease. *Brain* 136, 2419–2431. doi: 10.1093/brain/awt192

Liddelow, S. A., Guttenplan, K. A., Clarke, L. E., Bennett, F. C., Bohlen, C. J., Schirmer, L., et al. (2017). Neurotoxic reactive astrocytes are induced by activated microglia. *Nature* 541, 481–487. doi: 10.1038/nature21029

Lilleeng, B., Brønnick, K., Toft, M., Dietrichs, E., and Larsen, J. P. (2014). Progression and survival in Parkinson's disease with subthalamic nucleus stimulation. *Acta Neurol. Scand.* 130, 292–298. doi: 10.1111/ane.12224

Limousin, P., and Foltynie, T. (2019). Long-term outcomes of deep brain stimulation in Parkinson disease. *Nat. Rev. Neurol.* 15, 234–242. doi: 10.1038/s41582-019-0145-9

Limousin, P., Pollak, P., Benazzouz, A., Hoffmann, D., Le Bas, J. F., Broussolle, E., et al. (1995). Effect on parkinsonian signs and symptoms of bilateral subthalamic nucleus stimulation. *Lancet* 345, 91–95. doi: 10.1016/S0140-6736(95)90062-4

McGeer, P. L., and McGeer, E. G. (2008). Glial reactions in Parkinson's disease. *Mov. Disord.* 23, 474–483. doi: 10.1002/mds.21751

Mirza, B., Hadberg, H., Thomsen, P., and Moos, T. (2000). The absence of reactive astrocytosis is indicative of a unique inflammatory process in Parkinson's disease. *Neuroscience* 95, 425–432. doi: 10.1016/S0306-4522(99)00455-8

Ohama, E., and Ikuta, F. (1976). Parkinson's disease: Distribution of Lewy bodies and monoamine neuron system. *Acta Neuropathol.* 34, 311–319. doi: 10.1007/BF00696560

Pal, G. D., Ouyang, B., Serrano, G., Shill, H. A., Goetz, C., Stebbins, G., et al. (2017). Comparison of neuropathology in Parkinson's disease subjects with and without deep brain stimulation. *Mov. Disord.* 32, 274–277. doi: 10.1002/mds.26882

Pienaar, I. S., Lee, C. H., Elson, J. L., McGuinness, L., Gentleman, S. M., Kalaria, R. N., et al. (2015). Deep-brain stimulation associates with improved microvascular integrity in the subthalamic nucleus in Parkinson's disease. *Neurobiol. Dis.* 74, 392–405. doi: 10.1016/j.nbd.2014.12.006

Remple, M. S., Bradenham, C. H., Kao, C. C., Charles, P. D., Neimat, J. S., and Konrad, P. E. (2011). Subthalamic nucleus neuronal firing rate increases with Parkinson's disease progression. *Mov. Disord.* 26, 1657–1662. doi: 10.1002/mds.23708

Röhl, C., and Sievers, J. (2005). Microglia is activated by astrocytes in trimethyltin intoxication. *Toxicol. Appl. Pharmacol.* 204, 36–45. doi: 10.1016/j.taap.2004.08.007

Spieles-Engemann, A. L., Behbehani, M. M., Collier, T. J., Wohlgenant, S. L., Steece-Collier, K., Paumier, K., et al. (2010). Stimulation of the rat subthalamic nucleus is neuroprotective following significant nigral dopamine neuron loss. *Neurobiol. Dis.* 39, 105–115. doi: 10.1016/j.nbd.2010.03.009

Strafella, A. P., Sadikot, A. F., and Dagher, A. (2003). Subthalamic deep brain stimulation does not induce striatal dopamine release in Parkinson's disease. *Neuroreport* 14, 1287–1289. doi: 10.1097/00001756-200307010-00020

Tagliati, M., Martin, C., and Alterman, R. (2010). Lack of motor symptoms progression in Parkinson's disease patients with long-term bilateral subthalamic deep brain stimulation. *Int. J. Neurosci.* 120, 717–723. doi: 10.3109/00207454.2010.518777

Tawfik, V. L., Chang, S. Y., Hitti, F. L., Roberts, D. W., Leiter, J. C., Jovanovic, S., et al. (2010). Deep brain stimulation results in local glutamate and adenosine release: Investigation into the role of astrocytes. *Neurosurgery* 67, 367–375. doi: 10.1227/01.NEU.0000371988.73620.4C

Temel, Y., Visser-Vandewalle, V., Kaplan, S., Kozan, R., Daemen, M. A., Blokland, A., et al. (2006). Protection of nigral cell death by bilateral subthalamic nucleus stimulation. *Brain Res.* 1120, 100–105. doi: 10.1016/j.brainres.2006.08.082

Thobois, S., Fraix, V., Savasta, M., Costes, N., Pollak, P., Mertens, P., et al. (2003). Chronic subthalamic nucleus stimulation and striatal D2 dopamine receptors in Parkinson's disease. *J. Neurol.* 250, 1219–1223. doi: 10.1007/s00415-003-0188-z

Tong, J., Ang, L. C., Williams, B., Furukawa, Y., Fitzmaurice, P., Guttman, M., et al. (2015). Low levels of astroglial markers in Parkinson's disease: Relationship to α-synuclein accumulation. *Neurobiol. Dis.* 82, 243–253. doi: 10.1016/j.nbd.2015.06.010

Urbanc, B., Cruz, L., Le, R., Sanders, J., Hsiao Ashe, K., Duff, K., et al. (2002). Neurotoxic effects of thioflavin S-positive amyloid deposits in transgenic mice and Alzheimer's disease. *Proc. Natl. Acad. Sci. U.S.A.* 99, 13990–13995. doi: 10.1073/pnas.222433299

Vedam-Mai, V., Gardner, B., Okun, M. S., Siebzehnrubl, F. A., Kam, M., Aponso, P., et al. (2014). Increased precursor cell proliferation after deep brain stimulation for Parkinson's disease: A human study. *PLoS One* 9:e88770. doi: 10.1371/journal.pone.0088770

Vedam-Mai, V., van Battum, E. Y., Kamphuis, W., Feenstra, M. G., Denys, D., Reynolds, B. A., et al. (2012). Deep brain stimulation and the role of astrocytes. *Mol. Psychiatry* 17, 124–131. doi: 10.1038/mp.2011.61

Wallace, B. A., Ashkan, K., Heise, C. E., Foote, K. D., Torres, N., Mitrofanis, J., et al. (2007). Survival of midbrain dopaminergic cells after lesion or deep brain stimulation of the subthalamic nucleus in MPTP-treated monkeys. *Brain* 130, 2129–2145. doi: 10.1093/brain/awm137

Frontiers in Neuroscience

Provides a holistic understanding of brain function from genes to behavior

Part of the most cited neuroscience journal series which explores the brain - from the new eras of causation and anatomical neurosciences to neuroeconomics and neuroenergetics.

Discover the latest Research Topics

See more →

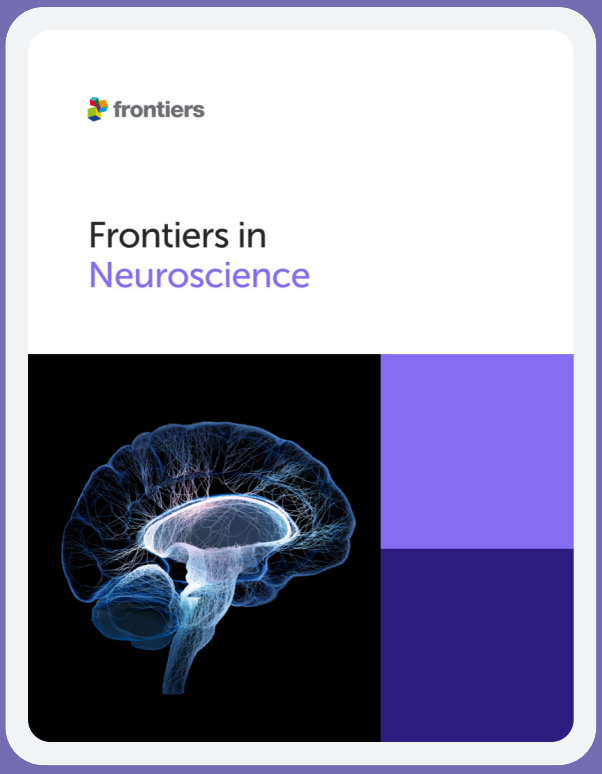

Frontiers

Avenue du Tribunal-Fédéral 34
1005 Lausanne, Switzerland
frontiersin.org

Contact us

+41 (0)21 510 17 00
frontiersin.org/about/contact